R-10-35

Äspö Hard Rock Laboratory

The TASS-tunnel

Geological mapping

Carljohan Hardenby, Vattenfall Power Consultant AB

Oskar Sigurdsson, HAskGeokonsult AB

December 2010

Svensk Kärnbränslehantering AB
Swedish Nuclear Fuel
and Waste Management Co

Box 250, SE-101 24 Stockholm
Phone +46 8 459 84 00

ISSN 1402-3091
SKB R-10-35

Äspö Hard Rock Laboratory

The TASS-tunnel

Geological mapping

Carljohan Hardenby, Vattenfall Power Consultant AB

Oskar Sigurdsson, HAskGeokonsult AB

December 2010

This report concerns a study which was conducted for SKB. The conclusions and viewpoints presented in the report are those of the author(s). SKB may draw modified conclusions, based on additional literature sources and/or expert opinions.

A pdf version of this document can be downloaded from www.skb.se.

Abstract

The project entitled “Sealing of tunnel at great depth” (Fintätning av tunnel på stort djup) needed a new tunnel in an area as undisturbed as possible and with cross-cutting water-bearing structures. The new tunnel, which was given the name TASS, was excavated on the –450 m level of SKB’s Äspö Hard Rock Laboratory (Äspö HRL). The length of the tunnel is approximately 80 m and the theoretical tunnel area 19 m^2. As is the case with all the other tunnels of the Äspö HRL, the new tunnel has been geologically mapped. In addition, laser scanning combined with digital photography has been carried out. The tunnel was also used to test various types of explosives, borehole layouts and drilling techniques.

The geological mapping of tunnel floor, walls and roof took place on four major occasions when a halt was made in tunnel excavation to allow for various tests. Before the mapping started on these occasions, laser scanning took place. The tunnel faces were mapped after each round (drilling, blasting and unloading).

The present report describes the geological features of the tunnel and briefly how the laser scanning was performed. Water-bearing structures have been compared to similar structures in the neighbouring tunnels.

The rock type names used here follow the old established Äspö HRL nomenclature. Narrow (<0.1 m wide) dykes are normally mapped as fracture fillings.

- The dominating rock type is *Äspö diorite,* which constitutes some 90% of the rock mass. It is mostly mapped as fresh rock.
- Minor constituents of the rock mass are: *fine-grained granite, hybrid rock, pegmatite, quartz veins/lenses* and *undifferentiated mafic rock*.

The mapping of fractures and deformation zones considers a number of parameters such as number of fractures, open/healed, width, length, description of fracture surfaces (roughness, planarity, etc), fracture filling, alteration and water. The deformation zones are discriminated into two main categories (“increased fracturing” and “deformation zones proper”). The orientation of the structures is measured with a compass, and magnetic north is used for reference purposes.

Two main *fracture sets* appear in the TASS-tunnel:

- East-west striking and steeply dipping. This fracture set dominates with a mean orientation of 097/86.
- Sub-horizontal to gently dipping with a more varying strike. This set may be divided into two sub-sets with the mean orientations 037/03 and 280/18 respectively.

The observed categories of *deformation zones* appear to fall within two major groups of orientation:

- Increased fracturing is oriented approximately ENE-WSW with a moderate dip to the north.
- Deformation zones proper (brittle/ductile) have a general orientation of approximately ESE-WNW strike with steep dip mostly to the south. These zones generally cross-cut the tunnel and their widths vary from 0.1–0.3 m.

The fractures and deformation zones normally contain secondary minerals. The most common *fracture-filling mineral* in the tunnel is chlorite, followed by calcite, epidote and prehnite. Quartz, pyrite and red feldspar are also quite common, while biotite, iron oxide and unconsolidated filling materials (grout and clay) have only been observed a few times.

Occurrences of *water* are of great interest since one of the major tasks of the project was to prove that the grouting compounds used could seal tunnels at the tentative final repository depth. The orientations of water-bearing fractures for the tunnel are dominated by sub-horizontal to gently dipping fractures, with mean orientations of 000/00 and 297/28. Two less prominent water-bearing fracture sets of 287/70 and 099/89 also occur.

Grouting was performed on a number of occasions while tunnel excavation was taking place. The quantity of water given by the geological mapping was, for the whole tunnel, approximately 1.2 litre/minute per 70 m of tunnel. According to the measurements in the weirs, the water inflow was, after tunnel completion, 1.5 litre/minute per 70 m of tunnel (=1.3 litre/minute per 60 m of tunnel – allowed inflow 1 litre/minute per 60 m of tunnel).

Comparisons of structures in the neighbouring tunnels show that there are strong similarities but also some differences. The fractures are commonly WNW-ESE striking and steeply dipping or sub-horizontal to gently dipping with more varying strike. The main difference is that the dominating steeply dipping fracture set in the TASS-tunnel is closer to E-W than the set in the TASA Prototype tunnel.

Some of the major structures identified in the TRUE Block Scale model were earlier interpreted to cut one of the pre-investigation boreholes (KI0010B01). These structures have now been extrapolated into the TASS-tunnel.

The *rock quality* is determined along the tunnel by using a simplified version of the RMR system. The RMR values vary from 58–81 with an average of about 70, which is in the middle of the rock mass class "good rock". The lowest RMR values are noted in the floor.

Laser scanning combined with digital photography was performed in the TASS-tunnel before the geological mapping of each stage. Successful tests to process the scan data using software other than that adapted to the laser scanner were performed by SKB. Laser scanning combined with digital photography was found to be a useful tool in the excavation work.

Sammanfattning

Projektet ”Fintätning av tunnel på stort djup” (Sealing of tunnel at great depth) krävde en ny tunnel i ett område som var så ostört som möjligt och med vattenförande sprickor som korsade tunnelsträckningen. Den nya tunneln, som kom att kallas TASS-tunneln, bröts på –450 m nivån i SKB:s Äspölaboratoriums tunnelsystem. Den nya tunneln är c:a 80 m lång med en teoretisk tunnelarea på c:a 19 m^2. Liksom alla tunnlar i laboratoriet karterades den nya tunneln. Dessutom utfördes laserskanning kombinerad med digital fotografering. Tunneln var även ämnad för att testa olika sprängmedel, borrhålslayouter och borrningsteknik.

Den geologiska karteringen av sula, väggar och tak ägde rum vid fyra huvudtillfällen då tunnelbrytningen gjorde uppehåll för att olika tester skulle kunna utföras. Före varje sådant karteringstillfälle utfördes laserskanningen. Tunnelfronterna karterades efter varje salva.

Denna rapport beskriver geologin och korta drag hur laserskanningen utfördes i tunneln. Vattenförande strukturer har jämförts med liknande strukturer i omgivningen.

De bergartsnamn som använts här följer den gamla etablerade Äspönomenklaturen. Smala (<0.1 m breda) gångar karterades vanligen som sprickfyllnader.

- Den dominerande bergarten *Äspödiorit* utgör omkring 90 % av bergmassan. Till största del har bergarten karterats som friskt berg.
- Underordnade bergarter är: *finkornig granit, hybridbergart, pegmatit, kvartsådror/gångar* och *odifferentierade mafiska bergarter*.

Karteringen av sprickor och deformationszoner omfattar ett antal parametrar såsom; antal sprickor, öppna/läkta, bredd, längd, beskrivning av sprickytor (råhet, planhet etc), sprickfyllnad, omvandling och vatten. Deformationszonerna har uppdelats i två huvudkategorier (”ökad sprickighet” och ”egentliga deformationszoner”). Orienteringen av strukturerna är mätt med kompass och som referens har magnetiskt norr använts.

Två *sprickgrupper* har noterats i TASS-tunneln:

- Strykning Ö-V och brant stupning. Denna sprickgrupp dominerar med medelorienteringen 097/86.
- Sub-horisontella till svagt stupande. Denna grupp skulle kunna delas upp i två undergrupper med medelorienteringen 037/03 respektive 280/18.

De två kategorierna av *deformationszoner* som har noterats i TASS-tunneln är:

- Ökad sprickighet som är orienterad ONO-VSV med moderat stupning mot norr.
- Egentliga deformationszoner (spröd/duktil) har en generell orientering OSO-VNV med brant stupning mestadels mot syd. Generellt skär dessa zoner tunneln med en bredd som varierar mellan 0.1–0.3 m.

Sprickor och deformationszoner innehåller vanligtvis sekundära mineral. Det vanligaste *sprickmineralet* i tunneln är klorit. Därefter kommer kalcit, epidot och prehnit. Kvarts, pyrit och röd fältspat är också tämligen vanliga, medan biotit, Fe-oxid och okonsoliderade fyllnadsmaterial (såsom injekteringsmedel och lera) har bara observerats ett fåtal gånger.

Förekomsten av *vatten* har varit av stort intresse eftersom ett av huvudsyftena med projektet var att visa de använda injekteringsmedlen kunde täta en tunnel på det tänkta slutförvaringsdjupet. Orienteringen av vattenförande sprickor i tunneln domineras av sub-horisontella till svagt stupande sprickor med medelorienteringarna 000/00 och 297/28. Två mindre tydliga vattenförande sprickgrupper förekommer också med orienteringen 287/70 och 099/89.

Under indriften injekterades tunneln vid ett antal tillfällen. Vid den geologiska karteringen noterades ett totalt inflöde av vatten på c:a 1.2 liter/minut och 70 meter tunnel. Enligt mätning som skedde i mätvallar efter det att tunneln var färdigsprängd var inflödet 1.5 liter/minut och 70 m tunnel (=1.3 liter/minut och 60 m tunnel – det tillåtna inflödet var 1 liter/minut och 60 m tunnel).

Vid en *jämförelse av strukturerna* i omgivande tunnlar så kunde det påvisas att stora likheter fanns. Sprickorna stryker ungefär VNV-OSO med brant stupning eller är horisontella till sub-horisontella med varierande strykning. Huvudskillnaden är att de brant stupande sprickorna inom TASS-tunneln stryker mera i Ö-V än de i TASA-Prototyptunneln.

Vissa av de i TRUE-Block Scale modellen förekommande strukturerna har ansetts klippa förundersökningsborrhålet KI0010B01. Dessa strukturer har extrapolerats till karteringen över TASS-tunneln.

Bergkvalitén har i tunneln bestämts med en förenklad version av RMR-systemet. RMR-värdena varierar mellan 58–81 med ett medelvärde kring 70 som faller inom bergklass ”bra berg”. De lägsta RMR-värdena har noterats i tunnelns sula.

Laserskanning kombinerad med digital fotografering utfördes i TASS-tunneln innan den geologiska karteringen av respektive etapp påbörjades. Skanndata levererades i ascii-format för att av SKB kunna hanteras med andra programvaror än de som tillhör laserskannern. Det kan konstateras att laserskanning kombinerad med digital fotografering kan vara ett bra hjälpmedel vid tunnelbyggande.

Contents

1 Introduction

1.1 Background

Svensk Kärnbränslehantering AB (SKB, Swedish Nuclear Fuel and Waste Management Co) decided in 2006 to execute tests on Silica sol as an alternative and/or complement to cement-based compounds to seal fractures. One advantage of Silica sol is its capability to seal very narrow fractures (about 0.01 mm in width). The compound has not, however, been tested at great depths such as those contemplated for the planned storage of nuclear waste (400–700 m below ground level). The SKB project in which the Silica sol tests were performed has been called "Fintätning av tunnel på stort djup" ("Sealing of tunnel at great depth") abbreviated to "Fintätningsprojektet" ("The Sealing Project").

SKB also decided to test different types of explosives, drilling techniques and borehole layouts to achieve as good tunnel contours as possible and to minimise the damage to the tunnel walls, roof and floor. These tests were to be performed as part of the same tunnel project as that used for testing silica sol.

In order to be able to perform both these sets of tests, a new tunnel was excavated, referred to as the TASS-tunnel (T=tunnel, AS=Äspö site, S=letter ID for the tunnel in question; this nomenclature is used in the SKB database, Sicada). The allowed inflow of water into the final repository has been set at 1 litre/min per 60 m of tunnel. This is also the target limit after grouting for the inflow into the new tunnel.

In addition, SKB decided to survey the entire tunnel with laser scanning combined with digital photography and to study the EDZ (excavation damage zone) in a section of the new tunnel.

1.2 Location of the TASS-tunnel

A suitable location for the new tunnel was found at the –450 m level of the Äspö Hard Rock Laboratory (Äspö HRL, Figure 1-1). The locality was chosen since it fulfilled a number of conditions, such as tunnel orientation in relation to water-bearing structures, location outside the main draw-down of the ground water surface and lack of major interference with other activities. Furthermore, the tunnel must be easily accessible for transportation /Hardenby et al. 2008/. The TASS-tunnel was ended at 80.7 m counted from the intersection of the centre line of the TASS-tunnel and the centre line of the TASI-tunnel from which it emanated (Figure 1-2). All specifications of sections refer to the centre line of the TASS-tunnel. The actual tunnel starts at approximately section 5 m from the right-hand wall of the TASI-tunnel or, depending on whether the right or left-hand wall of the TASS-tunnel is being considered, at a distance from the right-hand wall of the TASI tunnel of 3 or 7 m respectively. The theoretical tunnel area is 18.9 m^2. A section (approximately 22–48 m) of the TASS-tunnel is shown in Figure 1-3.

Two major references for North are used in the Äspö HRL tunnels. Drawings of the tunnel system use the coordinate system Äspö 96 as a reference whereas the measured orientation of geological features in the tunnels refers to magnetic north unless otherwise specified (see Figure 1-4). The orientation of the TASS-tunnel is 230° (Äspö 96) or 215.8° (Magnetic North). The NW tunnel wall will in the remainder of this report often be referred to as the right-hand wall, and hence the SE wall as the left-hand wall.

The EDZ study /Olsson et al. 2009/ and AP TD SU446-08-031 (internal controlling SKB document, Table 1-1) took place at section 36.4–44.4 m, where a slot had been cut in the right-hand wall (Figure 1-5). The slot was entitled US0036B01, where U = the Sicada-database notation for a slot, S = the tunnel S, 0036 = the tunnel section where the slot begins, B = the right-hand wall and 01 = the first slot in the section.

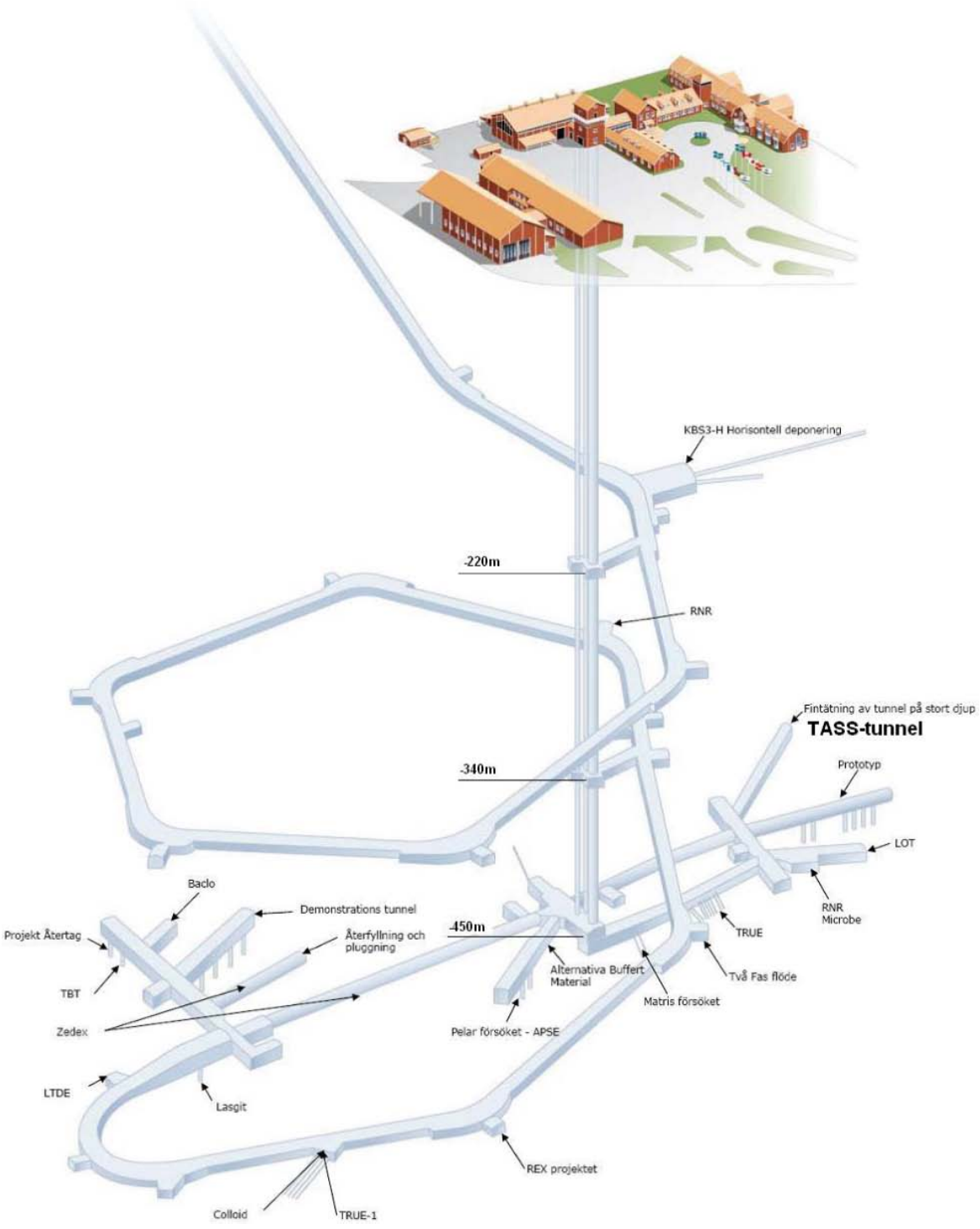

Figure 1-1. *The Äspö HRL, including location of the TASS-tunnel.*

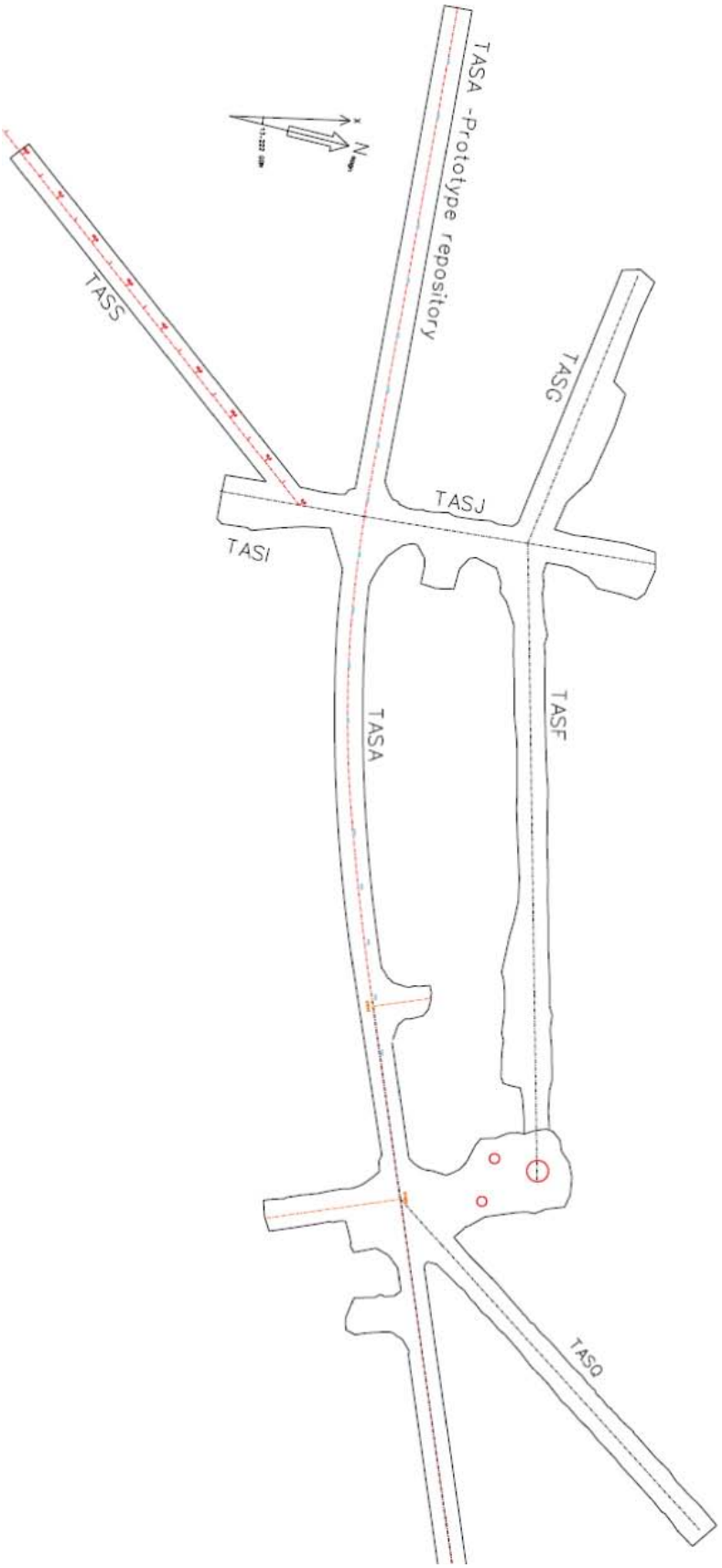

Figure 1-2. *Äspö HRL, contours of the tunnels at the –450 m level including location of the TASS-tunnel. The orientation of the TASS-tunnel is 230° (Äspö 96) or 215.8° (magnetic north). North arrow: N magn = magnetic north, x = north Äspö 96.*

Figure 1-3. *View of the TASS-tunnel, approximate section 22–48 m.*

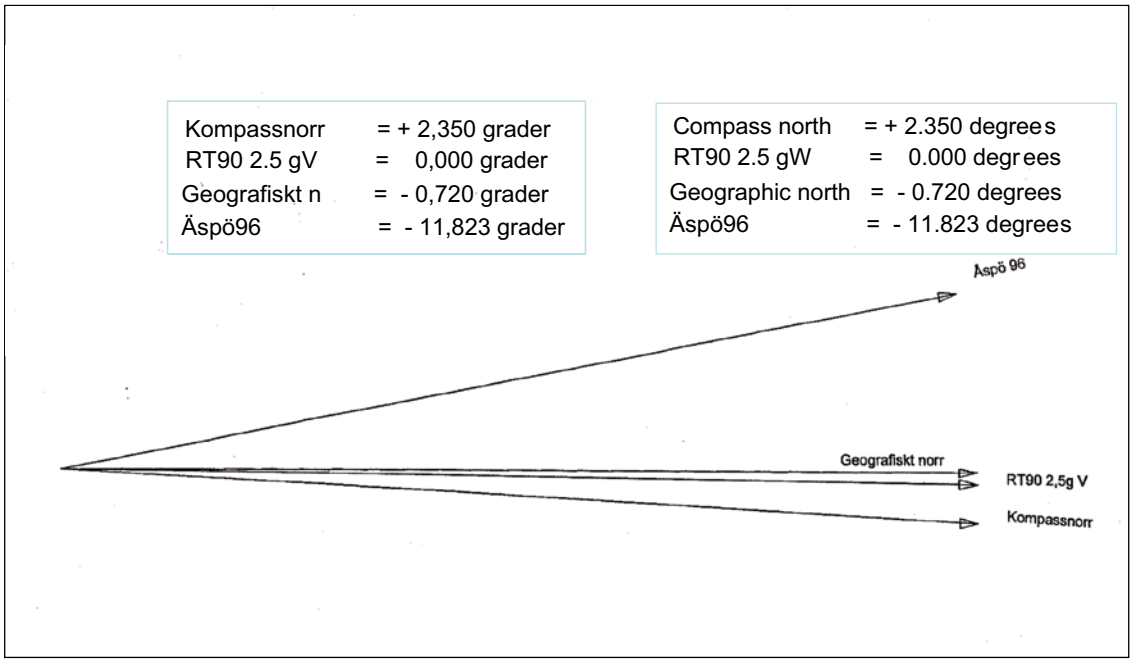

Figure 1-4. *Relationship between the various geographical systems used at Äspö HRL (modified from drawing made for SKB in 2006).*

Figure 1-5. *A part of the EDZ-slot in the right-hand wall of the TASS-tunnel, section 36.4–44.4 m.*

1.3 The aim of this study and report

As with all other tunnels/drifts at Äspö HRL, the new tunnel – including the EDZ-slot /Olsson et al. 2009/ – had to be geologically mapped. Apart from the mapping of the EDZ slot, no other work related to EDZ is dealt with in this report. All the geological mapping of the TASS-tunnel was executed by the authors (Carljohan Hardenby, Vattenfall Power Consultant AB and Oskar Sigurdsson, HAskGeokonsult AB).

The major purpose of the report is to:

- Describe the various geological features of the TASS-tunnel based on the geological mapping.

In addition the report will present:

- An attempt to identify mapped structures in the TASS-tunnel that may coincide with particularly water-bearing structures found in the three pre-investigation boreholes as well as those in the TRUE Block Scale hydro-structural model.
- The use of laser scanning combined with digital photography as a complementary documentation of the tunnel.

1.4 Internal controlling documents

To describe and control the various activities, a number of internal SKB documents have been used. These documents are not, however, accessible to the public and are only listed below in Table 1-1. Some of the unpublished documents may be submitted upon request to “document@skb.se”.

Table 1-1. Internal controlling documents.

Type of document	Document ID, version & year	Title	Author(s)/issuer
Project plan	Projektplan SU32516, ver 1.0, 2007	Fintätning av tunnel på stort djup. Genomförande, projektplan (Sealing of tunnel at great depth. Implementation, project plan)	Bergström, Martin
Activity plan	AP TD SU32516-07-057, ver 1.0, 2007	Geologisk kartering av S-Tunneln, Äspölaboratoriet (Geological mapping of the S-tunnel, Äspö HRL)	Hardenby, Carljohan
Activity plan	AP TD SU32516-08-006, ver 1.0, 2008	Laserskanning av tunnel S (TASS) [Laser scanning of the S-tunnel (TASS)]	Feng,Quanhong
Activity plan	AP TD SU446-08-031, ver 1.0, 2008	Dokumentation EDZ: Undersökning av block och modellering (Documentation EDZ: investigation of blocks and modelling)	Olsson, Mats, Markström, Ingemar and Pettersson, Anders
Method description	Teknisk PM nr. 25-95-018, 1994	Manual för tunnelkartering av front, nischer och sidotunnlar (Manual for mapping of tunnels, faces and niches)	Annertz, Kristian and Stenberg, Leif
Method description	Tekniskt Dokument TD-02-01, 2003	Djupförvarsteknik. Tunnel Mapping System (TMS) version 2.0. Användarmanual [Repository Technology. Tunnel Mapping System (TMS) version 2.0. User's manual]	Hardenby, Carljohan
Method description	SKB MD 143.008, ver 1.0, 2004	Nomenklatur vid Boremap-kartering (Boremap logging Nomenclature)	Larsson, Nils-Åke
Method description	SKB MD 132.004, ver 3.0, 2009	Regler för bergarters benämningar för Laxemar – Simpevarpsområdet och för Äspölaboratoriet	Peter Hultgren
Code list	SKBdoc 1252025 ver 0.2, 2009	Codes and information for the TMS mapping forms and the tables of the TMS data base	Hardenby, Carljohan

2 Preparation and mapping procedure

2.1 General mapping procedure

The geological mapping of the Äspö HRL tunnels is described in the document entitled "Manual för tunnelkartering av front, nischer och sidotunnlar" (Teknisk PM nr 25-95-018, internal controlling SKB document, see Table 1-1). The SKB application called TMS (Tunnel Mapping System) based on Micro Station is used for digitizing drawings and Microsoft's Access database is used to store data.

The following major items are registered during the mapping:

- rock types
- rock boundaries/contacts
- alteration
- fractures
- deformation zones
- occurrence of water/water leakage
- Rock Mass Rating (RMR).

The various parameters recorded for each of the major items can be found in the code chart called "Codes and information for the TMS mapping forms and the tables of the TMS database" (SKBdoc 1252025, internal SKB document, see Table 1-1). Many of the expressions and descriptions found in the code chart are used in the report.

Certain methods, definitions, descriptions, etc of the various subjects will be further dealt with in Chapter 3 under respective headings.

The rock type names that have been commonly used at Äspö HRL are basically those given by e.g. /Wikman and Kornfält 1995/.

Rock boundaries/contacts are described as being diffuse or sharp where sharp is subdivided into open and tight (closed).

Five weathering/alteration classes ("none" to "complete") based on those described by /ISRM 1977, pp 319–368/ are used.

Normally, the cut-off for fractures is 1 m in length. The fracture lengths are recorded as maximum trace length. The fracture width is defined as possible aperture plus possible fracture-filling measured across the fracture. Oxidation rims, when present, along fractures are measured in the same way and include the width (Figure 2-1). The width of dykes/veins drawn as rock types is >0.1 m. If these dykes/veins are <0.1 m in width, they are commonly regarded as fracture fillings and thus recorded together with fractures. The widths are frequently only estimated.

Deformation zones are divided into two major categories: *increased fracturing* that is defined as a zone with a large number of fractures that will not be drawn separately, and *deformation zones proper (brittle to ductile).*

The orientations of structural features are obtained by compass readings. A 0–360 degrees compass is used. Magnetic north is used for reference purposes and orientations of planar structures are given according to the right-hand rule as strike and dip (strike/dip). Thus the orientation of the strike is measured when the dip direction is on the right-hand side. The orientation of linear structures is given as trend and plunge (trend/plunge). Often the degree symbol ° is not used in the text.

The quantity of water leakage is wherever possible measured. Mostly, however, the quantity is only given in the terms of damp, wet or flow. The source (fracture, borehole, etc) of the leakage is recorded. Often, however, only a diffuse leakage can be observed from the rock surface, in which case the rock itself is regarded as the source.

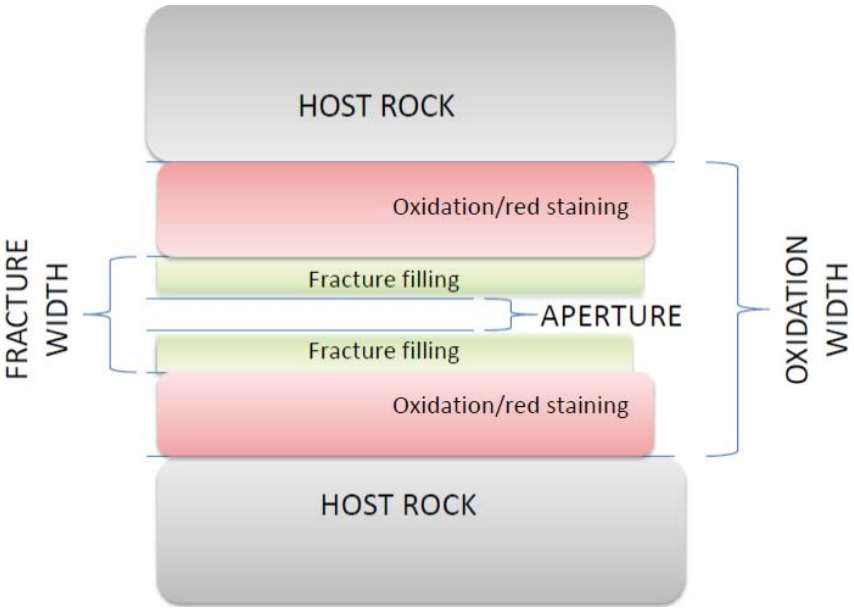

Figure 2-1. *Principle drawing of the parts of a fracture. The fracture width is defined as possible aperture plus possible fracture filling measured across the fracture. Oxidation rims along fractures are measured in the same way and include the fracture width.*

The rock quality has been determined on the basis of the RMR system, e.g. /Bieniawski 1973, pp 335–344, 1984, pp 97–133 and 1989, p 251, cited in Singh and Goel 1999, 34–46/. The RMR system is also described for example by /Hoek and Brown 1982, p 26/.

The standard mapping, which is an ocular examination of the rock surfaces, has been mostly performed on a scale of 1:100. Briefly, the documentation of the geological features is carried out in the following way. In the tunnel, the geological mapping is made on plastic-coated paper (Figure 2-2). Certain forms are used to record the characteristics of rock types, fractures, etc. The field documentation is later fed into a computer. All mapped objects such as fractures, rock boundaries etc are digitized and data are attached to each object by the use of the TMS system. The tunnel mapping is presented on a 2-D drawing where the tunnel walls have been unfolded to form a plane together with the tunnel roof (P, Figure 2-3).

The part of a tunnel that is currently being mapped is called a map cell. The ID of the map cell is normally the end section of the mapped tunnel segment. At present, fractures are given an ID-number from 1–999, the ID of deformation zones is Z0-Z29, rock types B0-B29, rock boundaries/contacts K0-K29, and water leakages A-Z and Aa-Zz. The IDs for water leakages will be accompanied by the symbols for the quantity of water (v = damp/moist, vv = wet/drops and vvv = flow of water; for example Av, Bvv etc). The ID-numbers are only valid within the map cell. When a new part of the tunnel is being mapped, this will be a new map cell and the numbering of fractures, etc will start all over again.

Note that in the TMS database the tables concerning deformation zones are still called fraczon1 and fraczon2 since deformation zones were earlier referred to as fracture zones.

As a supplement to the mapping, the tunnels have been photographed. All photos are stored in SKB's Sicada archive where they can be traced with the help of activity plan number AP TD SU32516-07-057 (internal SKB document, see Table 1-1) and/or referring to the TASS-tunnel.

Figure 2-2. *Tunnel floor mapping on plastic-coated paper (around section 24 m of the TASS-tunnel).*

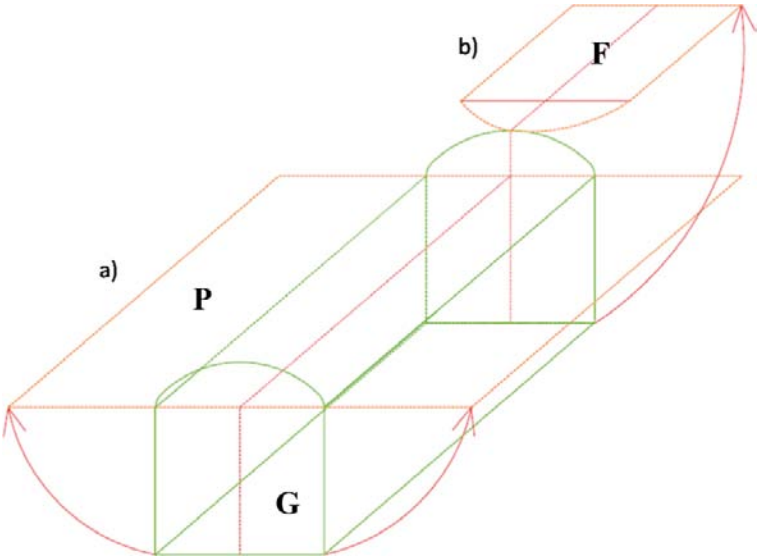

Figure 2-3. *Principle drawing showing the projection (light-brown) on which the geological mapping is performed. The light-brown planes show* ***a)*** *walls unfolded to form a plane together with the tunnel roof (P) and* ***b)*** *the tunnel face (F) unfolded. The tunnel faces (F) and floor (G) are drawn beside the tunnel walls and roof projection (see Figures 2-4 and 3-1). Green lines indicate the theoretical tunnel geometry. The transition area between tunnel walls and roof is here called shoulder.*

2.1.1 Specific TASS-tunnel mapping procedures

The geological mapping of the TASS-tunnel was basically performed in accordance with the standard procedure for tunnel mapping (Teknisk PM nr 25-95-018, internal SKB document, Table 1-1) as described in Section 2.1.

Owing to the time allowed for geological mapping in the TASS-tunnel a scale of 1:50 could be used. In this way, more detailed mapping could be performed than that specified in the standard procedure and in the internal SKB document AP TD SU32516-07-057 (Table 1-1). For example, the positions of geological features – such as fractures and rock boundaries – were determined with the help of a folding rule, and when possible all fractures exceeding 1 m were drawn.

As mentioned earlier, all fractures and deformation zones have been given an ID-number consisting of only numbers (1–999, fractures) or a combination of letter and number (Z0-Z29, deformation zones). These ID-numbers are only valid within the map cell where they are recorded. A further way of identifying an object was used when it continued into another map cell. For the mapping of the TASS-tunnel, the following system was used;

- If, for example, a fracture with the ID-number 1 in the first map cell of the floor continued into another map cell it was given the ID G1-1 in the drawing of the new map cell
- In a similar way, P2-Z0 means that the zone Z0 was first registered in the roof and/or walls of the second map cell 2 and continued into another map cell
- There is no new data entry for the object in the new map cell. The data may, however, be changed in a way that suits the extended structure (e.g. fracture length).

In addition to the general photography, laser scanning combined with digital photography was performed as complementary documentation of the TASS-tunnel.

Normally, only the unfolded tunnel walls and the roof (P in Figure 2-3) are presented on a 2-D drawing. For the TASS-tunnel, however, the tunnel floor (G) as well as the tunnel faces (F) are presented on the same 2-D drawing, but alongside the tunnel walls and roof (see Figure 2-4).

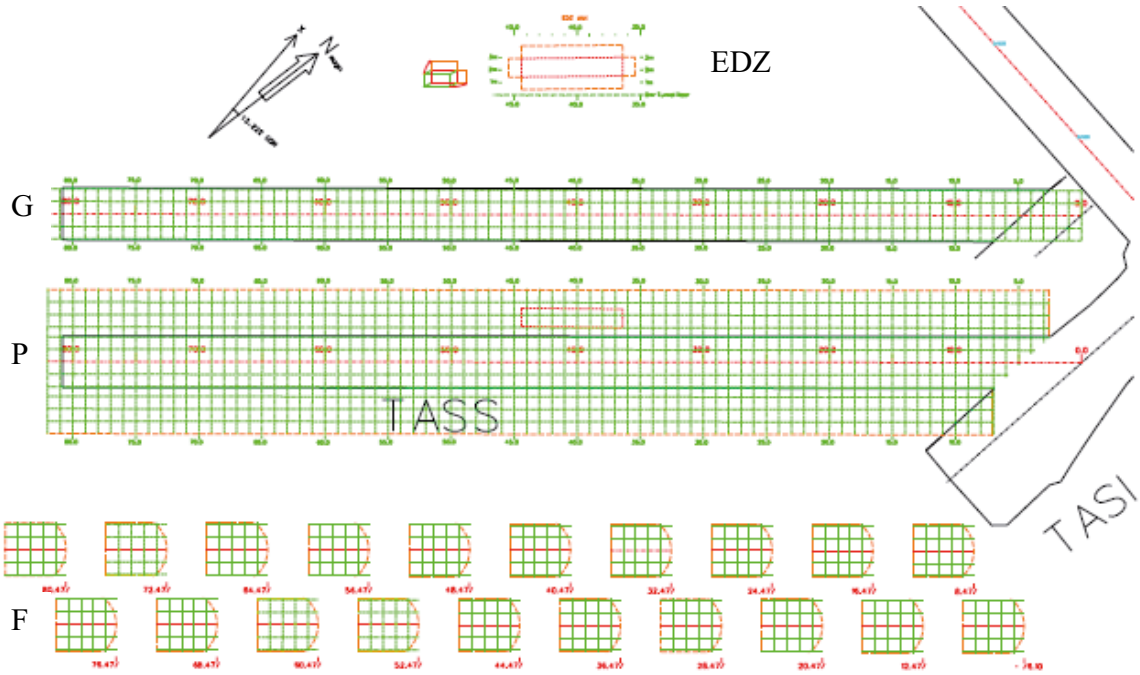

Figure 2-4. *Layout of 2-D drawing on which the mapping results from the TASS-tunnel will be drawn (EDZ = EDZ-slot, G = floor, P = walls and roof, and F = tunnel face, see Figure 2-3).*

Photos, drawings of the geological mapping and data tables were stored on CD:s that were delivered to SKB's Sicada archive. Data and photos are nowadays also stored in SKB's main database Sicada. Data etc. are traceable by using the activity plan number AP TD SU32516-07-057 (internal SKB document, see Table 1-1) and/or by referring to the TASS-tunnel. Data may be ordered from sicada.dataut@skb.se.

2.2 Preparations before mapping

Before the tunnel could be mapped, the tunnel walls, roof and floor had to be cleaned. The walls and roof were only flushed with water. The floor, however, had to be thoroughly cleaned with the aid of a front loader, brushes, flushing water and an industrial vacuum cleaner (Figure 2-5). Occasionally during the mapping of the floor, in-leaking water had to be pumped away.

The 1 m level above the theoretical tunnel floor and tunnel sections every second metre were marked with spray paint on the walls. On the floor, the centre line and 2 m sections were marked by painting. These features were marked out with the assistance of the surveyor.

A number of floodlights were positioned in the tunnel to make the mapping easier (Figure 2-6).

Figure 2-5. *Cleaning the tunnel floor with the help of water and an industrial vacuum cleaner somewhere within section 21–48 m.*

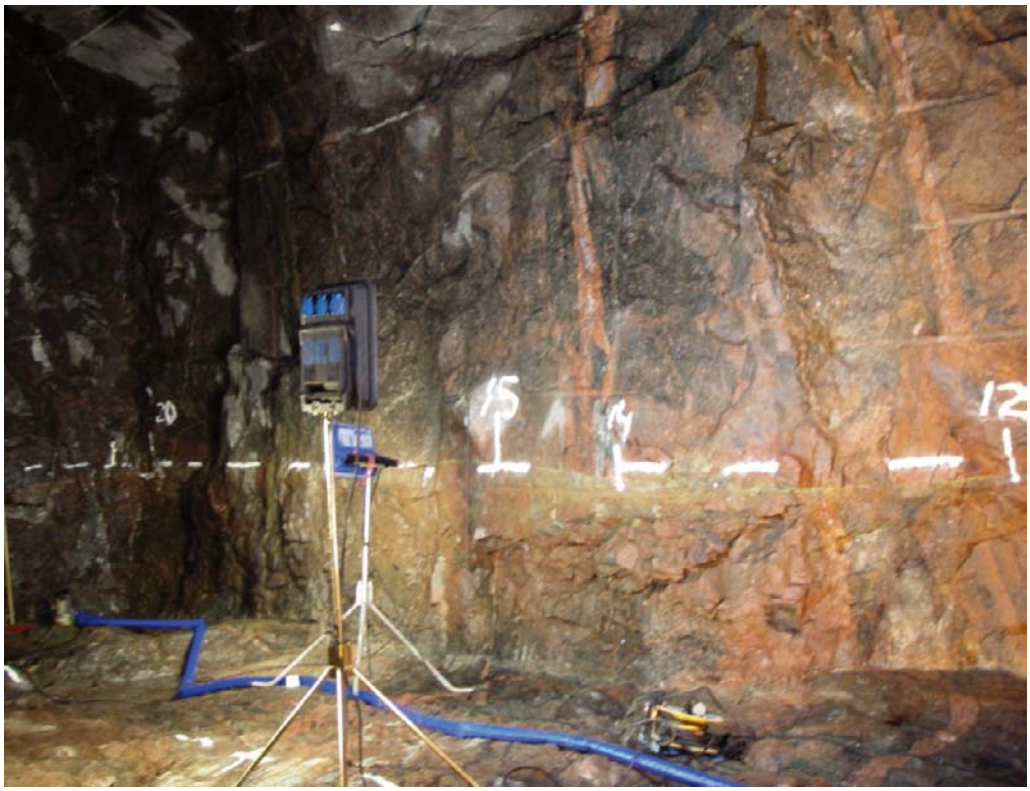

Figure 2-6. *Floodlights illuminating the TASS-tunnel, section 12–20 m. The figure also shows the painted white line marking on a level 1 m above the theoretical tunnel floor and some section markings on the wall. In the lower left-hand part of the figure, part of the painted floor centre line is visible.*

2.3 Mapping occasions

Tunnelling proceeded in six excavation steps, generally consisting of 3–4 rounds (Figure 2-7). Each round comprises drilling, blasting, unloading, scaling and possibly temporary support.

The tunnel faces were mapped after each round, whereas the tunnel walls, roof and floor were mapped on four principal occasions (Table 2-1). The latter mapping occasions are referred to here as stage mapping 1–4. Stage number two was divided into two sub-stages (2a and 2b) where Stage 2a did not include the floor. It was, however, mapped in Stage 2b. After each stage mapping, a number of experiments and tests were performed in the tunnel. These tests comprised grouting with silica sol, hydrogeological experiments/tests, etc (not included in this report, see /Funehag and Emmelin 2010/). During the course of these experiments/tests, the tunnel advance came to a halt.

Before the geological stage mapping started, laser scanning combined with digital photography was performed in the tunnel section concerned.

In Table 2-1, the specified sections are generally based on an average of five points on the tunnel face measured by the surveyor (Figure 2-8).

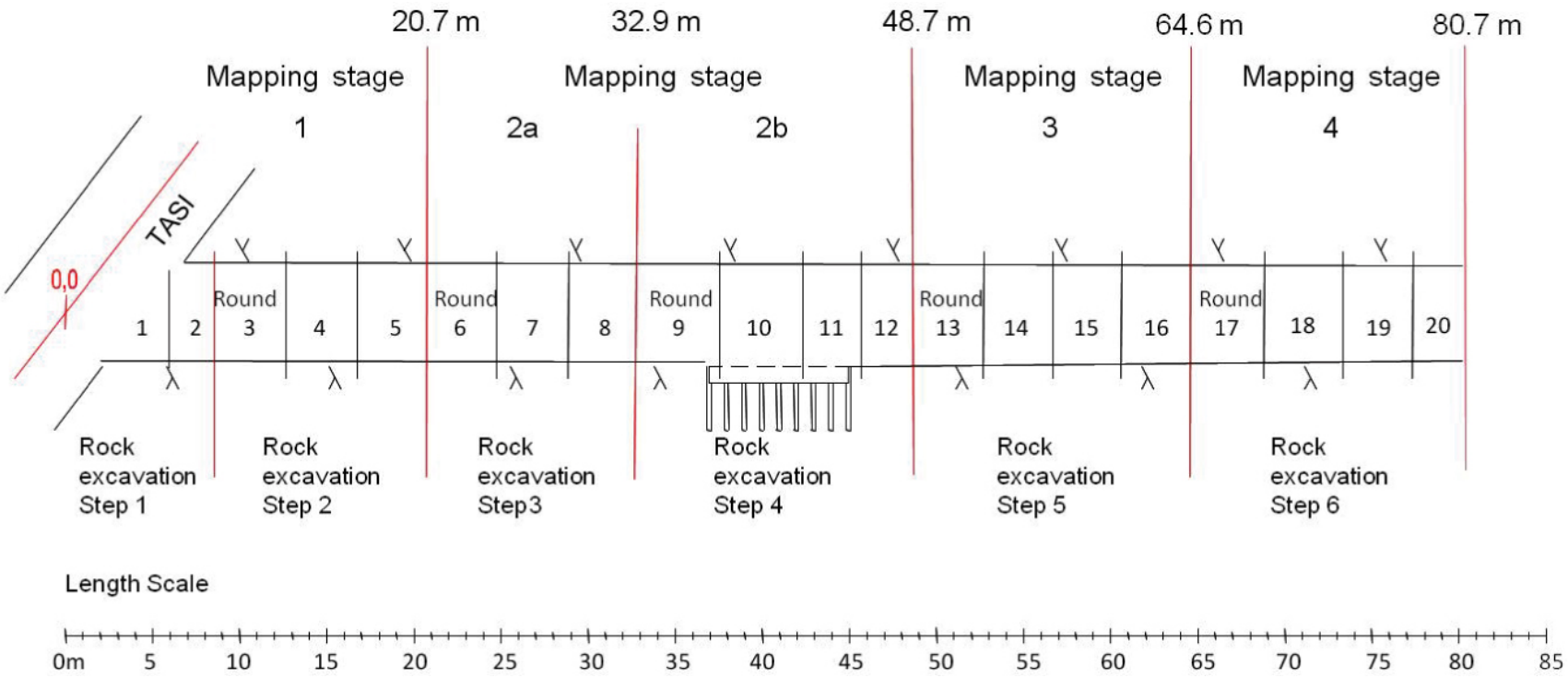

Figure 2-7. *The figure shows how the mapping stages 1–4 are related to the rock excavation steps 1-6 (modified after /Karlzén and Johansson, 2010/).*

Table 2-1. Summary of mapping occasions.

	Mapping Stage 1			Mapping Stage 2a			Mapping Stage 2b			Mapping Stage 3			Mapping Stage 4		
	Tunnel face	Tunnel floor	Tunnel walls & roof	Tunnel face	Tunnel floor	Tunnel walls & roof	Tunnel face	Tunnel floor	Tunnel walls & roof	Tunnel face	Tunnel floor	Tunnel walls & roof	Tunnel face	Tunnel floor	Tunnel walls & roof
Section m	6.1	–	–	24.8	–	–	37.5	–	–	52.7	–	–	68.9	–	–
Date	2007-12-12	–	–	2008-04-17	–	–	2008-06-09	–	–	2008-09-23	–	–	2008-12-05	–	–
Section m	8.7	–	–	28.9	–	–	42.1	–	–	56.8	–	–	73.2	–	–
Date	2007-12-20	–	–	2008-04-22	–	–	2008-06-11	–	–	2008-09-26	–	–	2008-12-09	–	–
Section m	12.8	–	–	32.9	–	20.7–32.9	45.7	–	–	60.6	–	–	77.1	–	–
Date	2008-02-12	–	–	2008-04-25	–	2008-04-28–05-06	2008-06-13	–	–	2008-10-01	–	–	2008-12-12	–	–
Section m	16.9	–	–	–	–	–	48.7	20.7–48.7	32.9–48.7	64.6	48.7–64.6	48.7–64.6	80.7	64.6–80.7	64.6–80.7
Date	2008-02-14	–	–	–	–	–	2008-07-01	2008-06-27–07-08	2008-07-02–07-10	2008-10-14	2008-10-14–10-17	2008-10-20–10-24	2008-12-17	2009-02-03–02-05	2009-02-09–02-23
Section m	20.7	3–20.7	3–20.7	–	–	–	–	–	–	–	–	–	–	–	–
Date	2008-02-21	2008-02-22–02-27	2008-02-27–03-06	–	–	–	–	–	–	–	–	–	–	–	–

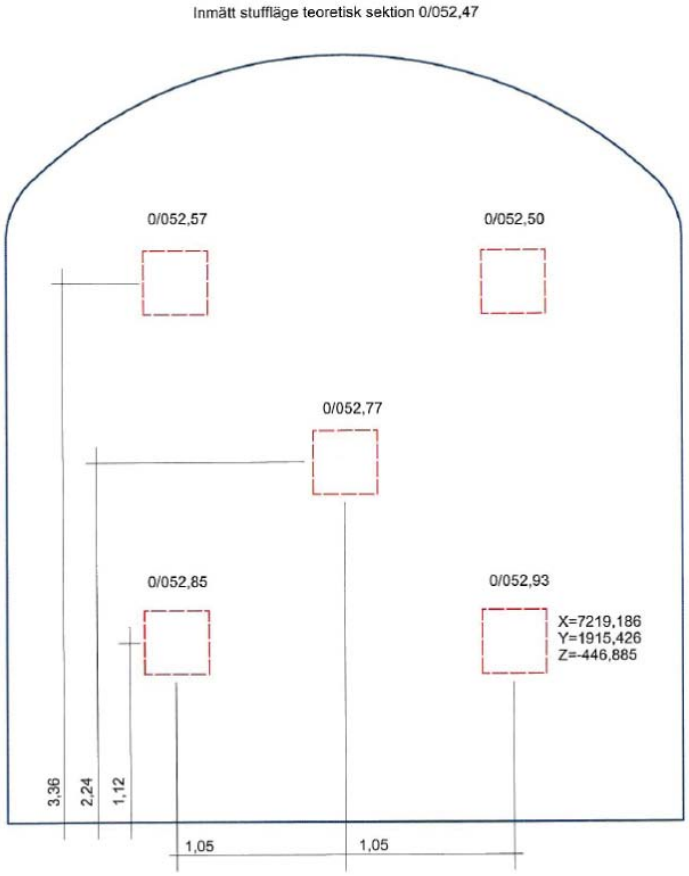

Figure 2-8. *Five points measured by the surveyor G. Johansson at Geocon AB on the tunnel face of the theoretical section 52.47 m. In this example, the average of these points will be 52.72 and will define the true section 52.72 m.*

3 Geological mapping – descriptions and results

3.1 General

To make it easier to interpret and compare the results of the changes in the drill and blast pattern, the rock volume of each mapping stage (Stages 1–4) has been dealt with separately. Section 3.2, dealing with the entire tunnel, will contain the main description of the various geological features as well as a compilation of the mapping results. The sections dealing with the tunnel faces and the mapping stages (including EDZ) respectively will only describe what is specific for these parts of the tunnel.

The mapping is described in the following order:

- rock types
- rock boundaries/contacts
- alteration
- fractures
- deformation zones
- occurrence of water/water leakage
- Rock Mass Rating (RMR).

Figure 3-1 summarises the geological mapping of the TASS-tunnel and shows how the mapping is presented on the TMS dgn-drawing. For a better resolution of the geological features, see Appendices I–VI. Appendices II–V also contain 3D-models of the mapping. In addition to which rock type each rock ID represents in the geological maps, Appendix VII also explains how the rock types are approximately distributed within the sections of the various stages and tunnel faces.

3.1.1 Definition of rock types

The various rock types found on the island of Äspö have earlier been described by, for example, /Kornfält and Wikman 1988, Wikman et al. 1988, Stanfors 1988, Stanfors et al. 1993, Wikman and Kornfält 1995, Rhén et al. 1997/. Common rock type names on the island of Äspö and in the Äspö HRL are Äspö diorite, Ävrö granite, fine-grained granite, pegmatite and undifferentiated mafic rocks (greenstone) that can be considered as the old established Äspö HRL nomenclature.

Following a number of attempts, consensus has been reached to synchronize the rock nomenclature used at Äspö HRL with that used on the mainland by the site investigation team at the tentative site area for the final repository at Oskarshamn. Therefore, the names of certain rock types have changed since mapping of the TASS-tunnel took place. Undifferentiated mafic rock/greenstone will in future be called gabbroid-dioritoid and Ävrö granite will be called Ävrö granodiorite. The “new” Ävrö granite will be a collective name designated undifferentiated Äspö diorite, Ävrö granodiorite and Ävrö quartz-monzodiorite as stated in the internal SKB document, SKB MD 132.004 (see Table 1-1).

The authors of the present report decided, however, to retain the old established Äspö HRL nomenclature because many of the tables and figures in the present report had already been prepared and work had already started on writing the report before the new rock type nomenclature was implemented. Furthermore, the TMS mapping system had not been updated with the new nomenclature when the mapping took place.

Figure 3-2 is a Streckeisen Q-A-P-diagram /Streckeisen 1976, pp 1–33/ in which rock type fields are used for reference purposes when defining the major rock types described below. No analyses have been made of the bedrock in the TASS-tunnel, however. The definitions are thus based on the earlier analyses of the rock types on the island of Äspö, e.g. /Wikman and Kornfält 1995/.

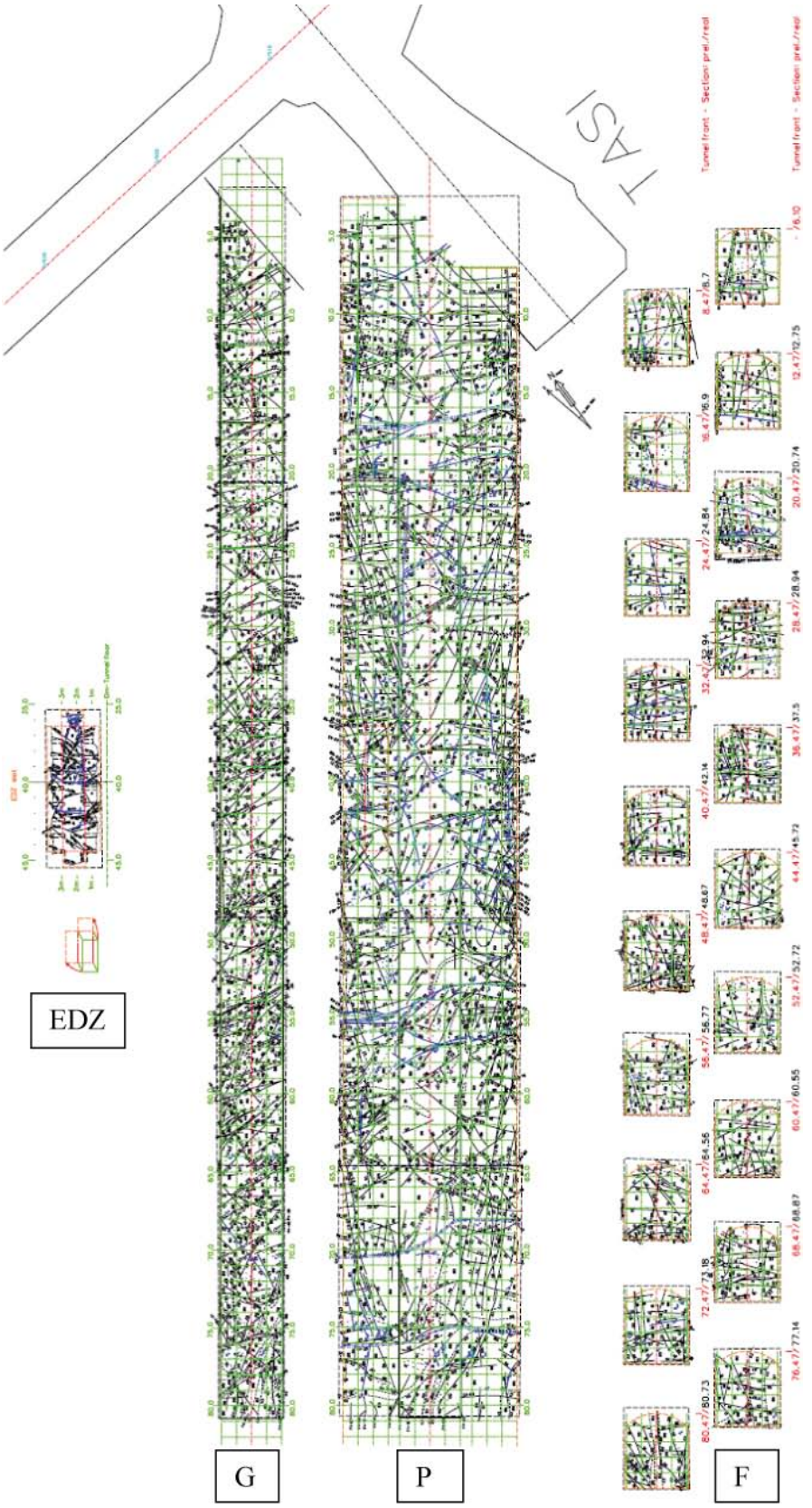

Figure 3-1. *Summary of the geological mapping of the TASS-tunnel as it is presented on the TMS dgn-drawing. EDZ = EDZ-slot, G = floor, P = walls and roof, and F = tunnel face (see Figures 2-3 and 2-4 and, for a better resolution, Appendices I to VI).*

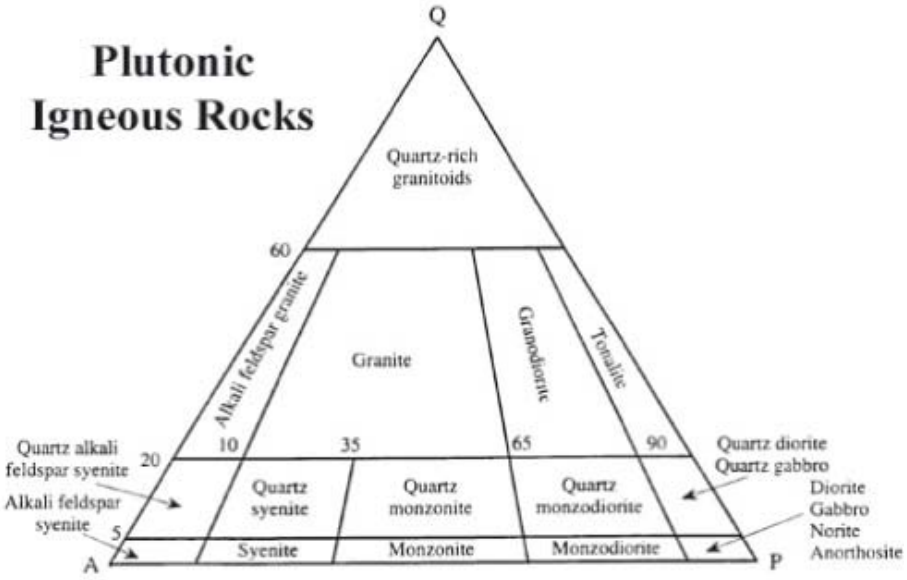

Figure 3-2. *Streckeisen Q-A-P-diagram (Q = Quartz, A = Alkali feldspar and P = Plagioclase).*

3.1.2 Graphical presentation of planar and linear structures

The orientations of planar geological structures, such as fractures, deformation zones and rock boundaries, are presented in equal area stereo nets and rosette diagrams, e.g. /Turner and Weiss 1963, pp 46–75, Hoek and Bray 1996, pp 37–63, Twiss and Moores 1992, pp 20–22/. To plot the structural data, the software Dips v.5.108 from Rocscience Inc. has been used.

The data plotted in the equal area nets have been projected on the lower hemisphere. The Fisher frequency distribution of points on a sphere has been used by the Dips software to calculate the concentrations of the plotted poles /Fisher 1953, pp 295–305, cited in Koch and Link 1980, pp 132–152/. The equal area stereo nets (Schmidt nets) are composed of two major parts: 1) a legend showing the concentration of the poles of the planes as a percentage of 1% of the net area and 2) the diagram itself showing the concentration of the poles as contours with fields of different colours. The mean value of a group of planes can be calculated and are shown in the diagram as 1m, 2m etc, and the mean plane/major plane of each group is shown as a great circle/arc.

The joint rosette diagrams (rose diagrams) consist of the actual diagram and explanations as to the number of fractures that have been plotted, what dips have been allowed and how the diagram is oriented. Here, trend/plunge of the face normal of the diagrams has been set at 0/90, which means that the diagram is represented by a horizontal base plane. In the rosette diagrams, the N-S trend is commonly caused by horizontal structures that have the designated structural orientation 000/00. To avoid this, horizontal to sub-horizontal structures could, of course, have been excluded when the data was plotted.

3.2 The entire tunnel – main geological description and results

This section presents the results of the mapping as well as the main description of the geological features of the entire tunnel: roof, walls, floor, all tunnel faces (6.1–80.7 m) and the EDZ-slot.

3.2.1 Rock types

The bedrock of the TASS-tunnel consists almost entirely of **Äspö diorite** and varieties of it. In addition, there are minor occurrences of **fine-grained granite**, **pegmatite**, **quartz veins/lenses or irregular minor bodies**, **undifferentiated mafic rocks** (formerly called greenstone) and **hybrid rock**. The Ävrö granite that is sometimes found on the island of Äspö and in parts of the Äspö HRL is lacking in the TASS-tunnel.

As has been mentioned before (in Section 2.1 General mapping procedure), rock types appearing as narrow veins and dykes of <0.1 m in width are commonly mapped as fracture filling and are thus not included in the rock type statistics.

The diagrams in Figure 3-3a–d show how the rock type distribution varies when they include the entire tunnel (roof, walls, floor, the last tunnel face and the EDZ-slot, Figure 3-3a), walls and roof (Figure 3-3b), only tunnel floor (Figure 3-3c) and all tunnel faces (from section 6.1–80.7 m, Figure 3-3d) respectively (see also Table 3-1). Figures 3-4 to 3-11 present photos to illustrate certain variations in the rock types and Figure 3-12 shows the occurrence of rock types in the tunnel walls and roof.

Table 3-1. Rock type distribution – the TASS-tunnel (walls, roof, floor, fronts and EDZ-slot).

Rock type	% of mapped area			
	Mapping of side walls & roof P (ca 885 m²)	Mapping of floor G (ca 305 m²)	Mapping of faces F (ca 360 m²)	Total P, G, F (80.7 m) & EDZ (ca 1,235 m²)
Äspö diorite	88.6	67.9	83.8	83.3
Äspö diorite (oxidized)	3.7	18.4	4.5	7.4
Hybrid	3.6	4.8	3.3	3.8
Fine-grained granite	3.3	7.8	7.8	4.6
Pegmatite	0.4	0.8	0.4	0.5
Quartz vein, lens, body	0.1	0.4	0.1	0.2
Mafic rock	0.2	0.0	0.1	0.2
Total	**99.9**	**100.1**	**100.0**	**100.0**

Rock type	Mapped area in m²			
	Mapping of side walls & roof P (ca 885 m²)	Mapping of floor G (ca 305 m²)	Mapping of faces F (ca 360 m²)	Total P, G, F (80.7 m) & EDZ (ca 1,235 m²)
Äspö diorite	784.2	207.0	301.6	1,029.2
Äspö diorite (oxidized)	33.0	56.0	16.2	92.0
Hybrid	32.0	14.7	11.8	47.2
Fine-grained granite	29.4	23.7	28.1	56.6
Pegmatite	3.5	2.5	1.4	6.0
Quartz vein, lens, body	0.9	1.1	0.5	2.0
Mafic rock	2.0	0.0	0.4	2.0
Total	**885.0**	**305.0**	**360.0**	**1,235.0**

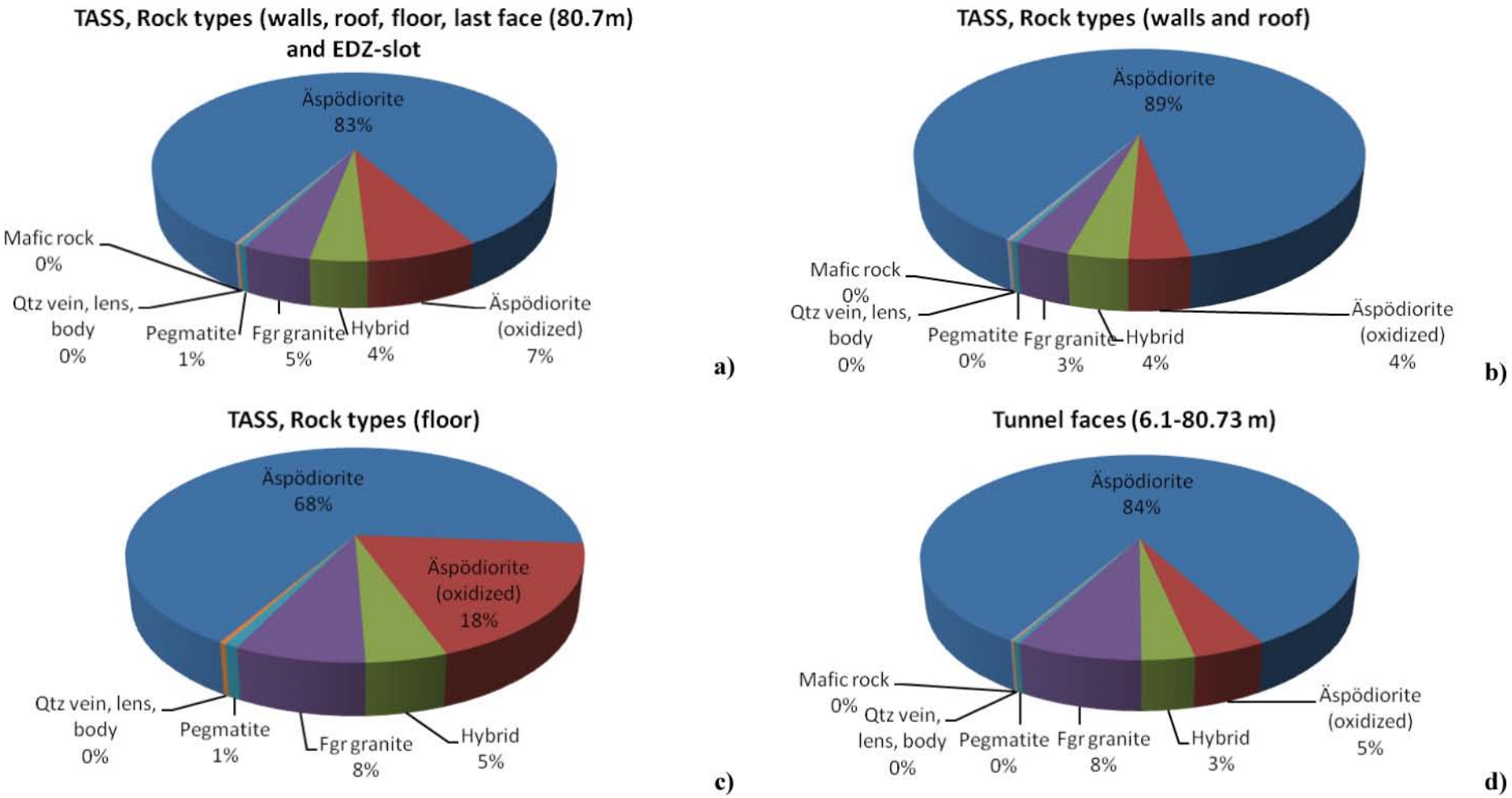

Figure 3-3a–d. *Rock type distribution of the TASS-tunnel (0% in the diagrams means >0 to <1%).* ***a)*** *the entire tunnel (walls, roof, floor and last tunnel face),* ***b)*** *walls and roof of the entire tunnel,* ***c)*** *the entire tunnel floor and* ***d)*** *all tunnel faces.*

Äspö diorite

When plotted in the Streckeisen Q-A-P-diagram (Figure 3-2), the Äspö diorite from other parts of the island of Äspö and Äspö HRL mostly occurs within the quartz-monzodiorite and granodiorite fields. Therefore, in spite of its name, it is not a true diorite. The rock type is commonly grey-dark grey, medium-grained and massive with 5–20 mm large, white-pinkish feldspar megacrysts (Figure 3-4a). Minor inclusions of mafic rocks may occur in the rock mass.

A minor portion of the Äspö diorite is composed of a more or less oxidized reddish variety (Figure 3-4b, cf. Section. 3.2.3 Alteration). Often this variety is related to zones of deformation.

Occurrence in the TASS-tunnel (Figure 3-3a–d and Table 3-1):

- Totally, over 90% of the mapped surfaces of the TASS-tunnel (including the EDZ-slot) consist of fresh and/or oxidized Äspö diorite.
- The fresh non-oxidized Äspö diorite constitutes 83% of the total surface of the roof, walls (including the EDZ-slot), floor and the last tunnel face, whereas the oxidized variety constitutes about 7%.
- Walls and roof are composed of 89% fresh and 4% oxidized Äspö diorite.
- Sixty-eight percent (68%) of the floor consists of fresh Äspö diorite, whereas almost 20% consists of the oxidized type.
- The distribution of the rock types in all tunnel faces shows that 84% are composed of fresh Äspö diorite and 5% of oxidized Äspö diorite.

The rather large percentage of oxidized Äspö diorite in the tunnel floor is due to sub-horizontal to gently dipping fractures or minor deformation zones of a few dm width that occur in the lower part of the tunnel walls and in the floor.

The domination of the various types of Äspö diorite in the TASS-tunnel is clearly demonstrated in Figure 3-12, which summarizes their occurrence in the tunnel walls and roof. Here, some Äspö diorite with the comment hybrid rock is regarded as Äspö diorite, whereas the diagrams in Figure 3-3 treat this variety as hybrid rock.

Fine-grained granite

When fine-grained granites have been plotted in the Streckeisen Q-A-P-diagram (Figure 3-2), they are clustered within the granite field of the diagram. This rock type is reddish-reddish brown-greyish red in colour, mostly massive, even-grained and commonly rather brittle (Figure 3-5a–b and Figure 3-6). The colour may in other parts of the tunnel system of Äspö HRL occasionally be more grey than red. The typical and characteristic fine-grained granite is, as the name indicates, fine-grained but the grain size often varies between very fine-grained, almost aphanitic, to medium-grained. The latter may resemble the equigranular and medium-grained varieties of the Ävrö granite that has also been noted by /Wikman and Kornfält 1995/.

Occasionally the rock is not massive but foliated and more or less sheared. This is demonstrated in, for example, the end section of the TASS-tunnel, where both varieties appear (Figures 3-5a and 3-6).

The fine-grained granite appears as veins, dykes and/or irregular bodies in the dominating rock mass of Äspö diorite (Figure 3-5a–b). Thin veins or dykes of fine-grained granite have been recorded as fracture filling. The dykes may often have pegmatitic boundaries. Sometimes the fine-grained granite even grades into pegmatite.

Occurrence in the TASS-tunnel (Figure 3-3a–d and Table 3-1):

- When all mapped surfaces of the TASS-tunnel are taken into account, the fine-grained granite constitutes about 5% of all rock types.
- Roof and walls consists to about 3% of fine-grained granite.
- The fine-grained granite constitutes about 8% of the tunnel floor and all tunnel faces respectively.

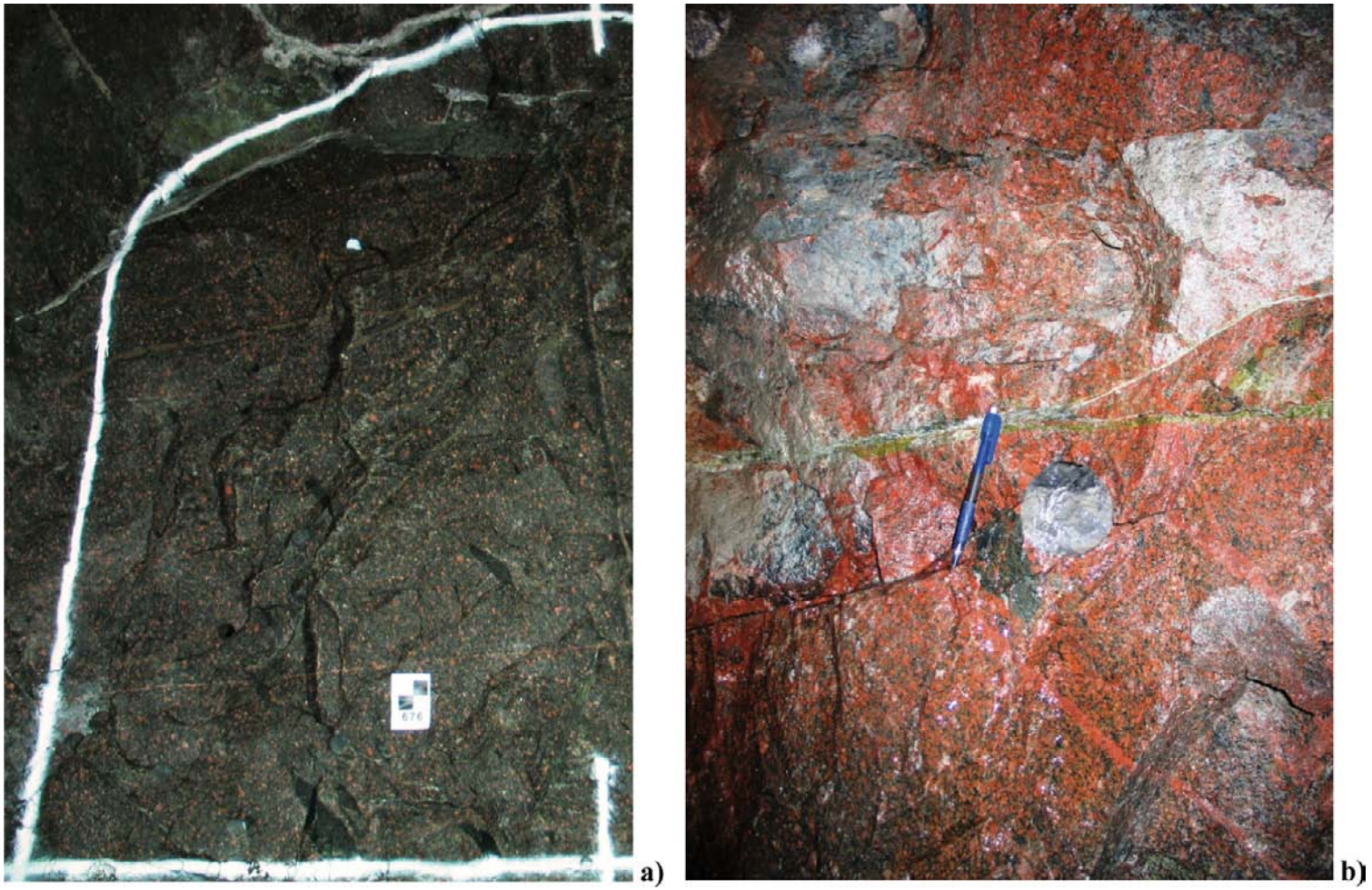

Figure 3-4a–b. *Äspö diorite.* ***a)*** *Upper left half of the tunnel face at section 64.56 m. Fresh Äspö diorite.* ***b)*** *Part of the tunnel face at section 6.6 m. Red, oxidized Äspö diorite surrounding epidote-filled fracture.*

a)

b)

Figure 3-5a–b. *Fine-grained granite.* ***a)*** *Right (NW) tunnel wall, section 78–80 m. Reddish fine-grained granite dyke.* ***b)*** *Tunnel floor, right (NW) side, section 8–9 m. Reddish fine-medium grained granite cross cutting reddish grey Äspö diorite, partly a hybrid.*

Figure 3-6. *Tunnel face at section 80.7 m. Part of fine-medium grained, red to pinkish granite, partly schistose dyke (see Appendix 1 B).*

Pegmatite

In the TASS-tunnel, pegmatite mostly appears as 0.1–0.3 m wide dykes (Figure 3-7a). A few observations of minor irregular bodies have, however, also been recorded (Figure 3-7b). They are medium- to coarse-grained and red to pinkish in colour. A few occurrences of pegmatite bordering fine-grained granite dykes have also been observed. A number of narrow pegmatite veins have been recorded as fracture filling. As mentioned above, pegmatite and fine-grained granite may grade into each other.

Occurrence in the TASS-tunnel (Figure 3-3a–b and Table 3-1):

- When all mapped surfaces of the TASS-tunnel are taken into account, pegmatite constitutes about 0.5% of all rock types.
- In walls and roof, and all tunnel faces respectively, pegmatite constitutes 0.4% of the rock.
- The floor is composed of 0.8% pegmatite.

Quartz veins/lenses and bodies

Quartz occurs as 0.05–0.1 m wide veins or lenses cross cutting the rock mass (Figure 3-8a–b) and as irregular minor bodies. Some of the occurrences show a diffuse lamination parallel to sub-parallel to the boundary of the vein/lens (Figure 3-9). At least some of the veins/lenses or bodies belong to the youngest rock types in the tunnel. Even pegmatites have been cut by quartz veins/lenses (Figure 3-8a and Figure 3-9). As in the case of pegmatite, thin veins of quartz have been recorded as fracture filling. Some of the recorded veins, recorded as rock type, could just as well have been regarded as fracture fillings.

The occurrence of quartz veins, lenses or bodies in the TASS-tunnel (Figure 3-3a–b and Table 3-1) is as follows:

- 0.2% when all mapped surfaces of the TASS-tunnel are taken into account.
- 0.1% for the walls and roof and all tunnel faces respectively.
- 0.4% of the floor.

Mafic rock – undifferentiated

This rock type, as the name indicates, is a collective name for all mafic rocks at Äspö HRL. Previously, the name greenstone was used but was changed to the present name some years ago. It will soon be changed again, and this time to gabbroid-dioritoid in accordance with the attempt to synchronize the Äspö HRL rock nomenclature with the site investigations in the Laxemar-Simpevarp area. The undifferentiated mafic rocks are normally greenish black to black, fine- to medium-grained and massive. In the TASS-tunnel they are not very common but appear occasionally as small irregular bodies and mappable xenoliths (Figure 3-10a–b). Minor xenoliths are regarded as a natural part of the Äspö diorite. When plotted in the Streckeisen Q-A-P-diagram (Figure 3-2), the undifferentiated mafic rock will mostly gather in the lower right-hand corner of the diagram within the quartz gabbro/diorite and the gabbro/diorite fields.

Occurrence in the TASS-tunnel (Figure 3-3a–b and Table 3-1):

- The occurrence of mafic rocks in the TASS-tunnel is even less than that of pegmatite and quartz, particularly when the number of occurrences is considered. Only 0.2% of all the mapped tunnel surfaces contain mafic rocks.
- When the walls and roof are considered, 0.2% of the exposed surfaces are made up of mafic rocks.
- The tunnel faces altogether contain only 0.1% of mafic rocks.
- No mafic rock has been recorded in the floor of the tunnel.

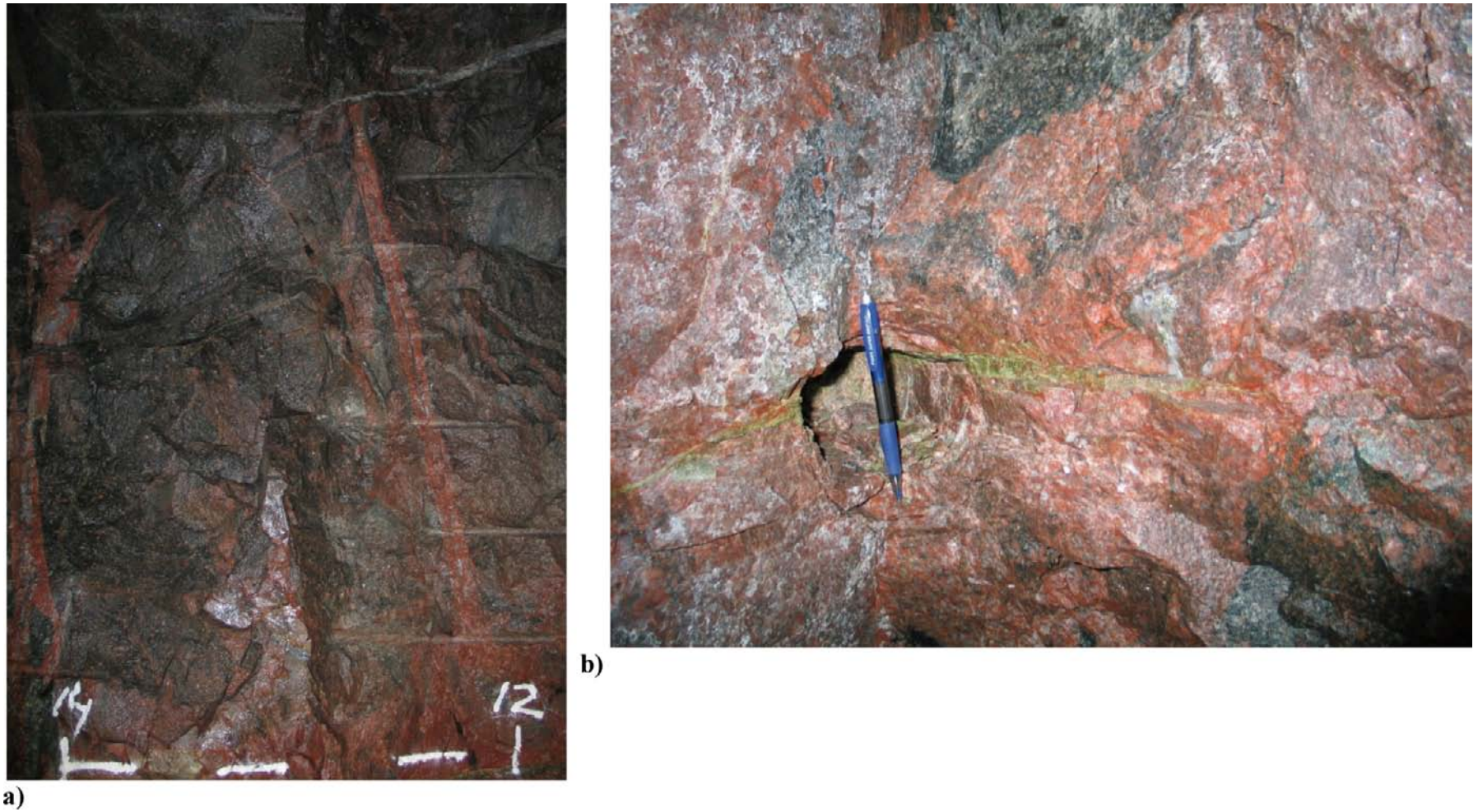

Figure 3-7a–b. *Pegmatite.* ***a)*** *Right (NW) tunnel wall, section 12–14 m. Reddish pegmatite dykes partly with quartz clustered in the middle. The surrounding rock is more or less oxidized and granitized, reddish grey Äspö diorite with diffuse boundaries to fresh Äspö diorite (greyish)* ***b)*** *Tunnel face at section 28.94 m. Irregular small reddish pegmatite body cut by an epidote-filled fracture.*

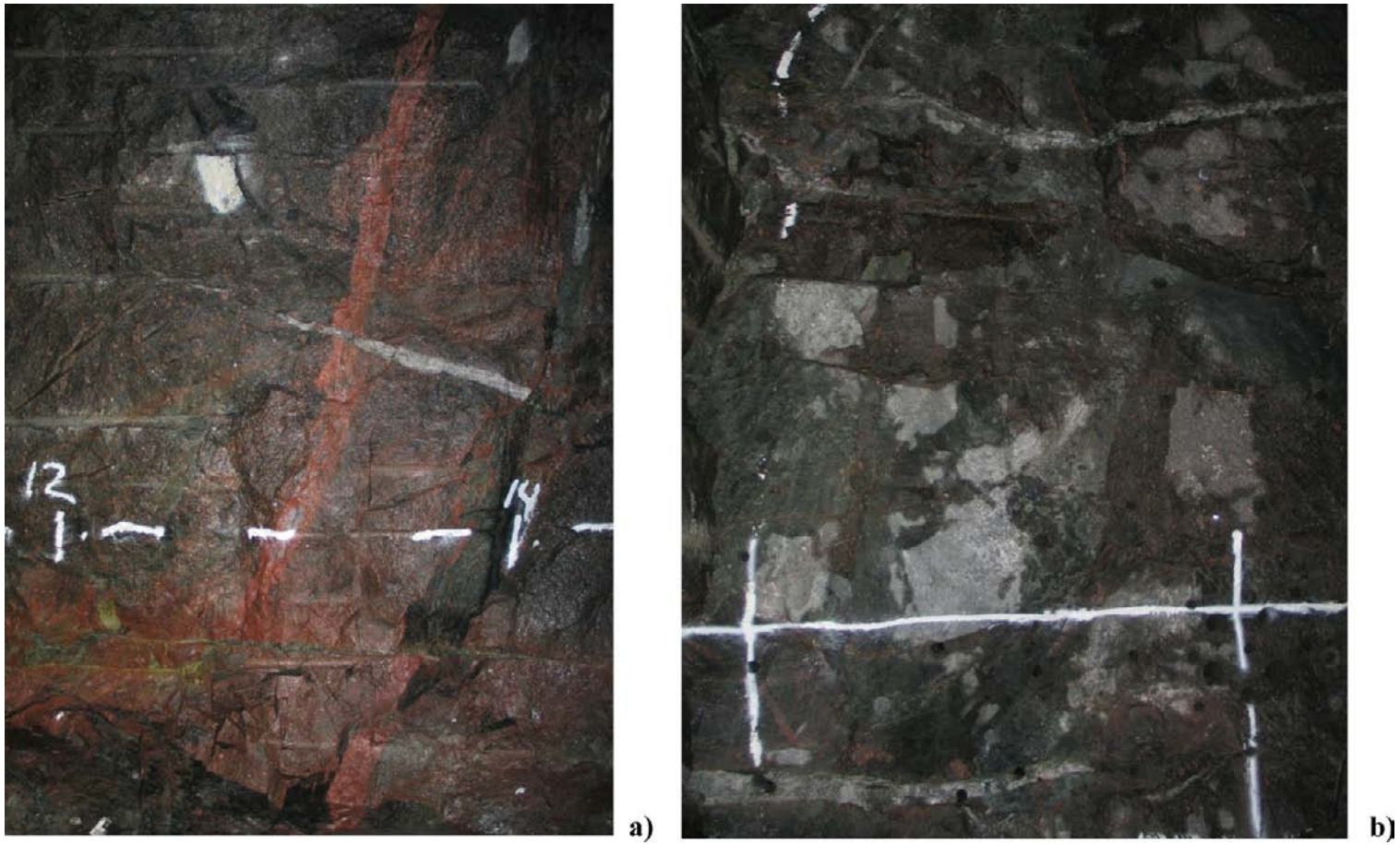

Figure 3-8a–b. *Whitish quartz veins/lenses.* ***a)*** *Left (SE) tunnel wall, section 12–14 m. Slightly laminated or banded quartz lens/vein cross cutting a pegmatite dyke (see also Figure 3-9). The pegmatite dyke has been displaced (lower part of the picture). The surrounding rock is more or less oxidized and granitized, reddish grey Äspö diorite.* ***b)*** *Tunnel face at section 56.77 m. Whitish quartz veins/lenses in the upper and lower parts of the picture.*

Figure 3-9. *Left (SE) tunnel wall, section 13–14 m. Slightly laminated <0.1 m wide quartz vein/lens cross cutting a pegmatite dyke (see Figure 3-8a). Along parts of the boundary, small dark tourmaline crystals can be found.*

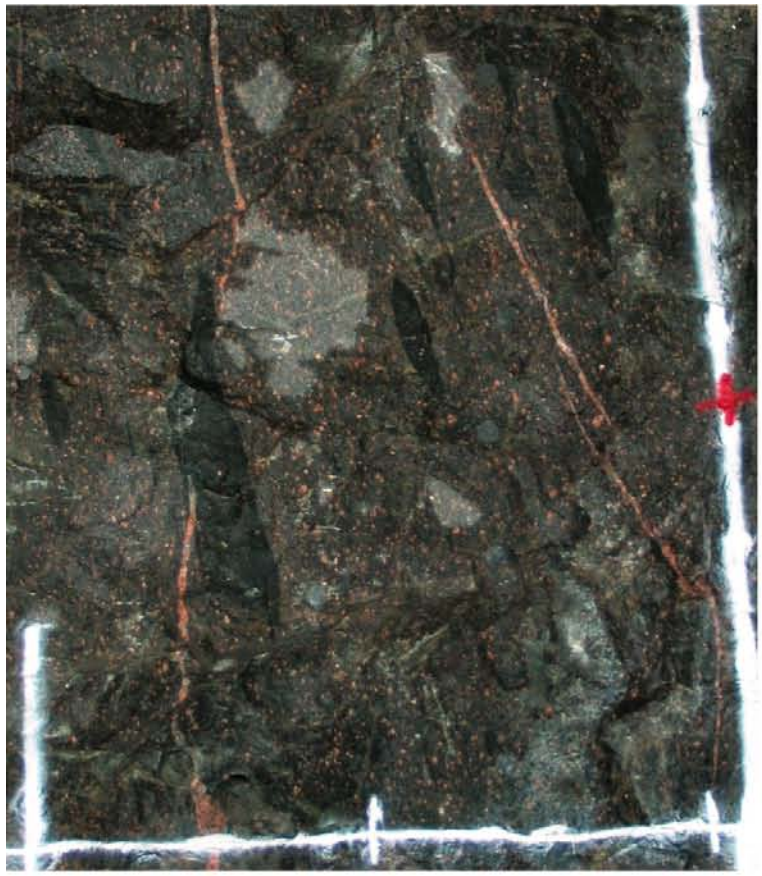

a)

b)

Figure 3-10a–b. *Mafic undifferentiated rock.* ***a)*** *Right-hand side of tunnel face at section 45.72 m. Dark grey-black, lens-shaped xenoliths of fine-medium grained undifferentiated mafic rock in ordinary Äspö diorite. The picture also shows narrow pinkish pegmatite veins/dykes mapped as fracture filling.* ***b)*** *Right (NW) tunnel wall, section 62–64 m. Just above the white line marking 1 m above the theoretical tunnel floor, a small irregular body of undifferentiated mafic rock in ordinary Äspö diorite.*

Hybrid rock

This is a collective name for bedrock that is mostly a mixture of Äspö diorite and fine-grained granite, but also more or less granitic varieties of what may originally have been Äspö diorite. Sometimes, the mapped rock type, however, has been given the name of the type that clearly dominates, often with the comment hybrid rock. In Table 3-1, all rock with the comment hybrid rock has been referred to as hybrid rock. The colour varies between reddish grey and greyish red, mostly depending on the degree of oxidation. The grain size varies between fine and medium, and structurally the rock is massive/irregular (mixture of textures and/or structures), sometimes diffusely laminated or banded Figure 3-11a–b). Mostly, the hybrid rock has diffuse boundaries to the surrounding rock types.

Occurrence in the TASS-tunnel (Figure 3-3a–b and Table 3-1):

There is very little difference in the occurrence of hybrid rock if all tunnel surfaces are considered, only walls and roof, only tunnel faces or only the floor.

- If all mapped rock surfaces are considered, hybrid rock constitutes 3.8% of the rock mass.
- Walls and roof show almost the same figure, i.e. 3.6%.
- 4.8% of the floor is composed of hybrid rock.
- Hybrid rock makes up 3.3% of the overall tunnel faces.

3.2.2 Rock boundaries/contacts

SKB defines the rock boundaries/contacts as being either diffuse or sharp. Sharp boundaries are sub-divided into open (with aperture) and tight (closed; no aperture).

Approximately 70% of the recorded rock boundaries are sharp and tight (closed) and about 30% are diffuse. The latter mostly represent the contacts between fresh Äspö diorite and oxidized Äspö diorite or hybrid rock. (Figures 3-7a, 3-8a and 3-11b). The contacts between fine-grained granite or pegmatite respectively and Äspö diorite are commonly tight and sharp (e.g. Figure 3-5a).

The orientation of the rock boundaries is often irregular. Those between fine-grained granite, pegmatite and quartz veins/lenses and surrounding rock could, however, often be measured. The diagrams in Figures 3-13, 3-14 and 3-15 show that the majority of the fine-grained granite contacts are oriented approximately northeast-southwest (066/87), while the pegmatite contacts are northwest-southeast (288/80) and finally the quartz veins/lenses have a more east-westerly orientation (091/24). In other words, the fine-grained granites are sub-vertical with some variation in strike (subordinate strike/dip: 200/74), the pegmatites are also sub-vertical but with less variation in strike. The quartz veins/lenses differ from these two with their relatively gentle dip.

a)

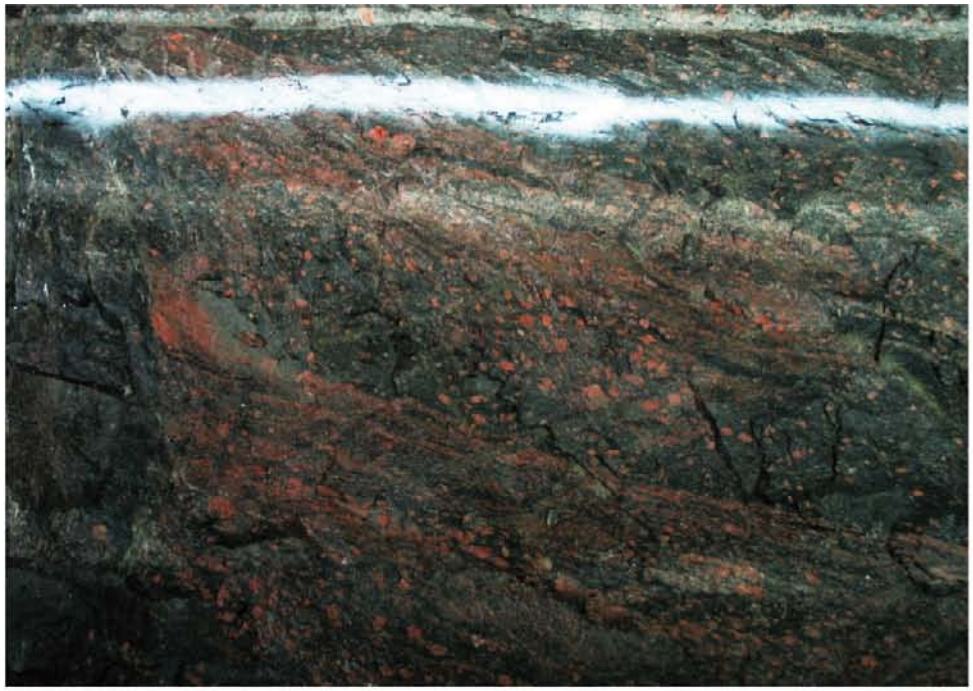

b)

Figure 3-11a–b. *Reddish to reddish grey varieties of hybrid rock.* ***a)*** *Lower part of right-hand (NW) tunnel wall and floor, section 77–79 m. Massive/irregular, partly foliated fine-medium grained reddish hybrid rock.* ***b)*** *Tunnel floor, section 74–75.5 m. Massive, partly laminated and/or banded and porphyritic, medium-grained reddish hybrid rock with diffuse boundaries to the surrounding ordinary Äspö diorite.*

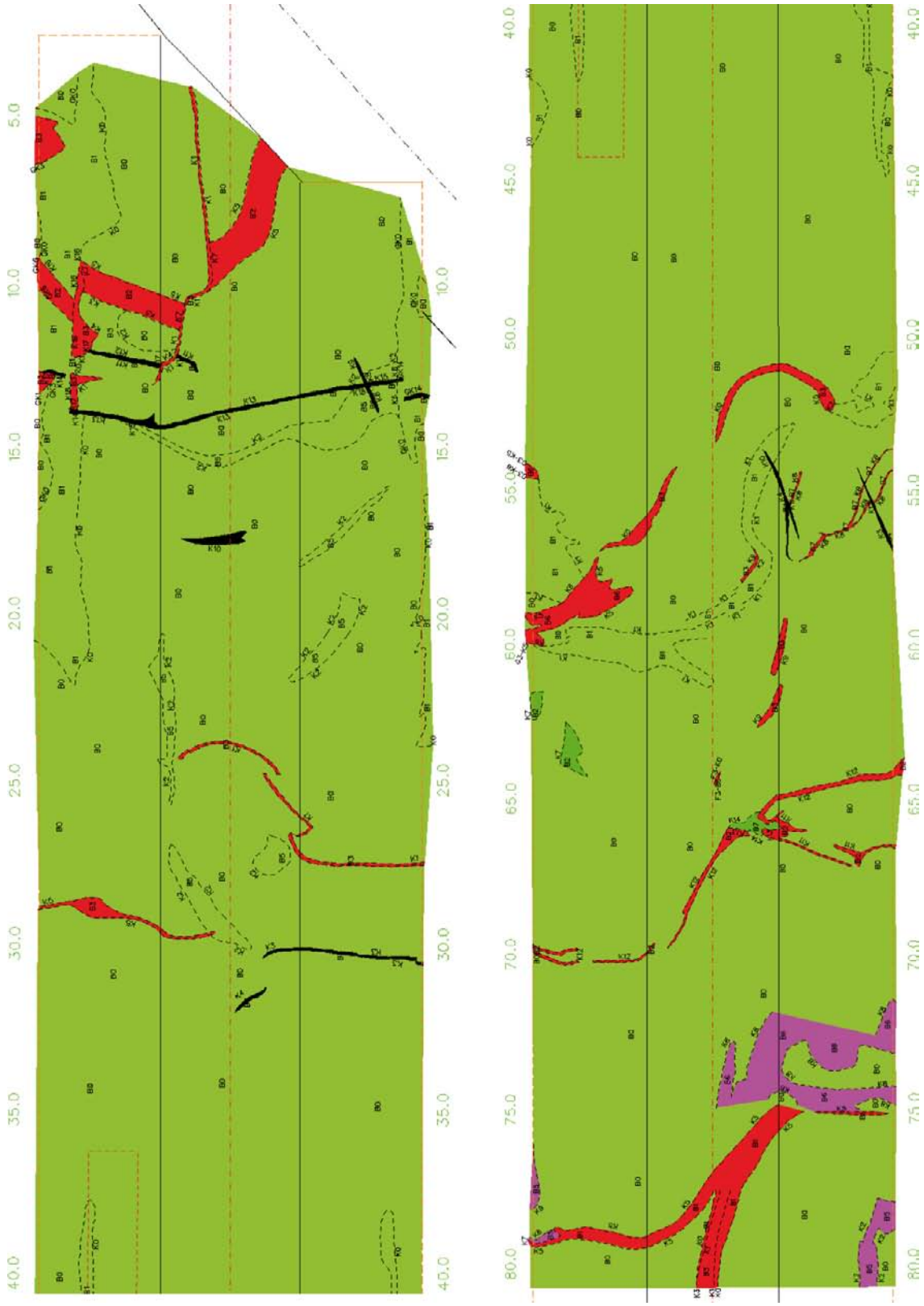

Figure 3-12. *Appearance and summary of rock types in the walls and roof of the TASS-tunnel. Green = Äspö diorite (various varieties), Dark green = Undifferentiated mafic rock (greenstone), Red = Fine-grained granite, Black = Pegmatite and/or quartz veins/lenses, Purple-violet red = Hybrid rock. Dashed black lines = rock boundaries. Note that Äspö diorite includes not only fresh and "normal" Äspö diorite but also hybrid and/or oxidized varieties of Äspö diorite. (Drawing compiled 2010 from TMS-drawing.)*

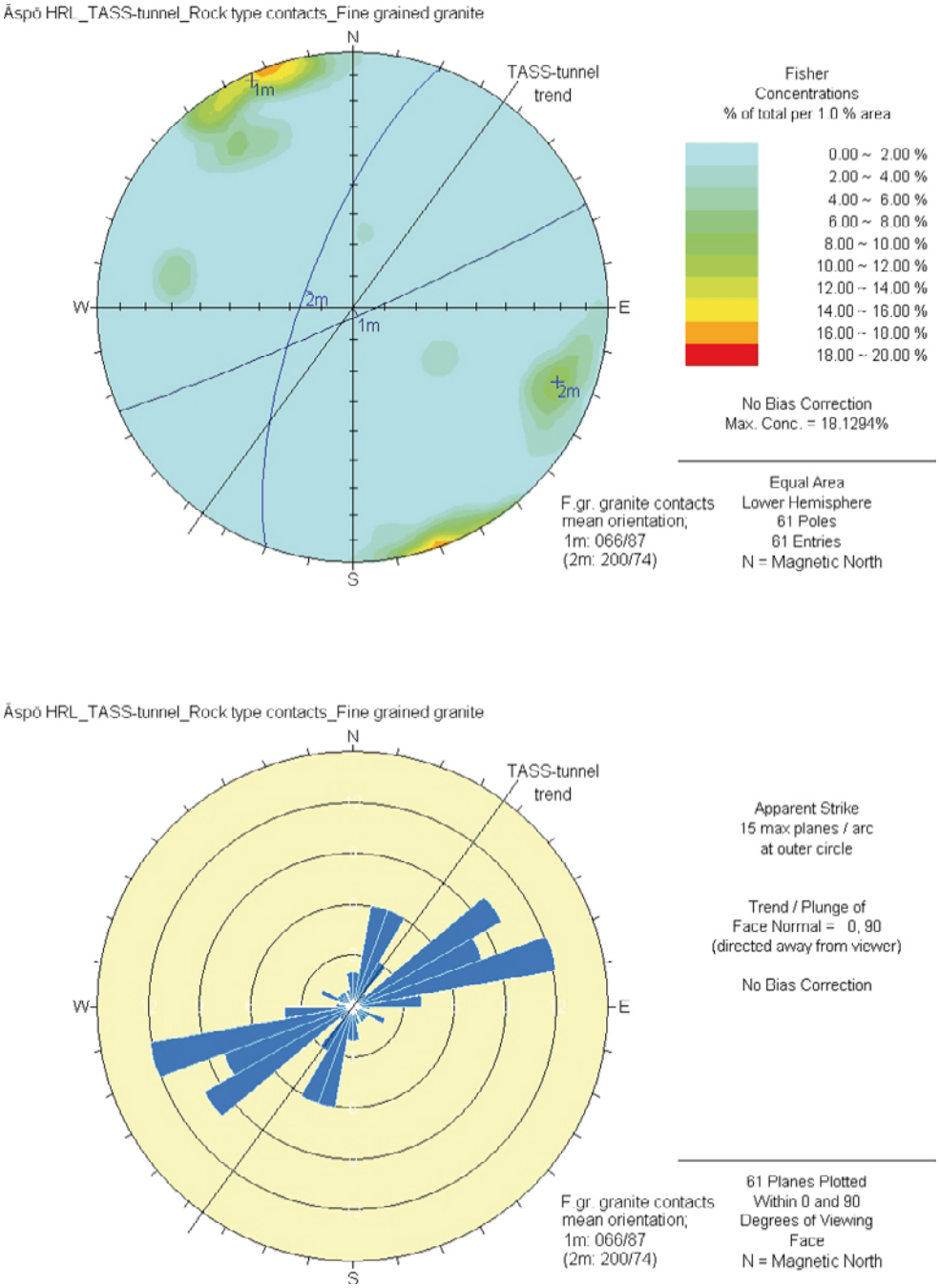

Figure 3-13. *Orientation of fine-grained (F.gr.) granite contacts in the TASS-tunnel presented in Schmidt equal area net (top) and joint rosette diagrams (bottom). Two major contact orientations can be distinguished particularly in the stereo diagram; 1m:066/87 and 2m:200/74. The trend of the TASS-tunnel is marked as a straight black line. N refers to magnetic north.*

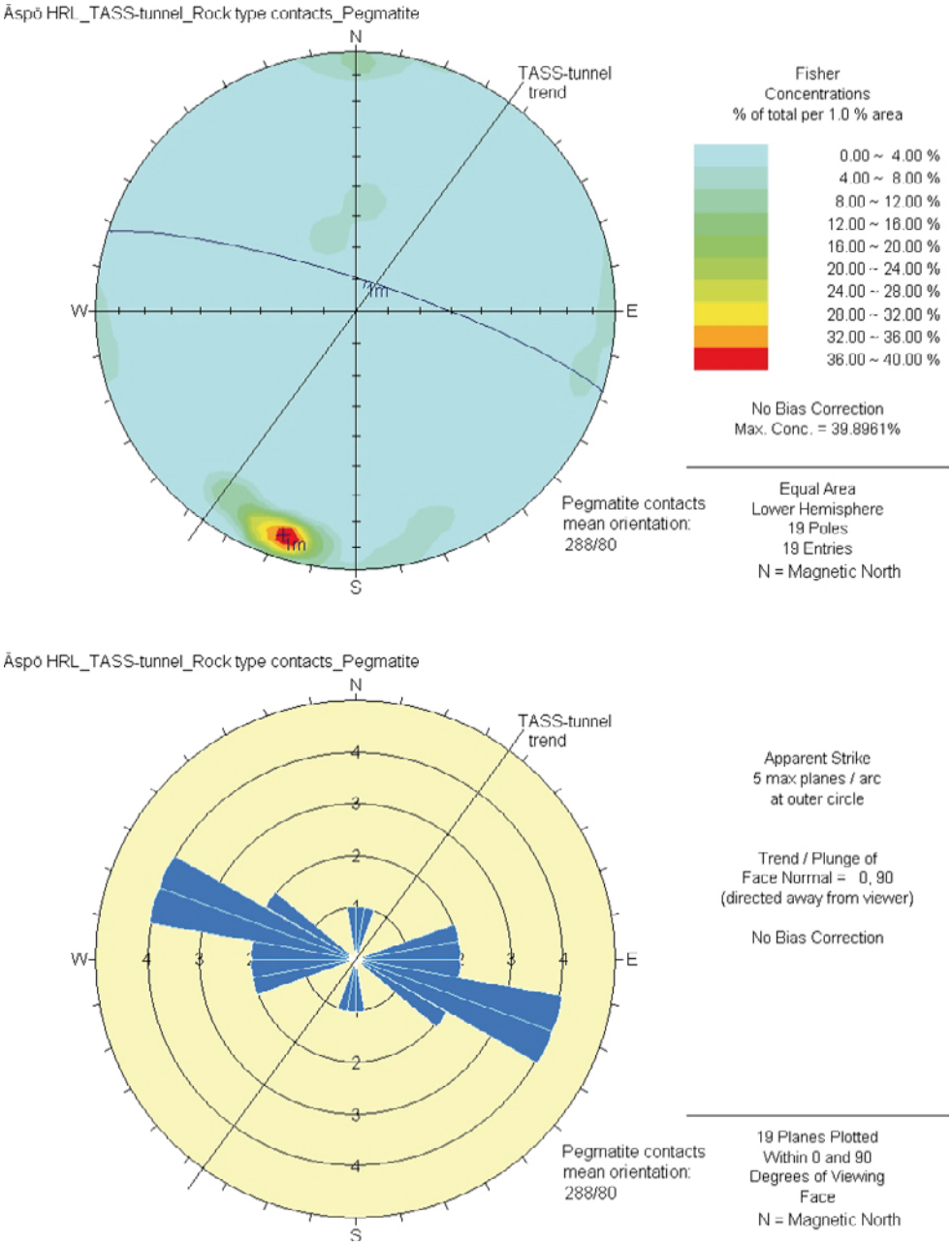

Figure 3-14. *Orientation of pegmatite contacts in the TASS-tunnel presented in Schmidt equal area net (top) and joint rosette diagrams (bottom). The trend of the TASS-tunnel is marked as a straight black line. N refers to magnetic north.*

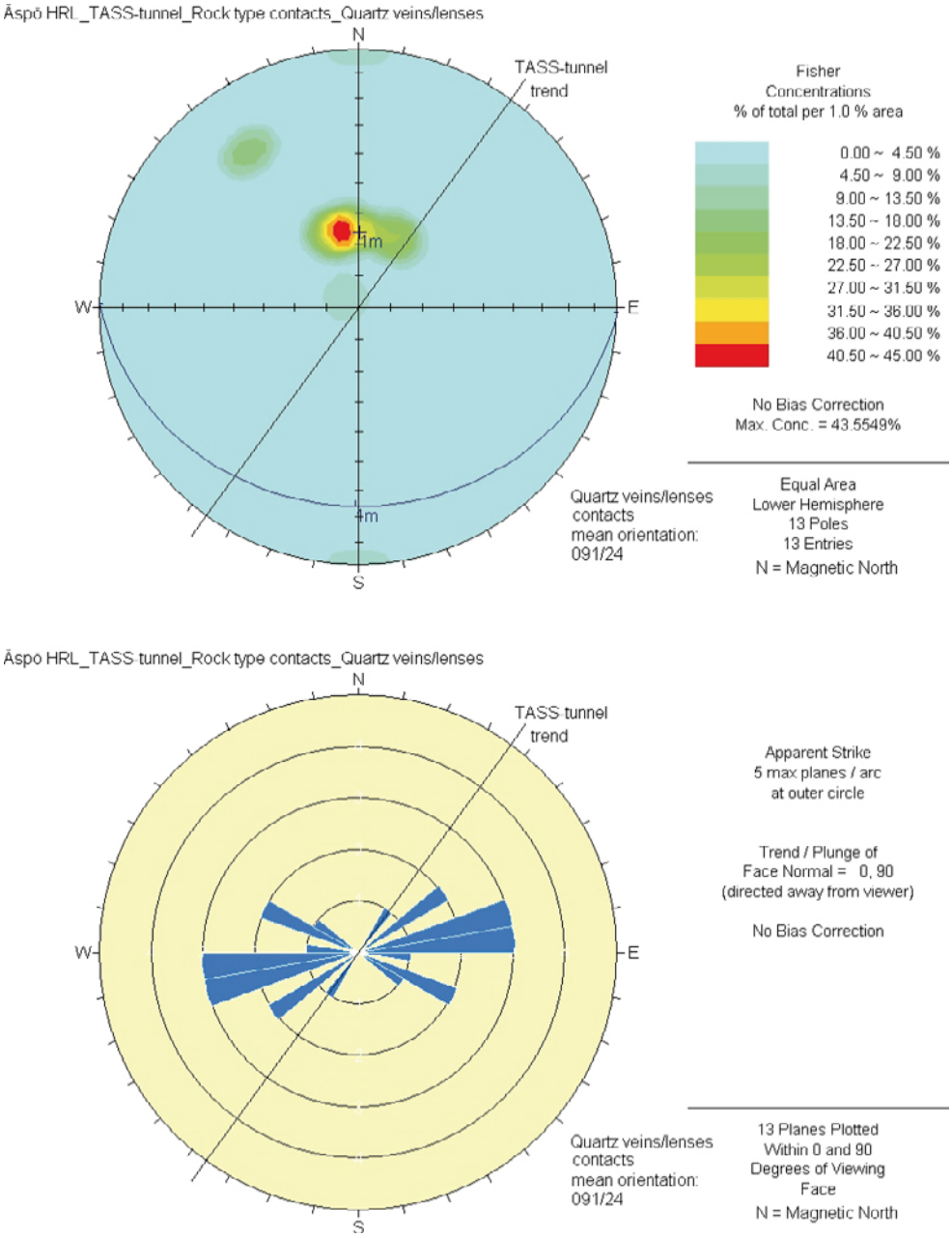

Figure 3-15. *Orientation of quartz vein/dyke contacts in the TASS-tunnel presented in Schmidt equal area net (top) and joint rosette diagrams (bottom). The trend of the TASS-tunnel is marked as a straight black line. N refers to magnetic north.*

3.2.3 Alteration

SKB's TMS mapping system uses five weathering/alteration classes based on those described by /ISRM 1977, pp 319–368/. The classes used are: none (fresh rock), weak, medium, strong and complete (totally disintegrated rock). Sometimes, however, there is a tendency to specify a higher degree of weathering/alteration than would otherwise have been the case if ISRM's nomenclature had been followed strictly.

Most of the bedrock found in the TASS-tunnel has been regarded as fresh. A minor portion of the rocks has, however, been recorded as being slightly weathered/altered. In this case, the rock has been stained more or less red due to various degrees of oxidation (cf. Section. 3.2.1 Rock types – Äspö diorite). The strength of the rock mass has probably only been affected to a minor degree or not at all.

The reddish staining is mostly visible in some of the Äspö diorite (about 7% of the rock mass, Figure 3-3a and 3-4b) but also in some of the fine-grained granite (<0.5% of the rock mass) and hybrid rock (<0.01% of the rock mass). Fine-grained granite and hybrid rock constitute about 5% and 0.1% respectively of the oxidized rock. Since the oxidized fine-grained granite and hybrid rock make up only such a small percentage of the rock mass, the diagrams in Figure 3-3 can be used to illustrate the distribution of altered/oxidized rock.

The oxidized rock is commonly related to larger sub-horizontal to gently dipping fractures. These fractures in turn very often include a network of minor epidote and/or prehnite healed fractures (Figure 3-16 and 3-17). Due to these sub-horizontal to gently dipping fractures that commonly appear in the lower parts of the TASS-tunnel, there is a rather large percentage of oxidized rock (almost 20% of all rock) exposed in the floor (Figure 3-3c).

Figure 3-16. *Front, section 12.75 m, right-hand side. Sub-horizontal, epidote/prehnite-healed fracture, partly fracture network in oxidized rock, mostly Äspö diorite. Upper left-hand corner, some smooth joints.*

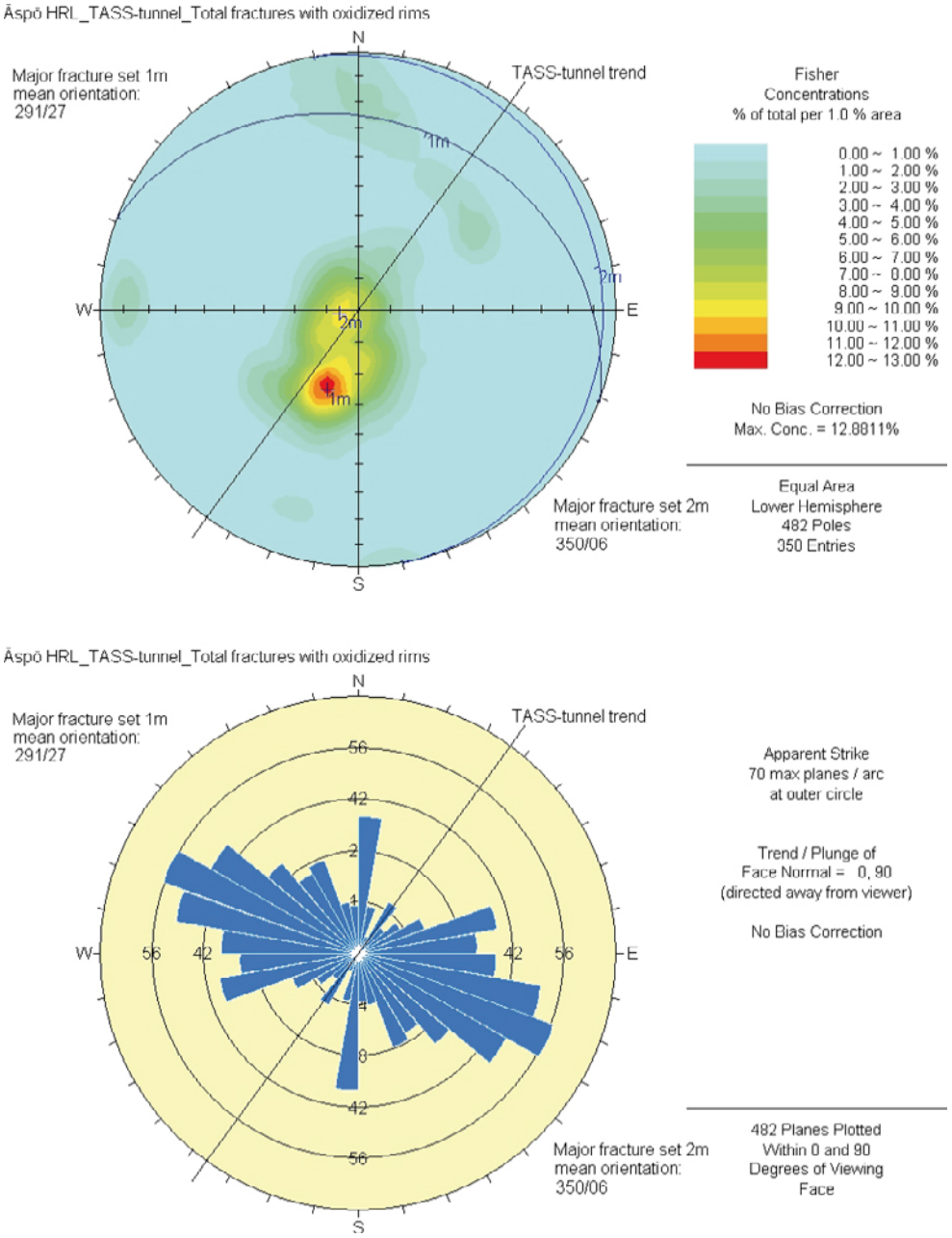

Figure 3-17. *Orientation of fractures showing oxidized rims in the TASS-tunnel presented in Schmidt equal area net (top) and joint rosette diagrams (bottom). The trend of the TASS-tunnel (216 degrees) is marked as a straight black line. The north-south striking trend on the rosette diagram is mainly caused by horizontal fractures that have the designated structural orientation 000/00. N refers to magnetic north.*

3.2.4 Fractures

The distribution of fractures can be seen in Figure 3-1, and in more detail in Appendices I to VI. Appendix I (mapping of faces), Appendices II A, III A, III B, IV A and V A (mapping of walls and roof), Appendices II B, III C, IV B and V B (mapping of floors), and Appendix VI (mapping of EDZ). Figures 3-18 to 3-39 illustrate certain varieties in fractures, fracture orientation, fracture distribution, displacements along fractures etc.

Fracture orientations are presented in Schmidt nets and joint rosette diagrams in Figures 3-24, 3-27 to 3-30 and 3-38 as well as in Appendices VIII and IX. No adjustments have been made for the orientation of the mapped surfaces in the diagrams. Nor has the compass readings been corrected for magnetic declination.

The fractures are recorded as open (truly open natural fractures), tight (sealed/healed natural fractures), re-opened (natural, formerly healed fracture, which are now more or less open due to e.g. blasting) and induced open (induced/mechanically-made fracture which is open due to e.g. blasting). These parameters are referred to as “type” in the TMS code list (SKBdoc 1252025, internal SKB document, see Table 1-1). Normally, only the trace of the fractures is visible on the rock surfaces. When excavating the tunnel, some fracture surfaces have occasionally been exposed (smooth joints) that commonly affect the tunnel geometry (Figure 3-18).

All fractures have a width (aperture + fracture filling), but only open and re-opened fractures have aperture (Figure 2-1, see also the TMS code list SKBdoc 1252025, internal SKB document, Table 1-1). The width and aperture (where present) are measured when possible and estimated when less than 1 mm.

Sometimes, the host rock has alteration rims along the fractures. Fracture borders that have a red colouring are recorded as oxidized zones/rims and measured across the fracture (width + oxidation rim), see Figures 2-1 and 3-19. Occasionally, however, the host rock close to the fractures has a lighter colour than that normal for the rock type in question (Figure 3-20). This may be similar to the situation described by /Mancktelow and Pennacchioni 2005, pp 645–661/. The light colour may be due to depletion, where certain components such as Fe and Mg have migrated away from the host rock. Sometimes these components may have moved towards the fracture to form fracture filling materials such as chlorite (Figure 3-20a) and epidote.

Width and type

Eight fractures were mapped with 0 mm width, six of which are fractures with no data and two are fractures with only a thin oxidation rim, see Table 3-2 and Figure 3-21. Fractures with widths of less than 2 mm dominate (almost 60% of all fractures). Most fractures, however, have no apertures. Where an aperture exists, it is mostly less than 1 mm in width (about 40% of all fractures). Most fractures (about 75%) have no alteration rim (mostly oxidation).

The distribution of fracture types is demonstrated in Table 3-3 and in Figure 3-22. The dominating fracture types are tight (55%) and re-opened (42%).

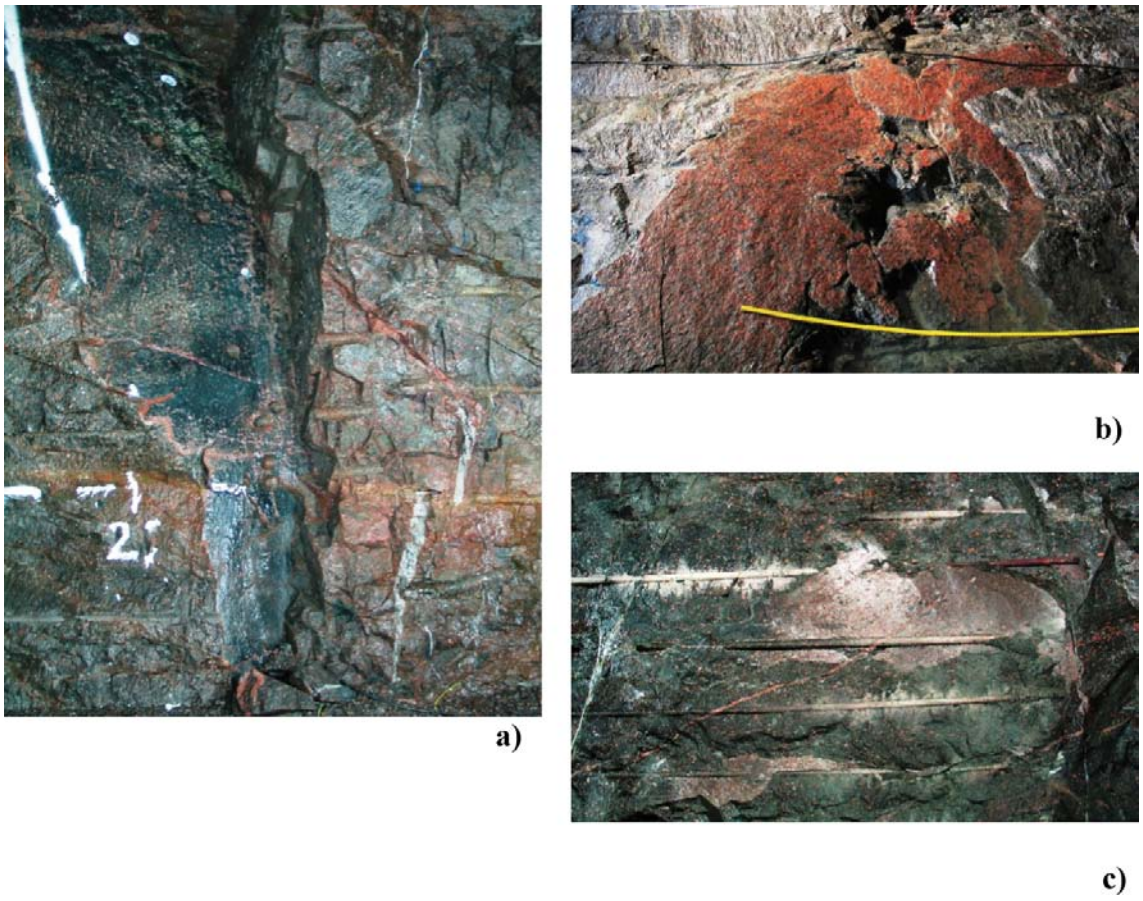

Figure 3-18a–c. *Exposed fracture surfaces (smooth joints).* ***a)*** *Right-hand wall, around section 21 m (fracture P2a-24, see Appendix III A). The picture also shows an oxidized, sub-horizontal fracture (fracture F-03, see Appendix I) that has displaced a quartz vein/dyke (fracture G2-77).* ***b)*** *Floor, around section 29 m (fracture G2-34, see Appendix III C).* ***c)*** *Roof, around section 55 m (fracture P3-132, see Appendix IV A).*

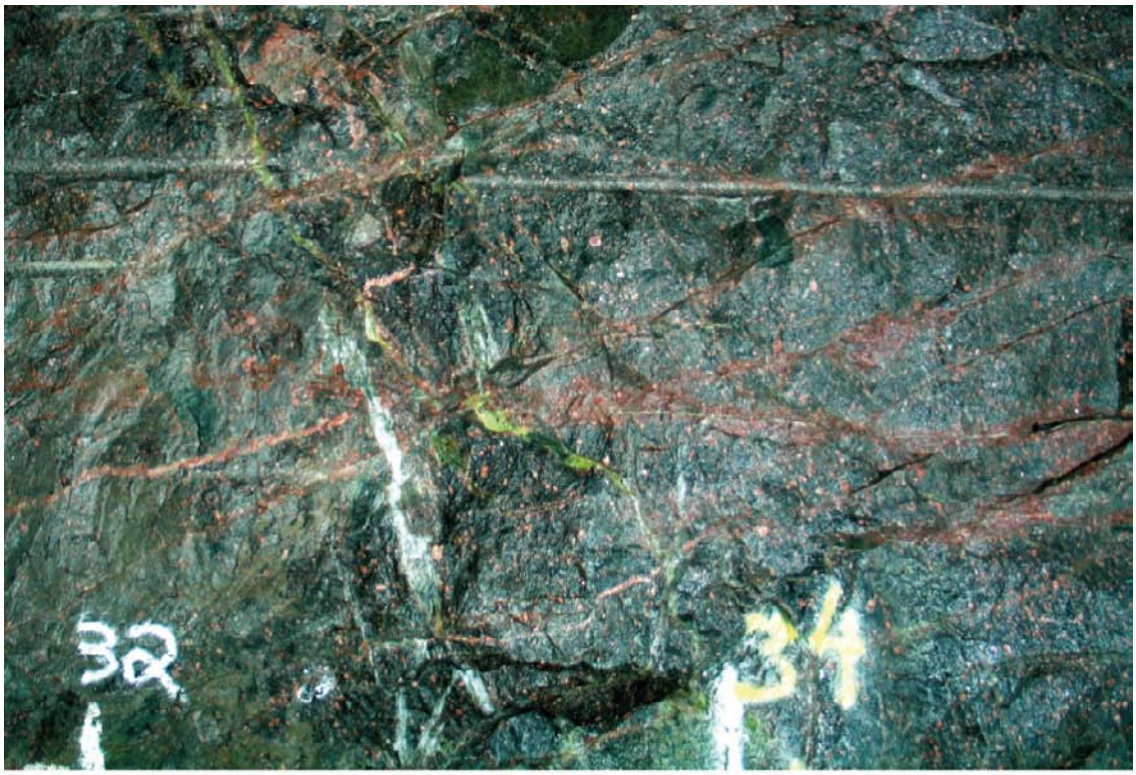

a)

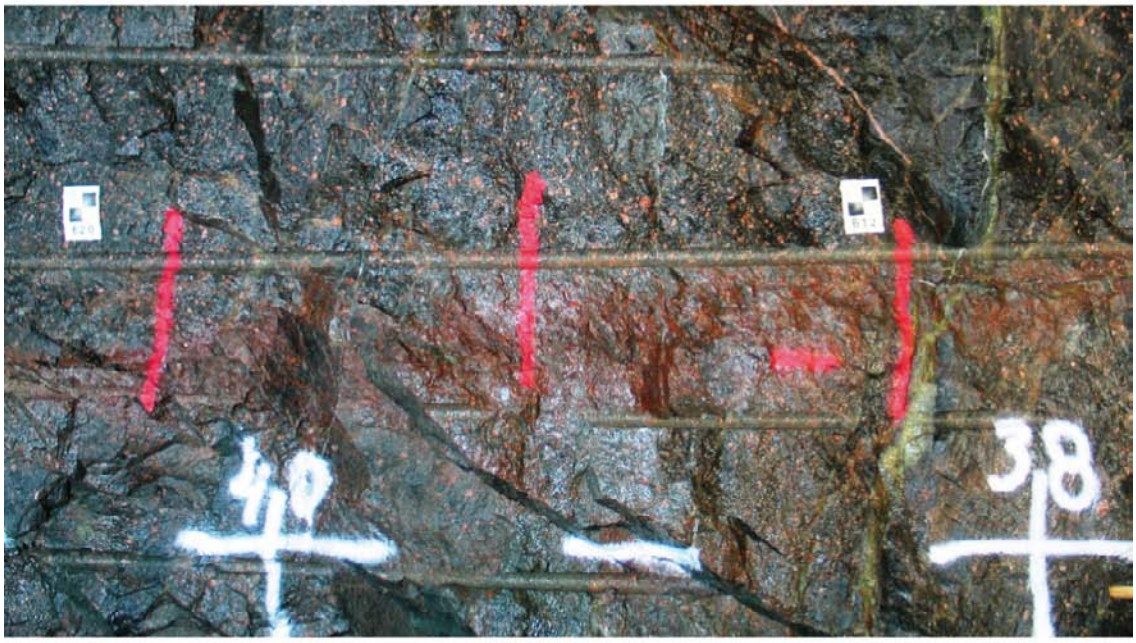

b)

Figure 3-19a–b. *Oxidized rims.* ***a)*** *Left-hand wall, section 32–34 m. Slightly irregular fracture pattern showing oxidized rims (fractures P2b-03 and 04, P2b-06 to 08 as well as F2a-10).* ***b)*** *Right-hand wall, section 38–40 m. Sub-horizontal fracture with oxidization rim (fracture P2b-35 and rock type P2b-B1).*

a)

b)

Figure 3-20a–b. *Fractures with alteration/depletion rims.* ***a)*** *Right-hand wall, section 36–38 m. Chlorite, prehnite and epidote-filled fractures with "alteration/depletion rims" (fractures P2b-60 to 62, see Appendix III B). Top left-hand corner shows part of fracture G2-109 (see Appendix III C).* ***b)*** *Left-hand wall, section 34–36 m. Fracture set showing depletion/epidote alteration within a diffuse deformation zone (G2-Z0, see Appendices III B and III C).*

Table 3-2. Recorded observations of fracture aperture, width and oxidation rims in the TASS-tunnel: P (walls and roof), G (floor), F (faces) and the EDZ-slot.

Interval (mm)	Aperture		Width (aperture + filling)		Oxidation rims or streaks (width + red colouring)	
	No of obs	% of all obs	No of obs	% of all obs	No of obs	% of all obs
0	820	58.74	8	0.57	1,059	75.86
> 0.0 – < 1	547	39.18	424	30.37	12	0.86
1 – < 2	23	1.65	385	27.58	10	0.72
2 – < 3	4	0.29	111	7.95	7	0.50
3 – < 4			98	7.02	3	0.21
4 – < 5			5	0.36		
5 – < 6	2	0.14	134	9.60	33	2.36
6 – < 7			6	0.43		
7 – < 10			14	1.00	1	0.07
10 – < 15			82	5.87	105	7.52
15 – < 20			24	1.72	22	1.58
20 – < 30			41	2.94	66	4.73
30 – < 40			39	2.79	26	1.86
40 – < 50			8	0.57	4	0.29
50 – < 100			17	1.22	22	1.58
100 – < 150					19	1.36
150 – < 200					2	0.14
200 – < 300					4	0.29
> 300					1	0.07
Total	**1,396**	**100.00**	**1,396**	**100.00**	**1,396**	**100.00**

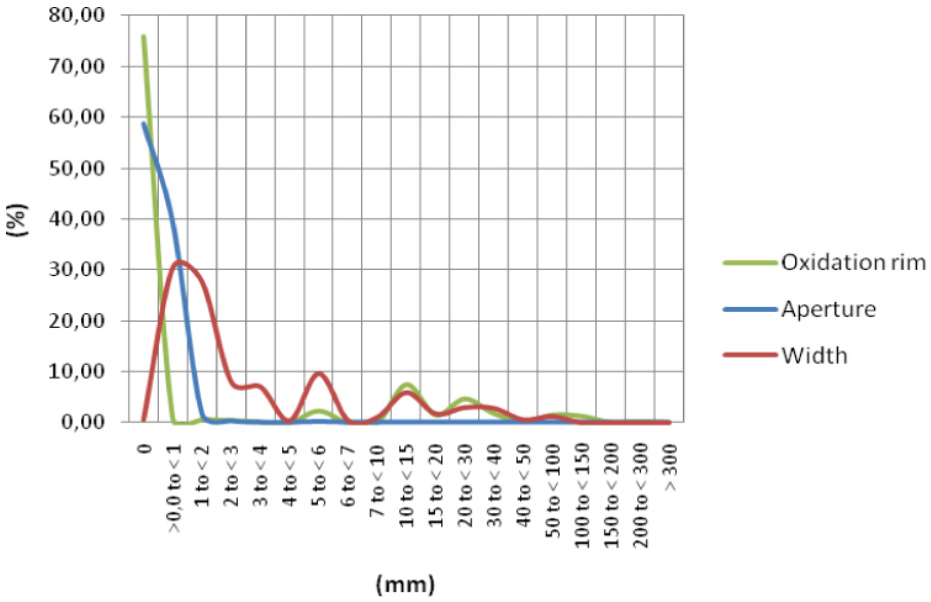

Figure 3-21. *Recorded fracture aperture, width and oxidation rims in the TASS-tunnel.*

Table 3-3. Recorded observations of fracture type in the entire TASS-tunnel: P (walls and roof), G (floor), F (faces) and the EDZ-slot.

Type	No of obs	%
Open	12	0.9
Tight	768	55.0
Re-opened	582	41.7
Induced open	28	2.0
No data	6	0.4
Total	1,396	100.0

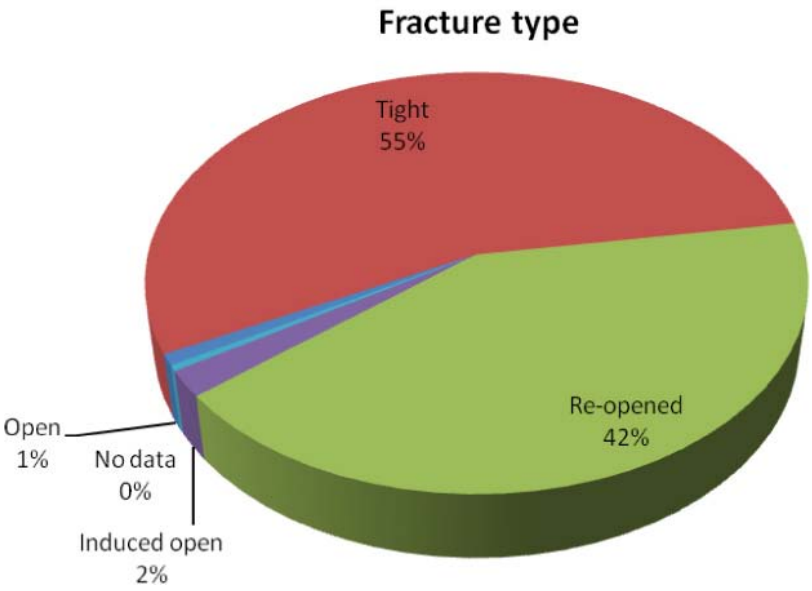

Figure 3-22. *Distribution of fracture types in the TASS-tunnel.*

Orientation

Orientation of fractures: The majority of the fractures in the TASS-tunnel are steeply dipping, although a number of sub-horizontal fractures have also been recorded (Figure 3-23). When all measured fractures in the TASS-tunnel, including all the tunnel faces, are plotted on a stereogram, two main fracture sets are apparent: 098/87 and 072/00 (right-hand rule), as well as a less prominent set 295/22, see Figure 3-24. The sub-horizontal fractures in the TASS-tunnel showing a north-south trend on the rosette diagram in Figure 3-24 are mainly caused by 30 almost horizontal fractures that were given the designated structural orientation 000/00.

Orientation of striation: Fractures containing visible lineations such as striation on fracture surfaces are mapped. The orientations can be seen in Figure 3-25, where an average trend/plunge is marked as approximately 023/28.

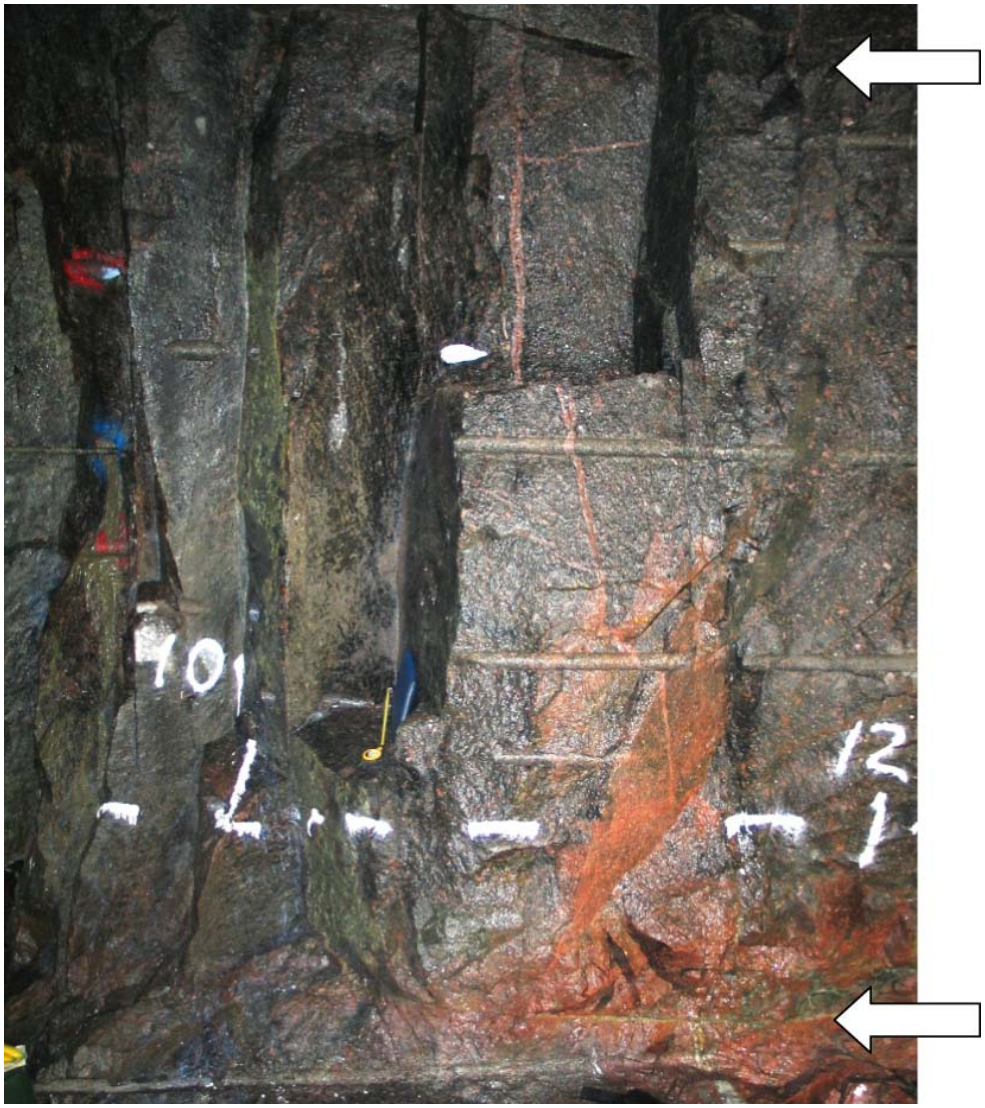

Figure 3-23. *Left-hand wall, section 10–12 m (see Appendix II A). Three sets of steeply dipping fractures forming pillar-shaped blocks , Set 1; fractures P-57, P-60 and 63 and P-65, orientation approx. 274/89 and Set 2; P-61 with orientation 057/88 and Set 3; P-67 with orientation: 341/77. Two sub-horizontal fractures (fractures F-03 and P-64, see arrows and Appendix II A) can also be seen. The one at the bottom of the picture (fracture F-03) shows some oxidation. A more evident oxidation rim can be seen in Figure 3-19b).*

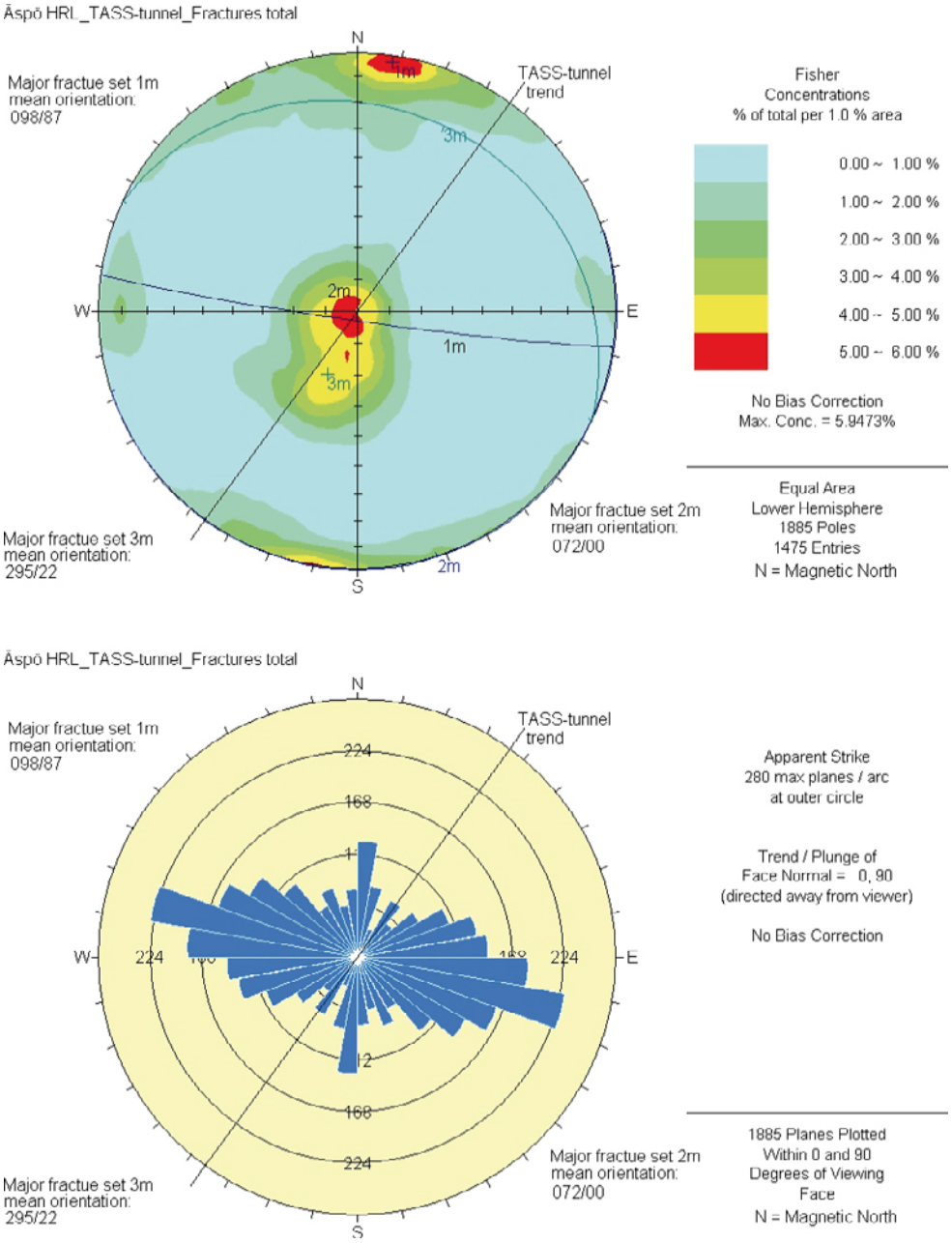

Figure 3-24. *All fracture orientations from the TASS-tunnel (walls and roof, floor, EDZ-slot and all tunnel faces) presented in Schmidt net and joint rosette diagrams. The 216° trend of the TASS-tunnel is marked as a black line. Three main orientation sets can be seen, namely 1m: 098/87 and 2m: 072/00 as well as a less prominent set 3m: 295/22. The north-south striking trend on the rosette diagram is mainly caused by 30 horizontal fractures that have the designated structural orientation 000/00. N refers to magnetic north.*

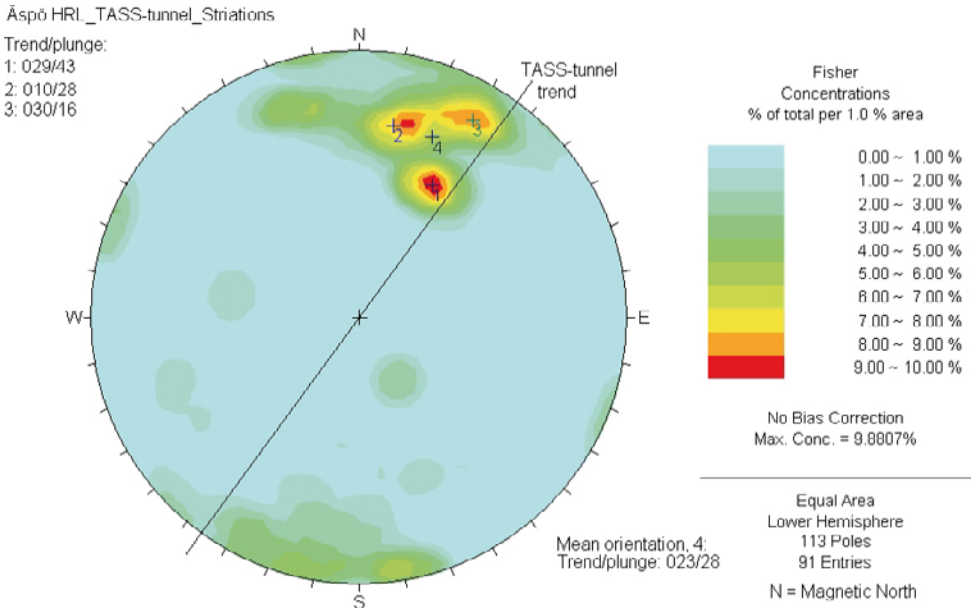

Figure 3-25. *Trend and plunge of visible striations on fracture surfaces from the TASS-tunnel presented in Schmidt net. The 216° trend of the TASS-tunnel is marked as a black line. Three major trend sets can be observed, namely 1: 029/43, 2: 010/28 and 3: 030/16. The average trend and plunge of all three is approximately 4: 023/28. N refers to magnetic north.*

Fracture filling

Rock types that are thinner than approximately 10 cm are also categorised as fracture fillings, e.g. fine-grained granite, pegmatite and breccia, as well as mylonite and quartz veins/lenses. It can even be concluded that the filling material red feldspar is thin granitic/pegmatitic veins, dominated by feldspar. In addition, the red colouring/staining of fracture rims (oxidation along a fracture/oxidation rim) is mapped as a fracture filling. In the statistics, all alteration rims have been included in the oxidation rims.

Several categories of fillings are identified when mapping the fractures of the TASS-tunnel. The most common fracture filling mineral in the tunnel is chlorite, followed by calcite, epidote and prehnite, see Table 3-4 and Figure 3-26. Quartz, pyrite and red feldspar are also quite common, while biotite, iron oxide and unconsolidated filling materials (grout and clay) have only been observed a few times. Four other filling categories have been observed: dull surface (very thin unidentified surface alteration), unidentified filling material, filling material that could exist (but is not seen) and finally fractures with no filling.

Most fractures contain more than one fracture filling mineral. They are mapped according to apparent quantity in each fracture so that the most abundant mineral is mapped as mineral 1 and so on to mineral 5. The orientation of fractures containing chlorite, calcite, epidote and prehnite as first mineral, respectively, are shown below in Figures 3-27, 3-28, 3-29 and 3-30. Examples of mapped fracture fillings from the TASS-tunnel can be seen in Figure 3-31 (calcite-filled fractures) and in Figure 3-32 (epidote-filled fractures).

Fractures with chlorite and prehnite as the most dominant fracture minerals are dominated by relatively gently dipping to sub-horizontal fractures, as can be seen in Figures 3-27 and 3-30 respectively. They show an average orientation of 291/24 for chlorite and 286/28 and 360/01 for prehnite. On the other hand, fractures with calcite and epidote as the most dominant fracture minerals are dominated by sub-vertical fractures, as can be seen in Figures 3-28 and 3-29 respectively. Fractures with calcite filling show an average orientation of 103/88, while the epidote-filled fractures have a mean orientation of 089/84.

As a comparison, the distribution of all occurrences of the most common fracture-filling minerals can be seen in Appendix IX (chlorite, calcite, epidote and prehnite as well as fractures containing both epidote and prehnite as fracture filling minerals).

Table 3-4. Distribution of fracture fillings – the TASS-tunnel total: P (walls and roof), G (floor), F (faces) and the EDZ-slot.

Filling	No of observations	% of all observations (total no: 2,876)	Number of observations against total number of fractures (1,396)
Chlorite	896	31.15	64.18
Calcite	460	15.99	32.95
Epidote	402	13.98	28.80
Prehnite	350	12.17	25.07
Quartz	111	3.86	7.95
Pyrite	33	1.15	2.36
Biotite	4	0.14	0.29
Iron oxide	9	0.31	0.64
Red feldspar	22	0.76	1.58
Grout	2	0.07	0.14
Clay	1	0.03	0.07
Dull surface	36	1.25	2.58
Unidentified filling	18	0.63	1.29
Filling could exist	22	0.76	1.58
No filling	15	0.52	1.07
Oxidation rim	320	11.13	22.92
Fine-grained granite	61	2.12	4.37
Pegmatite	108	3.76	7.74
Breccia	5	0.17	0.36
Mylonite	1	0.03	0.07
Total	**2,876**	**100.00**	**–**

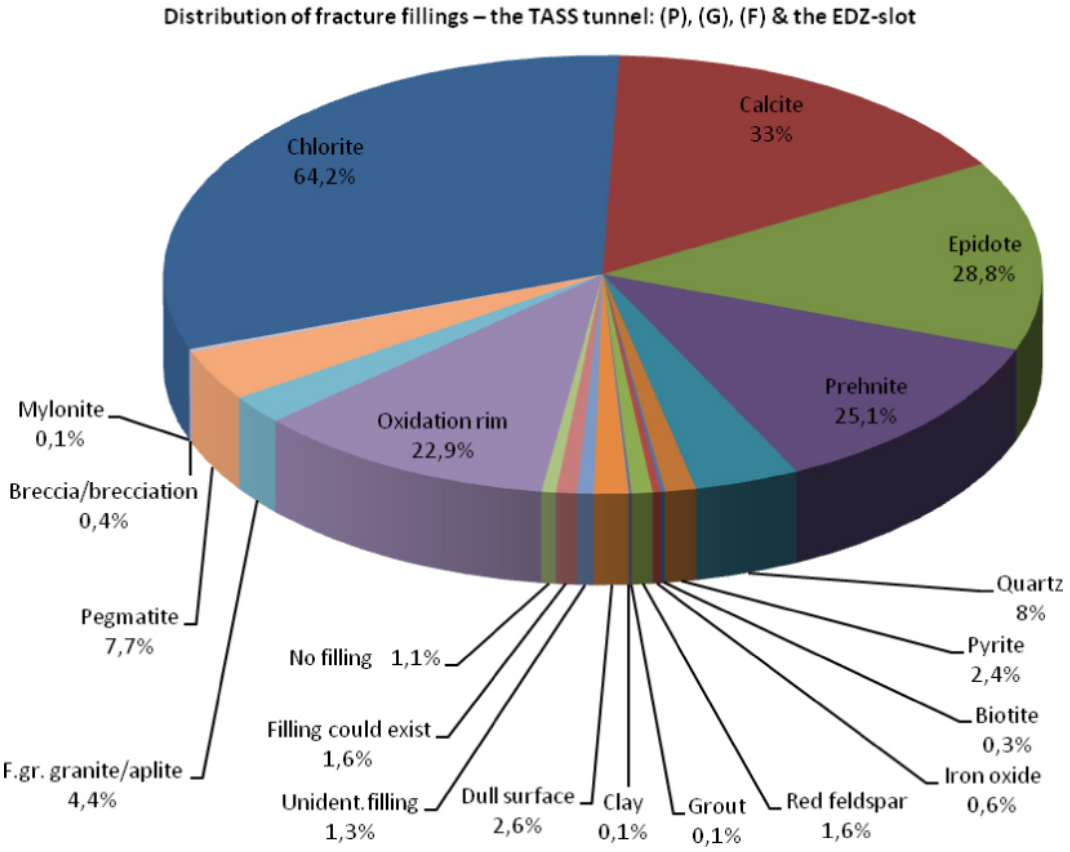

Figure 3-26. *Distribution of fracture fillings in the TASS-tunnel, including oxidation rim as well as rock types; fine-grained granite/aplite, pegmatite, breccia/brecciation and mylonite. Number of observations (2,876) against total number of fractures (1,396), see Table 3-4.*

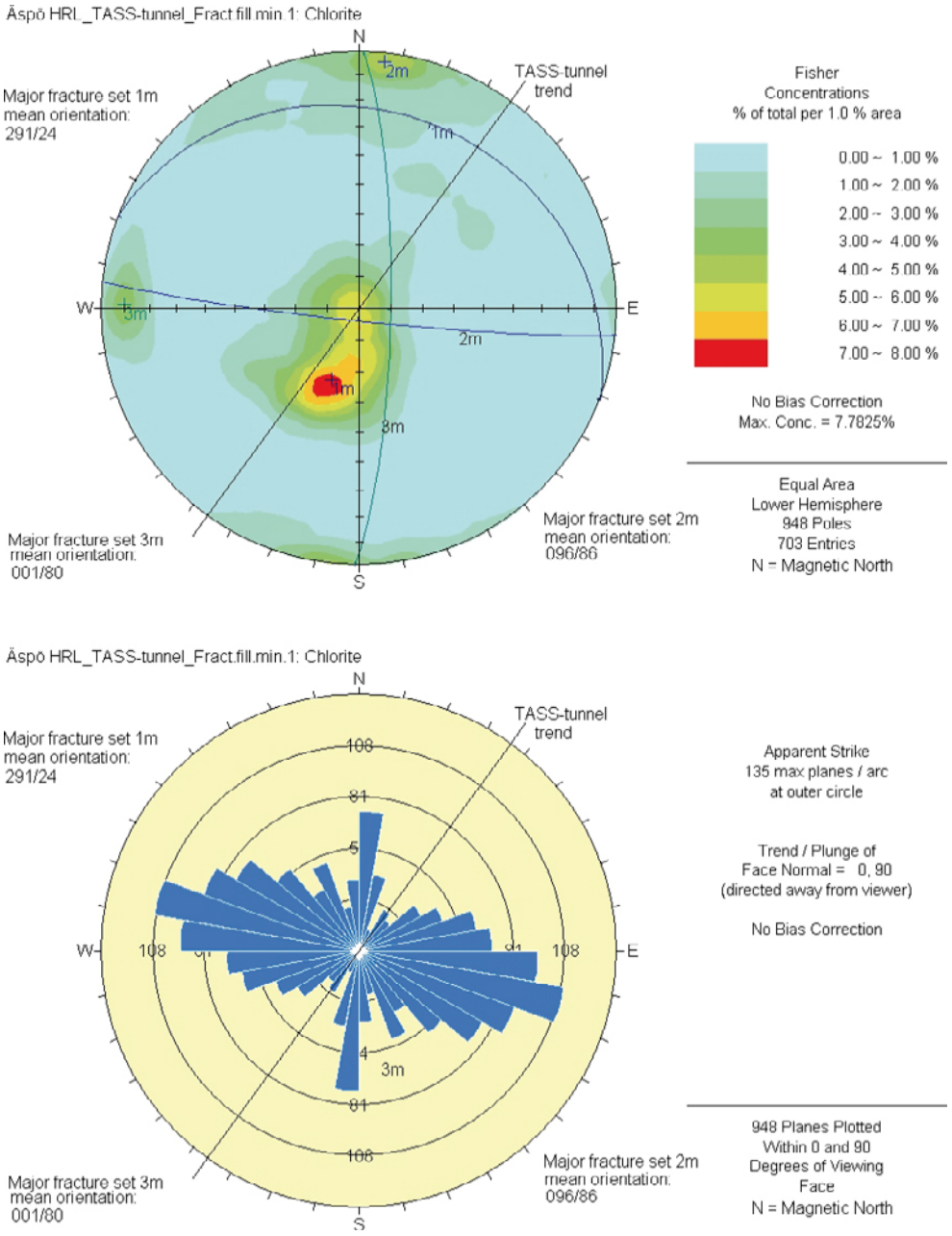

Figure 3-27. *Orientation of fractures that contain chlorite as the first fracture filling mineral in the TASS-tunnel presented in Schmidt net and joint rosette diagrams. The 216° trend of the TASS-tunnel is marked as a black line. The main orientation set is 1m: 291/24, and two less prominent sets can also be seen, namely set 2m: 096/86 and set 3m: 001/80. The north-south striking trend on the rosette diagram is mainly caused by sub-horizontal fractures that have the designated structural orientation 000/00 (see Figure 3-16). N refers to magnetic north.*

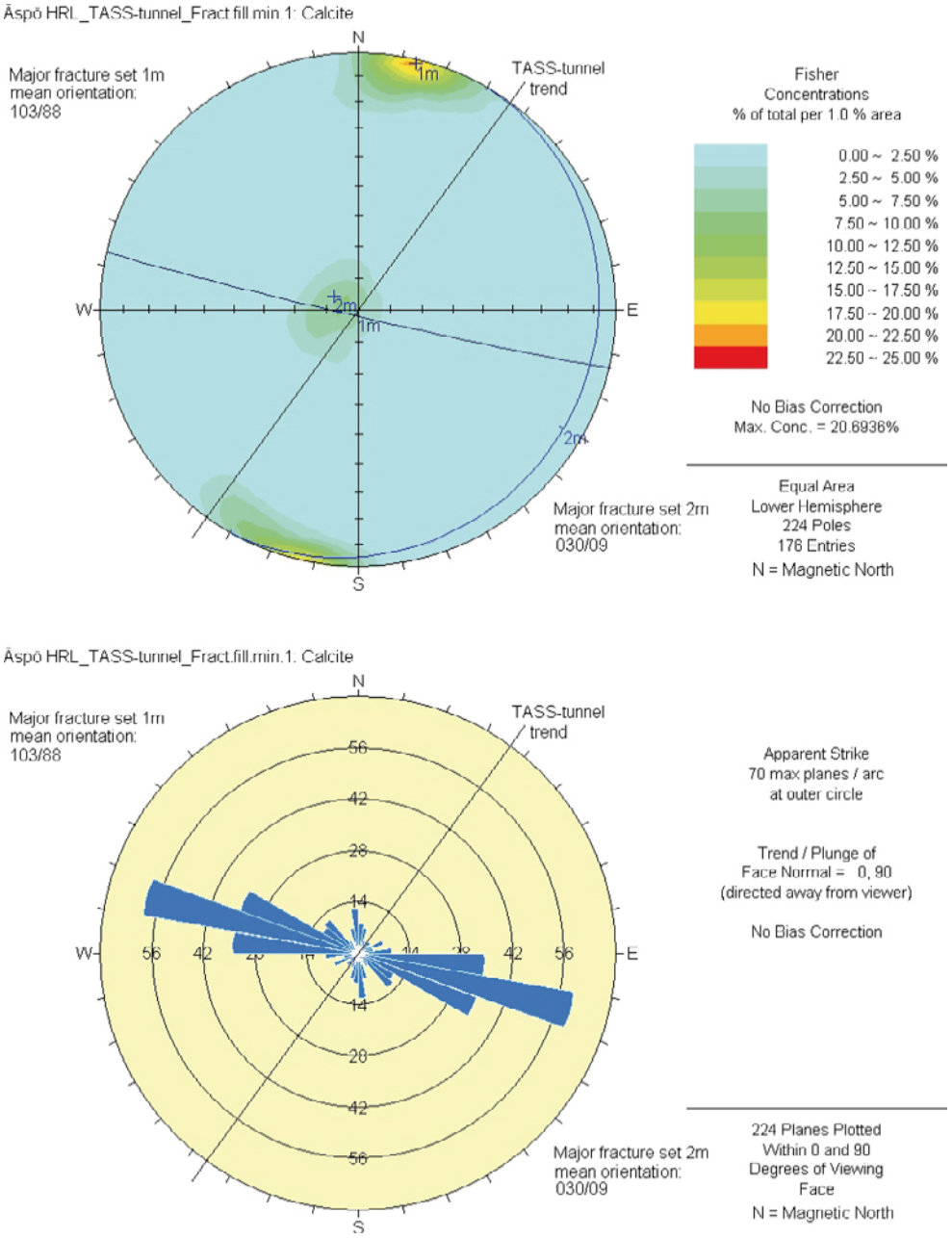

Figure 3-28. *Orientation of fractures that contain calcite as the first fracture-filling mineral in the TASS-tunnel presented in Schmidt net and joint rosette diagrams. The 216° trend of the TASS-tunnel is marked as a black line. The main orientation set is 1m: 103/88. One less prominent set can also be seen, namely set 2m: 030/09. N refers to magnetic north.*

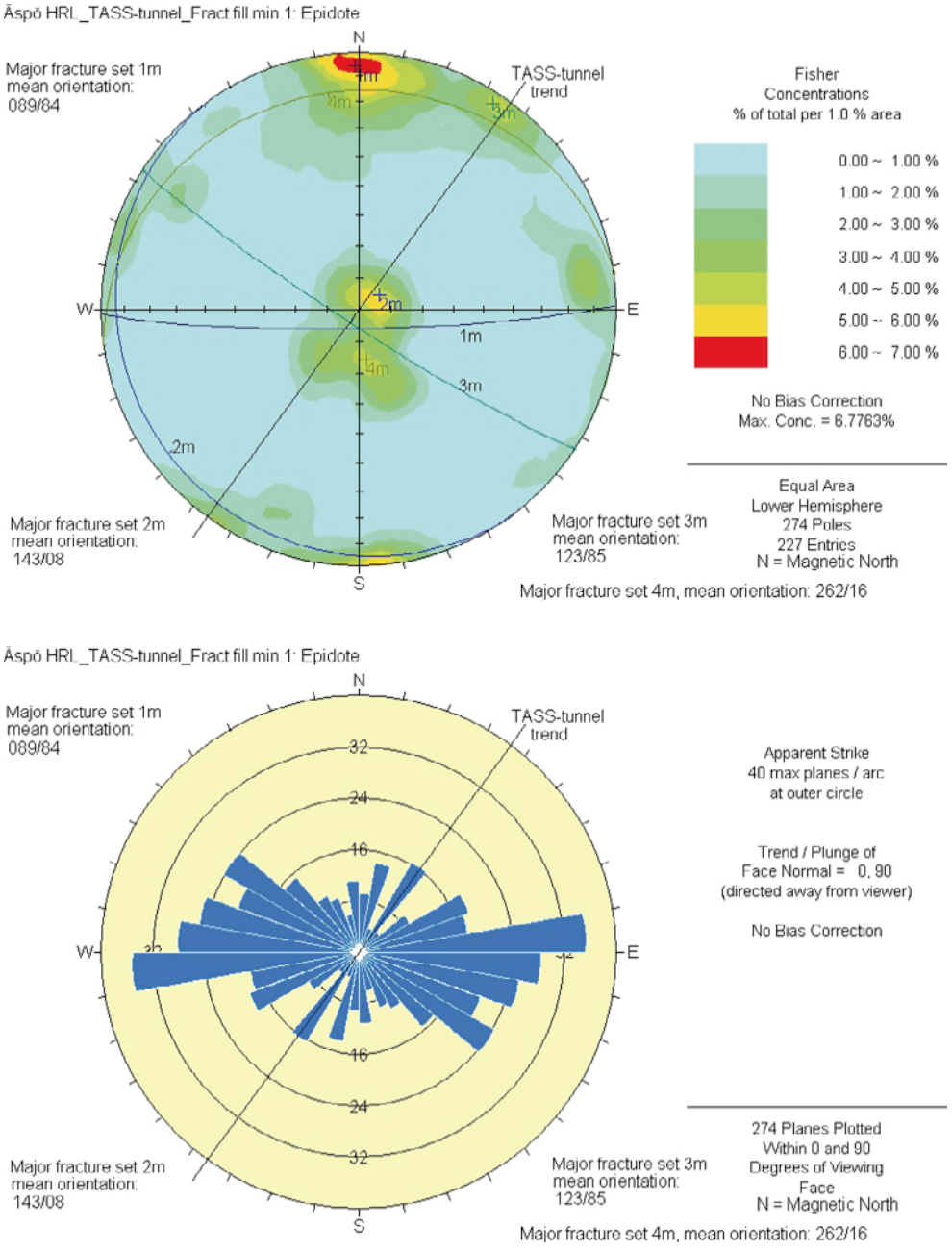

Figure 3-29. *Orientation of fractures that contain epidote as the first fracture filling mineral in the TASS-tunnel presented in Schmidt net and joint rosette diagrams. The 216° trend of the TASS-tunnel is marked as a black line. The main orientation set is 1m: 089/84. Three less prominent sets can also be seen, namely set 2m: 143/08, set 3m: 123/85 and set 4m: 262/16. N refers to magnetic north.*

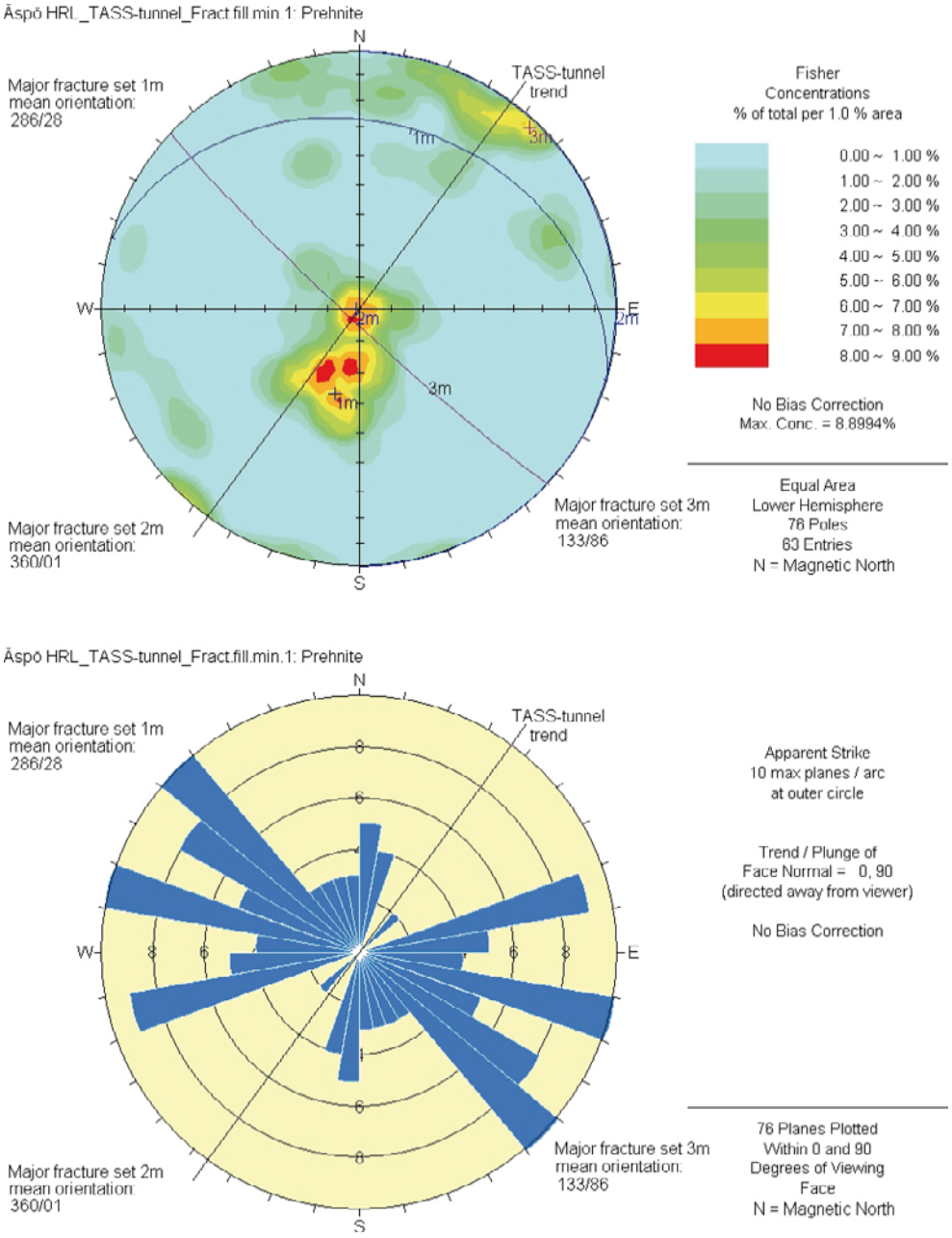

Figure 3-30. *Orientation of fractures that contain prehnite as the first fracture filling mineral in the TASS-tunnel presented in Schmidt net and joint rosette diagrams. The 216° trend of the TASS-tunnel is marked as a black line. There are two main orientation sets, namely set 1m: 286/28 and set 2m: 360/01. One less prominent set can also be seen, namely set 3m: 133/86. The north-south striking trend on the rosette diagram is mainly caused by horizontal fractures that have the designated structural orientation 000/00. N refers to magnetic north.*

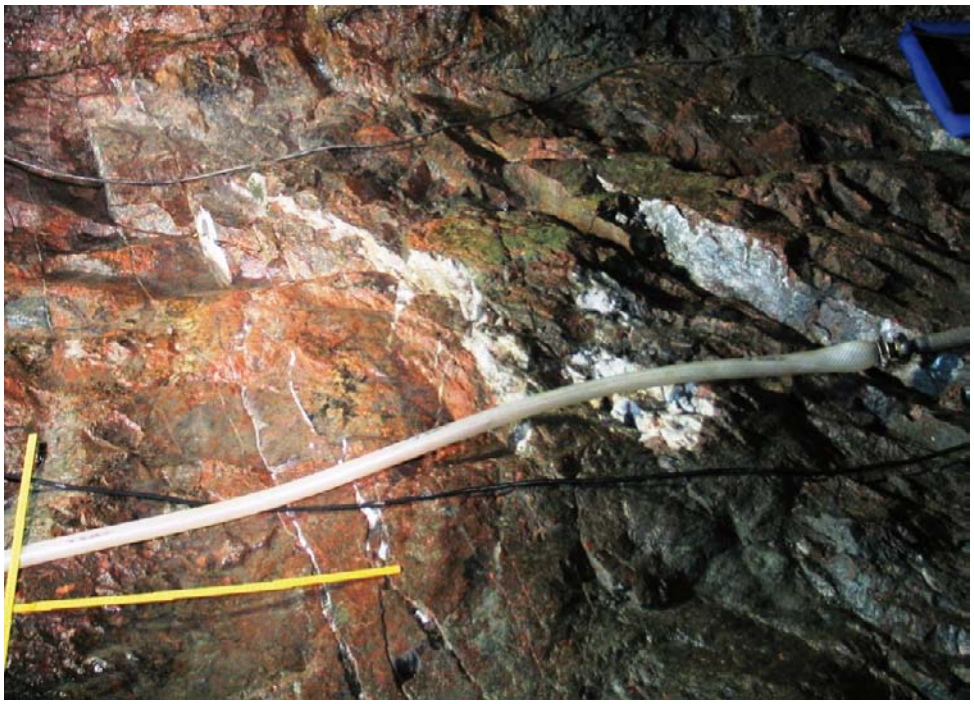

Figure 3-31. *Floor, approximate section 19–20 m, fracture ID: G-42, 2 fractures, width: 5 mm, orientation: 287/90 (see Appendix II B). Calcite-filled fractures (white).*

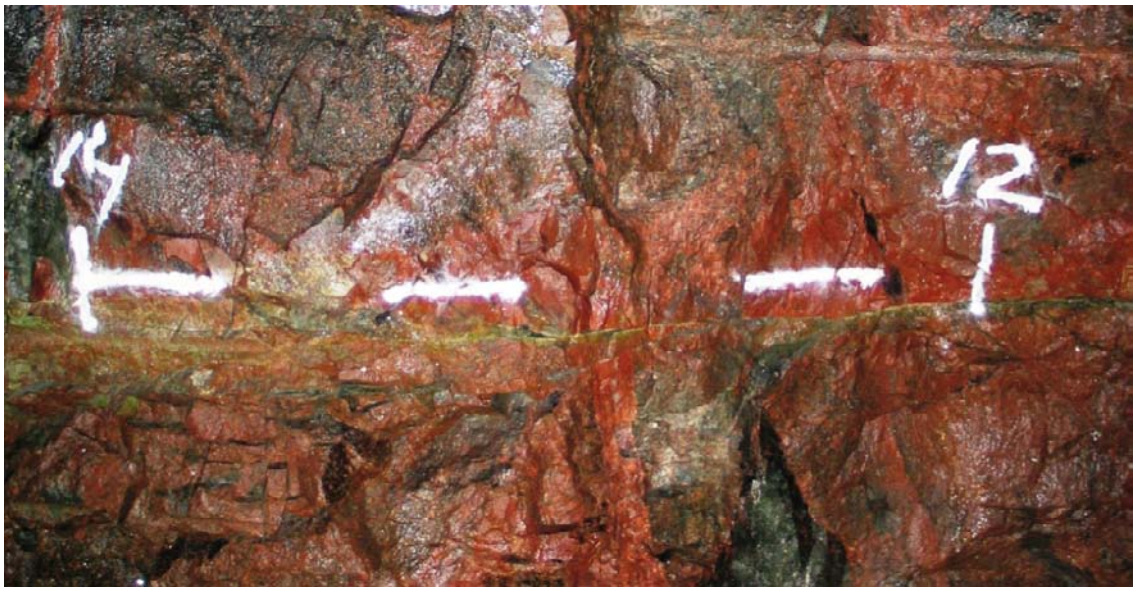

Figure 3-32. *Right-hand wall, section 12–14 m, sub-horizontal, fracture ID: F-03 (ID comes from first full-face mapping at 8.7 m tunnel length, Appendix I), width: 5 mm, designated orientation: 000/00 (see Appendix II A).The fracture is dominated by epidote, but both prehnite and calcite also occur.*

Fracture form and surface roughness

Form (planarity): The form (planarity) of fractures is in the TMS code chart (SKBdoc 1252025, internal SKB document, Table 1-1) divided into four categories: plane (or planar), undulating (amplitude over 0.1 m), arched (with height of arch over 0.1 × length of fracture) and stepped cf. /ISRM 1977, pp 338–346/. In Table 3-5 and Figure 3-33 it can be seen that fractures with the designation plane dominate.

Surface structure (roughness): According to TMS code chart (SKBdoc 1252025, internal SKB document, Table 1-1) the surface structure (roughness) of fractures is divided into rough, smooth and slickensided cf. /ISRM 1977, pp 338–346/. Closed fractures or other fractures that have no surface exposure are mapped as undefined.

In Table 3-6 and Figure 3-34 it can be seen that most fractures do not show their surface structure and therefore fall within the category undefined. Of those that do show their surface structure, the surface structure rough dominates.

Table 3-5. Form (planarity) of all fractures in the TASS-tunnel.

Form (planarity)	Number of fractures	% of all fractures
Plane (planar)	1,204	86.25
Undulating (amplitude >0.1 m)	155	11.10
Arched (height >0.1 × length)	30	2.15
Stepped	3	0.21
No data	4	0.29
Total	**1,396**	**100.00**

Table 3-6. Surface structure (roughness) of all fractures in the TASS-tunnel.

Surface structure (roughness)	Number of fractures	% of all fractures
Rough	648	46.42
Smooth	12	0.86
Slickensided	8	0.57
Undefined	719	51.50
No data	9	0.64
Total	**1,396**	**100.00**

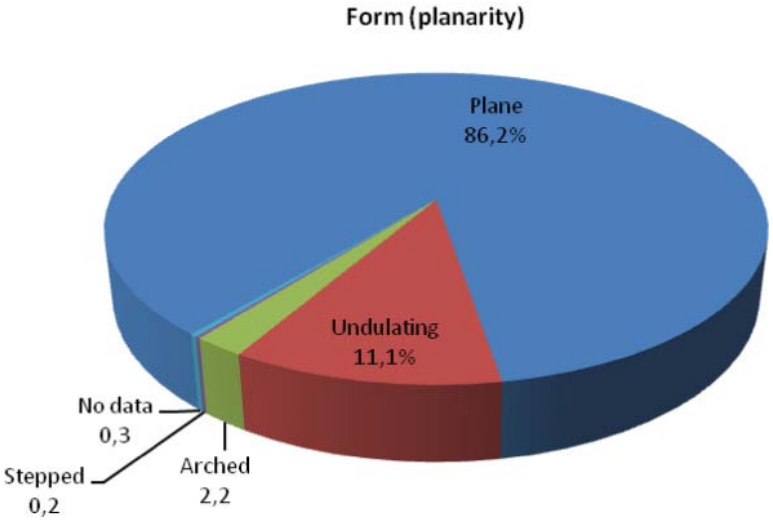

Figure 3-33. *Distribution of form (planarity) of all fractures in the TASS-tunnel.*

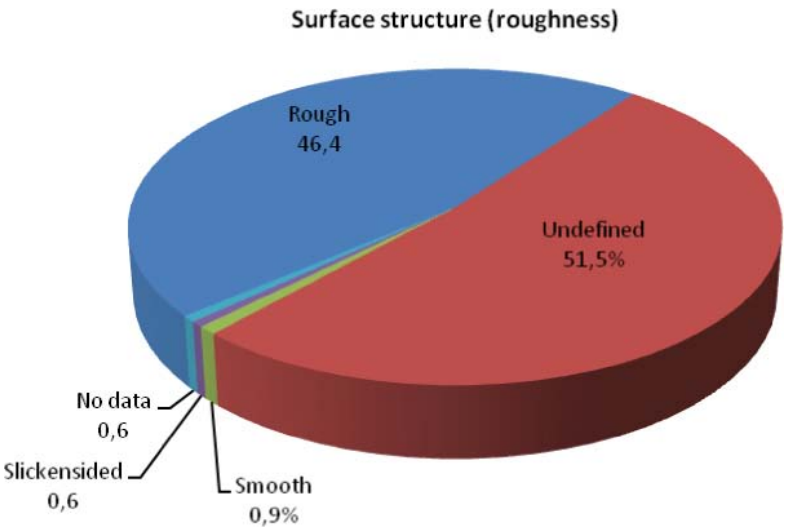

Figure 3-34. *Distribution of surface structure (roughness) of all fractures in the TASS-tunnel.*

Table 3-7 and Figure 3-35 shows the distribution of all fractures in the TASS-tunnel when the fracture form and fracture surface structure are combined. As is to be expected from the data presented in Tables 3-5 and 3-6 as well as in Figures 3-33 and 3-34, plane fractures with either undefined or rough surface structure dominate in Table 3-7 and Figure 3-35.

Table 3-7. Distribution of fracture surface categories – the TASS-tunnel: P (walls and roof), G (floor) and F (faces).

Surface category	Number of fractures	% of all fractures
Plane and undefined	640	45.85
Plane and rough	542	38.83
Plane and smooth	11	0.79
Plane and slickensided	6	0.43
Plane and no data	5	0.36
Undulating and rough	93	6.66
Undulating and undefined	59	4.23
Undulating and slickensided	2	0.14
Undulating and smooth	1	0.07
Arched and undefined	18	1.29
Arched and rough	12	0.86
Stepped and undefined	2	0.14
Stepped and rough	1	0.07
No data	4	0.29
Total	**1,396**	**100.00**

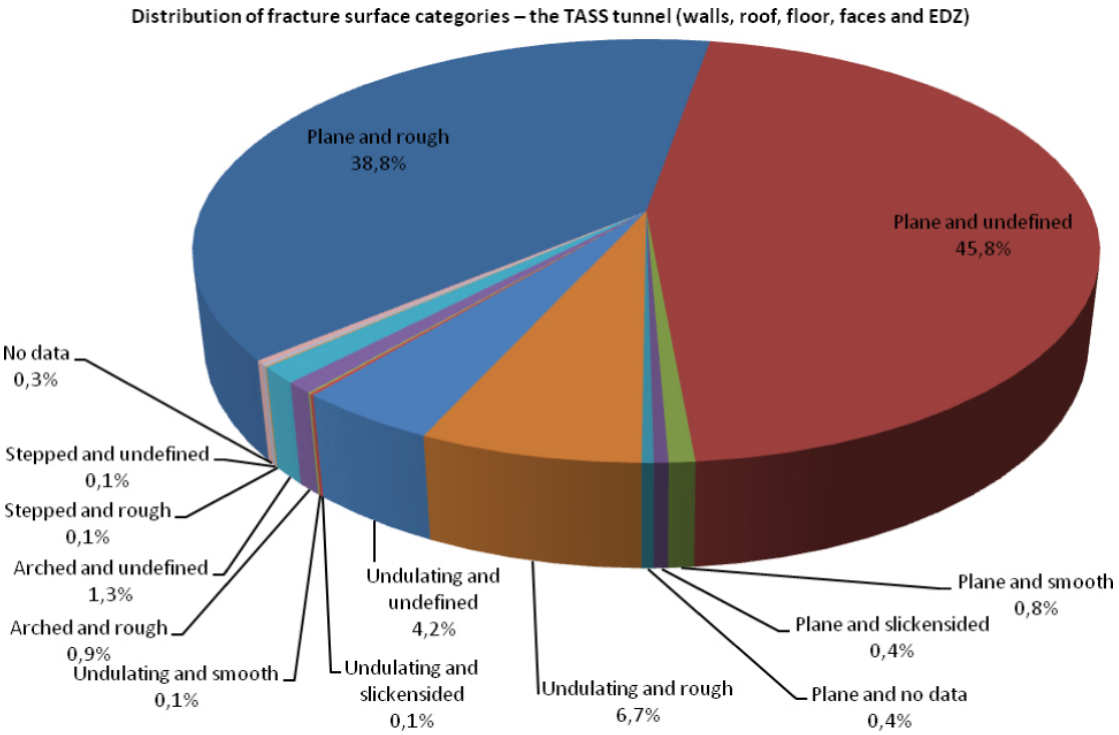

Figure 3-35. *Distribution of the combined fracture form and fracture surface structure categories for all fractures in the TASS-tunnel.*

Persistence/fracture length

The length of a fracture is defined as the distance along the fracture trace on the fracture map (trace length). The cut-off is about 1 m, except when the fractures are leaking water or there is some other aspect of importance to the fracture mapping (e.g. displacement). This means that in reality there are more fractures that are <1 m in length than those that have been mapped and are presented in Table 3-8 and Figure 3-36.

Figure 3-36 presents several curves showing the distribution of fracture lengths. Although the curves represent different numbers of fractures, they still show the same distribution pattern for the fracture lengths. Only one small exception can be seen in the distribution curve for tunnel faces, between 3–5 m lengths. The explanation for this could be that certain fractures mapped first in the tunnel face were during the stage mapping found to continue into the walls, roof and/or floor of the tunnel. This added to their maximum trace lengths, which were entered into the database.

Table 3-8. Fracture persistence in the TASS-tunnel: P (walls and roof), G (floor), F (faces) and the EDZ-slot.

Length interval in meters	Mapping of roof, walls, floor, all faces and EDZ	Mapping of roof, walls, floor, last face (80.7 m) and EDZ	Mapping of roof, walls, last face (80.7 m) and EDZ	Mapping of roof, walls and EDZ	Mapping of roof and walls	Mapping of tunnel floor	Mapping of tunnel faces
< 1	145	109	66	66	59	43	36
1 to 2	616	436	256	248	244	180	188
2 to 3	281	213	144	140	140	69	72
3 to 4	158	102	73	71	70	29	58
4 to 5	86	49	33	28	28	16	42
5 to 6	44	34	19	19	19	15	10
6 to 7	19	15	8	7	7	7	5
7 to 8	12	8	2	2	2	6	4
8 to 9	11	6	3	3	3	3	5
9 to 10	5	4	1	1	1	3	1
10 to 15	13	10	0	0	0	10	3
15 to 20	3	3	1	1	1	2	0
20 to 25	3	2	1	1	1	1	1
Totally	**1,396**	**991**	**607**	**587**	**575**	**384**	**425**

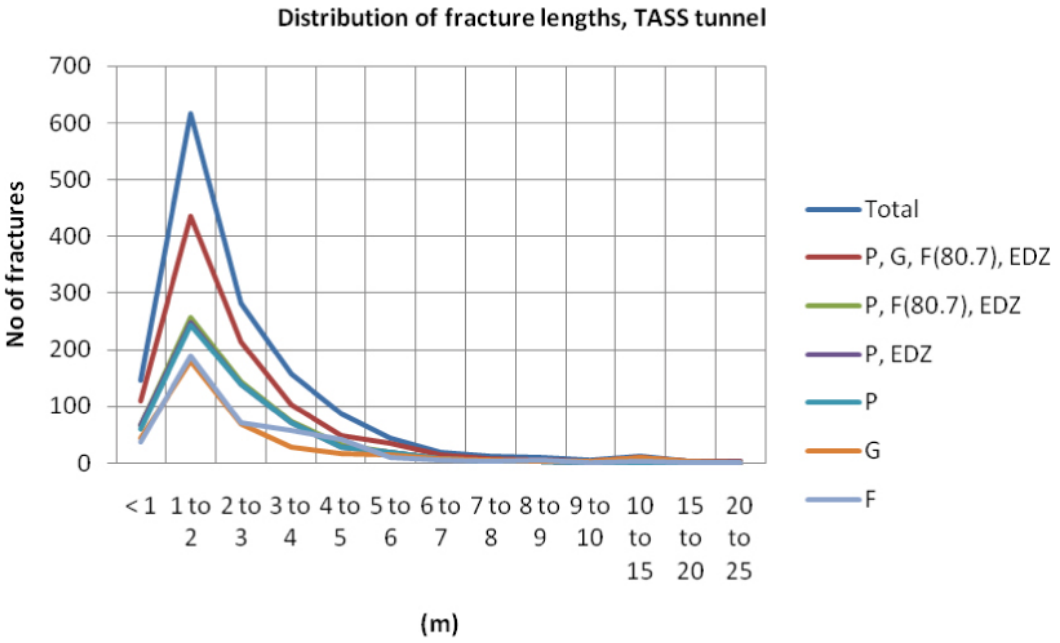

Figure 3-36. *Distribution of fracture lengths in the TASS-tunnel. Total = walls, roof, floor, all faces and the EDZ-slot, P = walls and roof, G = floor, F = faces, F(80.7) = face at 80.7 m tunnel length, EDZ = the EDZ-slot in the tunnel.*

Displacements

Mapped displacements along fracture planes occur in 87 fractures and are between 0.1–1.20 m in magnitude, with a strong preference for minor displacements, see Table 3-9 and Figure 3-37.

The majority of the displacements occur along sub-horizontal to gently dipping fracture planes, as can be seen in Figure 3-38, where the most prominent concentration of displacing fractures has a mean orientation of 294/26, with two subordinate orientations of 092/81 and 065/07. The subordinate orientation 092/81 is sub-parallel to the dominating fracture orientation of the TASS-tunnel (see Figure 3-24, mean orientation of major fracture set 1m: 098/87). Two examples of displacements along a vertical and sub-horizontal fracture respectively can be seen in Figure 3-39a–b.

Table 3-9. Displacements in the TASS-tunnel.

Length of displacements (m)	No of displacements
0	1,309
0.1	50
0.2	19
0.3	7
0.4	4
0.5	4
0.6	1
0.8	1
1.2	1
Total	**1,396**

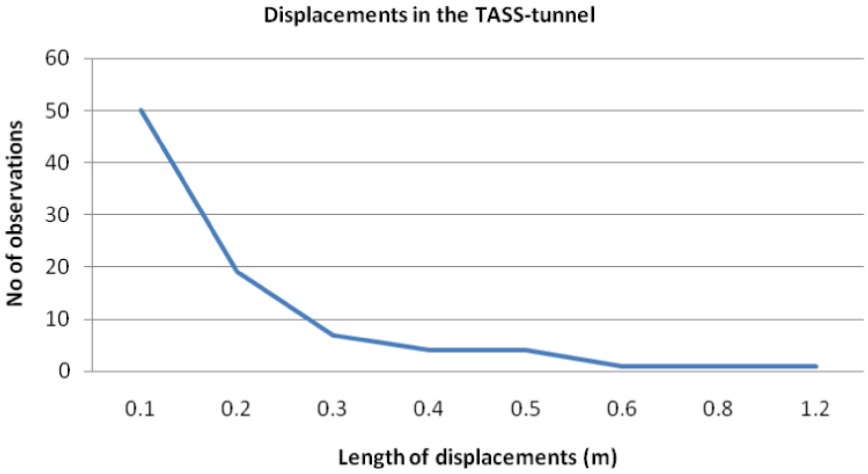

Figure 3-37. *Distribution of displacements in the TASS-tunnel. The category "no displacement" or "0 m displacement" is not included in the diagram.*

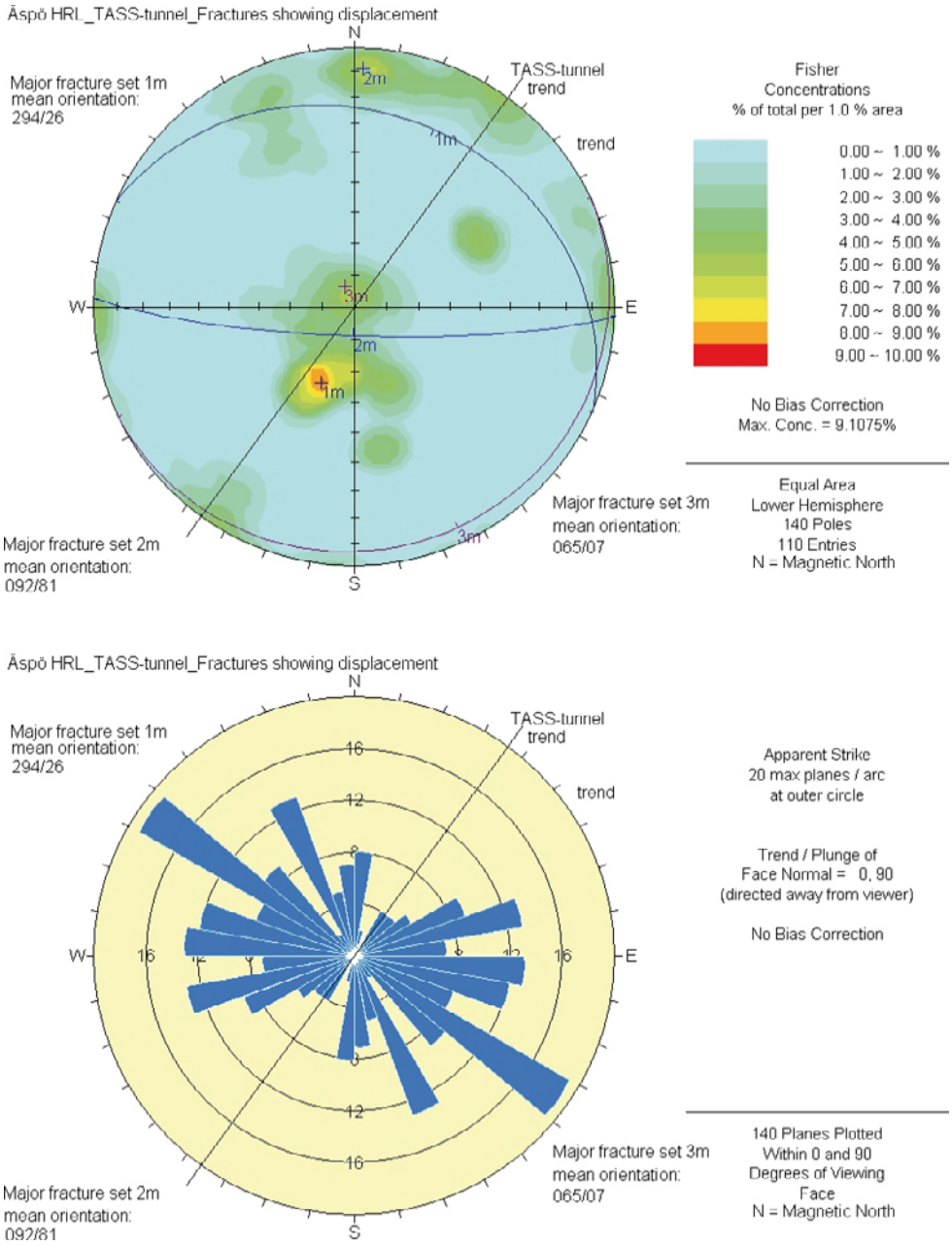

Figure 3-38. *Orientation of fractures that show displacements in the TASS-tunnel presented in Schmidt net and joint rosette diagrams. The 216° trend of the TASS-tunnel is marked as a black line. The main orientation set is 1m: 294/26. Two less prominent sets can also be seen, namely set 2m: 092/81 and set 3m: 065/07. The north-south striking trend on the rosette diagram is mainly caused by horizontal fractures that have the designated structural orientation 000/00. N refers to magnetic north.*

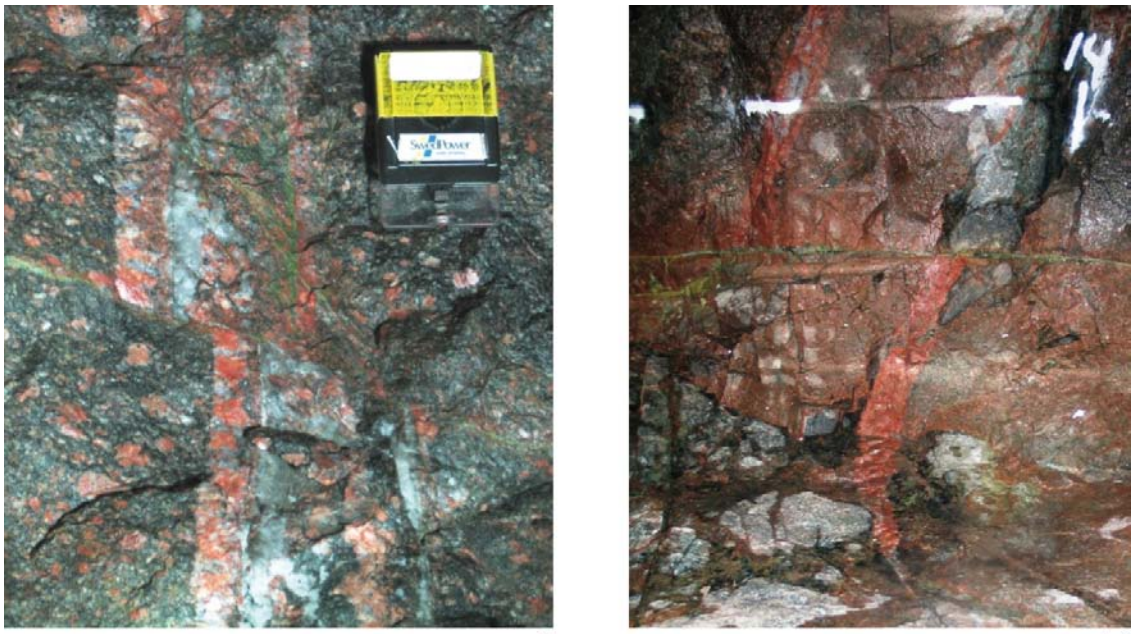

Figure 3-39a–b. *Displacements.* ***a)*** *Floor, section around 26 m. Minor (about 0.1 m) displacement of a pegmatite dyke (P2a-B3) along an almost vertical fracture (fracture G2-45, orientation 260/80, see Appendix III A and III C).* ***b)*** *Left-hand wall, section 13–14 m. About 0.5 m displacement of a pegmatite dyke (P-B4) by a sub-horizontal, persistent fracture (fracture F-03, designated orientation: 000/00, see Appendix II A).*

3.2.5 Deformation zones

Distribution of deformation zones as well as fractures can be seen in Appendices I–VI. Appendix I (mapping of faces), Appendices II A, III A, III B, IV A and V A (mapping of walls and roof), Appendices II B, III C, IV B and V B (mapping of floors), and Appendix VI (mapping of EDZ).

When a deformation zone or a fracture cross cuts the entire tunnel, the intersection is defined as a Full Perimeter Intersection (FPI, /Munier 2010/). Two examples of steeply dipping deformation zones that cross cut the tunnel can be seen in Figure 3-40.

Deformation zone orientations are presented in Schmidt nets and joint rosette diagrams in Figures 3-41, 3-42 and 3-43. No adjustments have been made in the diagrams for the orientation of the mapped surfaces. Nor have the compass readings been corrected for magnetic declination.

In the TMS code chart (SKBdoc 1252025, internal SKB document, Table 1-1), the table concerning deformation zones refers to them as fracture zones. In the column headed Zone category, however, the various zone-types are referred to as deformation zones.

The mapped deformation zones in the TASS-tunnel are divided into two categories. In consistence with the TMS code chart they have been called:

- *increased fracturing* (with apparent width 0.5–8 m) mainly visible in the floor of the tunnel and
- *deformation zones proper, brittle/ductile* (0.1–0.3 m wide) that cut the tunnel and commonly have well defined boundaries. Thinner zones (<0.1 m wide) were generally mapped as fractures. They are sometimes somewhat irregular and difficult to trace.

Orientation

Orientations of eight deformation zones in the TASS-tunnel are presented in Schmidt net and joint rosette diagrams in Figure 3-41. The two zone categories are given different colours: deformation zone proper, brittle/ductile are green (ID numbers: 1, 6, 7 and 8) and increased fracturing is red (ID numbers: 2, 3, 4 and 5).

Figure 3-40a–b. *Examples of steeply dipping brittle/ductile deformation zones cross cutting the tunnel (FPI = Full Perimeter Intersection).* ***a)*** *Left-hand wall, section 16–17 m, zone G-Z0 (see Appendix II A and II B), orientation: 110/85, ID: 1 in Figure 3-41. Lamellar to mylonitic deformation zone with epidote, prehnite, chlorite, calcite filling and slightly oxidized rims.* ***b)*** *Right-hand wall and floor, section about 76 m, zone G4-Z0 (see Appendix V A and V B), orientation: 114/90, ID: 7 in Figure 3-41. Lamellar deformation zone with prehnite, epidote, chlorite and calcite filling.*

Zones with increased fracturing are generally sub-horizontal to gently inclined, and often have borders that are more or less diffuse, while the proper deformation zones dip more steeply and have more clearly defined borders.

- In Figure 3-41, the average orientation of the *increased fracturing* is approximately 277/37 with the exception of 074/84 (no. 4), which is a zone consisting of a number of fractures with depleted borders, see Figure 3-20b.
- The average orientation of the *deformation zones proper* in Figure 3-41 is approximately 107/87 with the exception of 055/85 (no. 6). The latter zone (no. 6) is actually made up of two components, which partly merge in the left-hand wall of the TASS-tunnel at approximately section 53 m (see Appendix IV). The orientation of the dominating component (deformation zone proper) is plotted as no. 6 in Figure 3-41 and as G3-Z0 in Figure 3-42. The cross-cutting component containing several thinner fractures has an average strike/dip of approximately 099/82 (see 1m in Figure 3-42), which coincides approximately with deformation zone no. 1 in Figure 3-41 (110/85). None of the components are clearly FPI.

Thin deformation zones (less than approximately 10 cm) plot according to Figure 3-43a and those with breccias as in Figure 3-43b. Generally, the thin deformation zones strike approximately northwest or southeast, and dip relatively steeply, thereby giving them an approximately parallel orientation to the deformation zones in the TASS-tunnel, shown in Figures 3-41 and 3-42. The breccias (Figure 3-44), on the other hand, are predominantly sub-horizontal and can with certain exceptions be said to approximate the directions of the increased fracturing zones of the TASS-tunnel, see Figure 3-41.

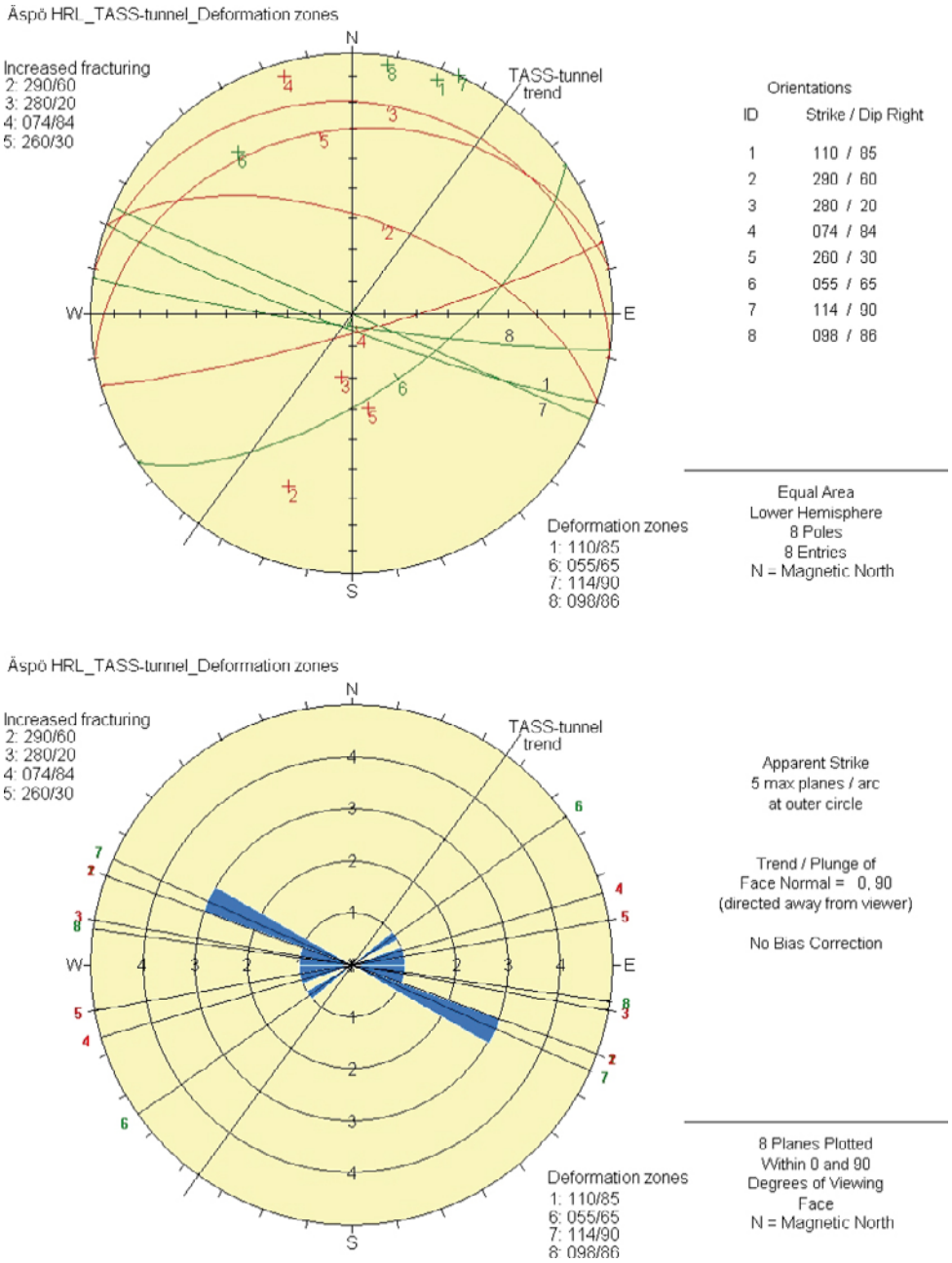

Figure 3-41. *Orientation of deformation zones in the TASS-tunnel presented as planes in a Schmidt net and joint rosette diagrams. The 216° trend of the TASS-tunnel is marked as a black line. Two zone categories occur in the TASS-tunnel: deformation zone proper brittle/ductile (green, 1, 6, 7 and 8) and increased fracturing (red, 2, 3, 4 and 5). N refers to magnetic north.*

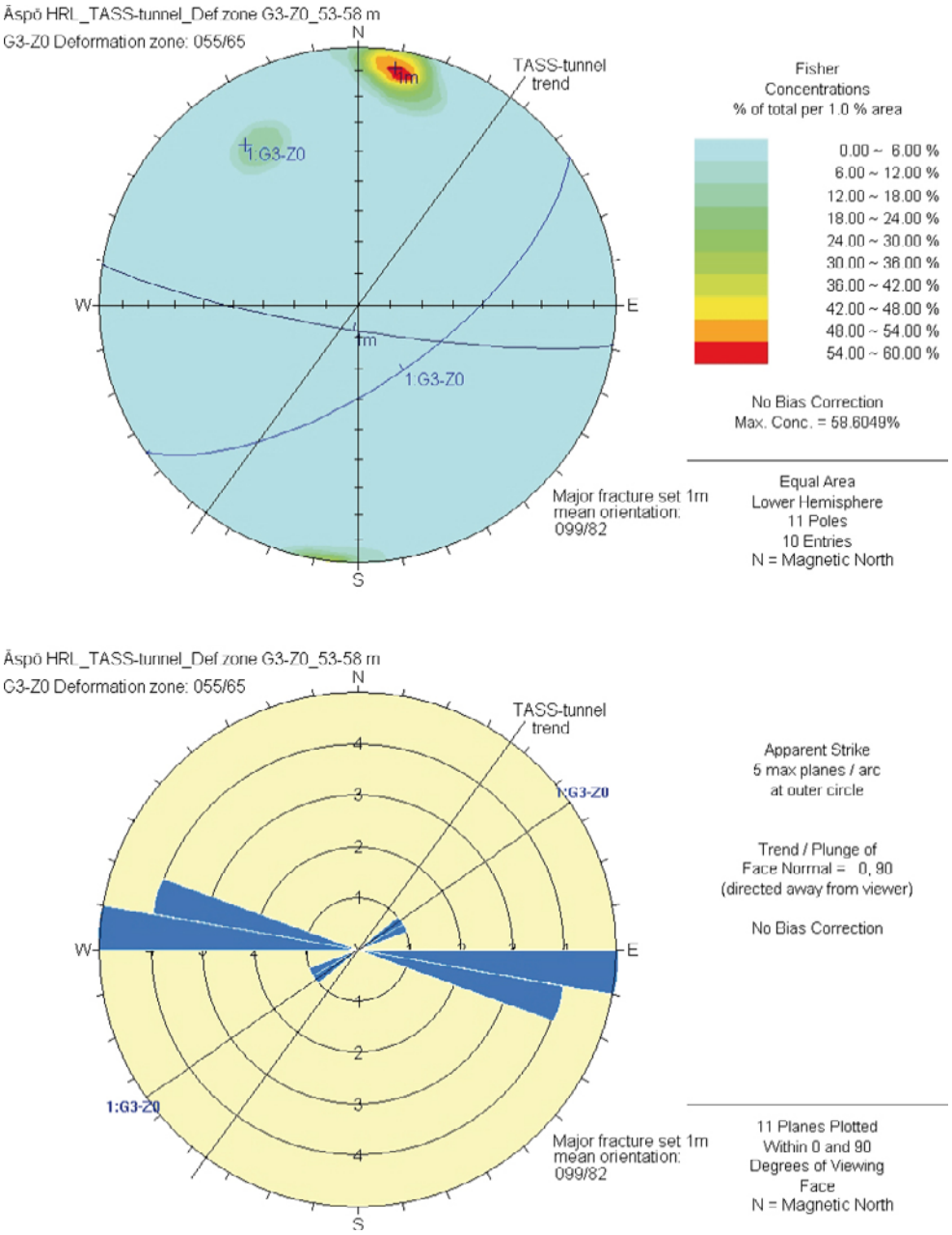

Figure 3-42. *Deformation zone G3-Z0 (zone no. 6 in Figure 3-41), with the orientation 055/65, which merges into a cross-cutting swarm of fractures with the average strike/dip of approximately 099/82 in the TASS-tunnel (see also Appendices IV A and IV B). The orientations of the zone and the fractures are presented in Schmidt net and joint rosette diagrams. The 216° trend of the TASS-tunnel is marked as a black line. N refers to magnetic north.*

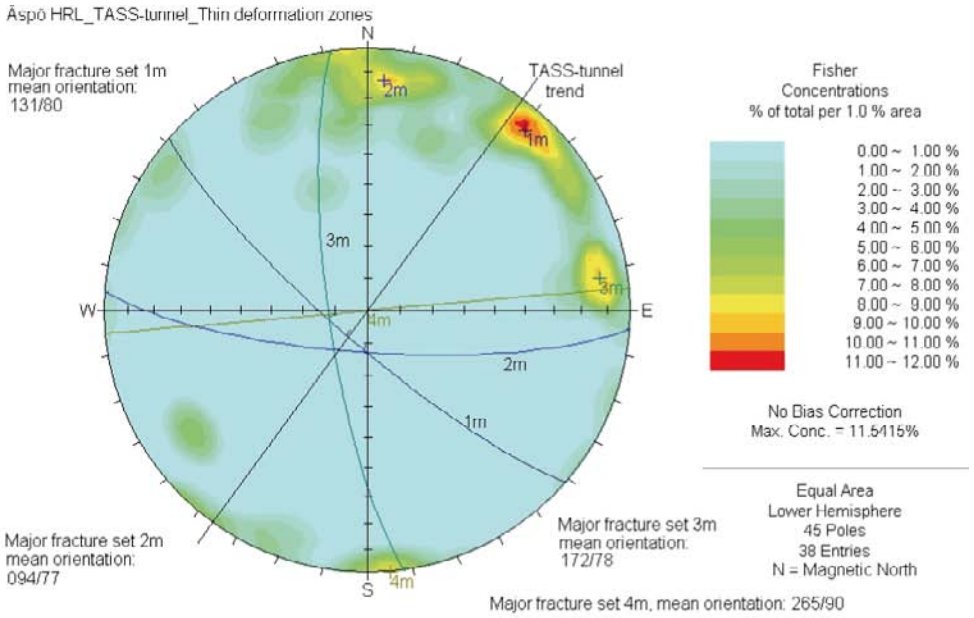
Äspö HRL_TASS-tunnel_Thin deformation zones
N
Major fracture set 1m
mean orientation:
131/80
TASS-tunnel
trend
2m
1m
3m
3m
W
E
4m
2m
1m
S
4m
Major fracture set 2m
mean orientation:
094/77
Major fracture set 3m
mean orientation:
172/78
Fisher
Concentrations
% of total per 1.0 % area
0.00 ~ 1.00 %
1.00 ~ 2.00 %
2.00 ~ 3.00 %
3.00 ~ 4.00 %
4.00 ~ 5.00 %
5.00 ~ 6.00 %
6.00 ~ 7.00 %
7.00 ~ 8.00 %
8.00 ~ 9.00 %
9.00 ~ 10.00 %
10.00 ~ 11.00 %
11.00 ~ 12.00 %
No Bias Correction
Max. Conc. = 11.5415%
Equal Area
Lower Hemisphere
45 Poles
38 Entries
N = Magnetic North
Major fracture set 4m, mean orientation: 265/90

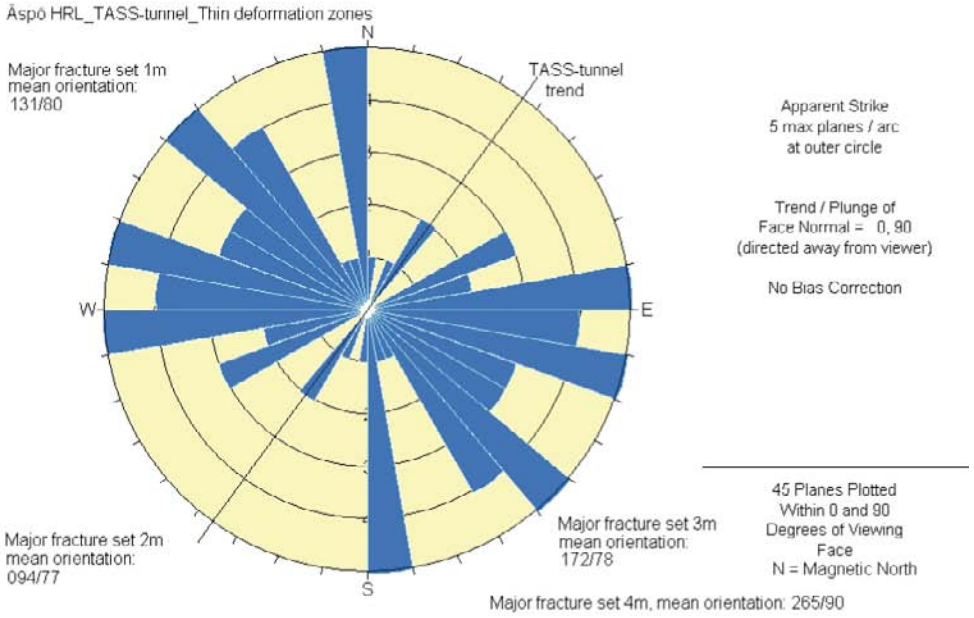
Äspö HRL_TASS-tunnel_Thin deformation zones
N
Major fracture set 1m
mean orientation:
131/80
TASS-tunnel
trend
W
E
S
Major fracture set 2m
mean orientation:
094/77
Major fracture set 3m
mean orientation:
172/78
Apparent Strike
5 max planes / arc
at outer circle
Trend / Plunge of
Face Normal = 0, 90
(directed away from viewer)
No Bias Correction
45 Planes Plotted
Within 0 and 90
Degrees of Viewing
Face
N = Magnetic North
Major fracture set 4m, mean orientation: 265/90

a)

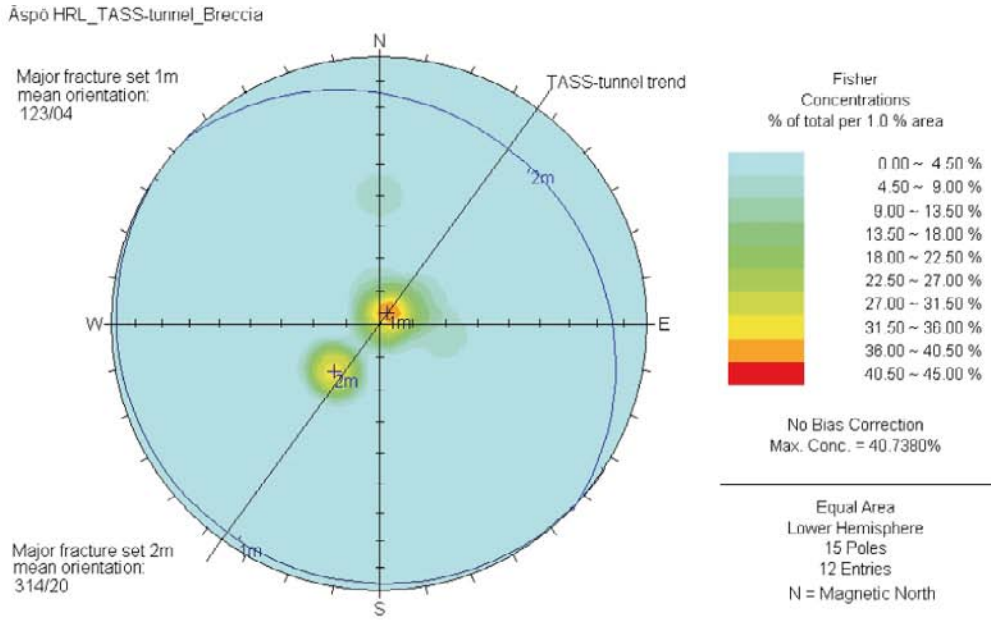

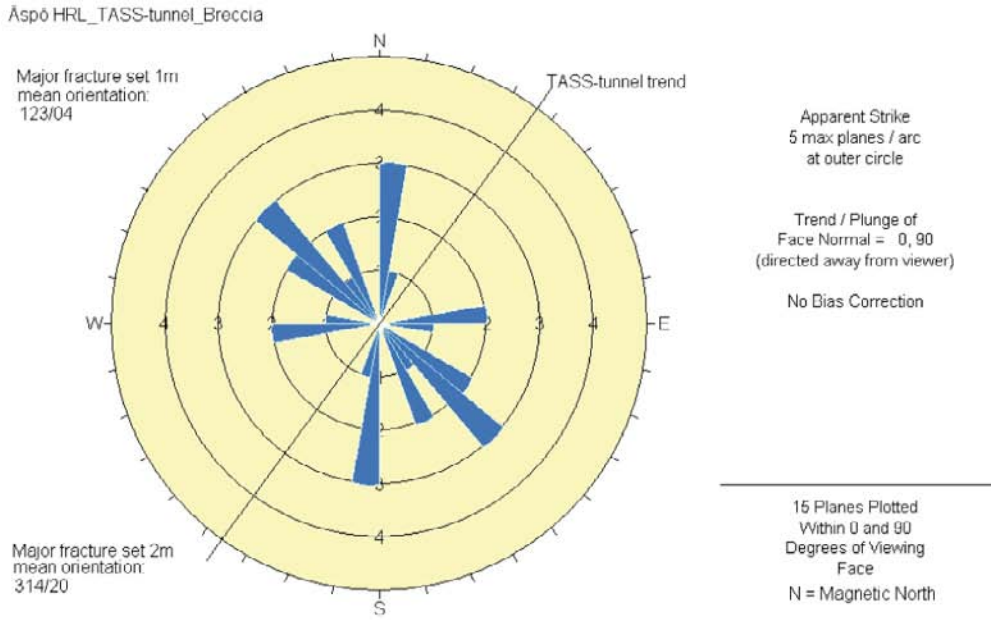

b)

Figure 3-43a–b. *Orientation of fractures that can be interpreted as thin deformation zones in the TASS-tunnel presented in Schmidt net and joint rosette diagrams. The 216° trend of the TASS-tunnel is marked as a black line. N refers to magnetic north.* ***a)*** *Thin deformation zones (less than approximately 10 cm), concentrating into three major fracture sets: 1m: 131/80, 2m: 094/77 and 3m: 172/78.* ***b)*** *Brecciated factures are mainly sub-horizontal and concentrate into two major fracture sets: 1m: 123/04 and 2m: 314/20. The north-south striking trend on the rosette diagram is partly caused by horizontal fractures that have the designated structural orientation 000/00.*

Figure 3-44. *Brecciated and oxidized Äspö diorite. Small fragments of Äspö diorite can be seen in an early epidote/prehnite filling. Note that some of this filling has in turn also been brecciated. Tunnel face 6.1 m, fractures 05 and 06 (see Appendix I B).*

3.2.6 Water leakage

The last aspect to be mapped on each mapping occasion was water leakage. Since the major reason for excavating the tunnel was to prove that the grouting compounds used could seal tunnels at the tentative depth of the final repository, occurrences of water were regarded to be of great importance. The water observations described below were used as input for further investigations that will not be dealt with in this report (see e.g. /Funehag and Emmelin 2010/).

Where possible, the quantity of water leakage is measured/estimated by counting drops of water (1 drop = approx. 0.25 ml or 0.00025 litres of water) or by using some sort of measuring vessel. Mostly, however, the quantity is only given in terms of damp/moist, wet or flow in accordance with the TMS code chart (SKBdoc 1252025, internal SKB document, Table 1-1). These leakage terms can be described as follows:

- Damp or moist refers to minor seepage, occasional drops or simply a moist fracture, area etc.
- Wet refers to seepage, minor flow or continuous dripping.
- Flow indicates that a continuous flow of water is present.

The source (fracture, bolt/borehole etc) of the leakage is recorded. When only a diffuse leakage can be observed from the rock surface, and no other source can be identified, the rock itself is regarded as the source. The term bolt/drill hole is used in the TMS code list (SKBdoc 1252025, internal SKB document, Table 1-1) to represent any kind of borehole, irrespective of diameter or length. In the TASS-tunnel, most of the water-bearing boreholes observed are grouting holes.

Since the planned tunnel sections were always sealed/grouted before excavation, major water inflows were rarely noted during geological mapping. The few major inflows that were registered within a mapping stage were grouted and sealed before the next rock excavation step (see Figure 2-7).

Table 3-10 shows the quantity of water that was measured or estimated and registered during the mapping (roof, walls, floor, all tunnel faces and EDZ-slot). The quantity from each of these observations has been summated in the "quantity" column of the table. This means that when leakage has been noted on more than one occasion, the quantity from each occasion has been added. It should be observed that the column headed "total number of observations" also includes observations in which the quantity of water could not be measured by counting drops or using a measuring device. In these conditions, it was frequently the case that the water merely formed a film or a moist patch on the rock surface. In the column headed "number of quantified observations", only the number of observations in which the quantity of water could be measured or estimated is listed.

On a few occasions, the flow of water was large enough to be measured by a measuring glass or bucket. This was, for example, the case with one of the grouted boreholes (KI0014B01) that was leaking (1.8–4.3 l/min) in each of the tunnel faces between sections 6.1–20.7 m. This leakage was observed and registered in five tunnel faces and the summated quantities are the main contributors to the large quantity of water (13.7 l/min) for bolt/boreholes in Table 3-10.

Table 3-10 and Table 3-11 include rock type with no data for "character of water leakage" and water quantity. This originates from the floor mapping of the first mapping stage (section 3–20.7 m), where the floor only had puddles of water owing to inflow from the walls and roof, but otherwise appeared to be dry. It is, however, acknowledged that a certain amount of water may seep through the floor itself, although no specific source can be found for it. Despite the fact that the water conditions regarding the floor were almost the same in the subsequent mapping stages as they were in Stage 1, it was decided that a certain amount of information should be given about them. In this context, the character of the leakage is mainly stated as being damp/moist and wet, where wet means that puddles of water had been formed.

Table 3-10 and Figure 3-45 show that for bolt/boreholes, the number of observations with the leakage character wet is higher than those with the leakage character moist. This is in contrast to other objects where moist is the most common character (has the highest number of observations). The reason for this may partly be that the bolt/boreholes have cut through more than one water-bearing fracture.

Table 3-10. Water leakage in the TASS-tunnel, all observations included (roof, walls, floor, all tunnel faces and EDZ-slot).

Object from which the water originates	Number of observations	Character of water leakage	Total number of observations	Number of quantified observations	Drop counting quantity (litre/minute)
Rock type	105	–	1	–	–
		Moist	63	12	0.0095
		Wet	23	6	0.0268
		Flow	–	–	–
Fracture	185	Moist	118	11	0.0046
		Wet	33	18	0.0513
		Flow	1	4	4.2
Fracture Zone	6	Moist	3	1	0.0003
		Wet	2	–	
		Flow	–	–	–
Bolt/Borehole	35	Moist	10	–	–
		Wet	13	5	0.0445
		Flow	1	6	13.7*
Total	**331**		**268**	**63**	**~18.0**

* Measured with measuring vessel.

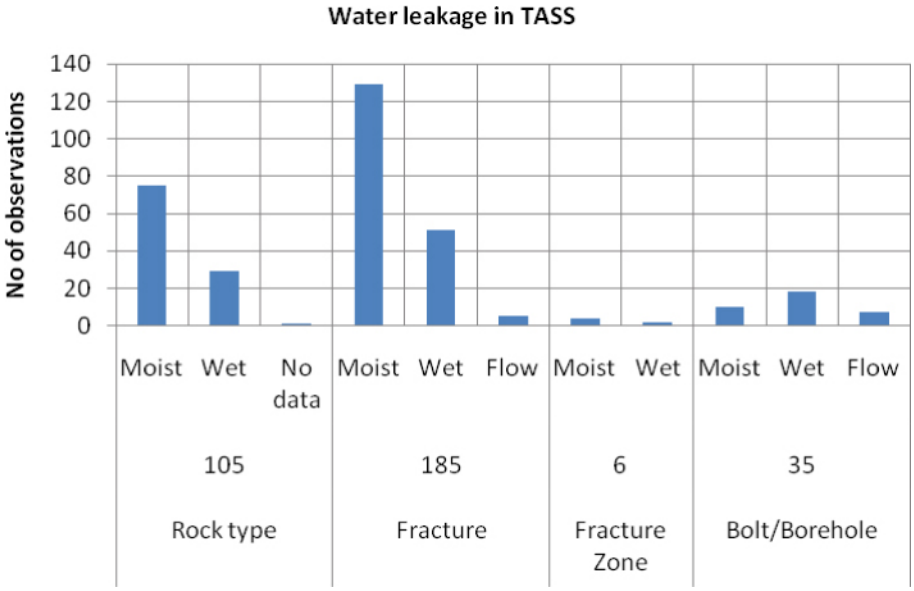

Figure 3-45. *Distribution of water leakage in the TASS-tunnel. The figures below represent the total number of observations for each category.*

Table 3-11 includes only observations from the TASS-tunnel as it was when completed (roof, walls, floor, EDZ-slot and last tunnel face at 80.7 m). Thus, borehole KI0014B01 (13.7 l/min) and all tunnel faces except the last one have been excluded from the table. Fracture P-35 (1.6 l/min) from Mapping Stage 1 has also been excluded from the table, since it is known to have been grouted and sealed before Mapping Stage 2 was excavated. The location of fracture P-35 can be found in Appendix II A, at approximately section 20 m and 2 m up from the floor on the right-hand wall.

The orientation of water-bearing fractures can be seen in Figure 3-46. The figure shows two distinct concentrations representing sub-horizontal and gently dipping fractures respectively. Steeply dipping fractures form less, but still rather distinct concentrations. It is worth mentioning that the strike is approximately the same for both the steeply dipping and the gently dipping fractures. The strike of the sub-horizontal fractures is more ambiguous.

Table 3-11. Water leakage in the completed TASS-tunnel (roof, walls, floor, EDZ-slot and last tunnel face at 80.7 m, i.e. all faces except for the last face at 80.7 m are excluded).

Object from which the water originates	Number of observations	Character of water leakage	Total number of observations	Number of quantified observations	Drop counting quantity (litre/minute)
Rock type	85	–	1	–	–
		Moist	47	12	0.0095
		Wet	19	6	0.0268
		Flow	–	–	–
Fracture	148*	Moist	90	11	0.0046
		Wet	26	18	0.0513
		Flow	1	2*	1.1000*
Fracture Zone	6	Moist	3	1	0.0003
		Wet	2	–	–
		Flow	–	–	–
Bolt/Borehole	15	Moist	4	–	–
		Wet	5	5	0.0445
		Flow	1	–	–
Total	**254**		**199**	**55***	**~1.2***

* Fracture P-35 (1.6 l/min) from Mapping Stage 1 has been excluded from the table since it was grouted and sealed before Mapping Stage 2 was excavated.

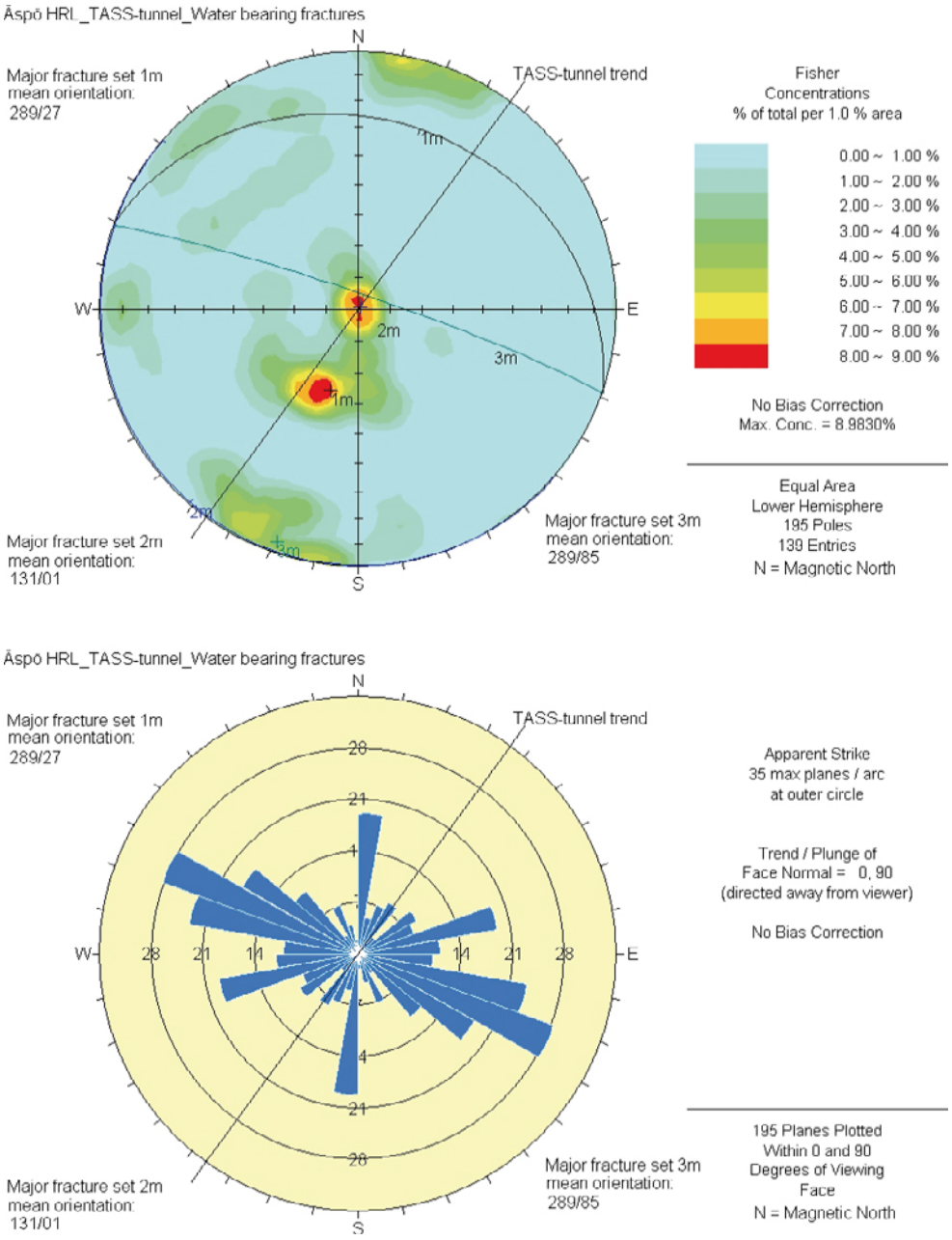

Figure 3-46. *Orientation of all water-bearing fractures in the TASS-tunnel presented in Schmidt net and joint rosette diagrams. The 216° trend of the TASS-tunnel is marked as a black line. Two main orientation sets can be seen, namely 1m: 289/27 and 2m: 131/01, as well as a less prominent set 3m: 289/85. The north-south striking trend on the rosette diagram is mainly caused by horizontal fractures that have the designated structural orientation 000/00 (see also Figure 3-24). N refers to magnetic north.*

Additional water measurements were conducted in the TASS-tunnel, measurements on the floor between each stage and detailed measurements of individual leaking points from the roof. These results are not discussed here /Funehag and Emmelin 2010/.

The total water inflow in the tunnel measured in a number of weirs (Figure 3-47), after completion but before the grouting that took place after the excavation, was 1.5 litre/minute per 70 m tunnel (1.3 litre/minute per 60 m tunnel). This is thus a little more than the allowed or target inflow limit of 1 litre/minute per 60 m tunnel. The water inflow recorded in the geological mapping is slightly less since not all leakage has been quantified.

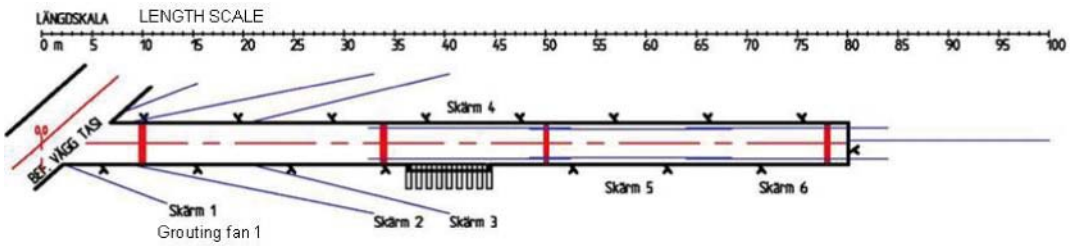

Figure 3-47. *Principal drawing of the TASS-tunnel. The pre-grouting fans are marked with blue lines and the weirs with thick red lines across the tunnel (Skärm 1, Skärm 2 etc = Grouting Fan 1, Grouting Fan 2 etc.). Drawing modified from /Funehag 2008/.*

3.2.7 Rock quality

In order to determine the rock quality, a slightly simplified version of the RMR system (Rock Mass Rating) has been used, e.g. /Bieniawski 1973, pp 335–344, 1984, pp 97–133 and 1989, p 251, cited in Singh and Goel 1999, pp 34–46, Hoek and Brown 1982, p 26/. The only difference between this rating and the RMR used by SKB is that the ratings 2, 1 and 0 have been omitted for the parameter "strength of intact rock material" and that the rating for "the joint orientation effect on tunnels, dip 0–20°" has been set at –10 instead of –5.

In Figure 3-48, the linear RMR trend line of the tunnel faces lies between 73 and 71 with a slightly negative trend. Single values range from 66 to 81. The trend line of the floor lies between RMR values 65 and 67 with a slightly positive trend and single values ranging between 58 and 73. The walls and roof have an almost identical trend as the tunnel faces, although slightly lower between RMR values 71 and 69 with single values varying between 67 and 74 (Figure 3-48). The negative trends of the trend lines for the tunnel faces and walls and roof may indicate a slightly decreasing rock quality as the tunnel proceeds, while the positive trend for the floor indicates the opposite conditions. It should, however, be mentioned that the difference between trends is very small.

The average RMR value for the TASS-tunnel is approximately 70. This is in the middle of the rock mass class "good rock", RMR = 61–80 (Figure 3-48b). It is only the floor in section 20.7–48.7 that will fall within the rock mass class "fair rock", RMR = 41–60 (Figure 3-48a). The large number of sub-horizontal to gently dipping fractures, mostly with unfavourable orientations, has a rather large impact on the RMR-values due to the negative effect (–10) on the joint orientation parameter.

3.3 Tunnel faces

The tunnel faces were mapped after each excavation round and the various occasions are shown in Table 2-1.

The geological mapping and photos of the tunnel faces are shown in Appendix I. The mapped tunnel faces presented are folded down and projected in the same way as the photos are, as opposed to Figures 2-3 and 3-1.

3.3.1 Rock types

The rock types are the same as in other parts of the TASS-tunnel. The overall distribution of the various rock types resembles that of the walls and roof (Figures 3-3b and d). It is only the amount of fine-grained granite that is slightly higher in the rock type distribution plot of all tunnel faces compared to all the walls and roof plot; 8% and 3% respectively. This is at the cost of a certain amount of Äspö diorite in the tunnel faces. How the rock types are distributed, in each single tunnel face, can be seen from the tables in Appendix VII C.

In some tunnel faces (sections 24.84, 32.94, 37.50, and 42.14 m), Äspö diorite is the sole rock type. The tunnel face at section 45.72 m also includes a certain amount of mafic rock that appears as xenoliths in the Äspö diorite. Normally, these mafic xenoliths are too small to be mapped, but are regarded as a part of the Äspö diorite.

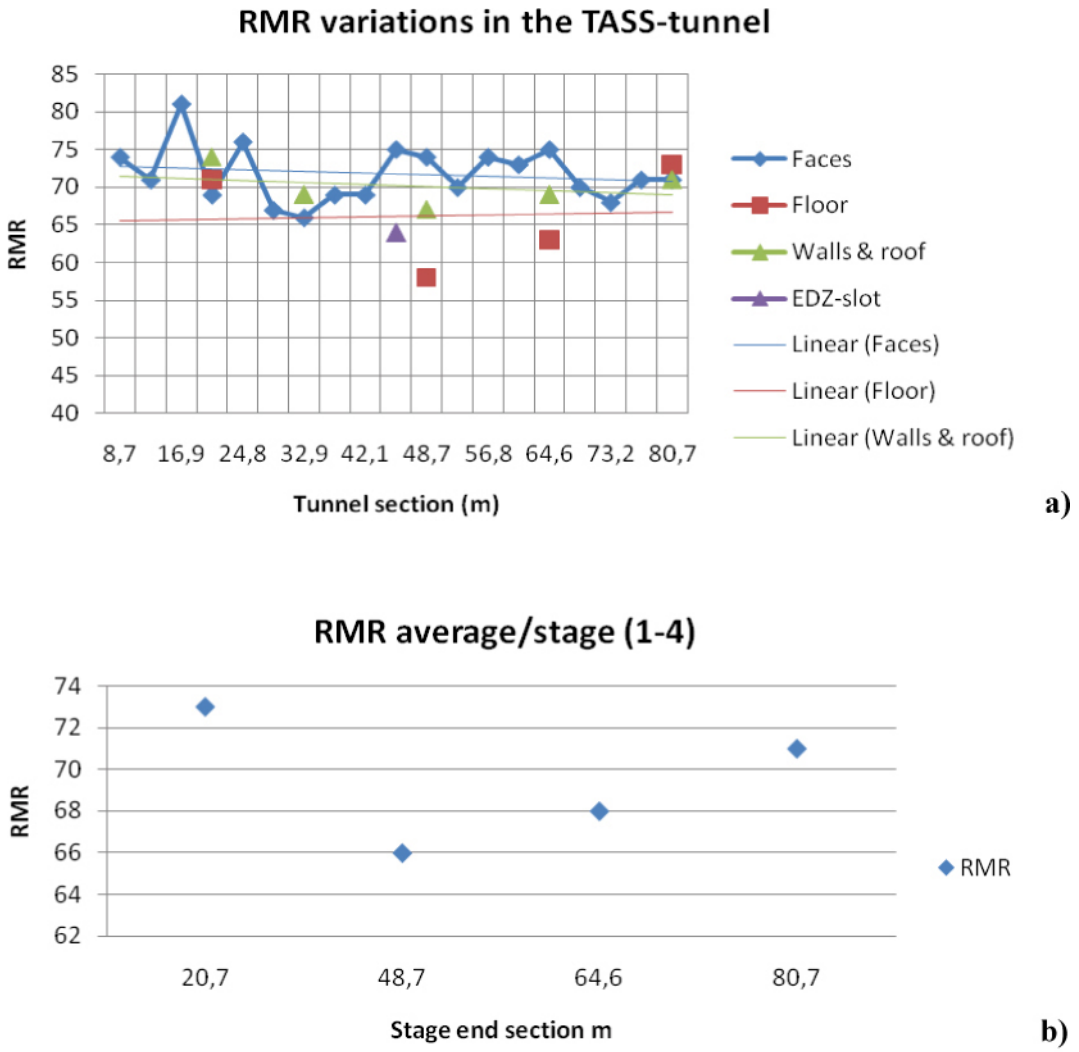

Figure 3-48a–b. *RMR variations in the TASS-tunnel.* ***a)*** *Tunnel section in m refers to the tunnel faces. The blue diamonds refer to each of the mapped tunnel faces. The reddish brown square markings (tunnel floor), the green triangles (walls and roof) and the violet triangle (EDZ-slot) are placed at the end of each mapped section but represent the whole section. Linear (linjär) trend lines have been marked out for the RMR values of the faces, floor and walls & roof.* ***b)*** *Average RMR value for the various stages (Stages 1, 2, 3 and 4).*

The major occurrences of fine-grained granite (exposure exceeding 10% of the tunnel face area) are found in the sections 6.1 m (approx. 44%), 8.7 m (22%), 56.77 m (11%), 77.14 m (36%), and 80.73 m (20%).

3.3.2 Fractures and deformation zones

When all fractures from the mapping of tunnel faces in the TASS-tunnel are plotted on a stereo diagram and a rose diagram, as in Figure 3-49, the general patterns are comparable with those of the diagrams shown in Figure 3-24 showing all the TASS-tunnel fractures. The mapping of the faces shows a clear domination of sub-horizontal fractures and thereby a relatively diversified strike direction in the rose diagram.

One explanation for the relative absence of the northwest to southeast striking fractures is the direction of the TASS-tunnel, which is roughly perpendicular to the dominating strike, thus yielding minimal exposure for those fractures in the faces as shown in the number of larger exposed fracture surfaces (smooth joints) that occur in some faces. See the geological mapping and photos of the tunnel faces in Appendix I.

Only one deformation zone was mapped in the faces. This occurred at the end of Mapping Stage 2 at a tunnel length of 48.7 m, and is of the increased fracturing category, see Figure 3-41 where it has ID 3 with an orientation of 280/20. It is only clearly visible in the lowest part of the front and to some extent in the floor and lower part of the right-hand wall, see maps in Appendices I, III B, III C, IV A and IV B.

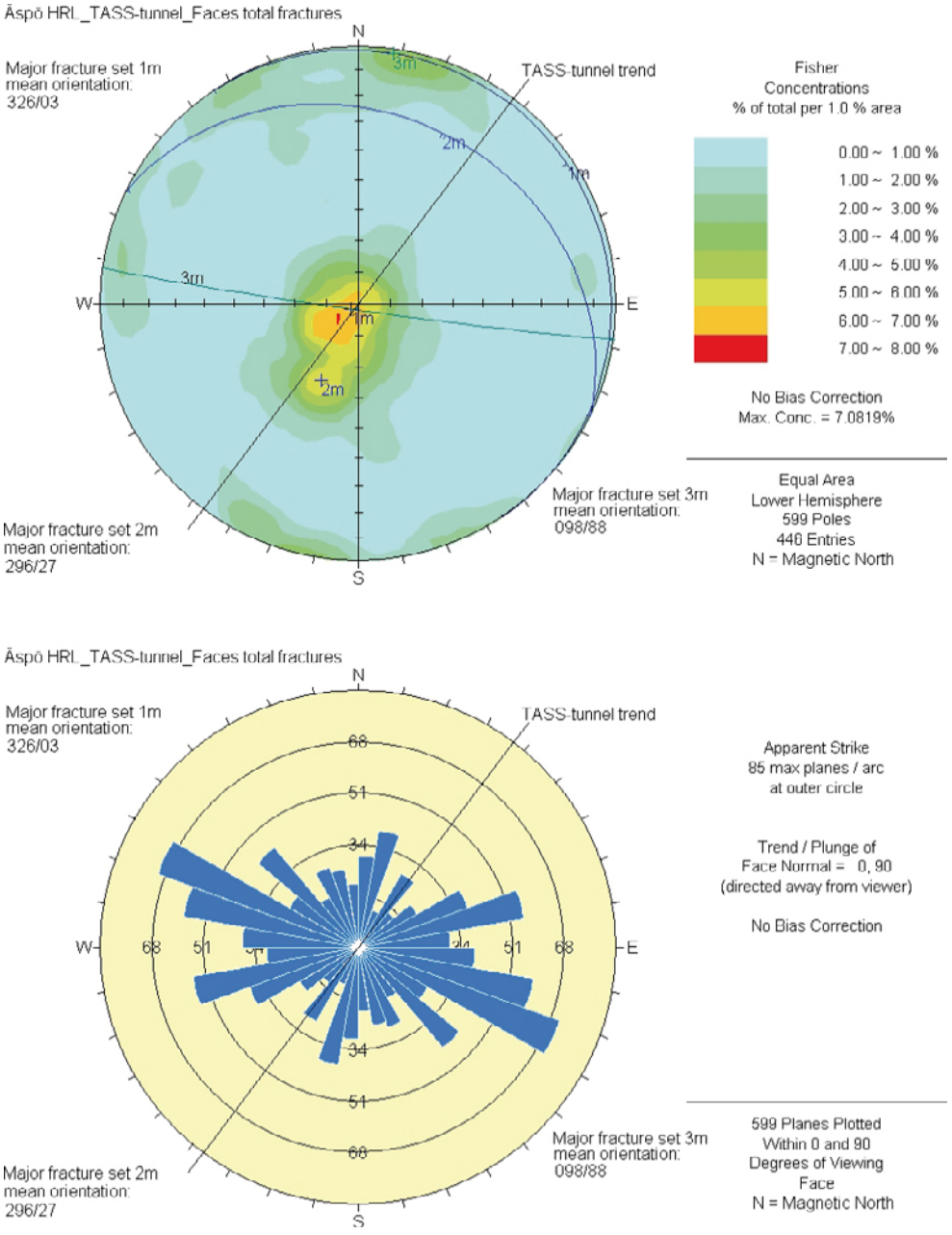

Figure 3-49. *Fracture orientations from all the faces in the TASS-tunnel presented in Schmidt net and joint rosette diagrams. The 216° trend of the TASS-tunnel is marked as a black line. One main orientation set can be seen, namely 1m: 326/03, as well as two less prominent sets 2m: 296/27 and 3m: 098/88. N refers to magnetic north.*

3.3.3 Water leakage

The orientation of water-bearing fractures can be seen in Figure 3-50, indicating that northwest to southeast striking and steeply dipping fractures (mean orientation: 298/80) yield most of the water in the faces of the TASS-tunnel. It coincides roughly with the steeply dipping orientation of all water-bearing fractures in the TASS-tunnel shown in Figure 3-46, where it is the least prominent of the three major sets with an orientation of: 289/85.

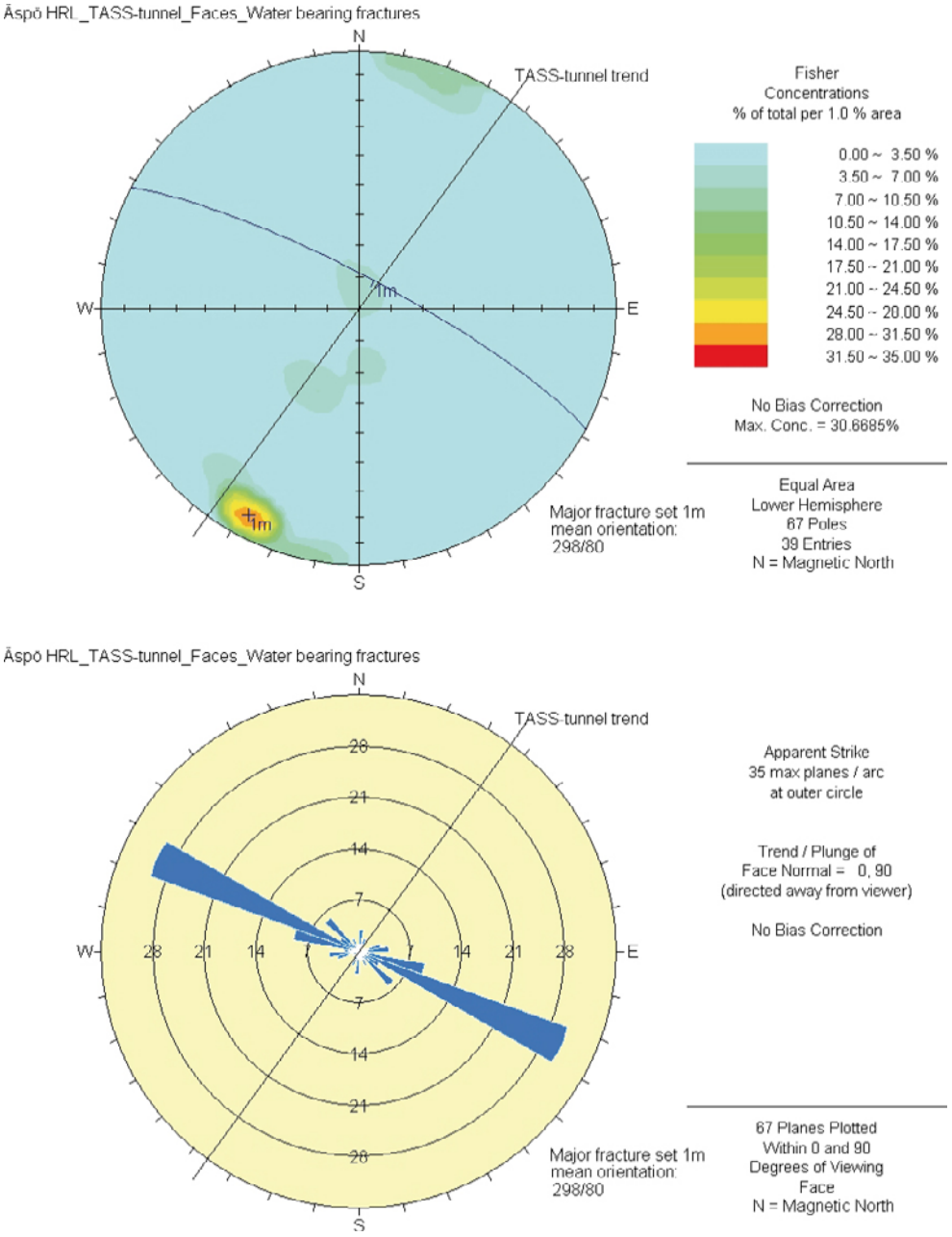

Figure 3-50. *Orientation of all water-bearing fractures in the faces of the TASS-tunnel presented in Schmidt net and joint rosette diagrams. The 216° trend of the TASS-tunnel is marked as a black line. One main orientation set can be seen, namely 1m: 298/80. N refers to magnetic north.*

3.3.4 Rock quality

The diagram in Figure 3-48a shows how the rock quality varies in the tunnel faces. The trend line runs between RMR 70–73 with a slightly negative trend. The individual RMR values vary approximately between 65 and 80, but still within the limits of good rock.

3.4 Stage mapping

Besides the tunnel face mapping, the walls, roof and floor of the TASS-tunnel were mapped during periods when there was a halt in excavation. These mapping occasions are shown in Figure 2-7 and in Table 2-1. There were four major halts and thus four major stage mapping occasions when all the rock surfaces of a certain tunnel section were cleaned and mapped. Stage Number 2 was, however, divided into two sub-stages (2a and 2b), where Stage 2a only included roof, walls and the current tunnel face whereas Stage 2b, in addition to roof, walls and tunnel face, also included the tunnel floor of Stages 2a and 2 b.

3.4.1 Mapping Stage 1; 3–20.7 m

The maps of the first mapping stage, namely tunnel faces (F), walls and roof (P) and floor (G) between 3–20.7 m tunnel length, can be found in Appendices I and II. Section 0 m of the TASS-tunnel is located on the centre line of the TASI-tunnel from which the TASS-tunnel emanates. The actual tunnel begins at about section 5 m (centre line) or at 3–7 m depending on whether the right- or left-hand wall is referred to.

Rock types

Most of the rock types found elsewhere in the TASS-tunnel are present in tunnel section 3–20.7 m. It is only mafic rock that has not been distinguished. The diagrams in Figure 3-51a–d illustrate how the rock type distribution varies in different parts of the tunnel segment (total, walls and roof, floor and all tunnel faces. See also Appendix VII for rock type distribution as a percentage). The overall rock type distribution (Figure 3-51a) of the tunnel segment is similar to that of the entire tunnel floor (Figure 3-3c and Appendix VII).

Äspö diorite

Almost 90% of the tunnel segment is composed of Äspö diorite. As can be seen in Figure 3-51, 64% of the rock mass has been regarded as fresh Äspö diorite. However, oxidized Äspö diorite constitutes a rather large proportion (23%) of the rock mass. This is a higher percentage than the average for the entire TASS-tunnel (7% oxidized Äspö diorite, Figure 3-3a). More than 50% of the tunnel floor of the 0-20.7 m tunnel section is composed of oxidized Äspö diorite (Figure 3-51c and Appendix VII). Often, the oxidized variety of Äspö diorite is associated with sub-horizontal fractures similar to the ones shown, for example, in Figures 3-8a and 3-16.

Fine-grained granite

Fine-grained granite constitutes a total of 7% of the rock mass. However, this rock type can be divided into fine-grained and medium-grained varieties, each of which constitutes 3 and 4% respectively. The medium-grained variety of "fine-grained granite" appears mainly as an approximately 1 m wide dike in the floor, roof and right-hand wall. The orientation of the dyke is approximately 245/85°. This dyke is cut by an approximately 0.1 m wide, 195–210° striking and 70–80° dipping dyke of fine-grained granite.

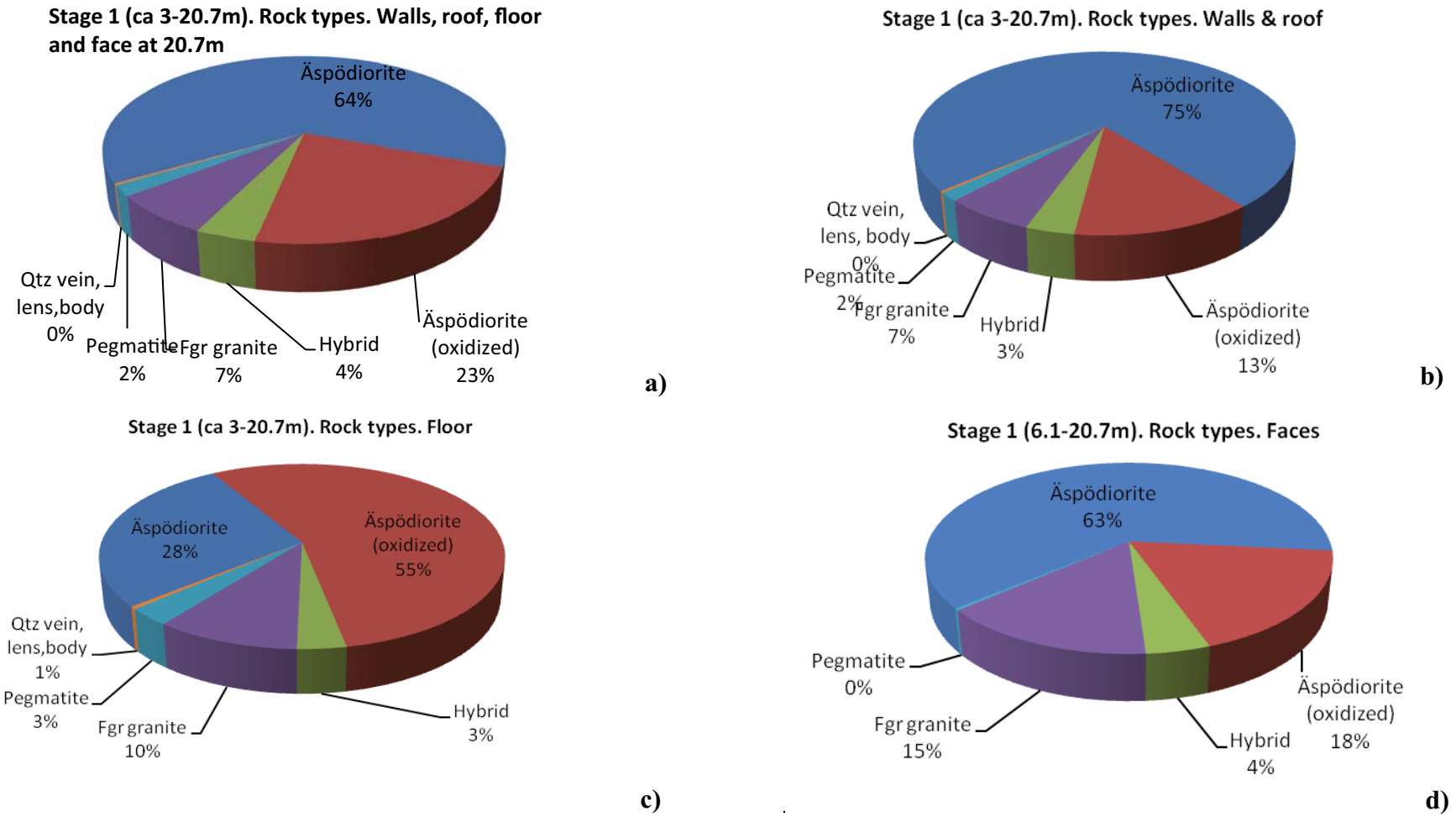

Figure 3-51a–d. *Rock type distribution in the tunnel segment 3–20.7 m of the TASS-tunnel. (0% in the diagrams means >0 to <1%).* ***a)*** *Walls, roof, floor and last tunnel face of the tunnel section,* ***b)*** *Walls and roof of the tunnel section,* ***c)*** *Floor of the tunnel section and* ***d)*** *All tunnel faces of the section (1st face to be mapped is at 6.1 m).*

Pegmatite and quartz

A 0.1–0.2 m wide, 290° striking and 80° dipping pegmatite dyke with elongated quartz inclusions/minor bodies cross-cuts the tunnel at about section 13–14 m. The same dyke is displaced 0.5 m by a prominent sub-horizontal fracture as can be clearly seen in the lower part of the left-hand wall (Figure 3-8a). Some of the quartz, mapped as a separate rock type, cross-cuts the same pegmatite in the left-hand wall at about section 12–14 m (Figures 3-8a and 3-9). The orientation of this approximately 1.5 m long and 0.02–0.1 m wide quartz lens is about 70/25°. At section 12 m, another approximately 0.1 m wide pegmatite dyke with an orientation of 303/75° cross-cuts the floor. Only minor proportions of the rock mass, i.e. 2% and 0.3% respectively, are composed of pegmatite and quartz.

Hybrid rock

Some hybrid rock (4%) forms a 0.1–0.5 m wide belt across the tunnel at about section 14–15 m, but also appears in patches at a number of places.

Rock boundaries/contacts

The contacts of the rock types follow the general pattern (see Section 3.2.2, Rock boundaries/contacts). Most of them are sharp and tight, and it is mainly between the oxidized variety of Äspö diorite and/or hybrid rock and surrounding rock types that the boundaries are diffuse. The orientations of the contacts are often irregular. Some, however, have been exemplified as the orientations of the dykes.

Fractures and deformation zones

When all mapped fractures in the first mapping stage, i.e. floor (G), walls and roof (P) and face (F) at 20.7 m tunnel length, are plotted on a stereogram one main fracture set becomes apparent: 097/87 (see 1m in Figure 3-52). It coincides well with the main fracture set of all fracture orientations from the TASS-tunnel as seen in Figure 3-24, where the main fracture set has a mean orientation of: 098/87. A less prominent orientation (2m), i.e. 360/78, can also be seen in Figure 3-52. This fracture set can also be seen in the total fracture diagram of Figure 3-24, but only very weakly.

Water leakage

The orientation of water-bearing fractures can be seen in Figure 3-53. The figure shows that northwest to southeast striking and steeply dipping fractures are the most common of the water-bearing fractures in the first mapping stage of the TASS-tunnel (1m and 2m with orientations 305/79 and 107/84 respectively). These orientations coincide roughly with the least prominent of the three major water-bearing fracture sets (orientation: 289/85) in the plots of all water-bearing fractures in the TASS-tunnel (Figure 3-46).

Two less prominent orientations are also shown in Figure 3-53, namely a north-south striking set (3m, 359/75) and a sub-horizontal fracture set (4m, 110/03), cf. Figure 3-46.

Rock quality

The average RMR value of the entire tunnel section 0–20.7 m is approximately 73 (Figure 3-48, good rock = 61–80). The RMR of the floor is 71 and that of the walls and roof 74. The RMR value of the tunnel faces within Mapping Stage 1 varies between 69 and 81 (Figure 3-48). Although the RMR value of the first complete tunnel face (8.7 m) to be mapped has been recorded as RMR = 74, the rock quality of the tunnel opening itself must be regarded as less than that. This is partly due to the acute angle (42°) between the TASS-tunnel and TASI-tunnel and the pillar-shaped blocks that appear on the left-hand side of the tunnel opening (Figure 3-23).

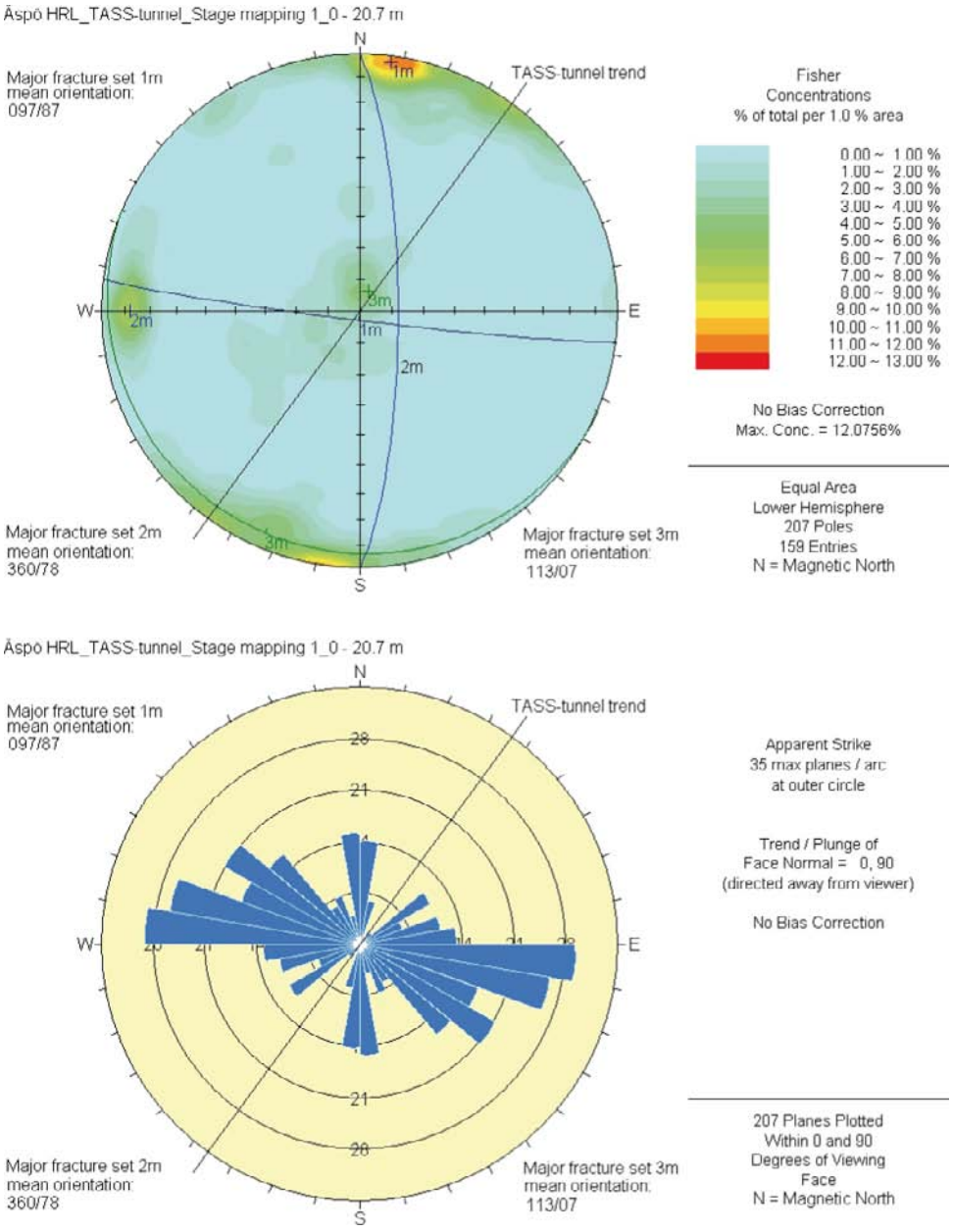

Figure 3-52. *Fracture orientations from the first stage mapping (3–20.7 m) of the TASS-tunnel presented in Schmidt net and joint rosette diagrams. The 216° trend of the TASS-tunnel is marked as a black line. One main orientation set can be seen, namely 1m: 097/87, as well as two less prominent sets, 2m: 360/78 and 3m: 113/07. The north-south striking trend on the rosette diagram is to some degree caused by horizontal fractures that have the designated structural orientation 000/00. N refers to magnetic north.*

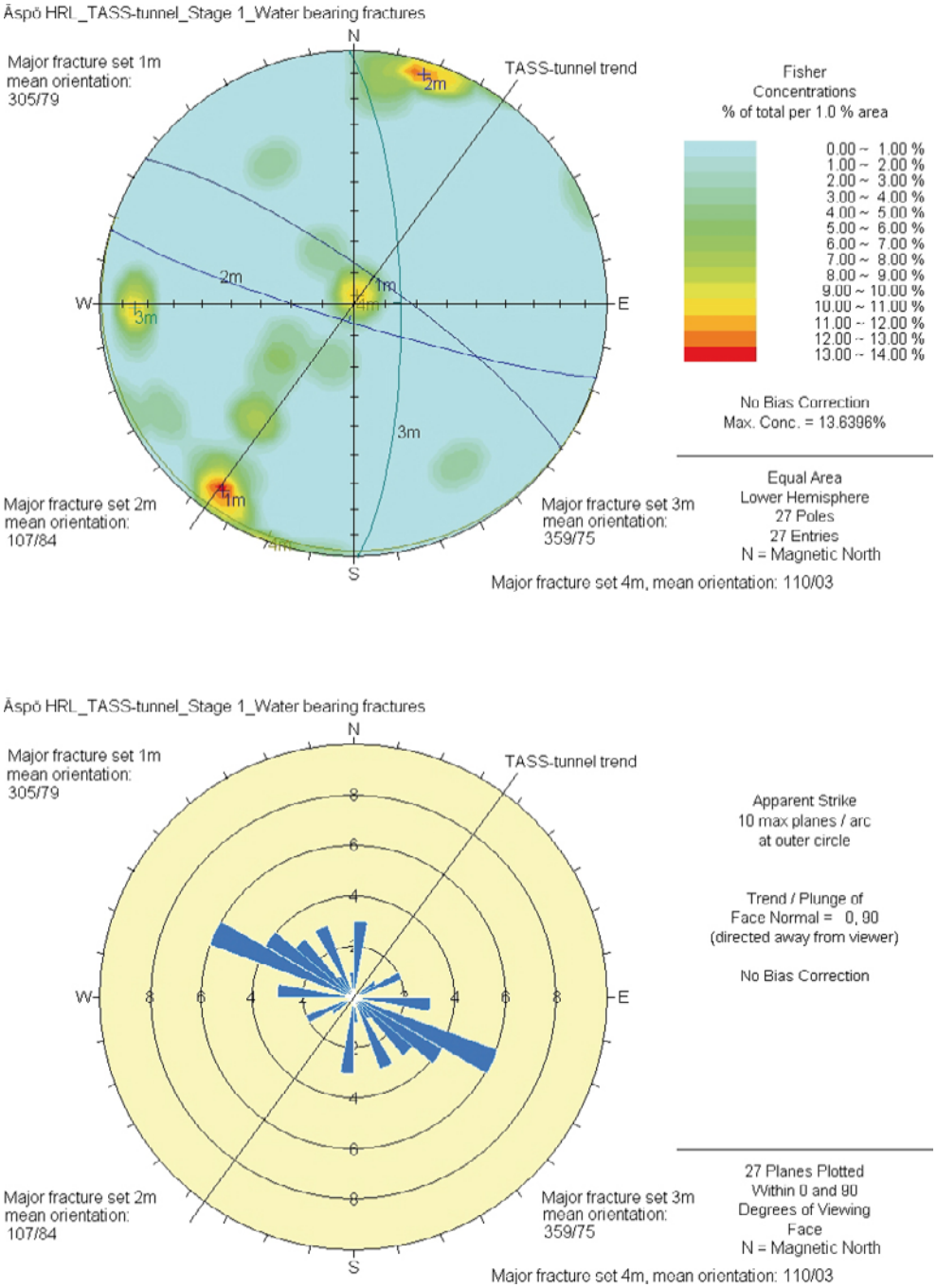

Figure 3-53. *Orientation of all water-bearing fractures from the first stage mapping (0–20.7 m) of the TASS-tunnel presented in Schmidt net and joint rosette diagrams. The 216° trend of the TASS-tunnel is marked as a black line. Two main orientation sets can be seen, namely 1m: 305/79 and 2m: 107/84, as well as two less prominent sets, 3m: 359/75 and 4m: 110/03. The north-south striking trend on the rosette diagram is partly caused by horizontal fractures that have the designated structural orientation 000/00. N refers to magnetic north.*

3.4.2 Mapping Stage 2; 20.7–48.7 m

The maps of the second mapping stage (Stage 2), i.e. tunnel faces (F), walls and roof (P) and floor (G) between 20.7–48.7 m tunnel lengths, can be found in Appendices I and III. This mapping stage was divided into two parts (Stages 2a and 2b).

Stage 2a included roof and walls between section 20.7 and 32.9 m and tunnel face at section 32.9 m

Stage 2b included roof and walls between section 32.9 m and 48.7 m, tunnel face at section 48.7 m and floor between section 20.7 and 48.7 m.

It is within this section of the TASS-tunnel that the EDZ-slot /Olsson et al. 2009/ is situated on the right-hand tunnel wall (NW wall), section 36.4–44.4 m. Although the mapping of the slot took place later than the mapping of Stage 2, it will be dealt with here (Appendix VI). The main reason for mapping the EDZ-slot was to connect fractures from the ordinary stage mapping with the fractures in the slot. However, some additional fractures were added, particular those that were found to be carrying water.

Rock types

All rock types are represented within this tunnel section and their distribution is shown in Figure 3-54 and Appendix VII.

Äspö diorite

The Äspö diorite constitutes 98% of rock volume and thus totally dominates this tunnel section. Mostly, this rock has been regarded as fresh, 92% of the rock mass, and up to about 6% as oxidized rock. Most of the oxidized Äspö diorite appears in the floor where it constitutes almost 20% of the rock mass (Figure 3-54c). One of the occurrences is found between section 37–39 m on the left half of the floor and another one on the right side of the floor between sections 42–47 m. Between sections 38–46 m in the lower part of the left-hand wall, oxidized Äspö diorite has been distinguished along a sub-horizontal fracture. No oxidized Äspö diorite has been recorded in the faces of the current tunnel section (diagram in Figure 3-54d). Here, it may form narrow oxidized borders to some of the fractures, and has thus either been recorded as such or included in the hybrid rock.

Only minor amounts of fine-grained granite, pegmatite, mafic rock and hybrid rock have been observed (1%, <1%, <1%, and 1% respectively).

Fine-grained granite

An example of fine-grained granite appears in the roof at about section 24 m and can be traced in the left-hand (SE) wall at about section 28 m and diagonally across part of the floor. This 0.05–0.2 m wide dyke has 0.01–0.02 m wide pegmatite borders and a mean orientation of 136/88°. Another fine-grained granite dyke, 0.1–0.3 m wide and oriented 346/86°, appears in the right-hand part of the roof and in the right wall, section 20–30 m. Altogether, the fine-grained granite constitutes only 1% of the rock mass in this section of the TASS-tunnel

Pegmatite

Pegmatite appears, for example, as a 0.1 m wide dyke with an orientation of 95/86° in the left-hand wall and roof at section 30.5 m. Some pegmatite also occurs in the left-hand side of the floor within section 31–33 m. Only <1% of the rock mass consists of pegmatite.

Mafic rock – undifferentiated

Mafic rock is almost absent (<1%) within the Mapping Stage 2 tunnel section. It has only been recorded in one of the tunnel faces, section 45.7 m. Here, mafic rock constitutes about 2% of the tunnel face area (Appendix VII) and appears as elongated xenoliths in Äspö diorite.

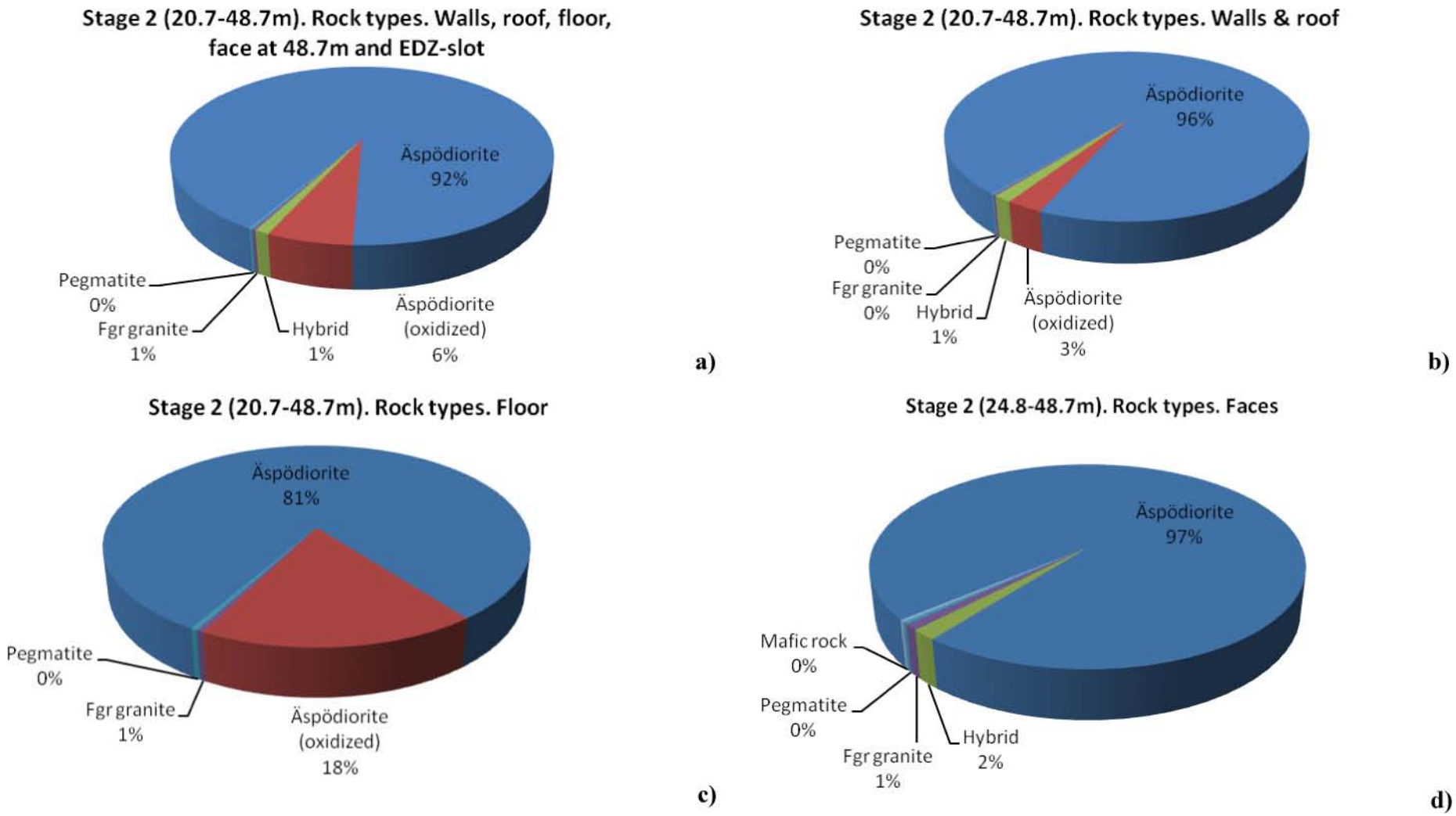

Figure 3-54a–d. *Rock type distribution in the tunnel segment 20.7–48.7 m of the TASS-tunnel (0% in the diagrams means >0 to <1%).* ***a)*** *Walls, roof, floor and last tunnel face of the tunnel section,* ***b)*** *Walls and roof of the tunnel section,* ***c)*** *Floor of the tunnel section and* ***d)*** *All tunnel faces of the section (the first face to be mapped is at 24.8 m).*

Hybrid rock

Most of the hybrid rock has been recorded in the right-hand side of the roof within section 22–30 m. A total of 1% of the rock mass within Stage 2 consists of hybrid rock.

Rock types of the EDZ-slot

The rock types of the EDZ-slot are included in diagram a) of Figure 3-54. Äspö diorite is the only rock type present. The predominant part – 89% – is considered to be fresh rock whereas 11% is considered to be oxidized (Appendix VII D). The oxidized Äspö diorite appears within section 38–42 m of the slot floor (Appendix VI).

Rock boundaries/contacts

The rock contacts of the current mapping section and stage follow the general pattern (see Section 3.2.2, Rock boundaries/contacts). Most of them are sharp and tight, and it is mainly between the oxidized variety of Äspö diorite and/or hybrid rock and surrounding rock types that diffuse boundaries appear.

Fractures and deformation zones

When all mapped fractures in the second mapping stage, i.e. floor (G), walls and roof (P2a and P2b), face (F) at 48.7 m tunnel length and EDZ-slot are plotted on a stereogram, three main fracture sets become apparent (see Figure 3-55). All three coincide fairly well with the main fracture sets in the TASS-tunnel as a whole (Figure 3-24). A slight difference in the concentrations of gently dipping fractures can, however, be noticed when the two diagrams are compared.

Major fracture set 1m of Stage 2 mapping: 285/27 coincides with major fracture set 3m in the total fracture plot (orientation 295/22, Figure 3-24). Major fracture set 2m of Stage 2 mapping: 094/87 coincides with major fracture set 1m of total fracture plot (orientation 098/87, Figure 3-24). Lastly, major fracture set 3m of Stage 2 mapping: 069/01 coincides with major fracture set 2m of total fracture plot (orientation 072/00, Figure 3-24).

In addition to the three major sets, a less prominent set 4m (orientation 178/89) is identified in Figure 3-55. The same set also occurs in Figure 3-24.

Water leakage

The orientation of water-bearing fractures can be seen from Figure 3-56, indicating that sub-horizontal fractures yield most of the water in the second mapping stage of the TASS-tunnel (designated orientation: 000/00). It coincides with the sub-horizontal orientation of all water bearing fractures in the TASS-tunnel shown in Figure 3-46, where it is one of the most prominent sets with an orientation of 131/01.

Rock quality

The mean RMR value based on all mapped surfaces of the tunnel section 20.7–48.7 m is about 66 (Figure 3-48, good rock = 61–80). The RMR value of the floor within the section is as low as 58, which is considered as fair rock (RMR = 41–60). The walls and roof together have a higher RMR value of 68. The RMR values of the tunnel faces within Mapping Stage 2 vary between 66–76, with an average of 71.

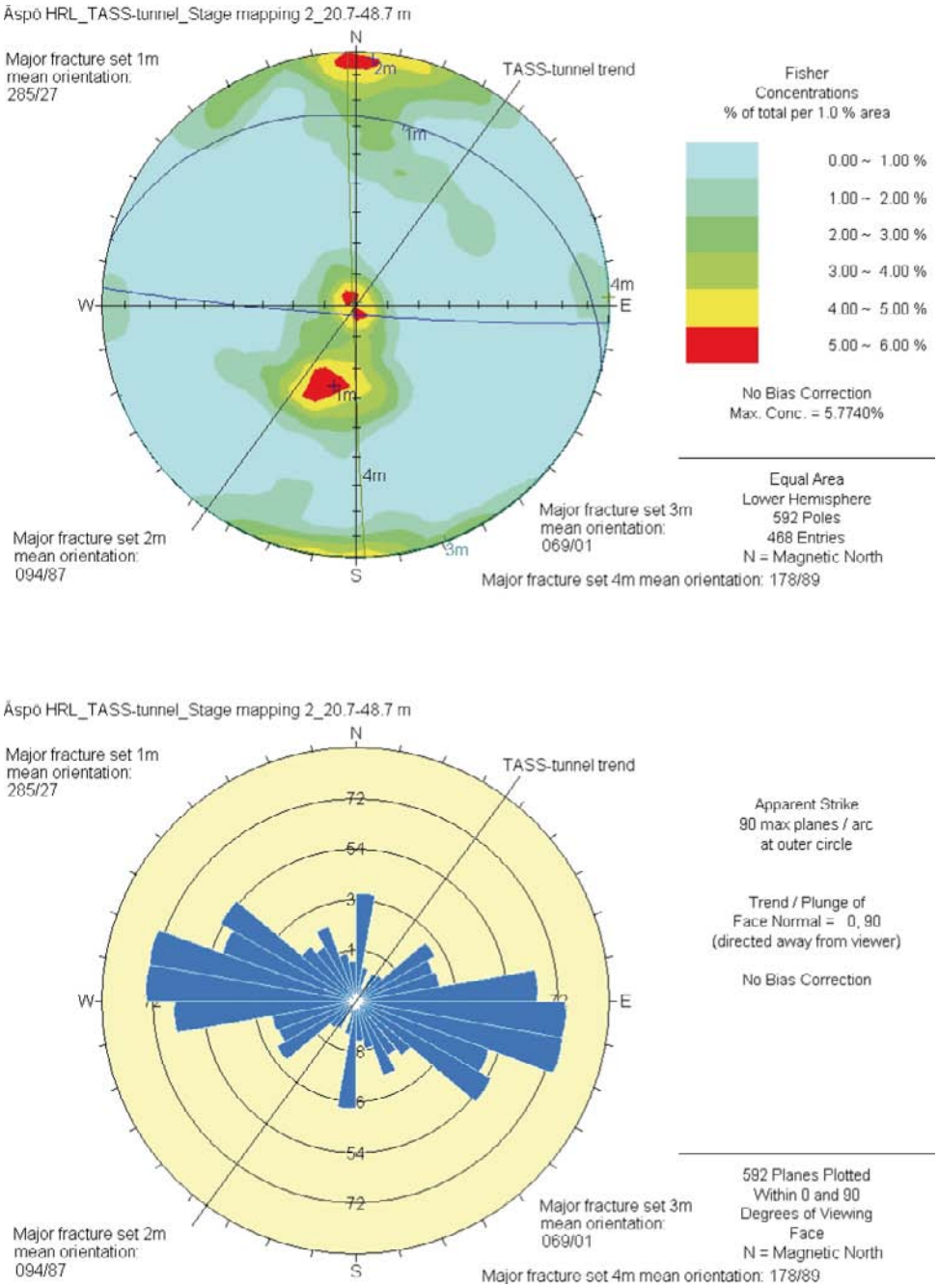

Figure 3-55. *Fracture orientations from the second stage mapping (20.7–48.7 m) of the TASS-tunnel presented in Schmidt net and joint rosette diagrams. The 216° trend of the TASS-tunnel is marked as a black line. Three main orientation sets can be seen, namely 1m: 285/57, 2m: 094/87 and 3m: 069/01, as well as one less prominent set 4m: 178/89. The north-south striking trend on the rosette diagram is partly caused by horizontal fractures that have the designated structural orientation 000/00. N refers to magnetic north.*

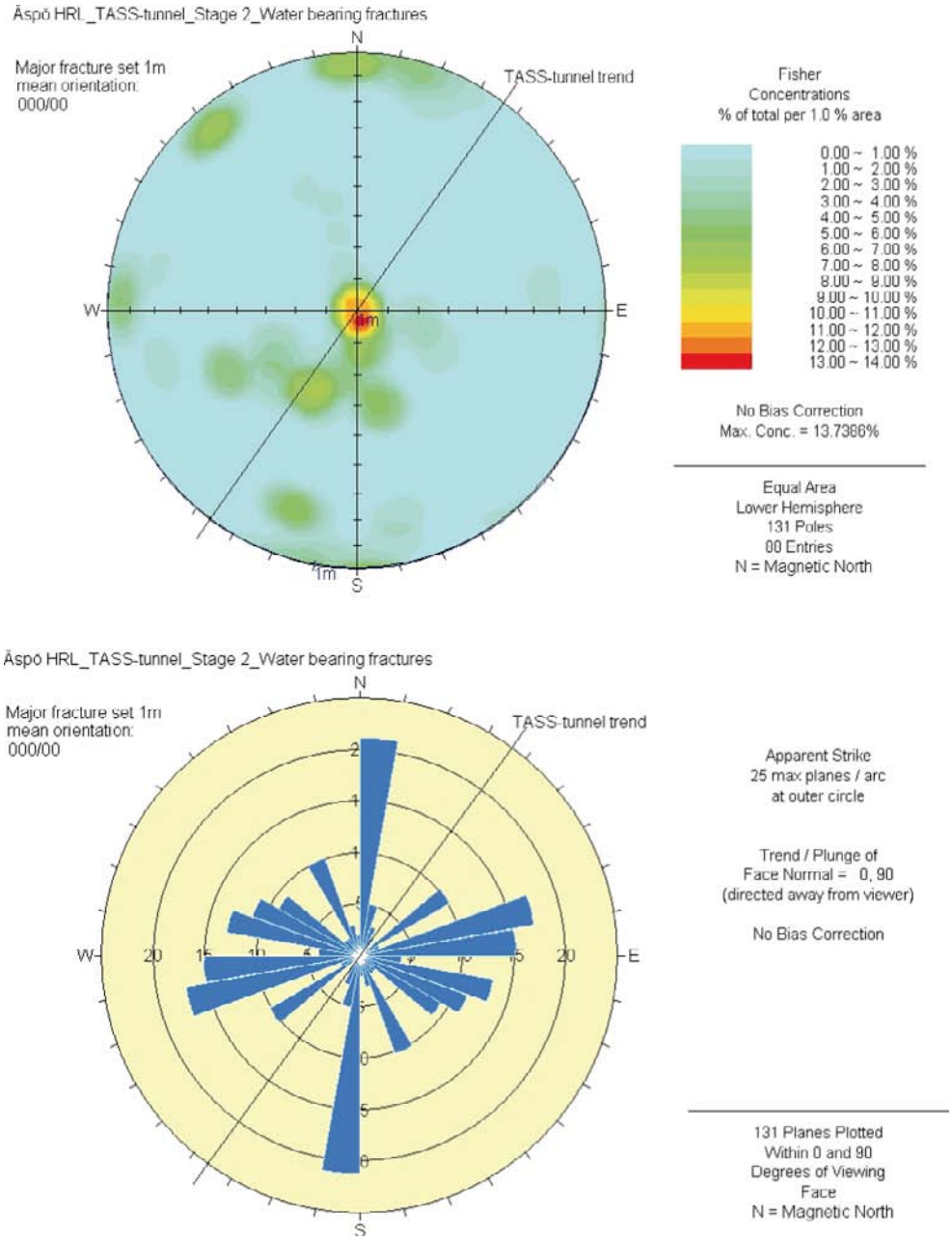

Figure 3-56. *Orientation of all water-bearing fractures from the second stage mapping (20.7–48.7 m) of the TASS-tunnel presented in Schmidt net and joint rosette diagrams. The 216°trend of the TASS-tunnel is marked as a black line. One main orientation set can be seen, namely 1m: 000/00. The north-south striking trend on the rosette diagram is mainly caused by horizontal fractures that have the designated structural orientation 000/00. N refers to magnetic north.*

3.4.3 Mapping Stage 3; 48.7–64.6 m

The maps of the third mapping stage (Stage 3) i.e. tunnel faces (F), walls and roof (P) and floor (G) tunnel segment 48.7–64.6 m, can be found in Appendices I and IV.

Rock types

The diagrams in Figure 3-57 show the distribution of the rock types in the tunnel section 48.7–64.6 m. Appendix VII includes the rock type distribution in figures for all the different mapping stages divided into roof and wall, floor and tunnel faces.

Äspö diorite

As usual, Äspö diorite is the completely dominating rock type (Figure 3-57a) and all of it has been regarded as fresh (87% of the rock mass). However, the area around section 50–55 m on the left-hand side of the tunnel to section 55–60 m on the right-hand side is structurally rather disturbed, which is particularly evident in the tunnel floor. Here, certain rock that may be considered as being oxidized Äspö diorite has been included in the hybrid rock. Some oxidized Äspö diorite may form narrow oxidized borders to some of the fractures, and has thus been recorded as such. The proportion of Äspö diorite in the floor is "only" 74%, whereas it occupies 91% of the roof plus walls.

Fine-grained granite

Fine-grained granite occupies the tunnel segment in about the same amount as the hybrid rock, i.e. 6% of the rock mass (Figure 3-57a). As mentioned above, some fine-grained granite is included in the hybrid rock. Minor slivers of Äspö diorite may be included in the fine-grained granite areas. The floor of the tunnel consists to about 15% of fine-grained granite (Figure 3-57c). Due to the partly tectonically disturbed area around section 50–60 m (Appendix X), a great deal of the fine-grained granite in the floor is sheared, i.e.12% of the rock mass (Appendix VII). The major part of the granite is found within the same belt as the hybrid rock (from the left-hand wall within section 50–55 m across the tunnel to the right-hand wall between sections 55–60 m. There are, however, also occurrences of more or less homogeneous fine-grained granite dykes. One dyke, oriented 75/85°, is found in the left-hand wall at section 52 m and ends in the right-hand wall at about section 57 m. This dyke appears to have been displaced about 1.5 m by one of the major fractures (G3-40), striking 98° and dipping 85°, as can be seen in the roof at about section 54 m (see also the section concerning fractures and deformation zones). Another dyke, oriented 255/85°, appears in the left-hand side of the floor at about section 55 m, intersects the centre line at 56.5 m and ends in the right half of the floor at section 57.5 m.

Pegmatite

Pegmatite has only been registered as a separate rock type in the tunnel face of section 60.5 m, where it constitutes 3% of the face area (Appendix VII).

Quartz veins and lenses

Some minor occurrences of quartz veins have been found at about section 55 m. Two veins/lenses, with an orientation of 85/25, appear in the left-hand wall. Another occurrence of quartz appears within a deformation zone registered in the floor, both with approximately the same orientation (55/65). In total, quartz veins/lenses constitute approximately 1% of the rock mass in this part of the tunnel.

Mafic rock – undifferentiated

Two small irregular bodies of mafic rock have been noted in the lower part of the right-hand wall between sections 62–64 m (Figure 3-10b). Less than 1% of the rock volume is composed of mafic rock.

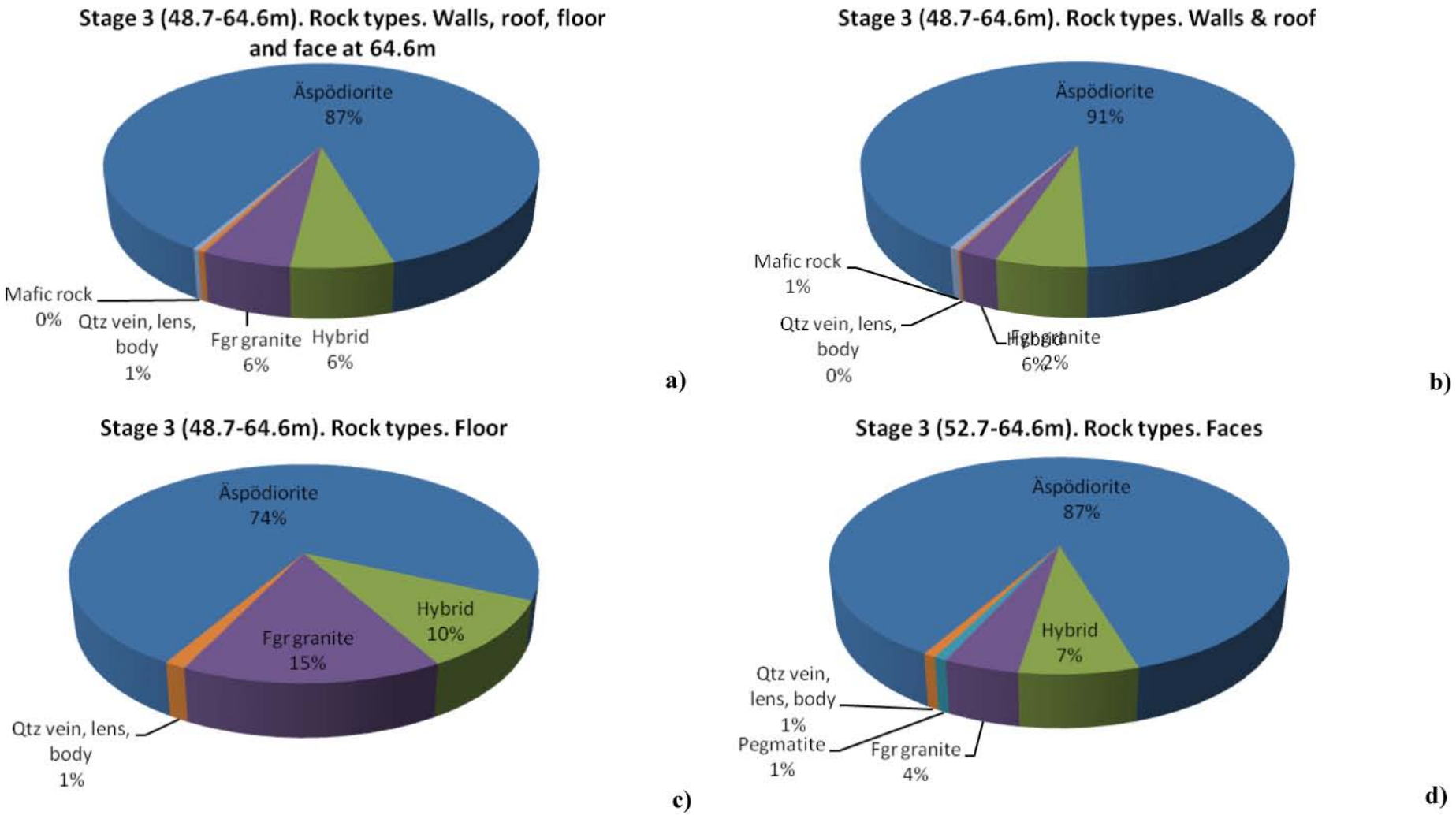

Figure 3-57a–d. *Rock type distribution in tunnel segment 48.7–64.6 m of the TASS-tunnel (0% in the diagrams means >0 to <1%).* ***a)*** *Walls, roof, floor and last tunnel face of the tunnel section,* ***b)*** *Walls and roof of the tunnel section,* ***c)*** *Floor of the tunnel section and* ***d)*** *All tunnel faces of the section (the first face to be mapped is at 52.7 m).*

Hybrid rock

Totally 6% of the rock mass of tunnel section 48.7–64.6 m is composed of hybrid rock (Figure 3-57a). This includes mainly irregular occurrences of oxidized Äspö diorite and fine-grained granite that could not be mapped separately. There are three major occurrences. One forms an approximately 0.5–1 m wide belt from the left shoulder at section 53 m, runs across the roof and ends in the lower part of the right-hand wall at section 60 m. The second occurrence forms an irregular body in the right-hand side of the floor and the lower part of the right-hand wall approximately between sections 55–60 m. Finally, the third major occurrence of hybrid rock is found in the lower part of the left-hand wall at about section 51–53 m and continues to roughly the middle of the floor at about section 54 m. These three occurrences are more or less related to each other and are normally separated by fine-grained granite, where it has been possible to map the latter as a separate rock type.

Rock boundaries/contacts

The rock contacts of the current mapping section and stage follow the general pattern (see Section 3.2.2, Rock boundaries/Contacts). Most of the contacts are sharp and tight, and it is mainly between the oxidized variety of Äspö diorite and/or hybrid rock and surrounding rock types that the boundaries are diffuse. The rock boundaries have been difficult to establish, particularly in the deformed zone mentioned above.

The orientations of the contacts are often irregular. As far as dykes are concerned, the rock boundaries run parallel to the dyke itself.

Fractures and deformation zones

When all mapped fractures in the third mapping stage, i.e. floor (G), walls and roof (P) and face at 64.6 m tunnel length (F) are plotted on a stereogram, two main fracture sets become apparent (1m and 2m, see Figure 3-58). Both coincide roughly with two of the main fracture sets in the plot of all fracture orientations from the TASS-tunnel as seen in Figure 3-24. Major fracture set 1m of Stage 3 mapping: 101/86 coincides with major fracture set 1m of total fractures: 098/87. Major fracture set 2m of Stage 3 mapping: 278/14 coincides with major fracture set 3m of total fractures: 295/22.

Water leakage

The orientation of water-bearing fractures can be seen from Figure 3-59, indicating that northwest to southeast striking and steeply dipping fractures are the most common water-bearing fractures (mean orientation: 099/83) in the third mapping stage of the TASS-tunnel. It coincides roughly with the orientation of the steeply dipping water-bearing fracture set 3m in the plot of all water-bearing fractures in the TASS-tunnel shown in Figure 3-46. Fracture set 3m is the least prominent of the major sets in Figure 3-46, with an orientation of: 289/85.

Rock quality

The variation of the RMR values is illustrated in Figure 3-48. Based on all mapped surfaces of the tunnel section 48.7–64.6 m, the mean RMR value is 68 (good rock = 61–80). The RMR value of the floor within the section is about 63 (good rock = 61–80). The walls and roof together have an RMR value of 69 which is close to the mean RMR value of the tunnel segment. The RMR values of the tunnel faces within mapping Stage 3 vary from 70–75, with an average of 73.

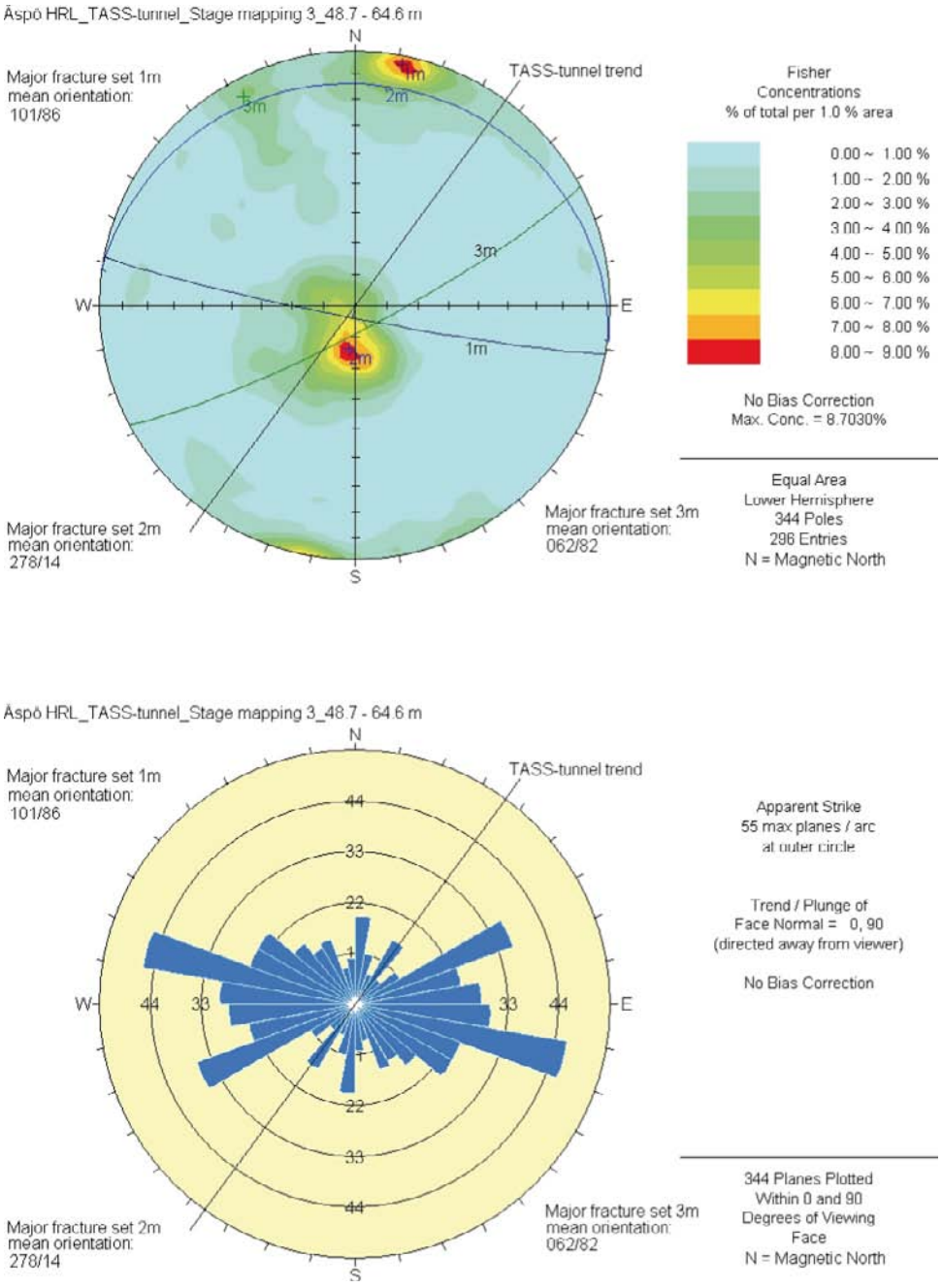

Figure 3-58. *Fracture orientations from the third stage mapping (48.7–64.6 m) of the TASS-tunnel presented in Schmidt net and joint rosette diagrams. The 216° trend of the TASS-tunnel is marked as a black line. The two main orientation sets that can be seen are 1m: 101/86 and 2m: 278/14 as well as one less prominent set 3m: 062/82. The north-south striking trend on the rosette diagram is mainly caused by horizontal fractures that have the designated structural orientation 000/00. N refers to magnetic north.*

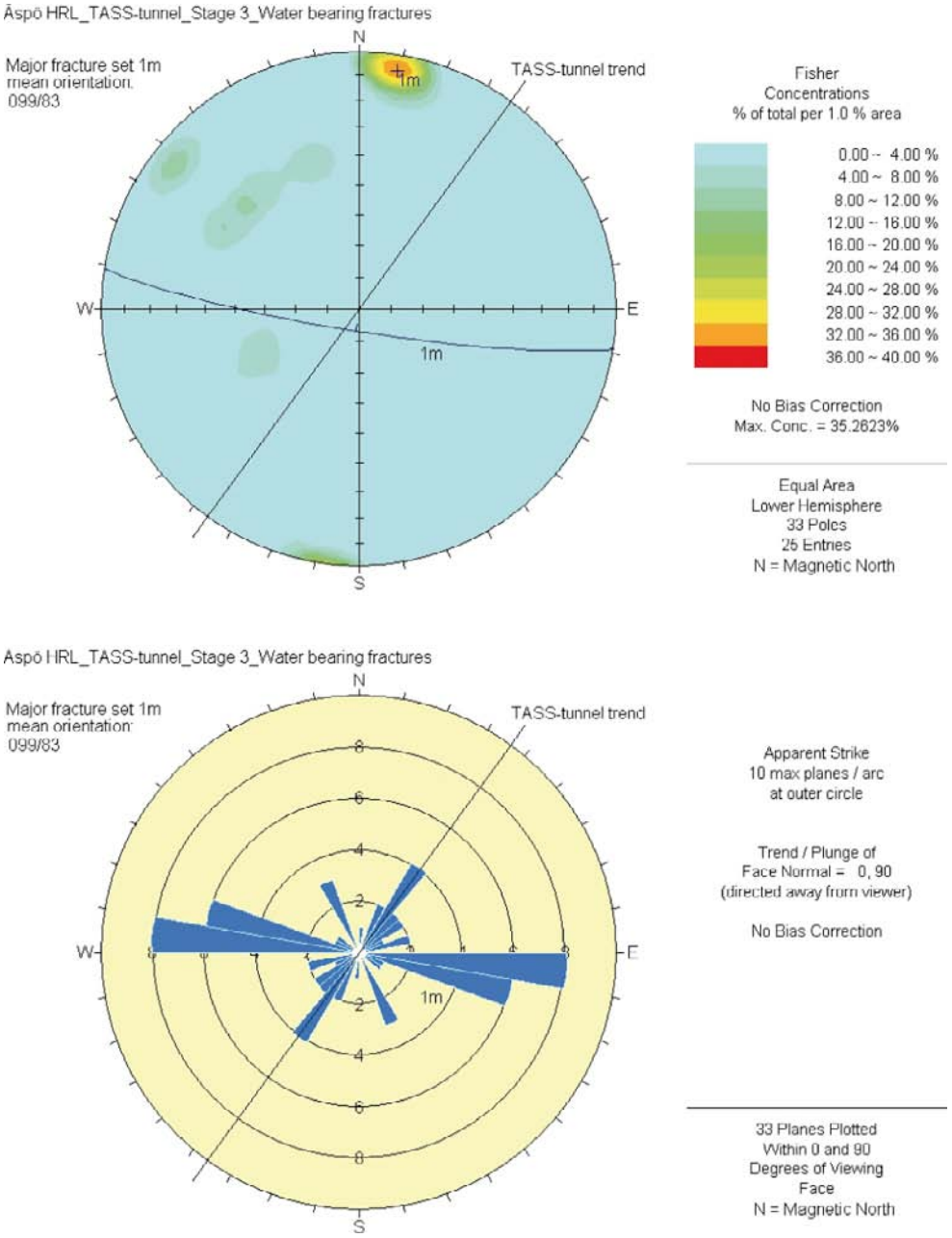

Figure 3-59. *Orientation of all water-bearing fractures from the third stage mapping (48.7–64.6 m) of the TASS-tunnel presented in Schmidt net and joint rosette diagrams. The 216° trend of the TASS-tunnel is marked as a black line. One main orientation set can be seen, namely 1m: 099/83. N refers to magnetic north.*

3.4.4 Mapping Stage 4; 64.6–80.7 m

The maps of the fourth and last mapping stage, i.e. tunnel faces (F), walls and roof (P) and floor (G) tunnel segment 64.6–80.7 m, can be found in Appendices I and V.

Rock types

The diagrams in Figure 3-60 show the distribution of the rock types in the tunnel section 64.6–80.7 m. Appendix VII includes the rock type distribution as a percentage for all the different mapping stages divided into roof and walls, floor and tunnel faces.

Äspö diorite

The Äspö diorite also dominates this section of the TASS-tunnel. Totally 85% of all mapped surfaces consist of fresh Äspö diorite. Minor occurrences of possible oxidized varieties are included in what has been regarded as hybrid rock. Where the Äspö diorite occurs as narrow oxidized borders to some of the fractures it has been recorded as fracture filling and not as a separate rock type. The percentage of the Äspö diorite distribution is about the same (80–87%) regardless of whether roof and walls, floor or tunnel faces are considered. Äspö diorite constitutes most of the tunnel section from 64.6 m to 73 m. Only a few minor dykes occur. Beyond section 73 m the rock type distribution is more irregular.

Fine-grained granite

Diagram a) in Figure 3-60 shows that 8% of the rock mass between sections 64.6–80.7 m consists of fine-grained granite. Its occurrence varies a little depending on which part of the current tunnel segment is being considered. The fine-grained granite occupies 6% of walls and roof, 11% of the floor and 15% (average) of the tunnel faces. There are three sub-varieties of fine-grained granite: fine grained, fine-medium grained and schistose. They all appear as dykes of various widths. A medium-grained variety appears as a 0.1–0.2 m wide dyke at section 64 m in the left-hand wall. It cross-cuts the centre of the roof at section 67 m and continues down the right-hand wall at section 70 m. The same dyke runs from section 64 m in the left-hand part of the floor to section 69 m on the right-hand side. This dyke, which is almost continuous, has the orientation 78/80. The medium-grained variety of the fine-grained granite also appears as pieces, some oriented 248/87, in the floor within sections 67–70 m and in the left-hand wall between sections 66–67 m.

The most conspicuous fine-grained granite in this part of the tunnel appears between sections 75–80.7 m (the end of the tunnel). An approximately 1 m wide, sub-vertical dyke occurs almost in the middle of the tunnel face at section 80.7 m. The dyke has a gneissic and medium-grained component (Figure 3-6) and a laminated fine-grained partly mylonitic component. In the roof, the dyke can be traced to the left shoulder, at about section 75 m where it almost disappears into the deformation zone G4-Z0. In the left-hand side of the floor, the dyke terminates in the same zone. At about section 78 m in the roof, the dyke is split and a branch of it runs down the right-hand wall (Figure 3-5a) to reach the floor at about section 79 m and re-unites with the main dyke at section 78 m in the central part the floor.

In the floor, the contacts and schistosity are sub-parallel with an orientation of about 55/85 and a lamination of 51/88. In the tunnel face, the outer contacts of the gneissic granite variety are oriented about 55/80 and the contacts between the laminated and gneissic varieties 70/86. Schistosity and lamination both have an orientation of 45/90.

Mafic rock – undifferentiated

Less than 1% of the rock volume of the tunnel segment 64.6–80.7 is composed of mafic rock. The only occurrence is a small irregular body on the left-hand side of the roof at section 66 m.

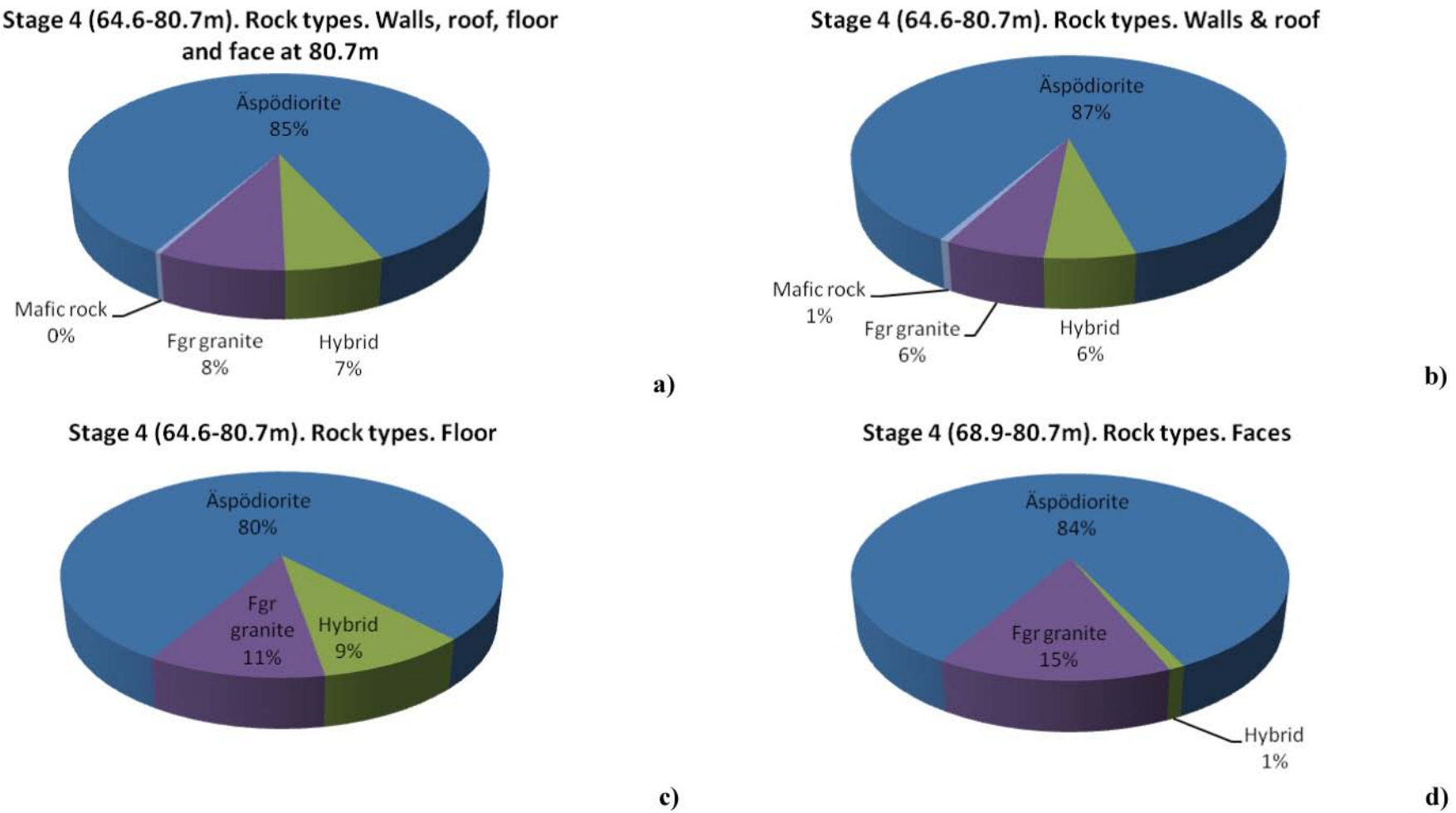

Figure 3-60a–d. *Rock type distribution in the tunnel segment 64.6–80.7 m of the TASS-tunnel (0% in the diagrams means >0 to <1%).* ***a)*** *Walls, roof, floor and last tunnel face of the tunnel section,* ***b)*** *Walls and roof of the tunnel section,* ***c)*** *Floor of the tunnel section and* ***d)*** *All tunnel faces of the section (the first face to be mapped is at 68.8 m).*

Hybrid rock

The hybrid rock that occupies 7% of the total rock volume of the current tunnel segment covers only an average of 1% of the tunnel faces. Some irregular occurrences appear in the left half of the tunnel from section 72–75 m (Figure 3-11b) and in the lower part of the left-hand wall and left side of the floor within section 78–80.7 m. Some hybrid rock, partially resembling fine-grained granite, also occurs in the lower part of the right-hand wall between sections 76–78 m (Figure 3-11a) and continues in the right-hand side of the floor between sections 76–79 m.

Rock boundaries/contacts

The rock contacts of the current mapping section and stage follow the general pattern (see Section 3.2.2, Rock boundaries/Contacts). Most of them are sharp and tight, and as usual it is mainly between the oxidized variety of Äspö diorite and/or hybrid rock and surrounding rock types that diffuse boundaries are common.

The orientations of the contacts are often irregular. In connection with dykes they have been considered to be parallel to the dykes although often undulating.

Fractures and deformation zones

When all mapped fractures in the fourth mapping stage, i.e. floor (G), walls and roof (P) and face (F) at 80.7 m tunnel length, are plotted on a stereogram, one main fracture set becomes apparent (1m, see Figure 3-61) plus two less prominent sets (2m and 3m). The main fracture set (1m: 003/13) coincides approximately with the sub-horizontal fracture sets in the plot of all fracture orientations from the TASS-tunnel as seen in Figure 3-24. The second fracture set (2m: 091/85) can be said to coincide roughly with fracture set 1m: 098/87 in Figure 3-24, while the third fracture set in Figure 3-60 (3m: 217/90) can only be seen as a minor set in Figure 3-24. In addition to the three fracture sets referred to above, a fourth weak, north-south striking set (4m, *358/89*) is present which is also represented in the total fracture plot in Figure 3-24 but where, however, it is not marked out.

Water leakage

The orientation of water-bearing fractures can be seen in Figure 3-62. Here, the plots indicate that northwest to southeast striking and gently dipping fractures are the most common water-bearing fractures in the tunnel section of the fourth TASS-tunnel mapping stage (set 1m, mean orientation: 279/28). It coincides with the orientation of gently dipping water-bearing fractures (set 1m) in the plot of all water bearing fractures in the TASS-tunnel shown in Figure 3-46, where it is the most prominent set with an orientation of 289/27. Two less prominent orientations can also be seen in Figure 3-61. One is a more north-south striking set (2m, 010/30), which can only be seen as a very weak concentration of poles in Figure 3-46. Another one is a northwest to southeast vertical fracture set (3m, 114/90), which coincides roughly with one of the weaker fracture sets (3m) in Figure 3-46 for the whole tunnel (289/85).

Rock quality

Based on all mapped surfaces of the tunnel section 64.6–80.7 m, the mean RMR value is 71 (Figure 3-48, good rock = 61–80). The RMR value of the floor within the section is about 73 (good rock = 61–80). The walls and roof together have an RMR value of 71 that is the same as the mean value of the tunnel segment. The RMR values of the tunnel faces within mapping Stage 4 vary from 68–71, with an average of 70.

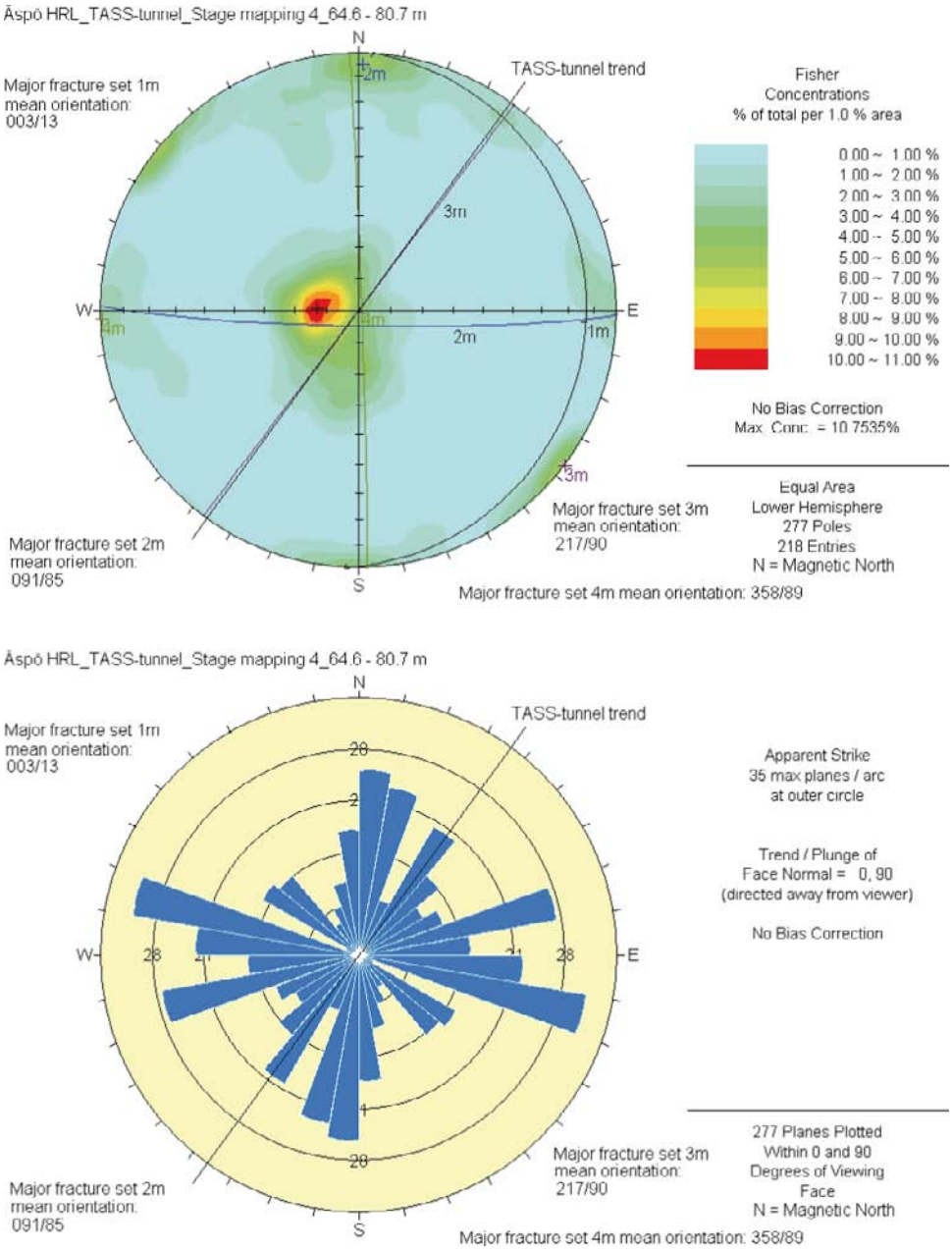

Figure 3-61. *Fracture orientations from the fourth stage mapping of the TASS-tunnel presented in Schmidt net and joint rosette diagrams. The 216° trend of the TASS-tunnel is marked as a black line. One main orientation set can be seen, namely 1m: 003/13 as well as three less prominent sets 2m: 091/85, 3m: 217/90 and 4m: 358/89. The north-south striking trend on the rosette diagram is partly caused by horizontal fractures that have the designated structural orientation 000/00. N refers to magnetic north.*

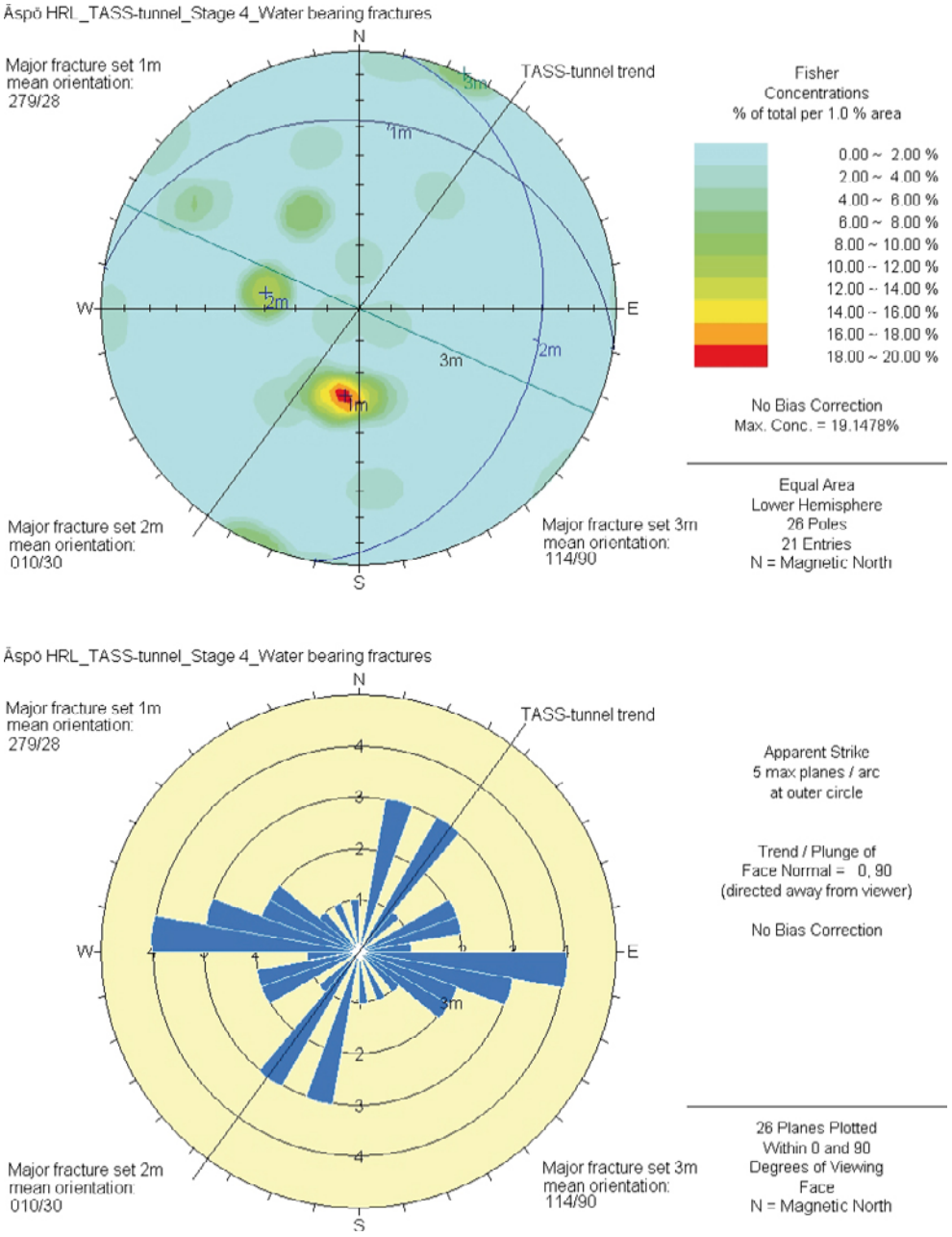

Figure 3-62. *Orientation of all water-bearing fractures from the fourth stage mapping (64.6–80.7 m) of the TASS-tunnel presented in Schmidt net and joint rosette diagrams. The 216° trend of the TASS-tunnel is marked as a black line. One main orientation set can be seen, i.e. 1m: 279/28, as well as two less prominent sets, 2m: 010/30 and 3m: 114/90. N refers to magnetic north.*

4 Relationships between geological features

4.1 The TASS-tunnel and hydraulic structures of the TRUE Block Scale model

The TASS-tunnel cuts through the northernmost part of the TRUE Block Scale model. This is a 200×250×100 m volume of rock which was characterised to furnish the basis for tracer experiments in a network of conductive structures in a 10–100 m large block, see Figure 4-1 /Anderson et al. 2002, Hermanson and Doe 2000/. In the pre-investigation report /Hardenby et al. 2008/, hydraulic measurements of the three boreholes KI0010B01, KI0014B01 and KI0016B01 were compared with the structural Block Scale model.

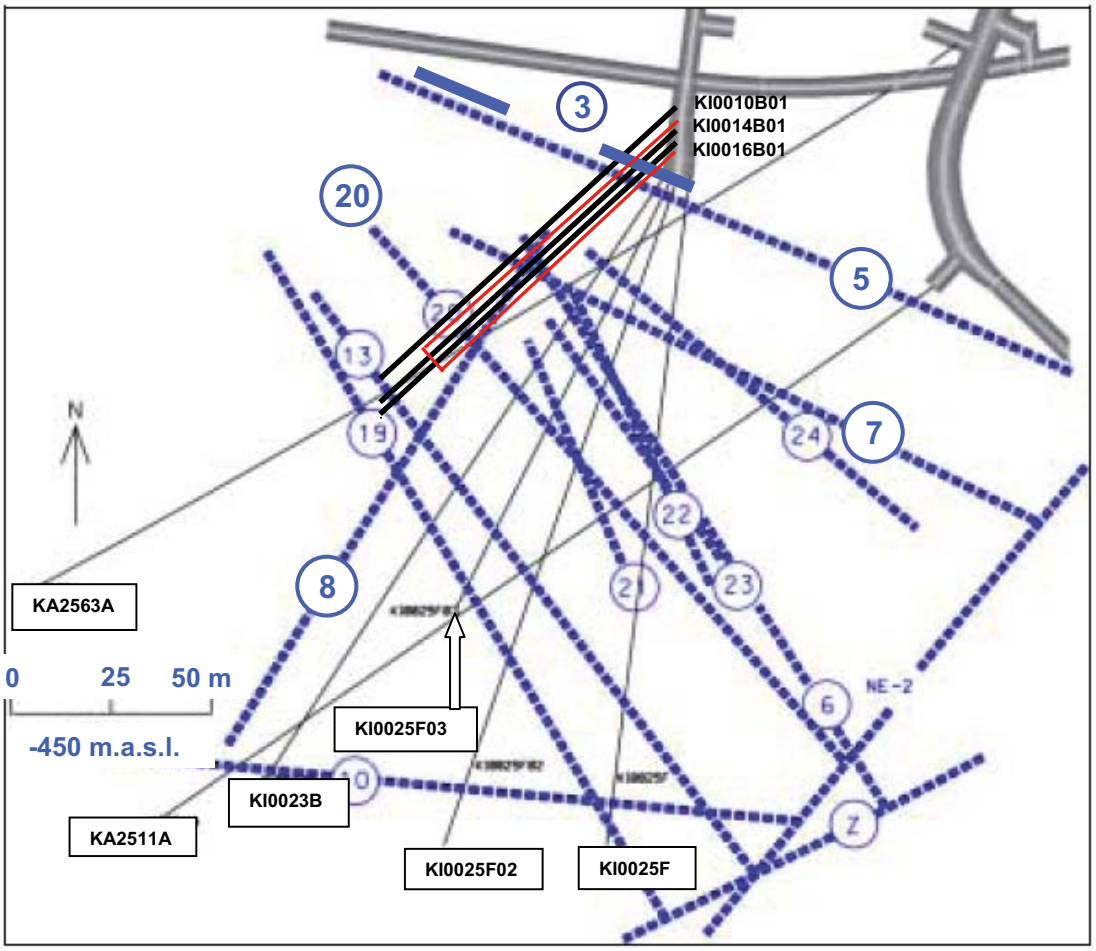

Figure 4-1. *Plan view of the TRUE Block Scale hydro-structural model (modified from Figure 4-6 in /Andersson et al. 2002/ and Figure 3-2 in /Hermanson and Doe 2000/), North arrow is in Äspö96. Structure #3 has been added (sub-parallel and in close proximity to structure #5), the approximate outline of the TASS-tunnel has been marked in red, the approximate locations of boreholes KI0010B01, KI0014B01 and KI0016B01have been indicated as black lines with labels, and labels have been inserted to mark boreholes KI0025F03, KI0025F02, KI0025F, KA2511A, KA2563A and KI0023B.*

The hydraulic measurements of borehole KI0010B01 indicated the possible identification of structures #5, #7, #8, #20 and #22, see Figure 4-2. These occurrences were in /Hardenby et al. 2008/ compared with BIPS images of the three boreholes and their mapping in Boremap. Identified open fractures and crush zones at lengths along the boreholes that approximated the location of inflow in the hydraulic measurements were interpreted as the possible intercepts of the appropriate TRUE Block Scale model structures. This interpretation is here compared in particular to water-bearing structures found in the TASS-tunnel at the sections that approximately coincide with the double packer positions of borehole KI0010B01. The results are shown in Table 4-1 and Table 4-2.

The position of borehole KI0010B01 is approximately 2.5 m up from the TASI-tunnel floor and 1 m NW of the theoretical TASS-tunnel contour, see /Hardenby et al. 2008, Figure 2-4/. The part of the TASS-tunnel that best corresponds to the location of borehole KI0010B01 is to be found at a height of approximately 1.5–3.5 m on the right-hand tunnel wall.

The length of the borehole was measured from the top of the casing while the tunnel is measured from the centre line of the TASI-tunnel. To compare the double packer positions in Figure 4-2 of borehole KI0010B01 with the geological mapping of the TASS-tunnel, approximately 0.5 m has been added to each packer position. These positions are marked as red and pink rectangles in Appendices X A, X C, X F and X H, with the interpreted appropriate TRUE Block Scale model structures marked (#5, #7 etc as in Figure 4-2). Photographs of the structures as they appear in the TASS-tunnel can be found in Appendices X B, X D, X E, X G and X I.

All observed water-bearing structures in the TASS-tunnel were mapped and given a water-ID (for locations see Appendices I–VI as well as X). Since the planned tunnel sections were always sealed/ grouted before excavation, no major water inflows were recorded during the geological mapping.

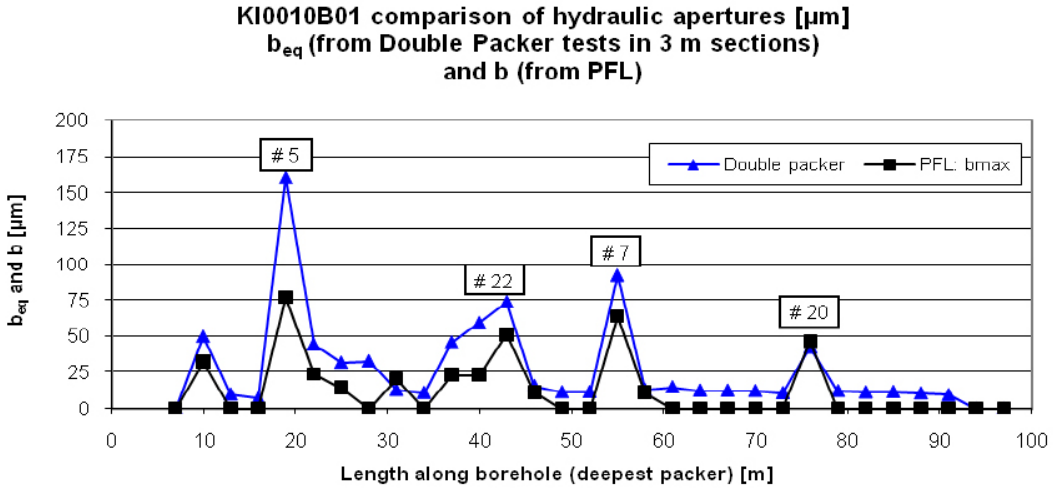

Figure 4-2. *Comparison between the largest b-value (hydraulic aperture) from PFL (Posiva Flow Log) within each 3 m section and the b_{eq} (equivalent hydraulic aperture) from double packer from the same sections in borehole KI0010B01. Hydraulic measurements indicating structures #5, #7, #8, #20 and #22, from /Hardenby et al. 2008/.*

Table 4-1 gives the compilation of water mapping on the right-hand wall of the TASS-tunnel within each extrapolated double packer area of borehole KI0010B01. All water-bearing structures, blast holes and rock surfaces at the appropriate positions that could contribute to the hydraulic apertures shown in Figure 4-2 are therefore listed in the table. To understand Table 4-1 a little better, its structure and columns (1–16) are described briefly below.

1. The relevant packer positions in borehole KI0010B01 are given in m along the borehole.
2. The packer positions are extrapolated into the tunnel (see also Appendices X C, X F and X H).
3–14. The water-bearing observations in the right-hand wall of the TASS-tunnel are listed.
3–8. Water-bearing observations related to open fractures and fracture zones in the tunnel are listed.
3. The water ID used during the mapping.
4. The mapped fracture ID or fracture zone ID.
5–6. Positions of the observations on the right-hand tunnel wall length (5) from start of tunnel and height (6) from floor.
7. Strike and dip for each structure.
8. Fracture fillings, when present (the same abbreviations are used in Table 4-2).
9–11. Water observations from rock surfaces.
9. The water ID used during the mapping.
10–11. Positions of the observations on the right-hand tunnel wall, length (10) from start and height (11) from floor.
12–14. Water observations from boreholes (blast and/or grouting holes).
12. The water ID used during the mapping.
13–14. Positions of the observations on the right-hand tunnel wall, length (13) from start and height (14) from floor.
15. The IDs of the TRUE Block Scale model structures (#5, #7 etc as in Figure 4-2).
16. Comment – Non-water bearing fractures related to the packer positions.

The uppermost double packer position at 7–10 m in borehole KI0010B01 is included in Table 4-1 since a minor peak of hydraulic aperture is indicated in the diagram in Figure 4-2. Other packer positions in Table 4-1 are based on information from /Hardenby et al 2008/. Thick black lines in the table illustrate either one double packer or groups of packers that are related to observed leakages in Figure 4-2.

The definitions of water IDs (Dv, Fv, Gvv etc), fracture IDs (P1-04, G1-15 etc) and deformation zone IDs (G1-Z0 and G4-Z0) have been described in Chapter 2. The mineral abbreviations in Columns 8 and 16 of Table 4-1 are the same as those found in the TMS code chart (SKBdoc 1252025, internal SKB document, see Table 1-1); BR = breccia, EP = epidote, KA = calcite, KL = chlorite, MY = mylonite, OX = oxidation “rim”, PR = prehnite, PY = pyrite, QZ = quartz. The same mineral abbreviations have also been used in Table 4-2.

Certain fractures and deformation zones in Table 4-1 that do not show water leakage are interpreted to be parts of TRUE Block Scale model structures. At packer position 16–19 m, fractures G1-37 and G1-40 are probably also part of model structure #5. Packer position 34–43 m contains fractures G2-106, G2-108, G2-109 and G2-110, which are probably part of model structure #22. Finally, model structure #7 at packer position 52–55 m also seems to contain fracture G3-39 and fracture zone G3-Z0 (see comments in Table 4-1).

Table 4-1. The compilation of water mapping on the right-hand wall of the TASS-tunnel within each extrapolated double packer area of borehole KI0010B01. See also Appendix X (maps and photographs from TASS mapping) and Figure 4-2. The main candidates for the TASS-tunnel observations to be TRUE block scale structures are written in bold type.

Packer position in borehole KI0010B01	Approx. packer posit. in TASS-tunnel (m)	Water-bearing observations in the right-hand wall of the TASS-tunnel												TRUE Block Scale model struc-tures	Comments Non-water-bearing fractures related to the packer positions
		Open fracture and fracture zone						Rock surface			Boreholes				
		Water ID	Fract./ fr.zone ID	Location in TASS-tunnel		Str./dip	Min.fill	Water ID	Location in TASS-tunnel		Water ID	Location in TASS-tunnel			
				Length (m)	Hight (m)				Length (m)	Hight (m)		Length (m)	Hight (m)		
1	**2**	**3**	**4**	**5**	**6**	**7**	**8**	**9**	**10**	**11**	**12**	**13**	**14**	**15**	**16**
7–10 m*	7.5–10.5	Dv Fv	P1-04 G1-15	7.8 9	2.5 2.5	98/80 354/76	KA+PR+KL KL+OX	Ev Hv Jv	8.9 8 10	3 1.8 2	Gvv Iv	9 9.5	2 2.5		
16–19 m	16.5–19.5	Vv Eev Qqvvv **Xv**	P1-69 G1-36 G1-39 **G1-Z0**	17 16.8 18.3 **17.2**	3 2.5 2.5 **2.5**	290/20 310/75 97/71 **110/85**	 KA+EP EP+PR+KA **EP+PR+KL+ KA+OX**	Uv Uuv	17.1 19.4	3.5 2.2	Ttvv	19.2	2.5	**#5**	 G1-37,16.8 m, floor, 138/76, KL+KA G1-40,17.6 m, floor, 289/90, EP+PR
19–22 m	19.5–22.5	Ppvvv Ssv	P1-35 P1-74	20.2 19.6	2.1 2.5	0/0 330/75	–	Rrvv	20.5	1.3	Xvv	22.1	3.3		
22–25 m	22.5–25.5							Tv	24.8	3.3					
25–28 m	25.5–28.5	Cv	P2a-98	28.8	3.4	0/0	KL								

* This packer position is not included in Table 4-2, which is partly based on information from /Hardenby et al 2008/. There is, however, a minor peak of hydraulic aperture in the diagram in Figure 4-2, and therefore it was included in the present table.

Table 4-1. Continuation.

Packer position in borehole KI0010B01	Approx. packer posit. in TASS-tunnel (m)	Water-bearing observations in the right-hand wall of the TASS-tunnel												TRUE Block Scale model struc-tures	Comments Non-water-bearing fractures related to the packer positions
		Open fracture and fracture zone						Rock surface			Boreholes				
		Water ID	Fract./ fr.zone ID	Location in TASS-tunnel		Str./dip	Min.fill	Water ID	Location in TASS-tunnel		Water ID	Location in TASS-tunnel			
				Length (m)	Hight (m)				Length (m)	Hight (m)		Length (m)	Hight (m)		
1	2	3	4	5	6	7	8	9	10	11	12	13	14	15	16
34–37 m	34.5–37.5	Vv	G2-30	35	2.5	5/85	KL+OX								
		Xvv	**P2b-35**	**34.5**	**2.1**	**190/20**	**PR+KL+KA +BR+OX**								
37–40 m	37.5–40.5	**Aavv**	**G2-107**	**39.5**	**2.5**	**100/82**	**KA**	Bbv	38.5	3.5					**G2-109, 38 m, roof, 145/80, KL+PR+EP+Qtz+BR**
		Ddvv	P2b-74	40.1	2.5	360/85	KL	Ccv	38.5	2					**G2-110, 38 m, roof, 100/83, KA+KL** **G2-106, 39 m, floor, 97/80, KA**
40–43 m	40.5–43.5	Hhvv	G2-132	42	2.5	360/85	KL+Qtz+KA							**#22 (?)**	
52–55 m	52.5–55.5	Ffv	P3-31	52.5	2.5	37/80	KL+EP+PR+KA							**#7**	
		Uv	**G3-40**	**54.8**	**2.5**	**98/85**	**KA+KL**								**G3-39, 53 m, roof, 104/75, KA+KL+PR+EP+MY**
		Vv	**G3-45**	**55.1**	**2.5**	**101/82**	**KA+KL**								
		Xv	**G3-45**	**55.2**	**2.5**	**101/82**	**KA+KL**								
		Yv	**G3-46**	**55.5**	**2.5**	**98/84**	**KA+KL**								**G3-Z0, 53 m, floor to approx. 1 m up on left-hand wall, 55/65, KL+PR+Qtz**
73–76 m	73.5–76.5	Ccv	P4-119	75.4	2.8	265/60		Aavv	75.7	1.6				**#20**	
		Ddv	P4-120	75.1	3.1										
		Eevv	P4-66	75.5	2.5	285/30	KL+PR+KA+OX								
		Ffv	P4-67	75	1.8	270/28	KL+PR+KA+OX								
		Iiv	P4-122	74.4	2.5	310/40	KL+OX								
		Xvv	P4-87	76.7	1.7	9/15	KL+KA								
		Zvv	**G4-Z0**	**76**	**2.5**	**114/90**	**PR+EP+KL+KA**								

There seems to be a relatively clear correlation between the mapped structures in the TASS-tunnel and the interpreted TRUE Block Scale model structure **#5** (Appendices X A and X B), TRUE Block Scale model structure **#7** (Appendices X F and X G) and **#20** (Appendices X H and X I). The correlation is more complex when it comes to TRUE Block Scale model structure **#22** (Appendices X C, X D and X E) where several structures can be extrapolated to cut the TASS-tunnel, as can be seen in Figure 4-1.

Table 4-2 is an attempt to compare the results from the Boremap mapping in the pre-investigation report /Hardenby et al. 2008/ with the interpretation from the TASS-tunnel mapping (Table 4-1) concerning the TRUE Block Scale model structures in Figure 4-1.

There is considerable uncertainty when comparing individual fractures from boreholes with mapped fractures in the tunnel. This uncertainty is caused by the large difference in diameter between the boreholes and the tunnel as well as the natural undulation of strike and dip for individual fractures in combination with variations in fracture filling minerals. Structures that are interpreted to be the same in the boreholes and tunnel are usually either fracture zones or groups of fractures with a number of factors in common (i.e. location, direction, fracture fillings and/or water).

In Table 4-2, the column headed "Structure (Description/type, aperture-width-oxidation width, filling minerals, no of fract., water ID)" contains as much relevant information from the TMS database as is possible to fit into the column.

The column contains first the description/type of observation and, if the observation concerns

1. fractures, the column includes aperture-width-oxidation in mm (with a zero-value if it does not exist) which is followed by abbreviations of fracture filling minerals, if any, in order of magnitude. After this, the number of fractures is given if they are more than one in number, and finally the water ID with "character" symbol (v-vvv) if any water leakage was mapped from the structure,
2. deformation zones, the column includes the total zone width in mm, which is followed by abbreviations of fracture filling minerals, if any, in order of magnitude. After this, the number of fracture sets is given if they are more than one and the orientation of each set. Finally, the water ID with "character" symbol (v-vvv) if any water leakage was mapped from the structure.

In addition to the fractures and deformation zones above, a thin pegmatite and an irregular quartz lens are also present. Quartz is marked in blue in the table and pegmatite in red to emphasise that they are rock occurrences rather than fractures. The only information in the structure column for these two features is the total width of the pegmatite and total area of the quarts lens.

The same mineral abbreviations as those used in Table 4-1 have also been used in Table 4-2;
BR = breccia, EP = epidote, KA = calcite, KL = chlorite, MY = mylonite, OX = oxidation "rim", PR = prehnite, PY = pyrite and QZ = quartz.

Most of the fractures from the BIPS images have no definite counterpart in the TASS-mapping of the right-hand wall. The structures that are interpreted as the same in the TASS-tunnel and the BIPS image are listed on the same row in Table 4-2. When fractures mapped in the right-hand wall of the TASS-tunnel have been interpreted as probable members of the TRUE Block Scale model structures (Table 4-1), but are not clearly identified in the BIPS images, the BIPS image part (left-hand part) of the row has been left empty in Table 4-2.

Table 4-2. Comparison of the intercept interpretation of structures in the Boremap mapping with BIPS images (Figure no.) from the three boreholes KI0010B01, KI0014B01 and KI0016B01 to the TRUE Block Scale model structure in /Hardenby et al. 2008/ to the intercept interpretation of mapped structures in the TASS-tunnel in this report. See also Appendix X (maps and photographs from TASS mapping). QZ (quartz) is marked in blue and pegmatite in red to indicate rock occurrence rather than fractures. The main structural candidates in the TASS-tunnel believed to be TRUE block scale structures are in bold text.

Borehole (packer length)	BIPS bore-hole length (m)	Strike (Äspö96)	Strike (Magn N)	Dip	Structure *	Figure no.	TASS struct ID	TASS-tunnel length (m)	Strike (Magn N)	Dip	Structure (Description/type, aperture-width-oxidation in mm, filling minerals, no of fract., water ID)	Possible TRUE Block Scale model structure
KI0010B01 (16–19 m)	16.74–16.92	128	114	90	Open fracture	6-2 a	**G1-Z0**	**17.25–17.35**	**110**	**85**	**Def. zone ca 100 mm wide, EP+PR+KL+KA+OX, water: Xv (+ Tv & Sv)**	**#5** (& #3?)
KI0010B01 (16–19 m)	18.27	110	96	82	Open fracture	6-2 b	**G1-39**	**ca 18.3**	**97**	**71**	**Ind/nat open fract, 0.5–5–0 mm, EP+PR+KA, water Qqvvv**	**#5**
KI0010B01 (19–22 m)	19.78	131	117	88	Open fracture	6-2 c						
KI0010B01	19.82	311	297	90	Open fracture	6-2 c						
KI0010B01	20.02	310	296	85	Open fracture	6-2 c						
KI0010B01	20.1	5	351	78	Open fracture	6-2 c						
KI0010B01 (19–22 m)	20.6	317	303	87	Open fracture	6-2 d						
KI0010B01	20.65	130	116	84	Open fracture	6-2 d						
KI0010B01	20.68	304	290	89	Open fracture	6-2 d						
KI0010B01 (22–25 m)	22.13	336	322	27	Open fracture	6-2 e						
KI0010B01	22.18	324	310	81	Open fracture	6-2 e						

Table 4-2. Continuation.

Borehole (packer length)	BIPS bore-hole length (m)	Strike (Äspö96)	Strike (Magn N)	Dip	Structure *	Figure no.	TASS struct ID	TASS-tunnel length (m)	Strike (Magn N)	Dip	Structure	Possible TRUE Block Scale model structure
KI0014B01	13.56 13.64	140 319	126 305	89 81	Crush zone	**6-2 f**	**G1-Z0**	**ca 17.4**	**110**	**85**	**Def. zone ca 100 mm wide, EP+PR+KL+KA+OX, water: Xv (+ Tv & Sv)**	**#5** (& #3?)
KI0014B01	14.8–14.9	125	111	65	Crush zone, Quartz	6-2 g	B6	18–19	270	90	QZ lens, area ca 0.5 m^2, irregular	
KI0014B01	16.63	309	295	69	Open fracture	6-2 h						
KI0014B01	16.68	305	291	78	Open fracture	6-2 h						
KI0014B01	16.8	308	294	66	Open fracture	6-2 h						
							G1-37 G1-40	16.8 17.6	138 289	73 90	Ind/nat open fract, 0.5–2–0, KL+KA Tight fract, 0–5–0, EP+PR	#5
KI0016B01	11.82	299	285	82	Open fracture	6-2 i	**G1-Z0**	**ca 16.5**	**110**	**85**	**Def. zone ca 100 mm wide, EP+PR+KL+KA+OX, water: Xv (+ Tv & Sv)**	**#5** (& #3?)
	11.88	305	291	75	Open fracture	6-2 i						
	12	308	294	88	Open fracture	6-2 i						
KI0016B01	13.31	310	296	89	Crush zone	6-2 j						
KI0016B01	14.79	297	283	89	Open fracture	6-2 k						
	14.7	71	57	82	Pegmatite	6-2 k	P1-37	18–24	240	88	Pegmatite, 10 mm wide	#5
KI0016B01	15.19	302	288	81	Open fracture	6-2 l						
	15.3	68	54	80	Pegmatite	6-2 l	P1-37	18–24	240	88	Pegmatite, 10 mm wide	
	15.4	142	128	85	Open fracture	6-2 l						
	15.43	135	121	73	Open fracture	6-2 l						

Table 4-2. Continuation.

Borehole (packer length)	BIPS bore-hole length (m)	Strike (Äspö96)	Strike (Magn N)	Dip	Structure *	Figure no.	TASS struct ID	TASS-tunnel length (m)	Strike (Magn N)	Dip	Structure	Possible TRUE Block Scale model structure
KI0010B01 (34–37 m)	35.1–35.3	151	137	18	Crush zone	6-3 a	P2b-35	32–39	190	20	Ind/nat open fract, 0.5–5–150 mm, PR+KL+KA+BR+OX, water: Xvv	
KI0010B01 (37–40 m)	37.32	134	120	90	Open fracture	6-3 b	**G2-109**	**38**	**145**	**80**	**Tight fract, 0–50–0 mm, KL+PR+EP+QZ+BR**	
KI0010B01 (37–40 m)	38.51	319	305	37	Open fracture	6-3 c						**#22** (& #8?)
	38.53	126	112	83	Open fracture	6-3 c						
	38.7	341	327	83	Open fracture	6-3 c	**G2-107**	**39.6**	**100**	**82**	**Ind/nat open fract, 0.2–3–0 mm, KA, water: Aavv**	
	38.81	131	117	88	Open fracture	6-3 c						
							P2b-74	40.15	360	85	Ind/nat open fract, 0.2–0.5 mm, KL, water: Ddvv	
KI0010B01 (40–43 m)	40.97	123	109	83	Open fracture	6-3 d						
	41.18	305	291	87	Open fracture	6-3 d						
KI0014B01	37.22	111	97	52	Open fracture	6-3 e						
		153	139	88	Open fracture	6-3 e						
		138	124	85	Open fracture	6-3 e						
		320	306	88	Open fracture	6-3 e						
		324	310	86	Open fracture	6-3 e						
							G2-106	**39**	**97**	**80**	**Ind/nat open fract, 0.2–2–0, KA**	
KI0016B01	33.49	209	195	79	Cataclastic		**G2-109**	**38**	**145**	**80**	**Tight fract, 0–50–0 mm, KL+PR+EP+QZ+BR, 2 fract**	**#22** (& #8?)
	33.51	326	312	82	Open fracture	6-3 f						
	33.57	306	292	31	Open fracture	6-3 f						
	33.65	123	109	77	Open fracture	6-3 f						
	33.76	322	308	24	Open fracture	6-3 f						
	33.77	141	127	79	Open fracture	6-3 f						
	33.77	140	126	77	Cataclastic		**G2-110**	**38.1**	**100**	**83**	**Tight fract, 0–3–0 mm, KA+KL**	**#22** (& #8?)

Table 4-2. Continuation.

Borehole (packer length)	BIPS bore-hole length (m)	Strike (Äspö96)	Strike (Magn N)	Dip	Structure *	Figure no.	TASS struct ID	TASS-tunnel length (m)	Strike (Magn N)	Dip	Structure	Possible TRUE Block Scale model structure
KI0010B01 (52–55 m)	54.3	326	312	86	Open fracture	6-4 a	**G3-40**	**54.8**	**98**	**85**	**Open fract, 0.1–0.5–0 mm, KA+KL, 2 fract**	#7
	54.5–54.65	304	290	84	Open fracture	6-4 a	**G3-45**	**55.1**	**101**	**82**	**Ind/nat open fract, 0.2–1–0 mm, KA+KL**	
							G3-46	**55-56**	**98**	**84**	**Ind/nat open fract, 0.2–1–0 mm, KA+KL**	
KI0014B01	51.13–51.16	123	109	85	Open fracture	6-4 b	**G3-40**	**54.2**	**98**	**85**	**Open fract, 0.1–0.5–0 mm, KA+KL, 2 fract**	#7
							G3-Z0	**53**	**55**	**65**	**Def. zone ca 100 mm wide, KL+PR+QZ**	
KI0016B01	48.76	113	99	87	Open fracture	6-4 c	**G3-39**	**53.3**	**104**	**75**	**Open fract, 0.5–5–0 mm, KA+KL+PR+EP+MY**	#7
	48.77	114	100	87	Open fracture	6-4 c						
KI0010B01 (73–76 m)	75.13	148	134	87	Open fracture	6-5 a	**G4-Z0**	**76.1**	**114**	**90**	**Def. zone ca 100 mm wide, PR+EP+KL+KA, >12 fract. 3 fract sets:100/90, 123/90, 115/90. Water: Kvv (left wall, drops), Zvv (right wall, drops)**	#20
	75.35	308	294	82	Open fracture	6-5 a						
	75.41	313	299	85	Open fracture	6-5 a						
	75.52	162	148	89	Open fracture	6-5 a						
	75.72	311	297	68	Open fracture	6-5 a						
KI0014B01	72.16	139	125	88	Open fracture	6-5 b	**G4-Z0**	**75.9**	**114**	**90**	**Def. zone ca 100 mm wide, PR+EP+KL+KA, >12 fract, 3 fract sets:100/90, 123/90, 115/90 Water: Kvv (left wall, drops), Zvv (right wall, drops)**	#20
	72.23	125	111	80	Open fracture	6-5 b						
	72.25	129	115	83	Open fracture	6-5 b						
	72.29	139	125	84	Open fracture	6-5 b						
KI0016B01	69.48	14	360	90	Open fracture	6-5 c						
KI0016B01	70.7–70.74	141	127	84	Open fracture	6-5 d	**G4-Z0**	**75**	**114**	**90**	**Def. zone ca 100 mm wide, PR+EP+KL+KA, >12 fract, 3 fract sets:100/90, 123/90, 115/90 Water: Kvv (left wall, drops), Zvv (right wall, drops)**	#20

* Structure nomenclature used by the Bips/Boremap core logging system: Cataclastic = fragmented rock dominated by fine-grained matrix, Crush zone = zone with fragmented rock, Open fracture = fracture with aperture.

4.2 Fracture orientations of the TASS-, TASA Prototype- and TASI-tunnels

The location of the TASS-tunnel can be seen in Figure 1-1 and Figure 1-2, and its orientation as well as the orientations of its neighbouring tunnels (TASA Prototype-tunnel and TASI-tunnel) in Table 4-3. The fracture orientations of the three tunnels are compared in Table 4-4 and Figure 4-3. All data originate from the TMS database.

There are strong similarities, especially between the TASS-tunnel and the TASA Prototype-tunnel. There are, however, some minor differences. One difference is that the dominating fracture orientation in the TASS-tunnel is closer to E-W than its equivalent in the TASA Prototype-tunnel. Sub-horizontal fractures seem to be more prominent in the TASS-tunnel than in the TASA Prototype-tunnel.

The sub-horizontal fractures also appear to be quite common in the TASI-tunnel, but there is not enough data from this tunnel for any detailed comparison to be made.

Table 4-3. Orientations in degrees of the TASS-tunnel, TASA Prototype-tunnel and TASI-tunnel.

Tunnel	Magnetic North (degrees)	Äspö 96 (degrees)
TASS	216	230
TASA Prototype	264	278
TASI	174	188

Table 4-4. Major fracture orientations based on all measured fractures in the TASS-tunnel, TASA Prototype-tunnel and TASI-tunnel. Strike and dip in degrees.

Tunnel	Major orientation (strike/dip)	Less prominent orientations (strike/dip)
TASS	097/86	037/03 & 280/18
TASA Prototype	118/90	
TASI	068/07	308/87, 078/85 & 006/80

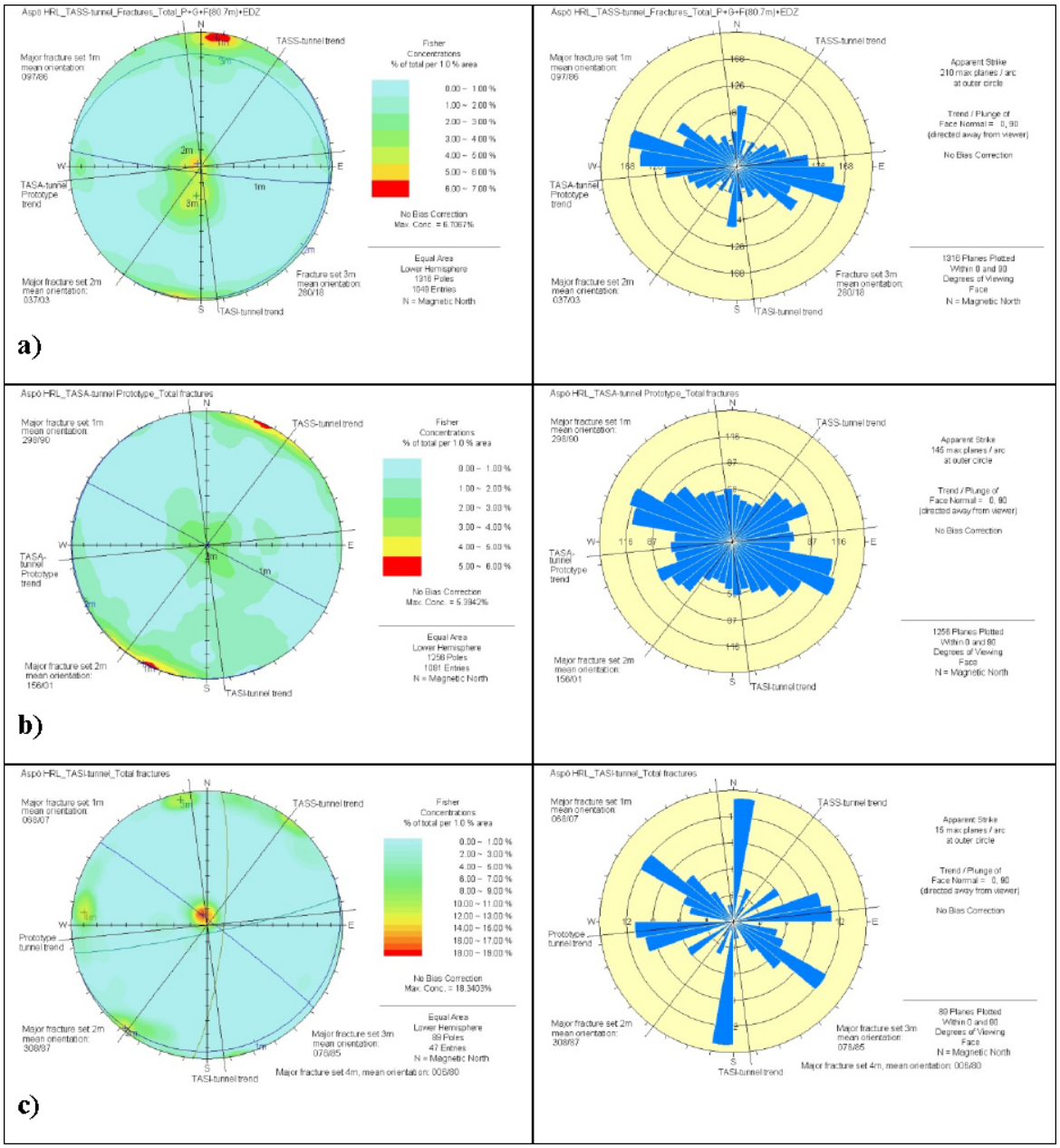

Figure 4-3a–c. *All fracture orientations from the TASS-tunnel, TASA Prototype-tunnel and the TASI-tunnel presented in separate Schmidt nets and joint rosette diagrams. The 216° trend of the TASS-tunnel, the 264° trend of the TASA Prototype-tunnel and the 174° trend of the TASI-tunnel are marked as black lines in the diagrams. N refers to magnetic north.* ***a)*** *The TASS-tunnel shows one main orientation set, namely 1m: 097/86, with two less prominent orientation sets 2m: 037/03 and 3m: 280/18.* ***b)*** *The Prototype-tunnel shows one main orientation set, 1m: 298/90.* ***c)*** *The TASI-tunnel shows one main orientation set, 1m: 068/07. Three less prominent orientation sets are, 2m: 308/87, 3m: 078/85 and 4m: 006/80.*

5 Laser scanning combined with digital photography

Tests with laser scanning combined with digital photography have been performed in the Äspö HRL on a number of occasions, mostly in connection with the RoCS-project (Rock Characterization System project /Magnor et al. 2006/). Since the results were promising it was decided to use laser scanning in the TASS-tunnel too.

Laser scanning in combination with digital colour photography was used for a number of purposes:

- To obtain complementary documentation of the TASS-tunnel.
- To be a possible part of future geological tunnel mapping, the RoCS project.
- The ongoing RoCS project was interested in testing whether it was possible to handle scan data irrespective of the software provided by the laser scanner brand.
- To create 3D-models and to show the geometries of the tunnel.
- To compare the real tunnel contours with the theoretical ones, compare the amount of overbreak and underbreak etc.

5.1 Theory and principles of laser scanning

The theory and principles of laser scanning are presented briefly in /Berlin and Hardenby 2008, Magnor et al. 2006/.

In short, the laser scanner sends out a beam of infrared light to the centre of a rotating mirror to spread the beam in a vertical plane. The laser also rotates in the horizontal plane. The laser scanner will cover 360° horizontally and 310–320° vertically. The latter is due to the tripod and the base of the laser itself, which prevent the beam from reaching the area underneath. The light is reflected against an object and back to the laser. Depending on whether "*phase shift technology*" or "*time of flight technology*" is used, registrations are made of the phase shift or the travel time, and the intensity of the reflected light. With the help of the phase shift or travel time, the distance to each point of an object can be calculated, as well the object's XYZ coordinates in a temporary coordinate system.

After being placed in position, the laser will perform a *scan* that will generate a so-called *3D point cloud***.** The latter can be converted into a "grey-scale" *3D-model or laser image/intensity image*. The intensity of the reflected light will determine the grey scale of the model and image. After having completed a scan the scanner has to be moved to another position.

Depending on different data formats and resolution, each scan will create an approximately 0.5 1 Gb large data file. However, with certain software this large amount of data can be reduced in volume to facilitate processing. Before the data can be fully used, a certain amount of noise (unwanted points) has to be eliminated.

To obtain a *coloured 3D-model or image,* complimentary digital photography has to be added to the scanning since the laser images are only in grey scale. Here a standard digital SLR camera is used, commonly mounted on the same tripod as the one used for the scanner. The camera is normally equipped with a wide angle or fish eye lens.

The laser scanner does not need any external light. However, it is needed for the digital photography. A good camera flash or ordinary floodlights should be sufficient for this purpose.

To fit the *XYZ-coordinates* of a point cloud into a specific coordinate system, *markers* with known coordinates must be included in the scanned area. These markers will have to be surveyed with, for example, a total station to determine their coordinates in the required coordinate system. Fitting several scans together to form one adjusted point cloud with coordinates is called *registration***.**

To achieve accurate *precision* of the points in a point cloud, it is essential for the marker survey to be accurate. The distance between points in the point cloud is called *resolution*. The better the resolution is, the smaller the objects that are visible in the point cloud and image will be. Both precision and resolution depend, apart from the type of scanner used, on the distance between the laser scanner and the object to be measured. Therefore, in order to achieve good scanning results a scan should not cover too large a tunnel segment. The higher the resolution required, the more time is needed for each scan. A scan will normally take about 5–10 minutes depending on the resolution chosen.

5.2 Scanning of the TASS-tunnel

5.2.1 Personnel and equipment

The laser scanning and digital photography of the TASS-tunnel (AP TD SU32516-08-006, internal SKB document, see Table 1-1) were performed by Feng Quanhong from ÅF AB (Ångpanneföreningen AB), Infrastructure Division. Gerry Johansson at Geocon AB conducted all the geodetic surveys.

A *Leica Scanner HDS4500* (the same as a Zoller & Frölich Imager 5003) was used in the TASS-tunnel (Figure 5-1a). This scanner, which is based on phase shift technology, is driven by a tool called *Laser Control*.

All scanning of the TASS-tunnel was performed with the laser set on high resolution. This gives a high standard of precision (±5 mm) for the points in the point cloud. The resolution is approximately 5 mm at a distance of 25 m and about 3 mm at a distance of 2–3 m from the laser. Depending on the software and graphic card used to process the laser data, the resolution of the laser/intensity image may be as good as 1 mm at a distance of <5 m.

Use has been made of the two software packages *Luposcan and Light former modeller* for the purpose of scan registration. The latter is used to check that the tools used have achieved the same results. To acquire good scanning results, each scan in the TASS-tunnel (with a cross-sectional area of approximately 18 m^2) covered tunnel segments that were some 8–10 m in length.

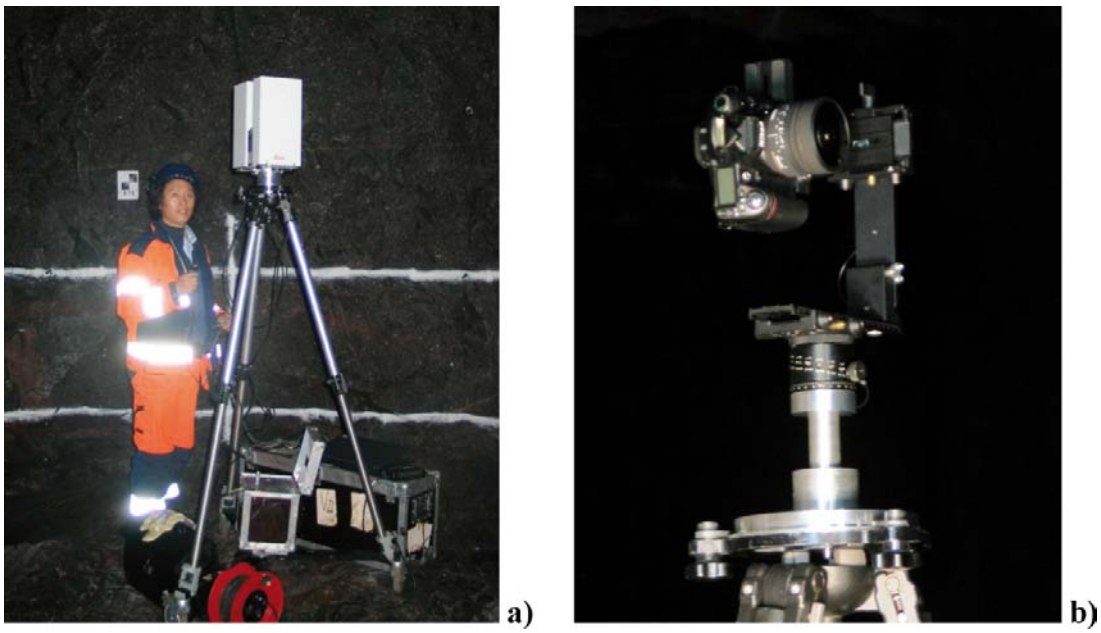

Figure 5-1a–b. *TASS-tunnel equipment at approximately section 48 m.* ***a)*** *Laser scanner on a tripod, marker (paper tag with black and white chequered pattern on the wall) and operator.* ***b)*** *Digital Nikon D80 SLR camera on a tripod.*

A *Nikon D80 10M pixel, 16×24 mm sensor digital SLR-camera* equipped with a *180° fisheye lens* was used for taking the digital photographs (Figure 5-1b, SLR-camera = single lens reflex camera). To start with, a Nikon D3 12M pixel, 24×36 mm full format sensor digital camera was tested to obtain the best possible picture quality. It was, however, concluded that the Nikon D80 camera produced sufficiently high quality for the photos. For each scan, 6 pictures were taken horizontally and one towards the roof – in other words a total of 7 pictures/scan.

5.2.2 Laser scanning events

Laser scanning combined with digital photography was performed on four occasions (see Table 5-1). The scanning was executed just after the current tunnel section had been thoroughly cleaned (Figure 2-5) and before the tunnel mapping commenced. On each occasion, about a day or a day and a half were needed for scanning, photography and geodetic survey. On the first occasion of scanning, both the Nikon D80 and the Nikon D3 were tested. On this occasion only, one person handled the laser and one the cameras. Normally, only one operator is needed for scanning and photography. The geodetic survey (Figure 5-2) was usually conducted immediately after the scanning had been completed.

Table 5-1. Laser scanning events.

Date	Stage	Tunnel section (m)	Activity
2008-02-26	1	0.0–20.7	Laser scanning and digital photography of the tunnel
2008-02-27	1	0.0–20.7	Geodetic measurements of reference markers
2008-06-26	2	20.7–48.7	Laser scanning and digital photography of the tunnel and geodetic measurements of reference markers
2008-10-13	3	48.7–64.6	Laser scanning and digital photography of the tunnel
2008-10-14	3	48.7–64.6	Geodetic measurements of reference markers
2009-02-02	4	64.6–80.7	Laser scanning and digital photography of the tunnel and geodetic measurements of reference markers
2009-02-02		36.4–44.4	Laser scanning, digital photography of the EDZ-slot US0036B and geodetic measurements of reference markers

Figure 5-2. *TASS-tunnel, section 20.7–48.7 m. Geodetic survey of complementary reference markers.*

5.3 Results and use of the results

5.3.1 Scan data delivery and treatment of the data

The outcome of the laser scanning combined with digital photography is merely a large number of points with coordinates that have RGB colour codes attached to them. In order to be able to use these points, they have to be processed in various ways, as described briefly below.

The scan results/point clouds were delivered to SKB in native and ascii (pts, ptx and ptc) formats. The pts-files carry both the xyz-coordinates and RGB-code (originating from the digital photos). In addition, the digital photos were delivered separately in panoramic jpg-format. These pictures are stitched together to form a spherical image that can be viewed with the software Quick Time player. With this tool, the picture can be rotated and viewed in a 3D panoramic field of vision (Figure 5-3). All scan data and digital photos have been delivered to SKB's Sicada archive where they are traceable by using the activity plan number AP TD SU32516-08-006 (internal SKB document, see Table 1-1) and/or by referring to the TASS-tunnel. The data may be ordered from sicada.dataut@skb.se.

The native format of the scan data requires a type of software that is specially made for the laser scanner brand. In order to be able to process the laser data with a type of software other than the one adapted to the laser scanner concerned, the files of various ascii formats are needed. In this way, the laser data can be handled and modified more freely. Besides recording tunnel geometries, this was one of the reasons for scanning the TASS-tunnel. Also some of the processed data in the form of a 3D tunnel model and cross sections of the TASS-tunnel have been delivered to the Sicada archive.

To process the laser data from the TASS-tunnel, the following software has been used by Pär Kinnbom (PKM Innovation AB):

Pointools has been used to check the point clouds and to make a first removal of unwanted points (noise, Figure 5-4).

The crudely cleaned point cloud was then imported into the software **VR Mesh Studio**. With this tool the previously registered point cloud was adjusted in order to achieve an even better fit between the scans. The tool was also used to make a point reduction to make the point cloud easier to handle.

The final cleaning of unwanted noise was done with the software **GEO,** which was equipped with the Tunnel and Mining module.

Coloured 3D mesh/wireframe models were created with the VR Mesh Studio software. The points in the point cloud have been connected with straight lines (triangulation) creating a mesh/wireframe that forms the surface of the models. It is also possible to create 3D mesh models with GEO, but in this case only in a grey scale.

Rhino 3D has been used to work with the laser scan models and to create various illustrations that are based on them.

5.3.2 Use of the scan data

The scan data were at this time not used for the geological mapping but merely as a complementary documentation of the TASS-tunnel. Laser scanning may, however, be a part of a future mapping/rock characterization system (RoCS, /Magnor et al. 2006/).

The scan data obtained from the TASS-tunnel have, on the other hand, been very useful for calculations and modelling in connection, for example, with tunnel geometries. Within the "Fintätningsprojektet" ("Sealing of tunnel at great depth" project), GEO software has been used by P. Kinnbom to determine, for example, the overbreak (part of the excavated tunnel that is outside the theoretical tunnel contour) and underbreak (part of the excavated tunnel that is inside the theoretical tunnel contour) respectively. The data have also been used for volume calculations and to calculate the outcome of look-out angles of the blast holes (look-out angle = "outward angle of the contour holes to the tunnel direction with the purpose of providing space for the rock drill when drilling the next round" /Rustan 1998, p 103/ see also the excavation report by /Karlzén and Johansson 2010/).

a)

b)

Figure 5-3a–b. *The TASS-tunnel, section 0–64.6 m, captured views from the Quick Time viewer. These illustrations are based solely on digital photos.* ***a)*** *The tunnel viewed from approximately section 48 m towards the tunnel mouth. To the left the EDZ-slot is visible.* ***b)*** *The tunnel viewed from approximately section 48 m towards the tunnel face, section 64.6 m.*

Figure 5-4. *The TASS-tunnel, section 70–80.7 m. Colour scan (laser image with RGB from digital photos) still with some unwanted noise such as, for example, the black dots.*

Figures 5-5 to 5-8 illustrate models of the TASS-tunnel based on all laser scans. Figure 5-5 illustrates the tunnel partially as a point cloud and partially as a mesh surface model. The model in Figure 5-6 also includes the colour photos. In Figure 5-7, Rhino 3D software has been used to wrap the geological mapping of the TASS-tunnel on a theoretical tunnel model that has been combined with the laser scan model. Appendices II C, III D, III E, IV C and V C are based on Figure 5-7 and illustrate the geological mapping in almost the same way, but without the laser scan model. A computer-generated triangulated model of the TASS-tunnel based on intensity laser scans is shown in Figure 5-8. This model illustrates the topography of the tunnel surfaces but also some theoretical cross sections of the tunnel that have been compared with the real outcome of the tunnel contour.

Figure 5-5. *A model of the TASS-tunnel that is based on all the laser scans and viewed from the outside. One part of the tunnel is illustrated as point cloud and the other as mesh surface. The beginning of the tunnel is in the upper left-hand corner and the final tunnel face in the lower right-hand corner.*

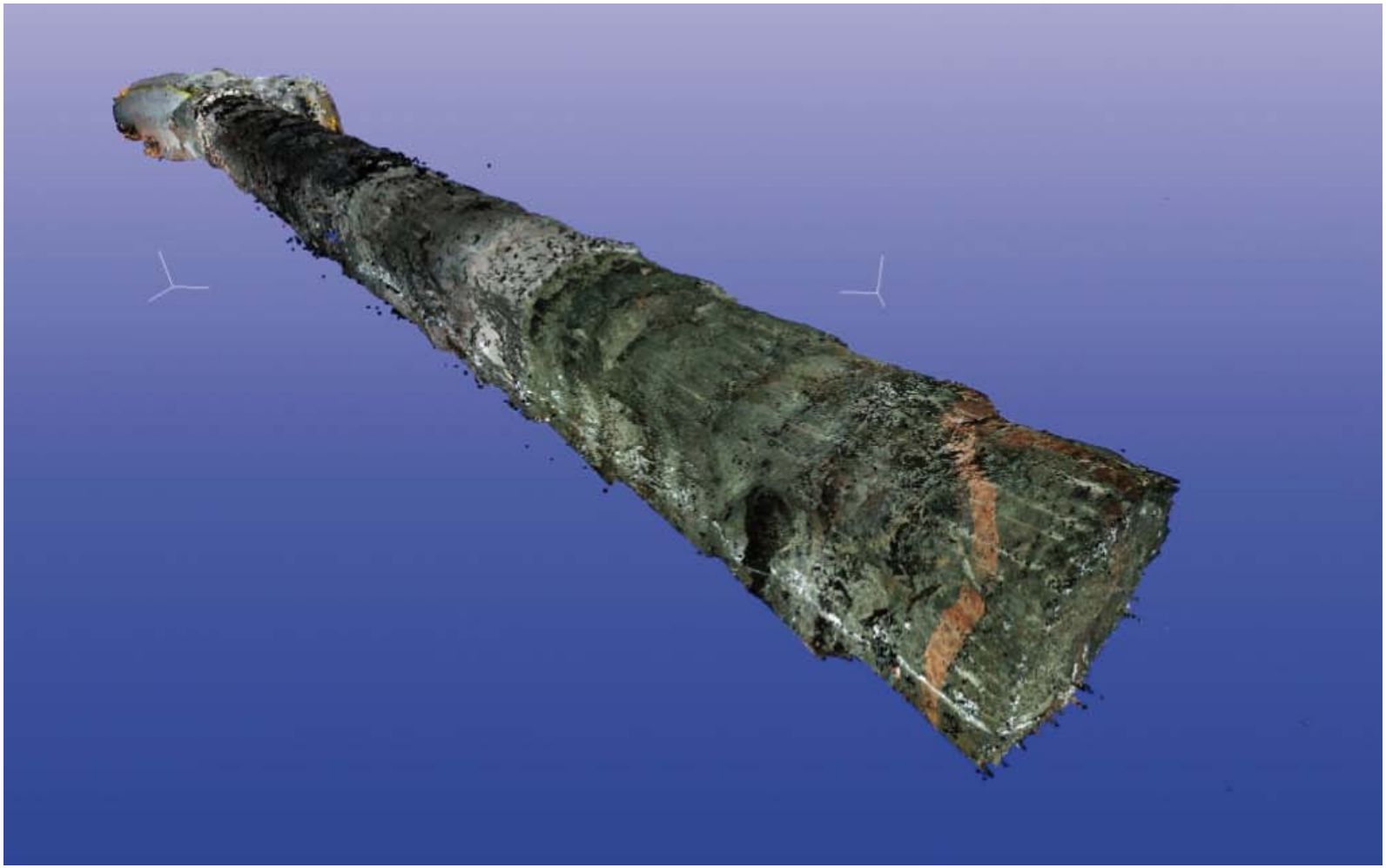

Figure 5-6. *A model of the TASS-tunnel that is based on all the coloured laser scans and viewed from the outside. The scans have been partially cleaned from noise by using Pointools software. Part of the TASI-tunnel is visible in the upper left-hand corner and the final tunnel face in the lower right-hand corner.*

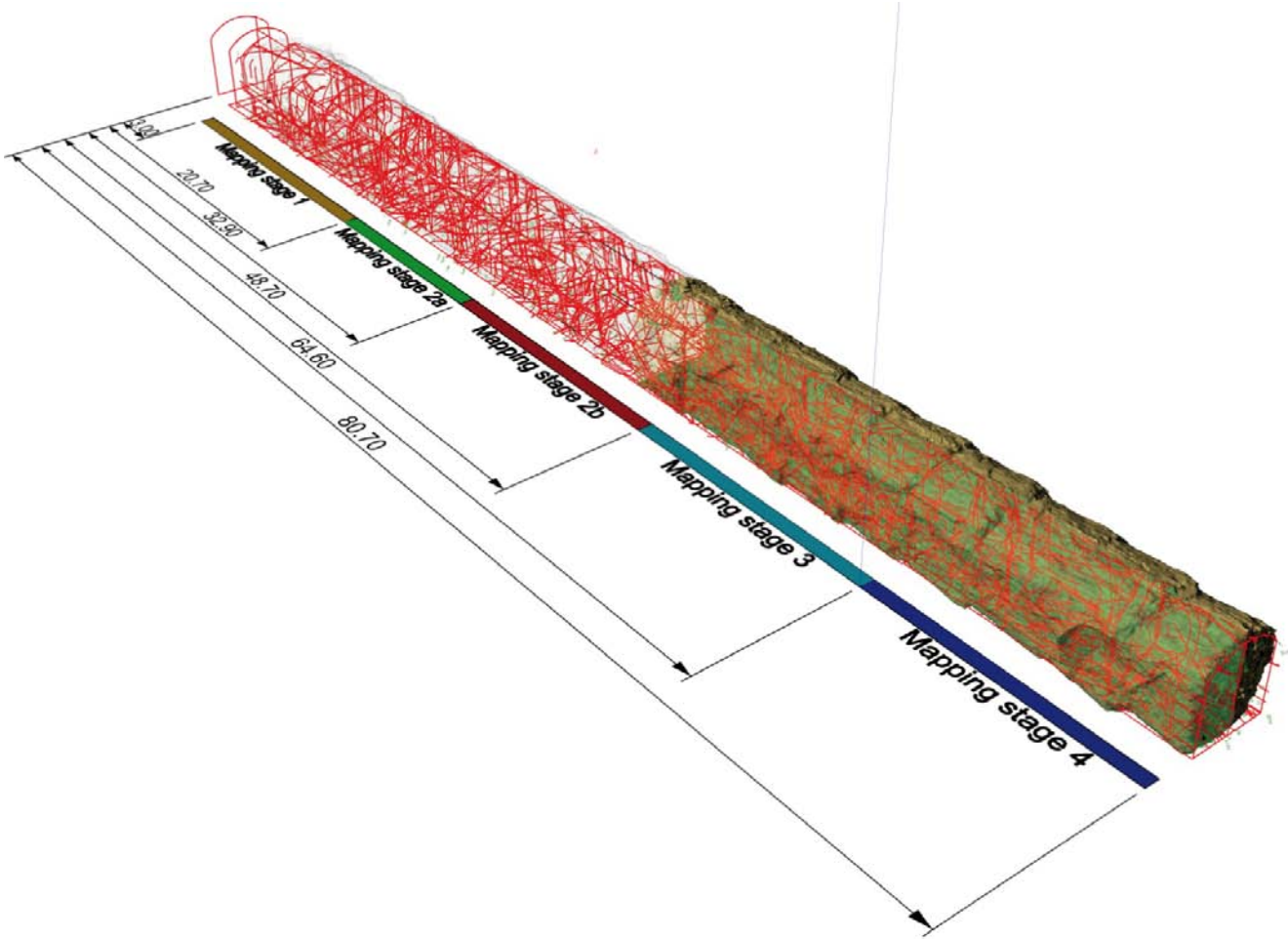

Figure 5-7. *The geological mapping of the TASS-tunnel has been wrapped around a theoretical tunnel model and then merged into the laser scan model of the TASS-tunnel. One part of the tunnel is illustrated as point cloud and the other as a partially transparent mesh surface. The figure also illustrates where the mapping stages started and ended. The beginning of the tunnel is in the upper left-hand corner and the final tunnel face in the lower right-hand corner. See also Appendices II C, III D, III E, IV C and V C.*

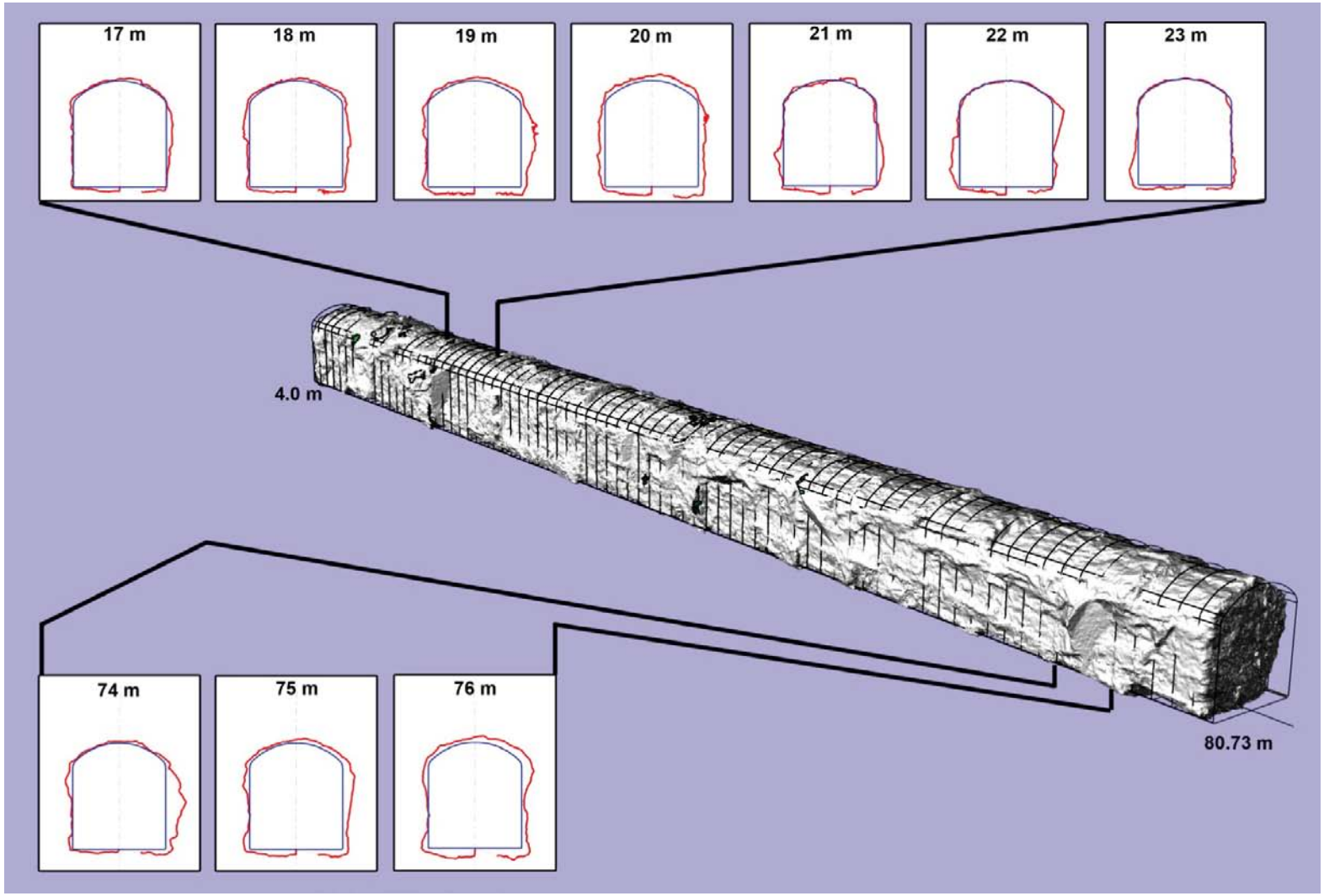

Figure 5-8. *Triangulated model of the TASS-tunnel based on intensity laser scans. Topography of the tunnel surfaces and some theoretical cross sections (blue) compared to the real contour (red).*

6 Concluding remarks and summing up

The aim of the report, as described in Section 1.3, was to:

1) Describe the geological features of the TASS-tunnel.
2) Briefly compare geological features found in the TASS-tunnel with features outside the tunnel.
3) Briefly describe how laser scanning combined with digital photography was used in the tunnel.

All three issues have been dealt with in the report.

The time allowed for the geological mapping as well as for the laser scanning of the tunnel was experienced as sufficient to conduct the required work properly. The tunnel, including the floor, was thoroughly cleaned and the equipment required was in place before the laser scanning and mapping took place.

6.1 Rock type distribution

- There is a certain difference in the rock type distribution from one mapping stage to another. Differences in the distribution are also found in the roof and walls, the floor and the tunnel faces.
- The *Äspö diorite* constitutes between 85–98% (89% average) of the rock mass. It is to some extent mapped as being oxidized, 0–23% (7% average) of the rock mass, but mostly as fresh, 64–92% (83% average). Most of the oxidized variety is found in the first two sections (0–20.7 m and 20.7–48.7 m) of the stage mapping. In the first section it occupies 23% of the rock mass and in the second section 6%. The majority of the oxidized Äspö diorite is found in the floor of these sections. This is evident in Stage 1, where it comprises >50% of the floor. Frequently, the oxidized Äspö diorite is related to sub-horizontal fractures. Some oxidized Äspö diorite may be included in the hybrid rock. In many cases, oxidized Äspö diorite forms a rim along fractures and has then been recorded as fracture filling. In the two tunnel sections mapped last, the oxidized Äspö diorite is absent as a separate rock type.
- The *fine-grained granite* (fine-medium grained) makes up 1–8% (5% average) of the rock mass. Some of it may be included in the hybrid rock. All stage sections, but number two (only 1% fine-grained granite) are composed of approximately equal amounts of fine-grained granite (6–8%).
- An average of some four per cent of the rock mass is composed of *hybrid rock*. The distribution varies between 1–6% of the rock mass. The second stage section (20.7–48.7 m) is composed of only 1% hybrid rock. In the other sections, it constitutes 4–7% of the rock mass. The hybrid rock is partially truly undefined rock and partially a mixture of mostly oxidized Äspö diorite and fine-grained granite. In this case it was regarded pointless to separate the two.
- Only a few occurrences of *pegmatite* have been registered. On *average, on*ly 1% of the rock mass is composed of pegmatite. Most of it appears in the first mapping stage section (0–20.7 m), where it constitutes 2% of the rock mass. In the following mapping stage section (20.7–48.7 m), <1% of the rock mass is composed of pegmatite and in the last two sections no pegmatite mapped as rock type is present at all. However, when the pegmatite dykes are narrow (<10 cm), they are recorded as fracture filling.
- *Quartz veins/lenses* constitute <1% of the rock mass of the TASS-tunnel. Commonly the width of the veins/lenses varies between 1–10 cm and the length from <1 m to some metres. The quartz veins/lenses have been recorded as a rock type in stage mapping sections one and three (3–20.7 m and 48.7–64.6 m respectively). Besides this, quartz appear as fracture filling.
- As with the quartz veins/lenses, *undifferentiated mafic rock* constitutes a very small portion (<1%) of the rock mass. It is only in the last two stage mapping sections (48.7–64.6 m and 64.6–80.7 m respectively) where mafic rock has been recorded as a separate rock type. In both sections, <1% of the rock mass consists of mafic rock. Commonly, mafic rock appears as small xenoliths in the Äspö diorite.

6.2 Fractures and deformation zones

The four mapping stages of the TASS-tunnel show a slight variation in *fracture orientations* as can be seen from Table 6-1 as well as Figures 3-52, 3-55, 3-58 and 3-61. The orientations of fractures in the TASS-tunnel as a whole show two main fracture sets: one striking roughly east-west and steeply dipping and one sub-horizontal to gently dipping with more varying strikes. The steeply dipping fracture set dominates with a mean orientation of 097/86. The sub-horizontal to gently dipping set may be divided into two sub-sets with the mean orientations of 037/03 and 280/18 respectively, see Table 4-4, Figure 4-3a) and Appendix VIII A.

- *Major fracture sets* appear in all the mapping stages, although their orientations vary. The major fracture set in the first mapping stage is east-west striking and steep. In Stages 2 and 3, two fracture sets dominate: the east-west striking and steeply dipping set and a sub-horizontal fracture set. In Stage 4, only one fracture set dominates: the sub-horizontal one.
- *Less prominent fracture sets* also appear in all the mapping stages. An almost N-S striking and steeply dipping set appears in Mapping Stages 1, 2 and 4, but is least prominent in Stage 2. A NE-SW striking and steeply dipping fracture set appears in all mapping stages, but is least prominent in Stage 1. In Stage 1, a sub-horizontal, not very prominent fracture set also appears.

There are *two categories of deformation zones* mapped in the TASS-tunnel.

- The first one is *increased fracturing*, mainly visible in the floor of the tunnel in Mapping Stages 1 and 2, with an apparent width of 0.5–8 m. Their general orientation is approximately ENE-WSW with a moderate dip to the north, see Figure 3-41.
- The second one is of the category *deformation zones proper (brittle/ductile)*, occurring in Mapping Stages 1, 3 and 4. These zones generally cross-cut the tunnel and their widths vary between 0.1–0.3 m. Their general orientation is approximately ESE-WNW and steeply dipping, see Figure 3-41.

Thinner deformation zones (3–50 mm wide) of the same category (brittle/ductile) occur in all mapping stages of the TASS-tunnel, but are mapped as fractures, see Table 6-2. Their general orientation coincides roughly with the mapped deformation zones proper (brittle/ductile), with a somewhat larger variation, see Figure 3-43 a). Some thinner deformation zones show brecciation in the first two mapping stages (see Figure 3-44 and Table 6-2). Their general orientation is sub-horizontal (see Figure 3-43 b).

Table 6-1. Main orientations of fractures in the TASS-tunnel (walls, roof, floor, faces and EDZ-slot). Strike and dip in degrees.

	Main orientation (strike/dip)	Less prominent orientation (strike/dip)
Mapping Stage 1	097/87	360/78 and 113/07
Mapping Stage 2	285/27, 094/87 & 069/01	178/89
Mapping Stage 3	101/86 and 278/14	062/82
Mapping Stage 4	003/13	091/85, 217/90 and 358/89

Table 6-2. Number of thin deformation zones in the TASS-tunnel with or without brecciation.

	Thin deformation zones	Thin deformation zones brecciated	Total number of deformation zones
Mapping Stage 1	9	3	12
Mapping Stage 2	10	10	20
Mapping Stage 3	7	0	7
Mapping Stage 4	21	0	21

6.3 Water-bearing fractures

The four mapping stages of the TASS-tunnel show variations in the orientations of water-bearing fractures, see Table 6-3 as well as Figures 3-53, 3-56, 3-59 and 3-62. When the orientations of water-bearing fractures for the whole tunnel are plotted, the sub-horizontal to gently dipping fractures dominate with the mean orientations of 000/00 and 297/28. Two less prominent fracture sets of 287/70 and 099/89 also occur, see Appendix VIII B.

The major fracture sets in Mapping Stages 1 and 3 are NW-SE striking and steep, while sub-horizontal fracture sets dominate Mapping Stage 2 and to a lesser degree Mapping Stage 1. In Mapping Stage 4, the dominating strike is NW-SE but with a moderate dip. A less prominent orientation of an approximately N-S strike and a steep dip to the east occurs in Mapping Stage 1 and in Mapping Stage 4, where the dip, however, is moderate. Water-bearing fractures mapped in the tunnel faces of the TASS-tunnel show a distinct domination of an orientation with a NW-SE strike and a steep dip towards the northeast, see Figure 3-50.

Table 6-3. Water-bearing fractures in the TASS-tunnel, main orientations (walls, roof, floor, faces and EDZ-slot). Strike and dip in degrees.

	Main orientation (strike/dip)	Less prominent orientation (strike/dip)
Mapping Stage 1	305/79 and 107/84	359/75 and 110/03
Mapping Stage 2	000/00	–
Mapping Stage 3	099/83	–
Mapping Stage 4	279/28	010/30 and 114/90

6.4 Rock quality – RMR

The *RMR values* vary between 58–81 depending on which part of the tunnel has been recorded. The lowest values (RMR = 58 and 63) are found in the floor, which may be due to the fact that this part normally suffers the most from blasting during tunnel excavation. The lowest value RMR = 58 in Stage 2, section 20.7–48.7 is likely to depend also on the fact that a number of zones with increased fracturing appear here. After Stage 2, the RMR values of the floor increase, which may be due to changes in the blasting technique. The average RMR value (RMR = 70) for the tunnel implies a good rock quality. This is also the general impression gained from the mapping of the tunnel. The frequent sub-horizontal, sometimes persistent fractures may, however, cause some instability of the roof.

6.5 Laser scanning combined with digital photography

- The *cleaning* of the tunnel before the laser scanning, photography and mapping was carried out in an excellent way.
- The *scanning and photography* of the four tunnel segments of Stages 1, 2, 3 and 4 proceeded as planned and took place as soon as possible after the current tunnel segment had been cleaned.
- The *scan data* was delivered in ascii-format as agreed upon. It is, however, essential that the delivered data be checked before delivery to ensure that the export files are in order and able to be used with the intended tools/software. In the situation described here, the data in native-format was in order but after the export to ascii-format the tunnel segments were delivered with random orientation. This was not observed in the case of the Luposcan software, which was used to process the native-format. This failure had been caused by an unknown bug in the software's export function, which was discovered when the data was opened with Pointools. After being processed with a new version of Luposcan, the laser data delivered in ascii-format was found to be in good order.
- The *tests* that were performed on the scan data have shown that it is possible to handle the data with software other than that adapted to the laser scanner. It can also be concluded that laser scanning combined with digital photography may be a useful tool in the excavation work.

7 References

SKB's (Svensk Kärnbränslehantering AB) publications can be found at www.skb.se/publications.

Andersson P, Byegård J, Dershowitz B, Doe T, Hermanson J, Meier P, Tullborg E-L, Winberg A (ed), 2002. Final report of the TRUE Block Scale project. 1. Characterisation and model development. SKB TR-02-13, Svensk Kärnbränslehantering AB.

Berlin R, Hardenby C, 2008. Äspö Hard Rock Laboratory. Laser scanning combined with digital photography. Tunnel TASQ and niche NASQ0036A at Äspö HRL. SKB IPR-08-10, Svensk Kärnbränslehantering AB.

Bieniawski Z T, 1973. Engineering classification of jointed rock masses. The Civil Engineer in South Africa, 15.

Bieniawski Z T, 1984. Rock mechanics design in mining and tunnelling. Rotterdam: Balkema.

Bieniawski Z T, 1989. Engineering rock mass cassifications: a complete manual for engineers and geologists in Mining, Civil and Petroleum Engineering. New York: Wiley.

Fisher R, 1953. Dispersion on a sphere. Proceedings of the Royal Society A, 217.

Funehag J, 2008. Injekteringen av TASS-tunneln. Delresultat t.o.m. september 2008. SKB R-08-123, Svensk Kärnbränslehantering AB.

Funehag J, Emmelin A, 2010. Injekteringen av TASS-tunneln. Design, genomförande och resultat från förinjekteringen. SKB R-10-39, Svensk Kärnbränslehantering AB.

Hardenby C, Sigurdsson O, Hernqvist L, Bockgård N, 2008. Äspö Hard Rock Laboratory. The TASS-tunnel project "Sealing of tunnel at great depth". Geology and hydrology – results from the pre-investigations based on the boreholes KI0010B01, KI0014B01 and KI0016B01. SKB IPR-08-18, Svensk Kärnbränslehantering AB.

Hermanson J, Doe T, 2000. Äspö Hard Rock Laboratory. TRUE Block Scale Project. Tracer test stage. March'00 structural and hydraulic model based on borehole data from KI0025F03. SKB IPR-00-34, Svensk Kärnbränslehantering AB.

Hoek E, Bray J, 1996. Rock slope engineering. 3rd ed. London: E & FN Spon (imprint of Chapman and Hall).

Hoek E, Brown E T, 1982. Underground excavations in rock. Hertford, UK: Stephen Austin & Sons Ltd. The institution of Mining and Metallurgy.

ISRM, 1977. Suggested methods for the quantitative description of discontinuities in rock masses. International Society for Rock Mechanics commission on standardization of laboratory and field tests. International Journal of Rock Mechanics and Mining Sciences & Geomechanics abstracts. Pergamon Press Ltd (1978), 15.

Karlzén R, Johansson E, 2010. Slutrapport från drivningen av TASS-tunneln. SKB R-10-31, Svensk Kärnbränslehantering AB.

Koch G S, Link R F, 1980. Statistical analysis of geological data. New York: Dover Publications.

Kornfält K-A, Wikman H, 1988. The rocks of the Äspö island. Description to the detailed maps of solid rocks including maps of 3 uncovered trenches. SKB HRL Progress Report 25-88-12, Svensk Kärnbränslehantering AB.

Magnor B, Hardenby C, Kemppainen K, Eng A, 2006. Rock Characterisation System – RoCS. Final report – feasibility study, phase I. State-of-the-art in 3D surveying technology. SKB IPR-06-07, Svensk Kärnbränslehantering AB.

Mancktelow N S, Pennacchioni G, 2005. The control of precursor brittle fracture and fluid-rock interaction on the development of single and paired ductile shear zones. Journal of Structural Geology, 27.

Munier R, 2010. Full perimeter intersection criteria. Definitions and implementations in SR-Site. SKB TR-10-21, Svensk Kärnbränslehantering AB.

Olsson M, Markström I, Pettersson A, Sträng M, 2009. Examination of the Excavation Damaged Zone in the TASS-tunnel, Äspö HRL. SKB R-09-39, Svensk Kärnbränslehantering AB.

Rhén I (ed), Gustafson G, Stanfors R, Wikberg P, 1997. Äspö HRL – Geoscientific evaluation 1997/5. Models based on site characterization 1986–1995. SKB TR-97-06, Svensk Kärnbränslehantering AB.

Rustan A (ed), 1998. Rock blasting terms and symbols: a dictionary of symbols and terminology in rock blasting and related areas like drilling, mining and rock mechanics. Rotterdam: Balkema.

Singh B, Goel R K, 1999. Rock mass classification: a practical approach in civil engineering. Amsterdam: Elsevier Science Ltd.

Stanfors R (compilation), 1988. SKB Hard Rock Laboratory. Geological borehole description KAS02, KAS03, KAS04, KLX01. SKB/Swedish Hard Rock Laboratory PR 25-88-18, Svensk Kärnbränslehantering AB.

Stanfors R, Liedholm M, Munier R, Olsson P, Stille H, 1993. SKB Hard Rock Laboratory. Geological-structural evaluation of data from section 700–1,475 m. SKB HRL Progress Report 25-93-05, Svensk Kärnbränslehantering AB.

Streckeisen A, 1976. To each plutonic rock its proper name. Earth Science Reviews, 12.

Turner F J, Weiss L E, 1963. Structural analysis of metamorphic techtonites. New York: McGraw-Hill Book Company.

Twiss R J, Moores E M, 1992. Structural geology. New York: W. H. Freeman and Company.

Wikman H, Kornfält K-A, 1995. Updating of a lithological model of the bedrock of the Äspö area. SKB HRL Progress Report 25-95-04, Svensk Kärnbränslehantering AB.

Wikman H, Kornfält K-A, Riad L, Munier R, Tullborg E-L, 1988. Detailed investigation of the drillcores KAS 02, KAS 03 and KAS 04 on Äspö island and KLX 01 at Laxemar. SKB HRL Progress Report 25-88-11, Svensk Kärnbränslehantering AB.

Acknowledgements

The Bergteamet AB excavation crew are remembered for being good work colleagues both on and off duty.

Magnus Kronberg (SKB, project coordinator) is acknowledged for organizing the work in the tunnel and providing us with necessary equipment.

Gerry Johansson (Geocon AB, surveyor) helped us with various surveying issues, such as the marking out of tunnel sections and the measuring of complementary markers for laser scanning as well as contributing with the drawing, now modified, in Figure 1-4.

Quanhong Feng (ÅF AB, laser scanning expert) performed the laser scanning and the digital photography, participated in trouble shooting related to these issues and reviewed the laser scanning section of the report.

We would also like to thank all the other people who gave us a helping hand during the tunnel excavation work.

Our gratitude is also extended to Pär Kinnbom (PKM Innovation AB, modeller) who performed all the tests on the laser scan data and provided us with some of the figures (Figures 5-5 to 5-8) and models (Appendices II C, III D and E, IV C and V C) related to the laser scanning and to Ingemar Markstöm (Golder Associates AB) who contributed with Figure 3-12.

Appendices

Appendix I

Tunnel face mapping, all faces section 6.1–80.73

I A Legends to the geological maps of the TASS-tunnel faces

I B Geological maps and photos of the TASS-tunnel faces

Appendix I A

Legends to the geological maps of the TASS-tunnel faces

General:

Scale: The squares of the grid in the drawing = 1×1 m.

Legends to the tunnel faces of Stage 1, section 6.1–20.74

Legend: F (face). Section: 6.1 m:

Rock types:

- B0 = Äspö diorite/granodiorite, grey, medium-grained (1–5 mm), porphyritic texture, showing no alteration and homogeneous structure.
- B1 = Äspö diorite/granodiorite, reddish grey, medium-grained (1–5 mm), porphyritic texture, showing weak alteration (red staining/oxidation) and homogeneous structure.
- B2 = Fine-grained granite/aplite, greyish red, medium-grained (1–5 mm), uniform texture, showing weak alteration (red staining/oxidation) and homogeneous structure.
- B3 = Fine-grained granite/aplite, red, fine-grained (< 1 mm), uniform texture, showing no alteration and homogeneous structure.

Contacts: K0–K4 and dashed line.

Fractures: 01–09 and continuous line.

Water: A–B and v and vvv (v = occasional drops, minor seepage or patch of moisture; vvv = flow).

Legend: F (face). Section: 8.7 m

Rock types:

- B0 = Äspö diorite/granodiorite, grey, medium-grained (1–5 mm), porphyritic texture (partly only slightly porphyritic), showing no alteration and homogeneous structure.
- B1 = Äspö diorite/granodiorite, reddish grey, medium-grained (1–5 mm), porphyritic texture, showing weak alteration (red staining/oxidation) and massive/irregular structure. Partly banded, weak oxidation, yellowish tint, partly oxidized, reddish.
- B3 = Fine-grained granite/aplite, reddish grey, fine-grained (< 1 mm), uniform texture, showing no alteration and homogeneous structure. Including fine-medium-grained (< 1–5 mm) granite, partly with pegmatite contacts.

Contacts: K0–K3 and dashed line.

Fractures: 01–09 and continuous line.

Water: A–C and v and vvv (v = occasional drops, minor seepage or patch of moisture; vvv = flow).

Legend: F (face). Section: 12.75 m

Rock types:

- B0 = Äspö diorite/granodiorite, grey (to reddish grey), medium-grained (1–5 mm), porphyritic texture, showing no alteration and homogeneous structure. Contains mafic xenolith lenses 20–40 cm long, approx. 1% of area.
- B1 = Äspö diorite/granodiorite, greyish red, medium-grained (1–5 mm), uniform (to irregular) texture, showing weak alteration (red staining/oxidation) and homogeneous structure.
- B2 = Äspö diorite/granodiorite, greyish red, medium-grained (1–5 mm), uniform texture, showing no alteration and massive/irregular structure. Laminated with sub-irregular bands of granitic material 5–10 cm wide.
- B3 = Fine-grained granite/aplite, red, fine-grained (< 1 mm), uniform texture, showing no alteration and massive/irregular structure. Slightly laminated (deformed sub-parallel to contact).

Contacts: K0–K4 and dashed line.

Fractures: 01–15 and continuous line.

Water: A–C and v–vvv (v = occasional drops, minor seepage or patch of moisture; vv = drops, seepage or wet surface; vvv = flow).

Legend: F (face). Section: 16.9 m

Rock types:

- B0 = Äspö diorite/granodiorite, grey, medium-grained (1–5 mm), porphyritic texture, showing no alteration and homogeneous structure. Mafic xenolith lenses ≤ 10 x 40 cm big, ca 1% of area.
- B1 = Äspö diorite/granodiorite, reddish grey, medium-grained (1–5 mm), porphyritic texture, showing weak alteration (red staining/oxidation) and homogeneous structure.
- B3 = Fine-grained granite/aplite, greyish red, fine-grained (< 1 mm), uniform texture, showing no alteration and massive/irregular structure. Possible rests of more felsic granite.

Contacts: K0–K1 and dashed line.

Fractures: 01–14 and continuous line.

Water: A–G and v–vvv (v = occasional drops, minor seepage or patch of moisture; vv = drops, seepage or wet surface; vvv = flow).

Legend: F (face). Section: 20.74 m

Rock types:

- B0 = Äspö diorite/granodiorite, grey, medium-grained (1–5 mm), porphyritic texture, showing no alteration and homogeneous structure.
- B1 = Äspö diorite/granodiorite, greyish red, medium-grained (1–5 mm), uniform texture, showing weak alteration (red staining/oxidation) and homogeneous structure.
- B3 = Fine-grained granite/aplite, red, fine-grained (< 1 mm), uniform texture, showing no alteration and homogeneous structure. Schlieren that ends in right-hand wall.
- B5 = Äspö diorite/granodiorite, reddish grey, medium-grained (1–5 mm), uniform texture, showing no alteration and homogeneous structure. Probably granitized Äspö diorite to hybrid rock.
- B7 = Pegmatite, white, coarse-grained (> 5 mm), uniform texture, showing no alteration and homogeneous structure. Pegmatite consists mainly of quartz.

Contacts: K0–K3 and dashed line.

Fractures: 01–23 and continuous line.

Water: A–G and v and vvv (v = occasional drops, minor seepage or patch of moisture; vvv = flow).

Legends to the tunnel faces of Stage 2, section 24.84–48.67 m

Legend: F (face). Section: 24.84 m:

Rock types:

- B0 = Äspö diorite/granodiorite, reddish grey (to grey), medium-grained (1–5 mm), porphyritic texture, showing no (to weak) alteration and massive/irregular (to homogeneous) structure.

Fractures: 01–14 and continuous line.

Water: A–C and v–vv (v = occasional drops, minor seepage or patch of moisture; vv = drops, seepage or wet surface).

Legend: F (face). Section: 28.94 m

Rock types:

- B0 = Äspö diorite/granodiorite, grey, medium-grained (1–5 mm), porphyritic texture, showing no alteration and homogeneous structure.
- B3 = Fine-grained granite/aplite, red, fine-grained (< 1 mm), uniform texture, showing no alteration and homogeneous structure. Possibly hybrid rock.
- B4 = Pegmatite, light red, coarse (to medium) grained (> 5 to 1–5 mm), uniform texture, showing no alteration and homogeneous structure.
- B5 = Äspö diorite/granodiorite, reddish grey, medium-grained (1–5 mm), porphyritic texture, showing weak alteration (red staining/oxidation) and homogeneous structure. Hybrid rock.

Contacts: K0–K3 and dashed line.

Fractures: 01–18 and continuous line.

Water: A–C and v–vv (v = occasional drops, minor seepage or patch of moisture; vv = drops, seepage or wet surface).

Legend: F (face). Section: 32.94 m

Rock types:

- B0 = Äspö diorite/granodiorite, grey, medium-grained (1–5 mm), porphyritic texture, showing no alteration and gneissified structure. Approximately 70% of rock is weakly deformed, rest is massive to homogeneous.

Fractures: 01–26 and continuous line.

Water: A–G and v–vv (v = occasional drops, minor seepage or patch of moisture; vv = drops, seepage or wet surface).

Legend: F (face). Section: 37.5 m

Rock types:

- B0 = Äspö diorite/granodiorite, grey, medium-grained (1–5 mm), porphyritic texture, showing no alteration and homogeneous structure.

Fractures: 01–31 and continuous line.

Water: A–G and v–vvv (v = occasional drops, minor seepage or patch of moisture; vv = drops, seepage or wet surface, vvv = flow).

Legend: F (face). Section: 42.14 m

Rock types:

- B0 = Äspö diorite/granodiorite, grey, medium-grained (1–5 mm), porphyritic texture, showing no alteration and homogeneous structure.

Fractures: 01–19 and continuous line.

Water: A–C and v (v = occasional drops, minor seepage or patch of moisture).

Legend: F (face). Section: 45.72 m:

Rock types:

- B0 = Äspö diorite/granodiorite, grey, medium-grained (1–5 mm), porphyritic texture, showing no alteration and homogeneous structure. Elongated xenoliths of mafic rock occur approximately 20–100 cm long and 5–20 cm wide.
- B2 = Mafic rock (undifferentiated)/greenstone (to gabbro/gabbroic rock), black, medium-grained (1–5 mm), uniform texture, showing no alteration and homogeneous structure. Elongated xenoliths approximately 20–100 cm long and 5–20 cm wide.

Contacts: K0 and dashed line.

Fractures: 01–24 and continuous line.

Water: A–G and v–vv (v = occasional drops, minor seepage or patch of moisture; vv = drops, seepage or wet surface).

Legend: F (face). Section: 48.67 m:

Rock types:

- B0 = Äspö diorite/granodiorite, grey, medium-grained (1–5 mm), porphyritic texture, showing no alteration and homogeneous structure. Mafic rock (undifferentiated) / greenstone lenses on right-hand side of front, size: approximately ≤ 10×40 cm, << 1%.
- B3 = Fine-grained granite/aplite, reddish grey, medium-grained (1–5 mm), irregular texture, showing no alteration and massive/irregular structure. Thin band parallel to fracture number 03, partly pegmatite.
- B5 = Hybrid rock, greyish red, medium-grained (1–5 mm), irregular texture, showing weak alteration (red staining/oxidation) and massive/irregular structure. Thin band parallel to fracture number 03.

Contacts: K0–K1 and dashed line.

Fractures: 01–36 and continuous line.

Fracture zone: Z0 and dash-dot-dashed line. The zone category is increased fracturing; structure is irregular and alteration is weak.

Water: A–C and v (v = occasional drops, minor seepage or patch of moisture).

Legends to the tunnel faces of Stage 3, section 52.72–64.6 m

Legend: F (face). Section: 52.72 m:

Rock types:

- B0 = Äspö diorite/granodiorite, grey, medium-grained (1–5 mm), porphyritic texture, showing no alteration and homogeneous structure.
- B3 = Fine-grained granite/aplite, red, fine (to medium) grained (< 1 to 1–5 mm), uniform texture, showing no alteration and homogeneous structure. Approximately 30 cm wide.
- B5 = Äspö diorite/granodiorite, greyish red, medium-grained (1–5 mm), irregular (to partly porphyritic) texture, showing no alteration and massive/irregular structure. More or less granitized Äspö diorite (hybrid rock).

Contacts: K0–K1 and dashed line.

Fractures: 01–21 and continuous line.

Water: A–E and v–vv (v = occasional drops, minor seepage or patch of moisture; vv = drops, seepage or wet surface).

Legend: F (face). Section: 56.77 m

Rock types:

- B0 = Äspö diorite/granodiorite, grey (with weak red grey tone), medium-grained (1–5 mm), porphyritic texture, showing no alteration and homogeneous structure.
- B2 = Fine-grained granite/aplite, red, fine (to medium) grained (< 1 to 1–5 mm), uniform texture, showing no alteration and homogeneous structure.
- B3 = Fine-grained granite/aplite, greyish red, fine-grained (< 1 mm), uniform texture, showing no alteration and schistified (to laminated) structure.

- B5 = Äspö diorite/granodiorite, greyish red, medium-grained (1–5 mm), irregular texture, showing no alteration and massive/irregular (to partly schistified) structure.
- B9 = Quartz vein/dyke, white, coarse (to fine) grained (> 5 to < 1 mm), uniform texture, showing no alteration and homogeneous structure. Quartz dyke.

Contacts: K0–K5 and dashed line.

Fractures: 01–20 and continuous line.

Water: A–E and v (v = occasional drops, minor seepage or patch of moisture).

Legend: F (face). Section: 60.55 m

Rock types:

- B0 = Äspö diorite/granodiorite, grey, medium-grained (1–5 mm), porphyritic texture, showing no alteration and homogeneous structure.
- B4 = Pegmatite, red, coarse-grained (> 5 mm), uniform texture, showing no alteration and homogeneous structure. Approximately 2–10 cm wide.
- B5 = Äspö diorite/granodiorite (to fine-grained granite/aplite), greyish red, medium-grained (1–5 mm), irregular texture, showing weak alteration (partly very weakly oxidized/red stained) and massive/irregular structure. Hybrid rock.

Contacts: K0–K1 and dashed line.

Fractures: 01–25 and continuous line.

Legend: F (face). Section: 64.56 m

Rock types:

- B0 = Äspö diorite/granodiorite, grey, medium-grained (1–5 mm), porphyritic texture, showing no alteration and homogeneous structure.
- B3 = Fine-grained granite/aplite, red, fine-grained (< 1 mm), uniform texture, showing no alteration and gneissified structure. Weak foliation/lineation occurs.
- B6 = Fine-grained granite/aplite, greyish red, medium-grained (1–5 mm), porphyritic texture, showing no alteration and homogeneous structure. Laminated granitic hybrid band approximately 5 cm wide with < 5 cm wide mafic borders.

Contacts: K0 and K4 and dashed line.

Fractures: 01–27 and continuous line.

Water: A and v (v = occasional drops, minor seepage or patch of moisture).

Legends to the tunnel faces of Stage 4, section 68.87–80.73 m

Legend: F (face). Section: 68.87 m:

Rock types:

- B0 = Äspö diorite/granodiorite, grey, medium-grained (1–5 mm), porphyritic texture, showing no alteration and homogeneous structure. Occasional mafic rock (undifferentiated) / greenstone lenses/xenoliths occur (≤ 20 cm long).
- B2 = Fine-grained granite/aplite, light red, coarse (to fine) grained (> 5 to < 1 mm), irregular texture, showing no alteration and massive/irregular structure. Thin dykes, with various directions.

Contacts: K0–K2 and dashed line.

Fractures: 01–24 and continuous line.

Legend: F (face). Section: 73.18 m

Rock types:

- B0 = Äspö diorite/granodiorite, grey, medium-grained (1–5 mm), porphyritic texture, showing no alteration and homogeneous structure.
- B6 = Äspö diorite/granodiorite, greyish red, medium-grained (1–5 mm), porphyritic texture, showing no alteration and massive/irregular structure. Hybrid rock, consisting of Äspö diorite and fine-grained granite, ca 50:50, irregular.

Contacts: K0 and dashed line.

Fractures: 01–32 and continuous line.

Water: A–G and v–vv (v = occasional drops, minor seepage or patch of moisture; vv = drops, seepage or wet surface).

Legend: F (face). Section: 77.14 m

Rock types:

- B0 = Äspö diorite/granodiorite, grey, medium-grained (1–5 mm), porphyritic texture, showing no alteration and homogeneous structure.
- B3 = Fine-grained granite/aplite, greyish red, fine-grained (< 1 mm), uniform texture, showing no alteration and gneissified (or shear) structure. Dip ± 5°.
- B8 = Fine-grained granite/aplite, greyish red, medium-grained (1–5 mm), uniform texture, showing no alteration and homogeneous structure. Medium-grained granite, towards B3 more gneissic.

Contacts: K0–K3 and dashed line.

Fractures: 01–19 and continuous line.

Water: A–C and v–vv (v = occasional drops, minor seepage or patch of moisture; vv = drops, seepage or wet surface).

Legend: F (face). Section: 80.73 m

Rock types:

- B0 = Äspö diorite/granodiorite, grey, medium-grained (1–5 mm), porphyritic texture, showing no alteration and homogeneous structure. Lens (size approximately 0.5×1.5 m) rich in mafic rock (undifferentiated) / greenstone fragments occurs.
- B3 = Fine-grained granite/aplite, reddish grey, fine-grained (< 1 mm), uniform texture, showing no alteration and gneissified (to shear) structure.
- B5 = Hybrid rock, reddish grey, medium-grained (1–5 mm), porphyritic texture, showing no alteration and massive/irregular structure. Approximately 50:50 mix of Äspö diorite and medium-grained granite.
- B8 = Fine-grained granite/aplite, red, fine-grained (< 1 mm), uniform texture, showing no alteration and gneissified structure.

Contacts: K0–K3 and dashed line.

Fractures: 01–20 and continuous line.

Water: A and v (v = occasional drops, minor seepage or patch of moisture).

Appendix I B

Geological maps and photos of the TASS-tunnel faces

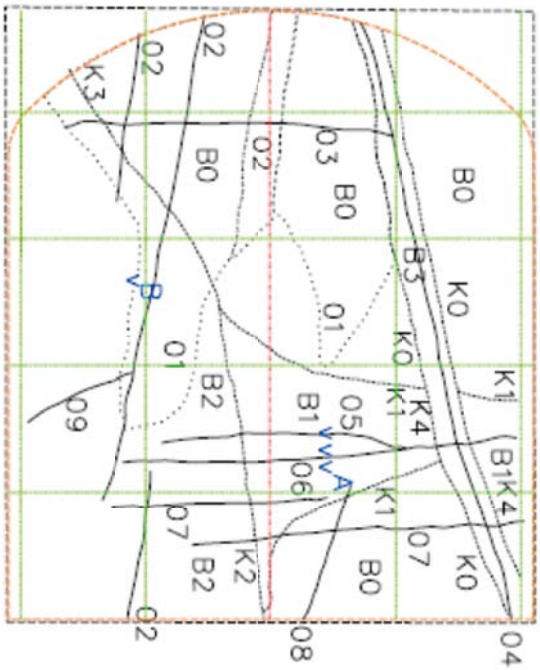

Tunnel face section 6.1 m

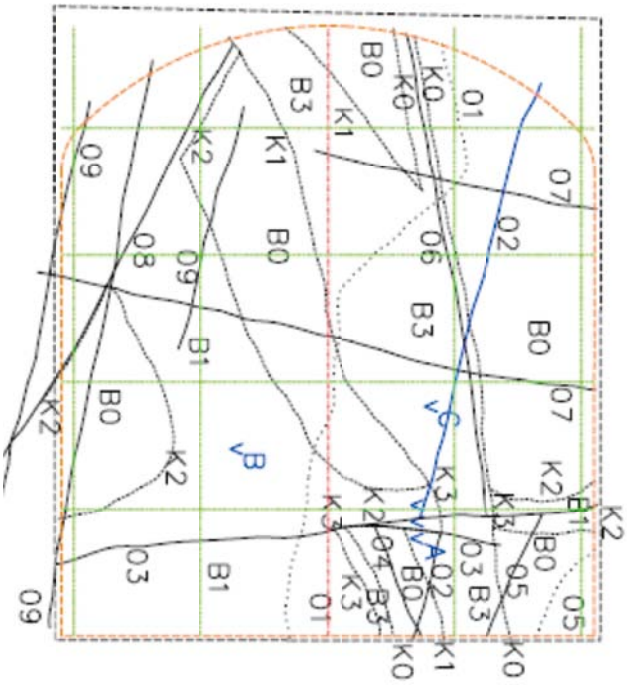

Tunnel face section 8.7 m

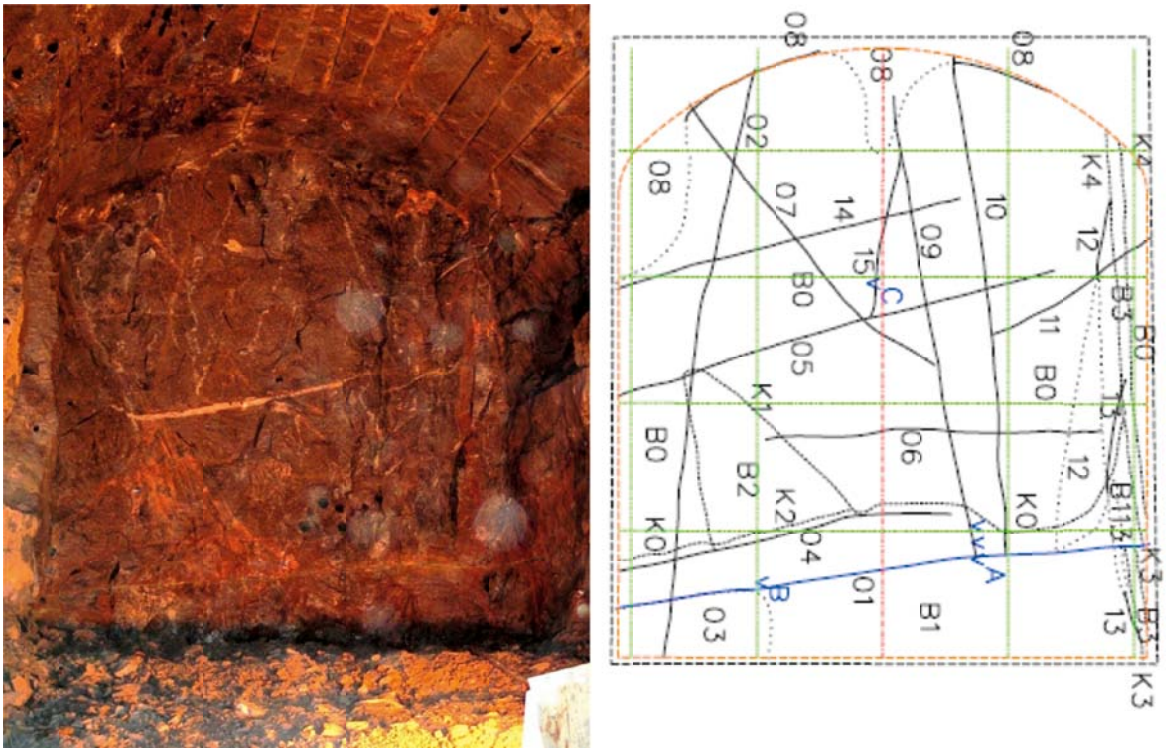

Tunnel face section 12.75 m

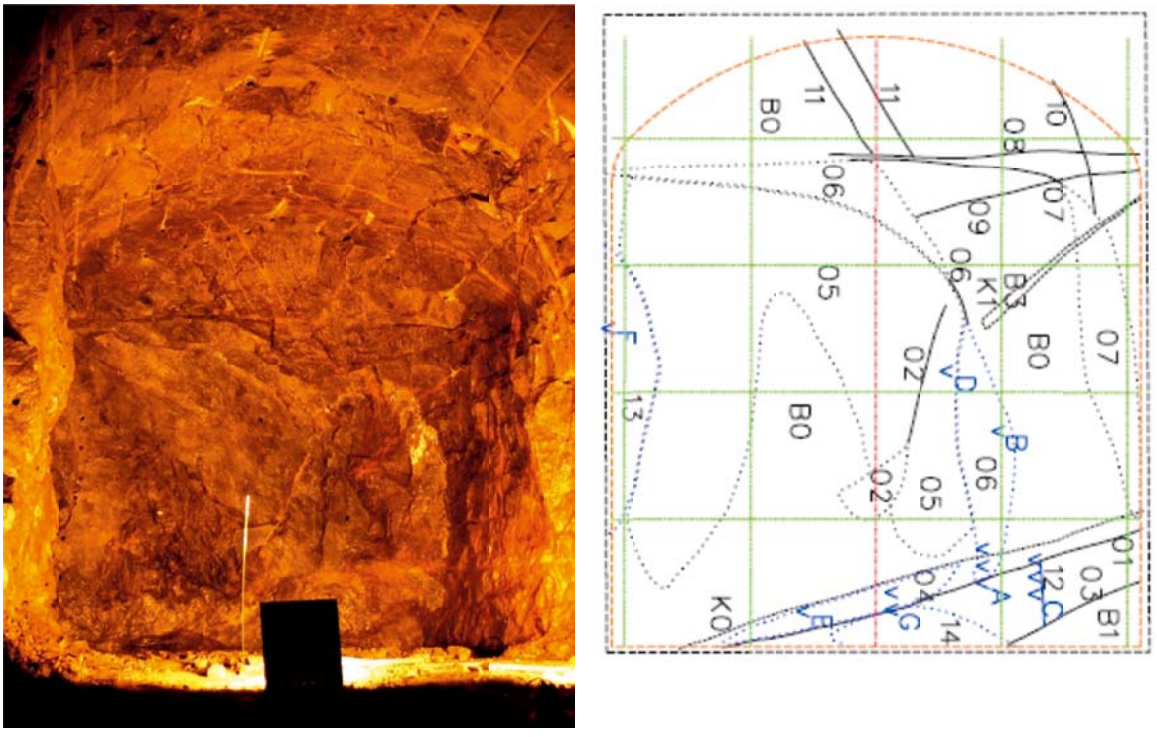

Tunnel face section 16.9 m

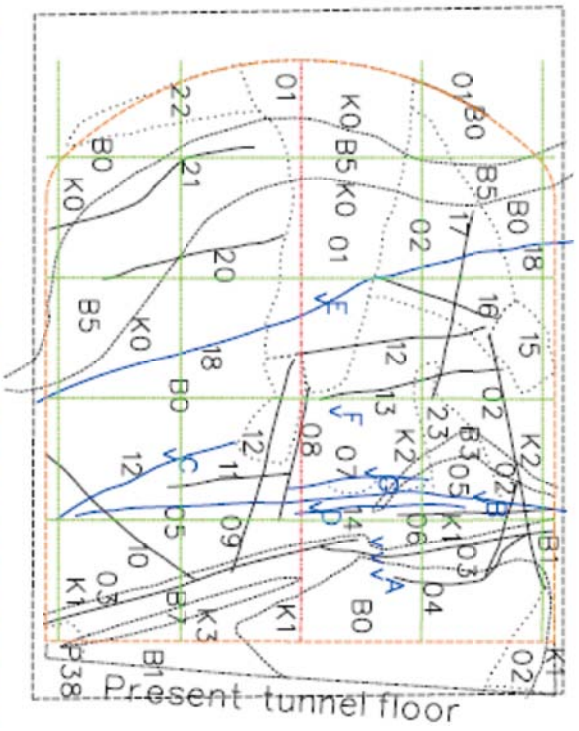

Tunnel face section 20.74 m

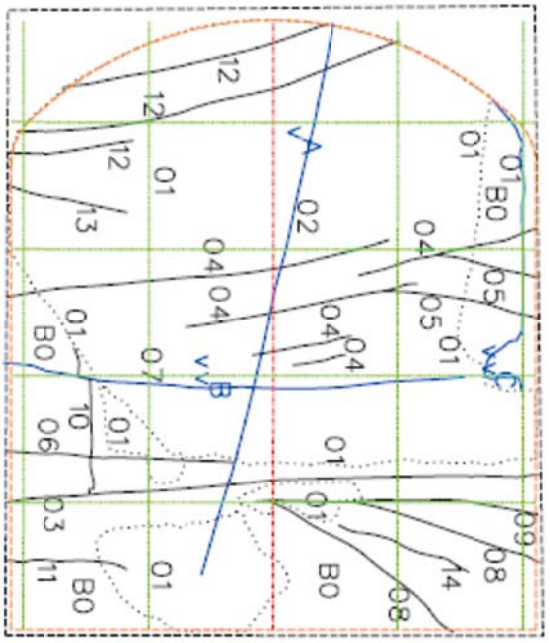

Tunnel face section 24.84 m

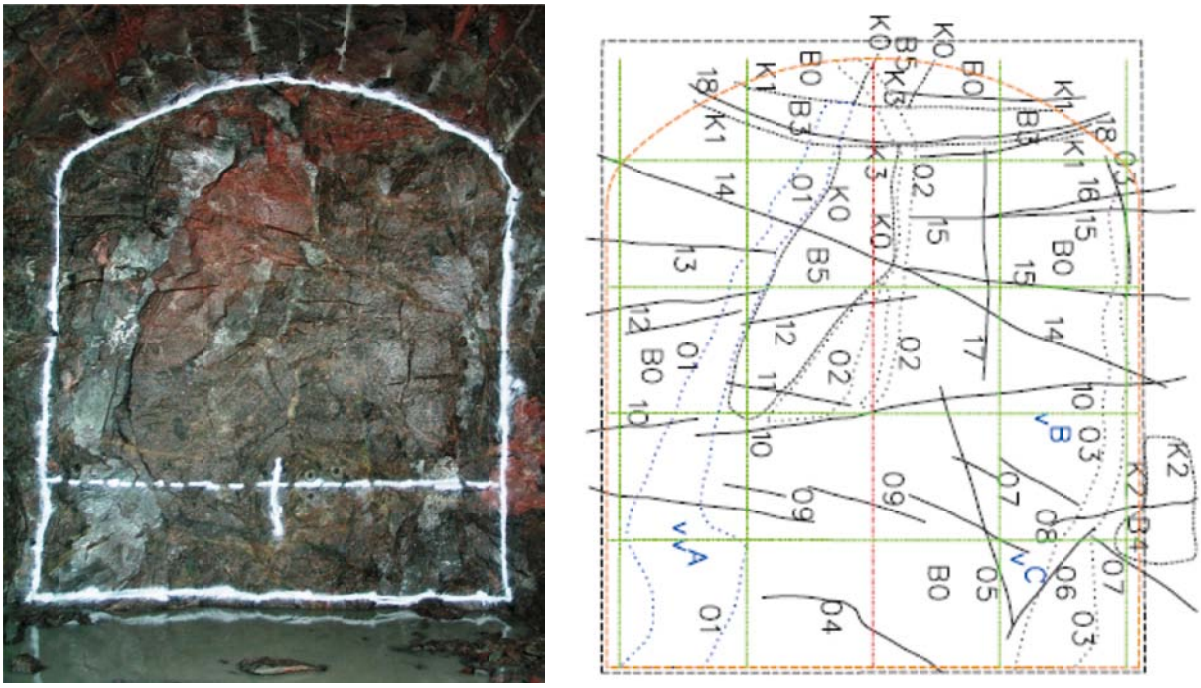

Tunnel face section 28.94 m

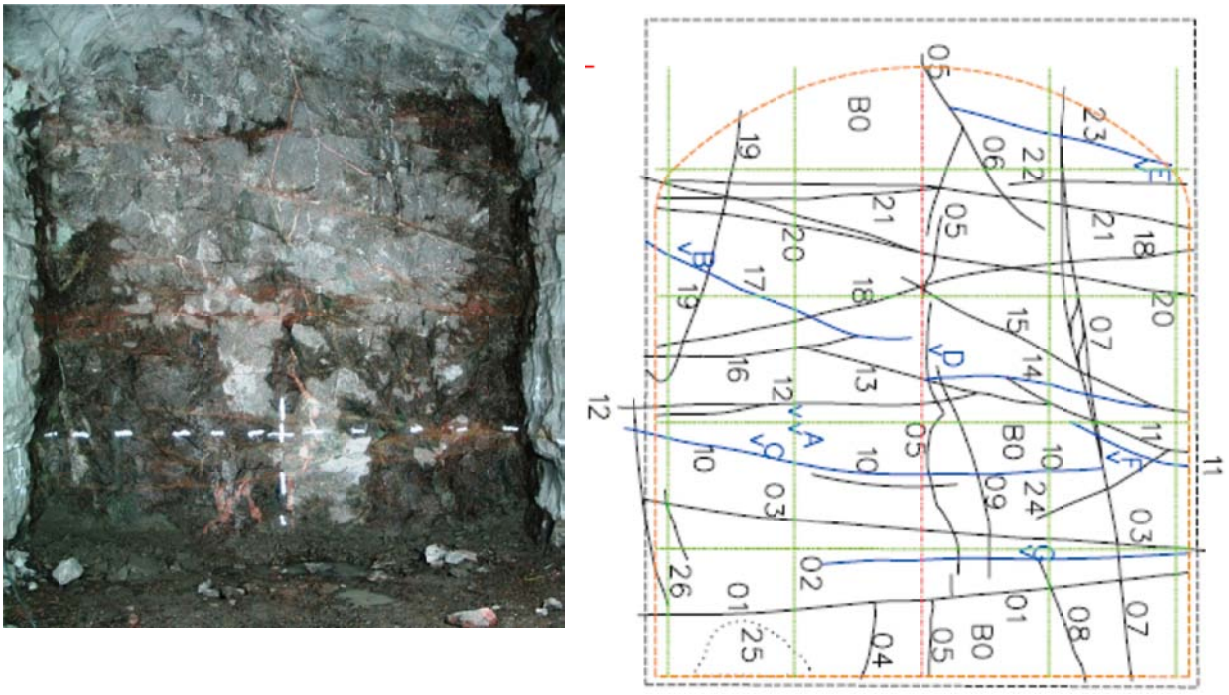

Tunnel face section 32.94 m

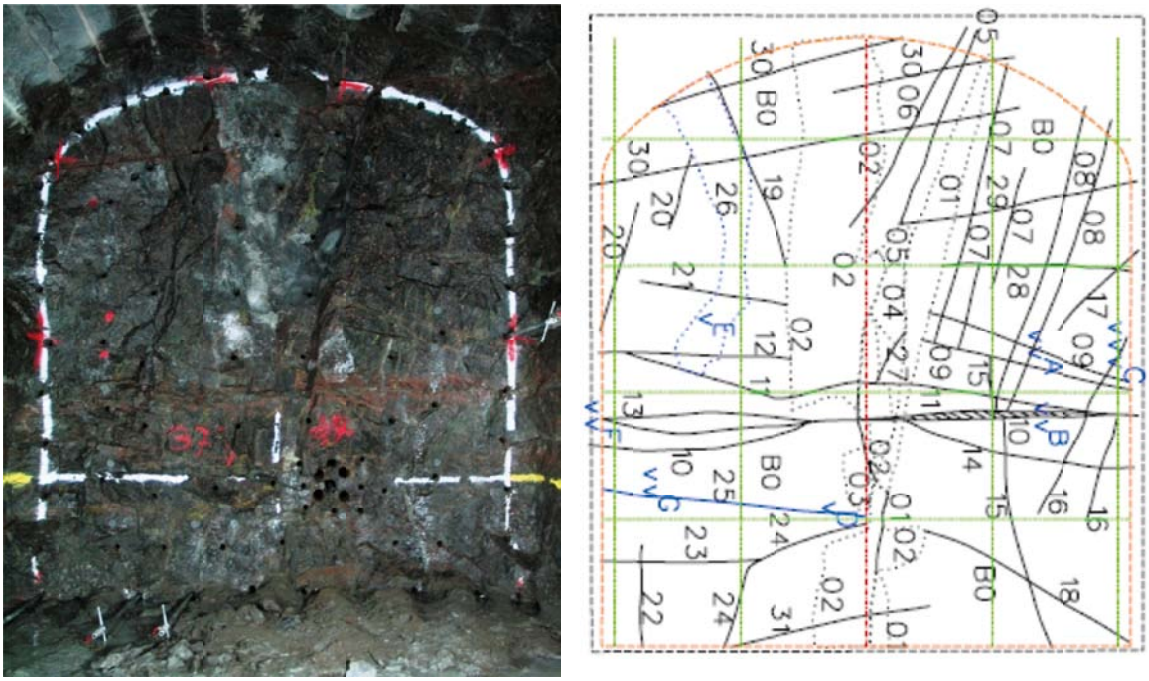

Tunnel face section 37.5 m

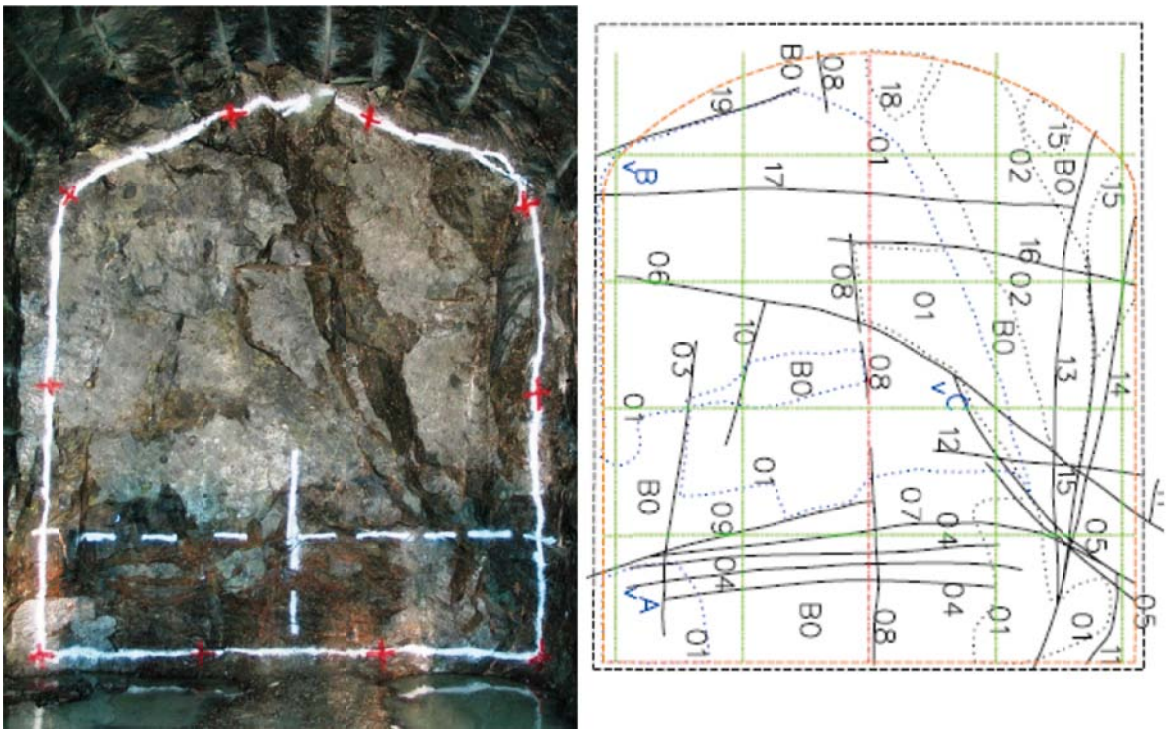

Tunnel face section 42.14 m

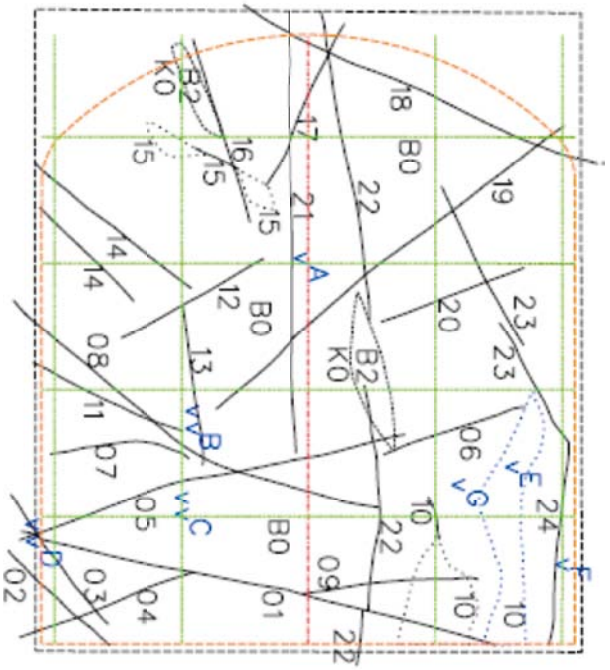

Tunnel face section 45.72 m

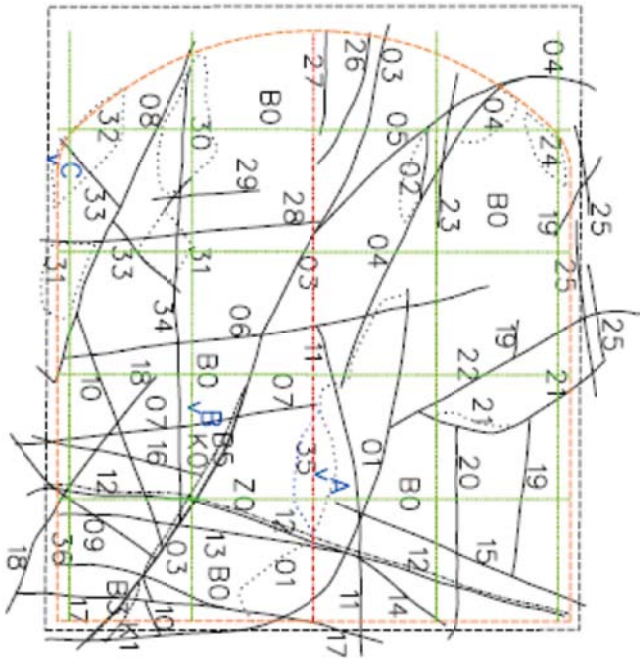

Tunnel face section 48.67 m

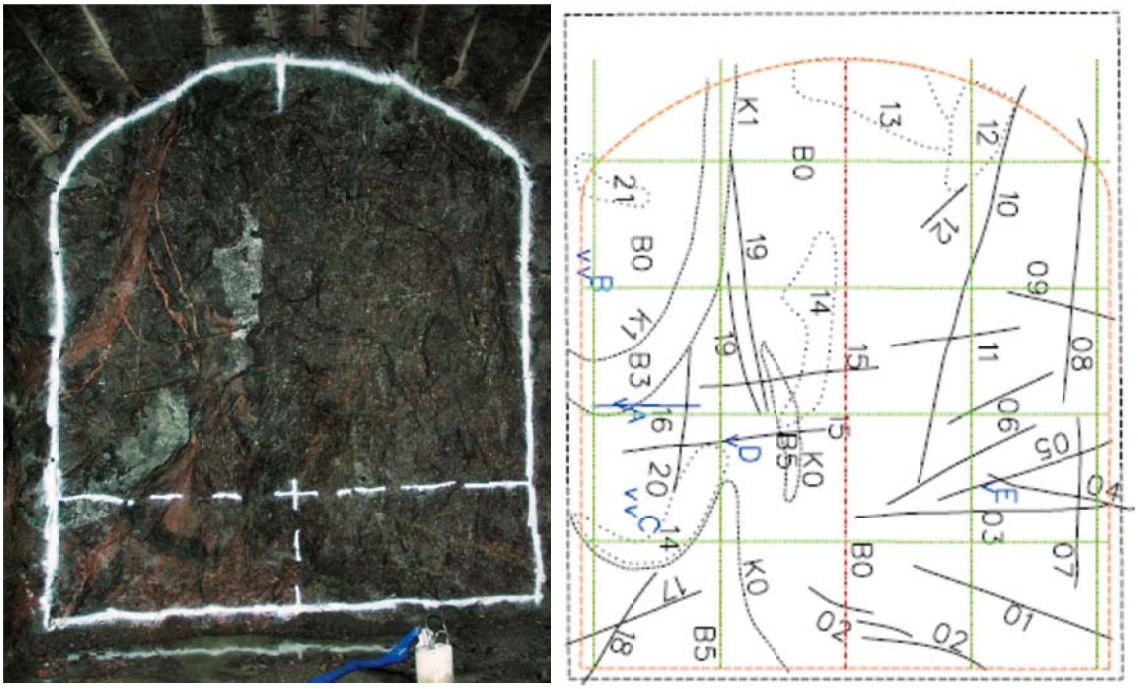

Tunnel face section 52.72 m

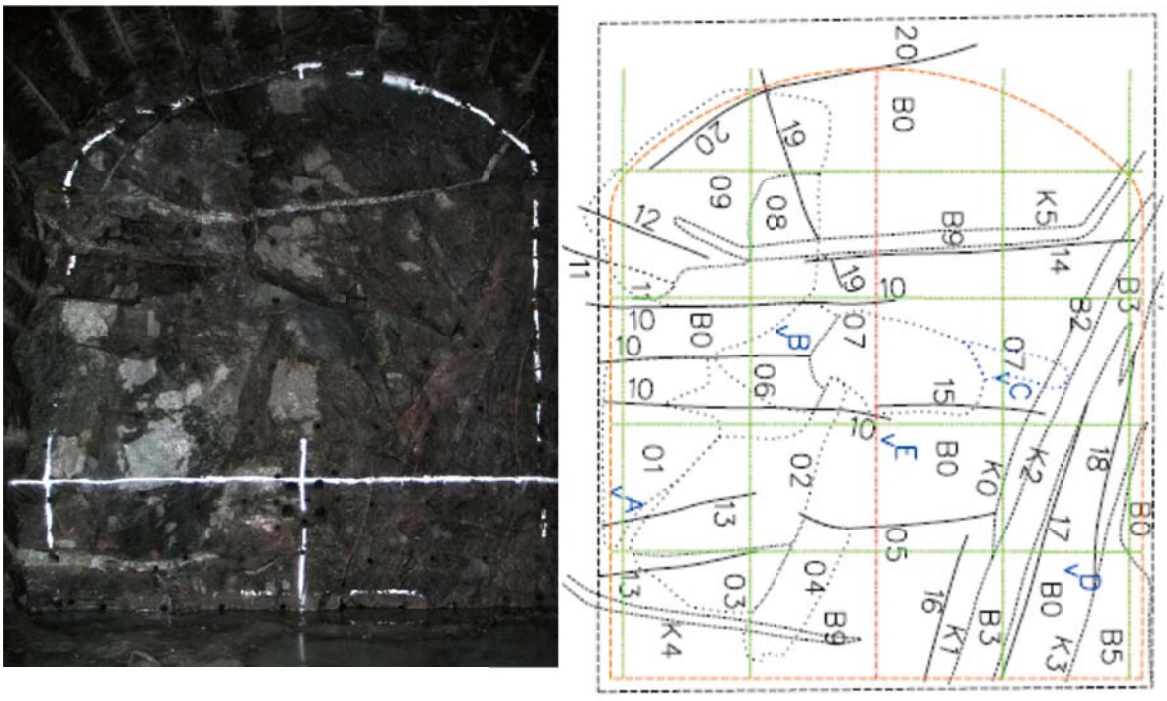

Tunnel face section 56.77 m

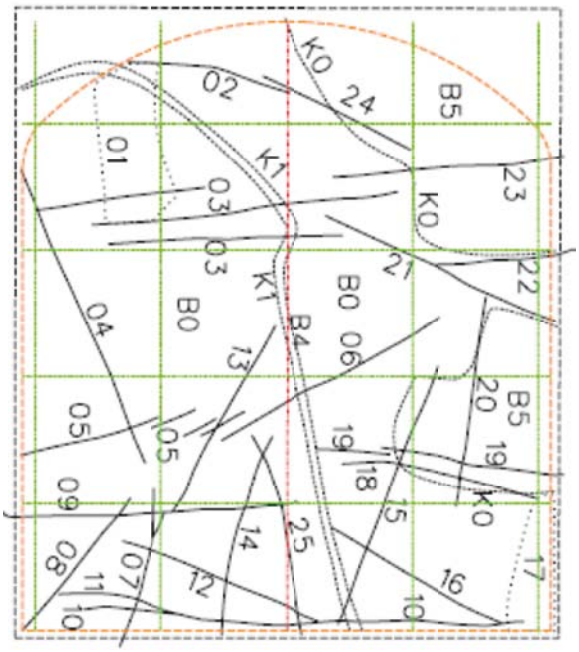

Tunnel face section 60.55 m

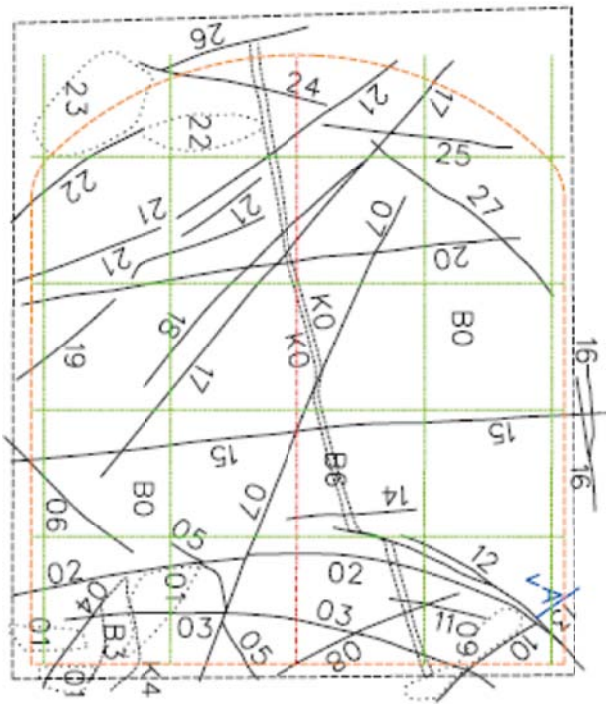

Tunnel face section 64.56 m

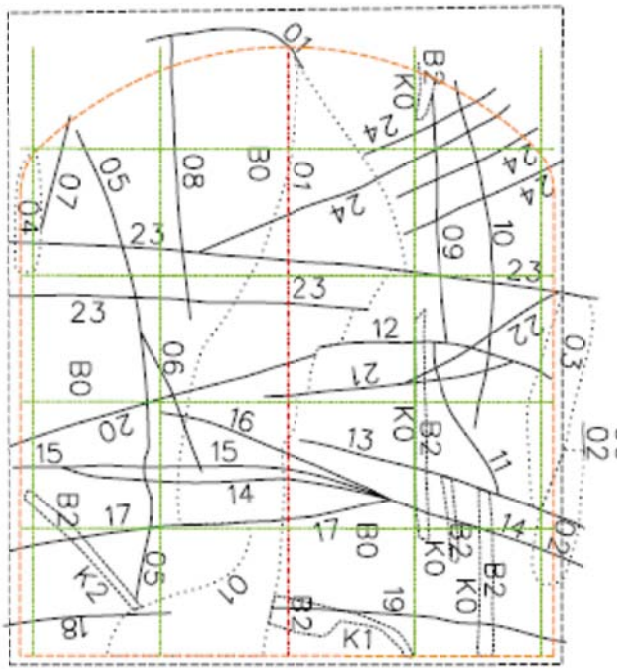

Tunnel face section 68.87 m

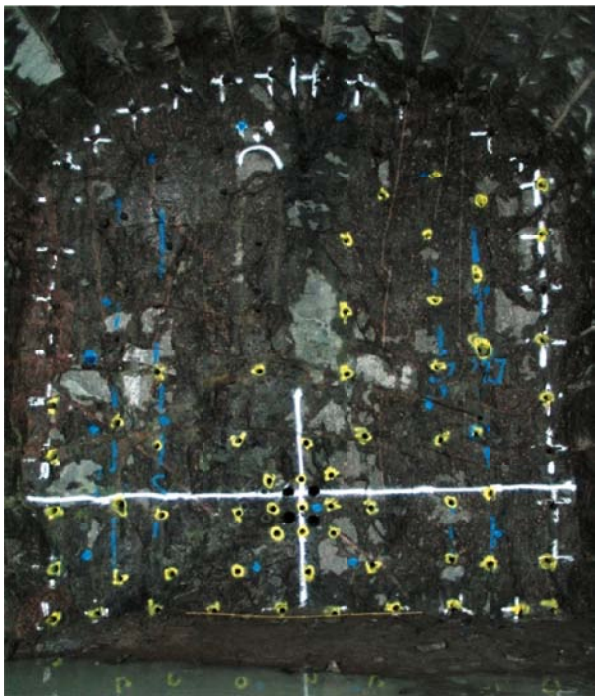

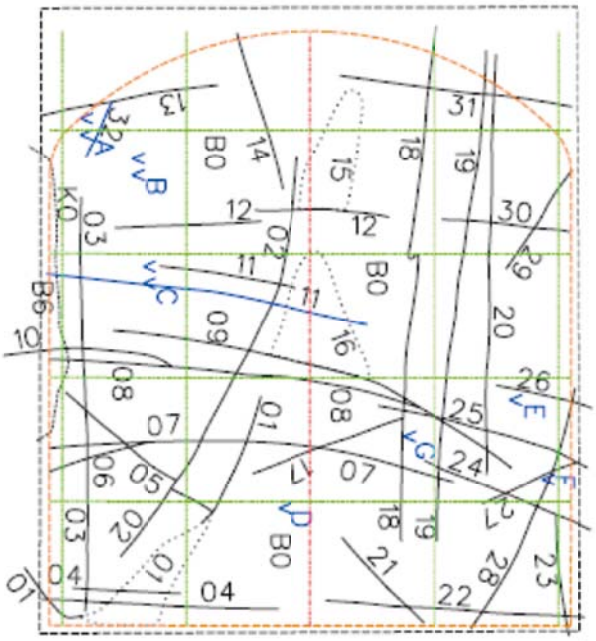

Tunnel face section 73.18 m

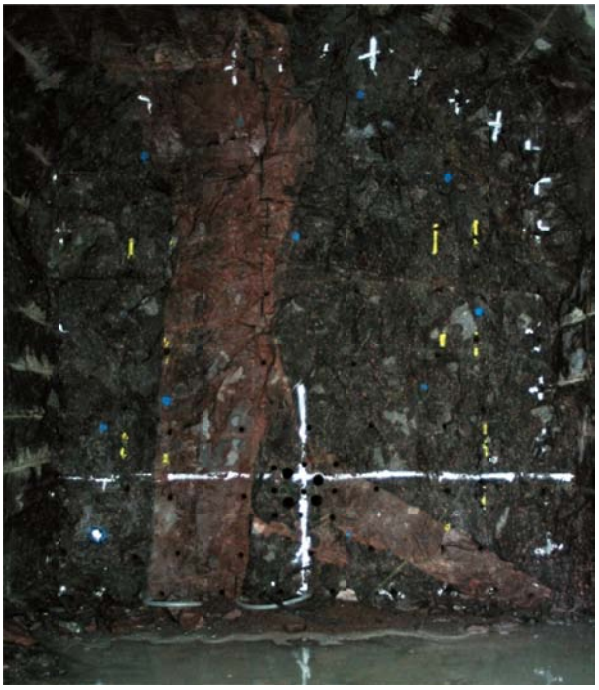

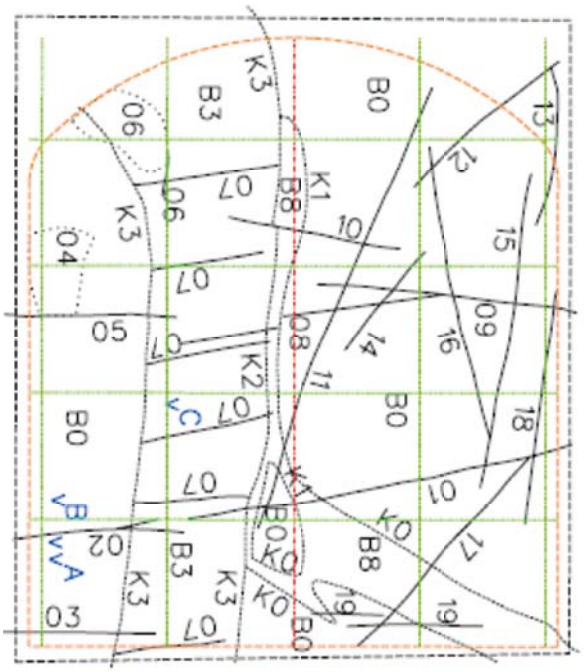

Tunnel face section 77.14 m

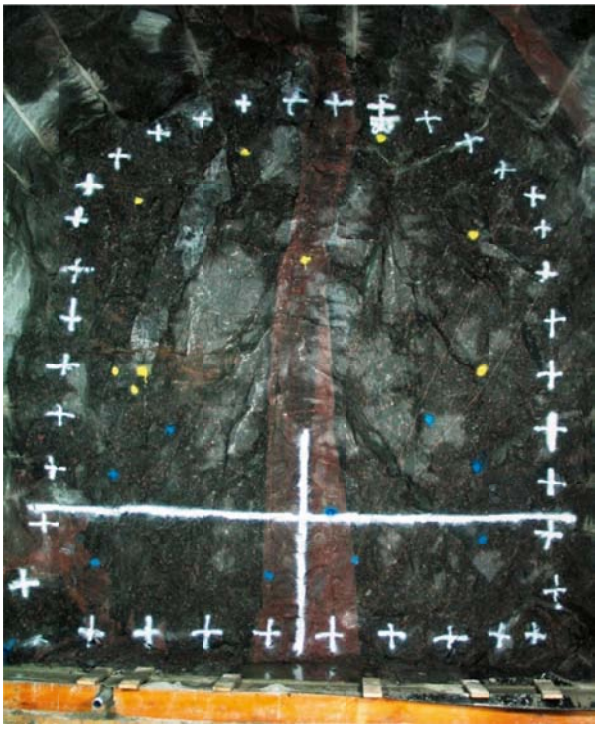

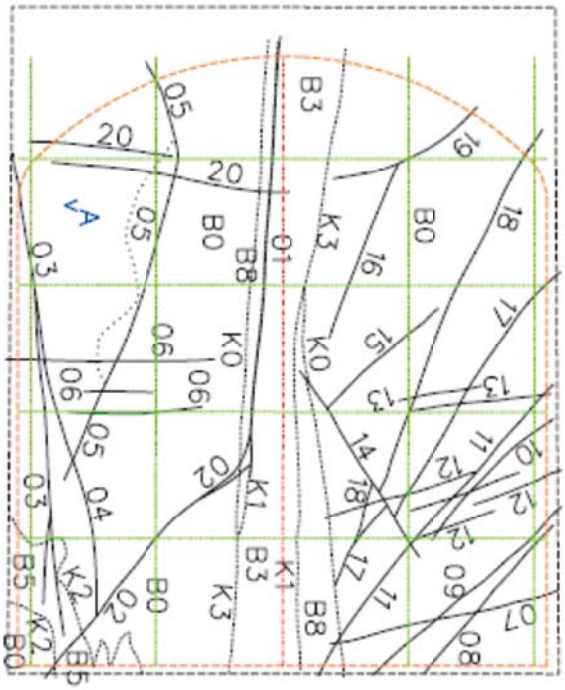

Tunnel face section 80.73 m

Appendix II

Stage mapping: Stage 1, section 0–20.74 m

II A Geological map of tunnel walls and roof with legend

II B Geological map of tunnel floor with legend

II C 3D model with the geological mapping wrapped around a theoretical tunnel model

Appendix II A

Geological map of tunnel walls and roof, with legend

Legend: P (walls and roof). Section: 3–20.74 m:

Rock types:

- B0 = Äspö diorite/granodiorite, grey, medium-grained (1–5 mm), porphyritic texture, showing no alteration and homogeneous structure. Small areas with weakly oxidized (red stained) rock occur.
- B1 = Äspö diorite/granodiorite, greyish red, medium-grained (1–5 mm), porphyritic texture, showing weak alteration (red staining/oxidized) and massive/irregular structure. More or less porphyritic and oxidized (red stained).
- B2 = Fine-grained granite/aplite, reddish grey, fine (to medium) grained (< 1 to 1–5 mm), uniform texture, showing no alteration and homogeneous structure.
- B3 = Fine-grained granite/aplite, red, fine-grained (< 1 mm), uniform texture, showing no alteration and homogeneous structure.
- B4 = Pegmatite, red, coarse-grained (> 5 mm), uniform texture, showing no alteration and homogeneous structure. Centre is often quartz-enriched.
- B5 = Äspö diorite/granodiorite, reddish grey, medium-grained (1–5 mm), irregular texture, showing no alteration and massive/irregular structure. More or less granitized Äspö diorite (hybrid rock?).
- B6 = Quartz vein/dyke, white, fine-grained (< 1 mm), uniform texture, showing no alteration and stratified structure.
- B7 = Quartz vein/dyke, white, fine-grained (< 1 mm), irregular texture, showing no alteration and massive/irregular structure.

Contacts: K0–K19 and dashed line.

Fractures: 01–74 and continuous line.

Water: A–Z and Aa–Uu and v–vvv (v = occasional drops, minor seepage or patch of moisture; vv = drops, seepage or wet surface; vvv = flow).

Scale: The squares of the grid in the drawing = 1×1 m.

Section: Numbers on the left and right-hand sides of the drawing.

North arrow: N indicates magnetic north whereas x indicates north in Äspö 96 coordinate system.

Geological map: P (walls and roof). Section: 3–20.74 m:

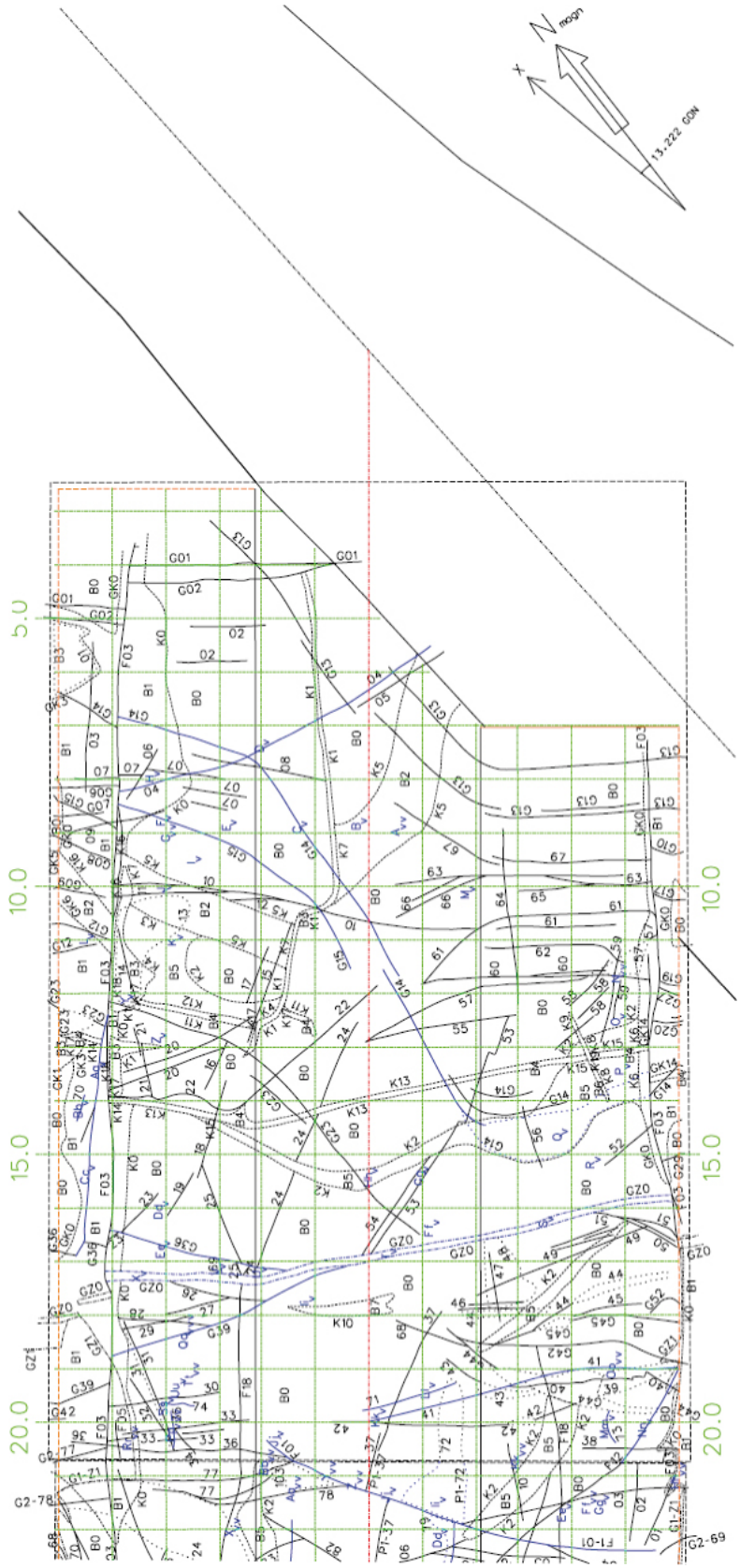

Appendix II B

Geological map of tunnel floor, with legend

Legend: G (floor). Section: 3–20.74 m:

Rock types:

- B0 = Äspö diorite/granodiorite, grey, medium-grained (1–5 mm), porphyritic texture, showing no alteration and homogeneous structure.
- B1 = Äspö diorite/granodiorite, reddish grey (to grey red), medium-grained (1–5 mm), porphyritic texture, showing weak alteration (more or less oxidized/red stained) and homogeneous structure.
- B2 = Fine-grained granite/aplite (both Äspö diorite and pegmatite occur also), greyish red, fine (to medium) grained (< 1 to 1–5 mm), uniform texture, showing no alteration and homogeneous structure.
- B3 = Fine-grained granite/aplite, red, fine-grained (< 1 mm), uniform texture, showing no alteration and homogeneous structure.
- B4 = Pegmatite (with quartz aggregations), red, coarse (to medium) grained (> 5 to 1–5 mm), uniform texture, showing no alteration and homogeneous structure.
- B5 = Äspö diorite/granodiorite, reddish grey, medium-grained (1–5 mm), uniform texture, showing no alteration and homogeneous structure. Hybrid rock?
- B6 = Quartz vein/dyke, white, coarse-grained (> 5 mm), irregular texture, showing no alteration and massive/irregular structure. Quartz aggregation/lens.

Contacts: K0–K17 and dashed line.

Fractures: 01–52 and continuous line.

Fracture zone: Z0–Z1 and dash-dot-dashed line.

Water: A–C and v–vv (v = occasional drops, minor seepage or patch of moisture; vv = drops, seepage or wet surface).

Scale: The squares of the grid in the drawing = 1×1 m.

Section: Numbers on the left and right-hand sides of the drawing.

Geological map: G (floor). Section: 3–20.74 m

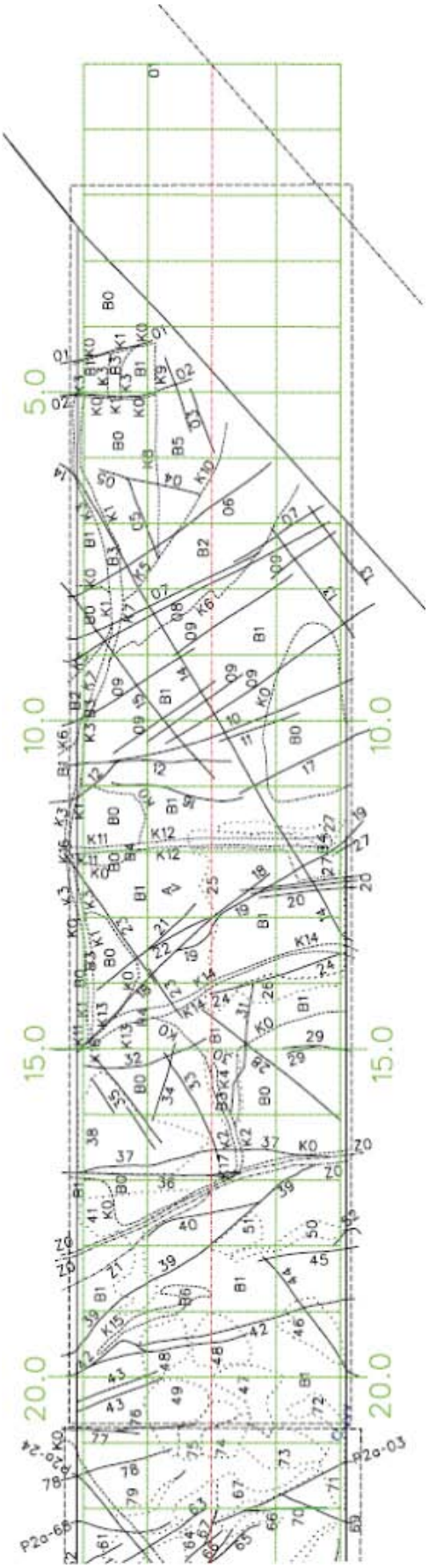

Appendix II C

3D model with the geological mapping wrapped around a theoretical tunnel model
Section: 3-20.74 m.

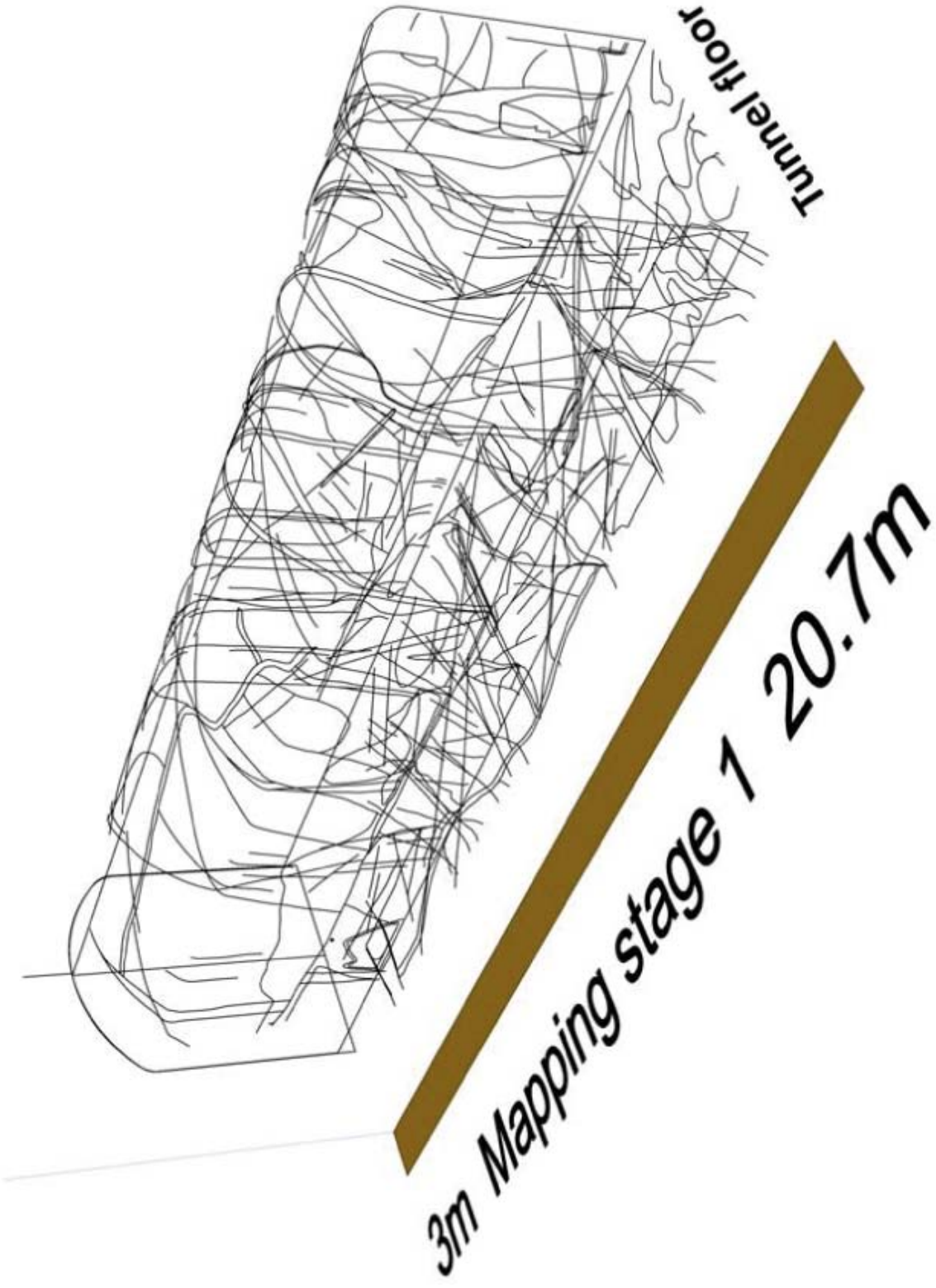

Appendix III

Stage mapping: Stage 2a, section 20.74–32.94 m
Stage 2b, section 32.94–48.67 m

III A Geological map of tunnel walls and roof, with legend (Stage 2a)

III B Geological map of tunnel walls and roof, with legend (Stage 2b)

III C Geological map of tunnel floor, with legend (Stages 2a and 2b)

III D 3D model with the geological mapping wrapped around a theoretical tunnel model

III E 3D model with the geological mapping wrapped around a theoretical tunnel model

Appendix III A

Geological map of tunnel walls and roof, with legend (Stage 2a)

Legend: P (walls and roof). Section: 20.74–32.94 m:

Rock types:

- B0 = Äspö diorite/granodiorite, grey, medium-grained (1–5 mm), porphyritic texture, showing no alteration and homogeneous structure.
- B1 = Äspö diorite/granodiorite, red, medium-grained (1–5 mm), porphyritic texture, showing weak alteration (red staining/oxidation) and homogeneous structure.
- B3 = Fine-grained granite/aplite, red, fine (to medium) grained (< 1 to 1–5 mm), uniform texture, showing no alteration and homogeneous structure. Pegmatite borders 1–2 cm wide.
- B4 = Pegmatite, red, coarse-grained (> 5 mm), uniform texture, showing no alteration and homogeneous structure. Diffuse banding occurs.
- B5 = Äspö diorite/granodiorite, reddish grey, medium-grained (1–5 mm), irregular texture, showing no alteration and massive/irregular structure. More or less granitized Äspö diorite (hybrid rock?).
- B6 = Pegmatite, red, coarse-grained (> 5 mm), uniform texture, showing no alteration and homogeneous structure.

Contacts: K0–K5 and dashed line.

Fractures: 01–103 and continuous line.

Water: A–Z and Aa–Kk and v–vv (v = occasional drops, minor seepage or patch of moisture; vv = drops, seepage or wet surface).

Scale: The squares of the grid in the drawing = 1×1 m.

Section: Numbers on the left and right-hand sides of the drawing.

Geological map: P (walls and roof). Section: 20.74–32.94 m:

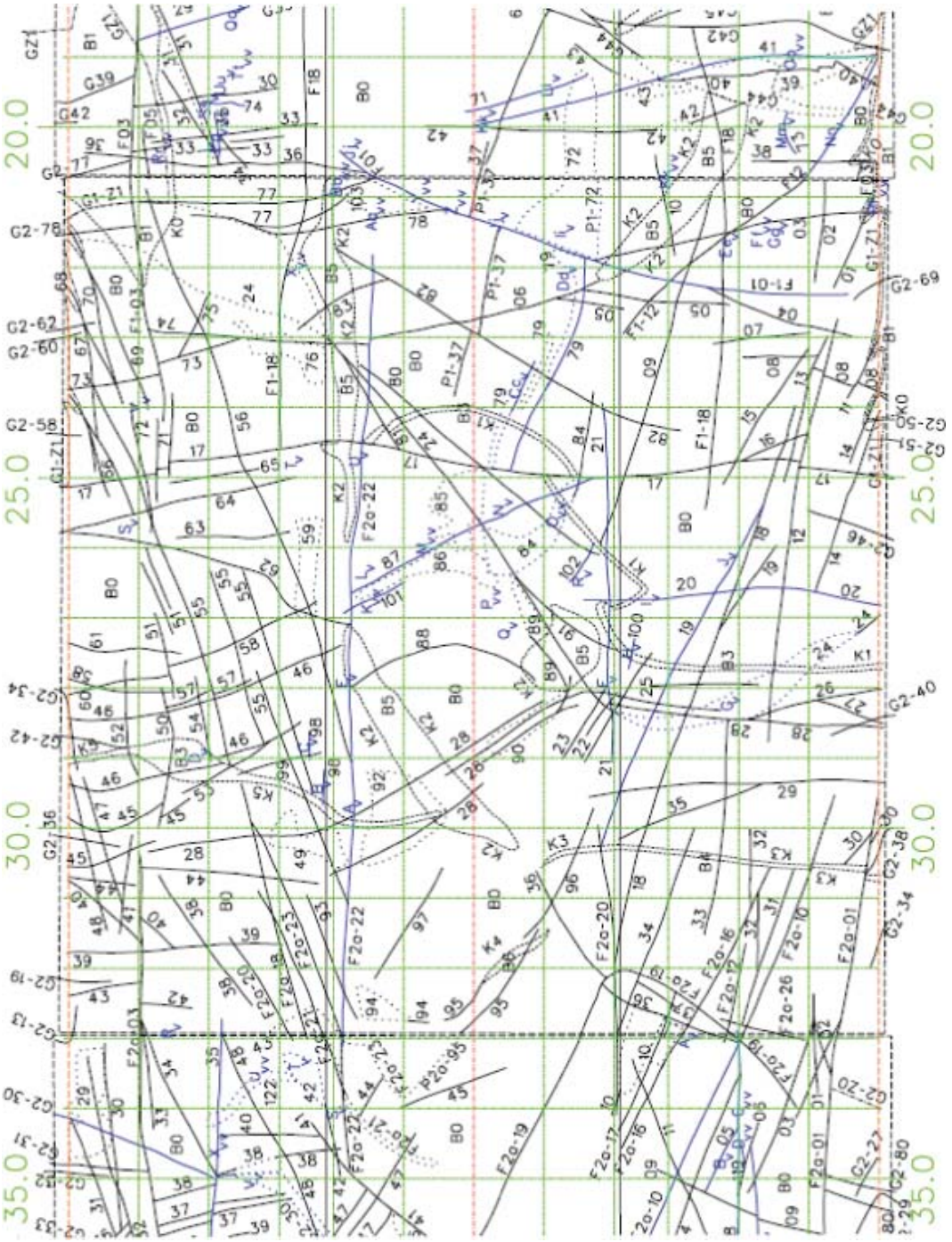

Appendix III B

Geological map of tunnel walls and roof, with legend (Stage 2b)

Legend: P (walls and roof). Section: 32.94–48.67 m:

Rock types:

- B0 = Äspö diorite/granodiorite, grey, medium-grained (1–5 mm), porphyritic texture, showing no alteration and homogeneous structure.
- B1 = Äspö diorite/granodiorite, greyish red, medium-grained (1–5 mm), porphyritic texture, showing weak alteration (red staining/oxidation) and homogeneous structure. Texture partly porphyritic.

Contacts: K0 and dashed line.

Fractures: 01–130 and continuous line.

Water: A–Z and Aa–Zz and Ab–Rs and v–vvv (v = occasional drops, minor seepage or patch of moisture; vv = drops, seepage or wet surface; vvv = flow).

Scale: The squares of the grid in the drawing = 1×1 m.

Section: Numbers on the left and right-hand sides of the drawing.

Geological map: P (walls and roof). Section: 32.94–48.67 m:

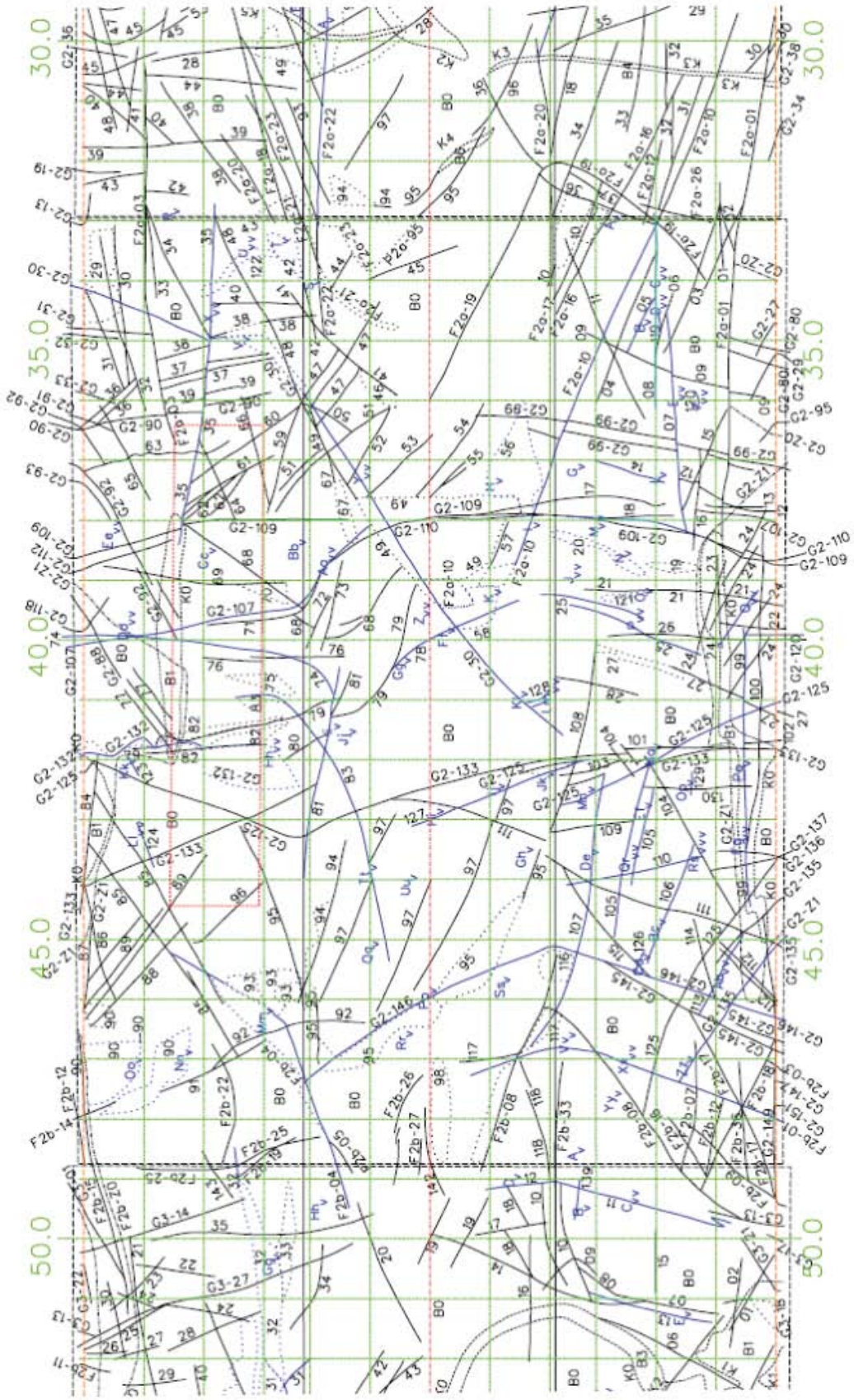

Appendix III C

Geological map of tunnel floor, with legend (Stage 2a and 2b)

Legend: G (floor). Section: 20.74–48.67 m:

Rock types:

- B0 = Äspö diorite/granodiorite, grey, medium-grained (1–5 mm), porphyritic texture, showing no alteration and homogeneous structure.
- B1 = Äspö diorite/granodiorite, greyish red, medium-grained (1–5 mm), porphyritic texture, showing weak alteration (red staining/oxidation) and homogeneous structure.
- B4 = Pegmatite, light red, coarse-grained (> 5 mm), uniform texture, showing no alteration and homogeneous structure. Partly laminated in left-hand side of dike.

Contacts: K0–K4 and dashed line.

Fractures: 01–153 and continuous line.

Fracture zone: Z0–Z1 and dash-dot-dashed line.

Water: A–C and v–vvv (v = occasional drops, minor seepage or patch of moisture; vv = drops, seepage or wet surface; vvv = flow).

Scale: The squares of the grid in the drawing = 1×1 m.

Section: Numbers on the left and right-hand sides of the drawing.

Geological map: G (floor). Section: 20.74–48.67 m:

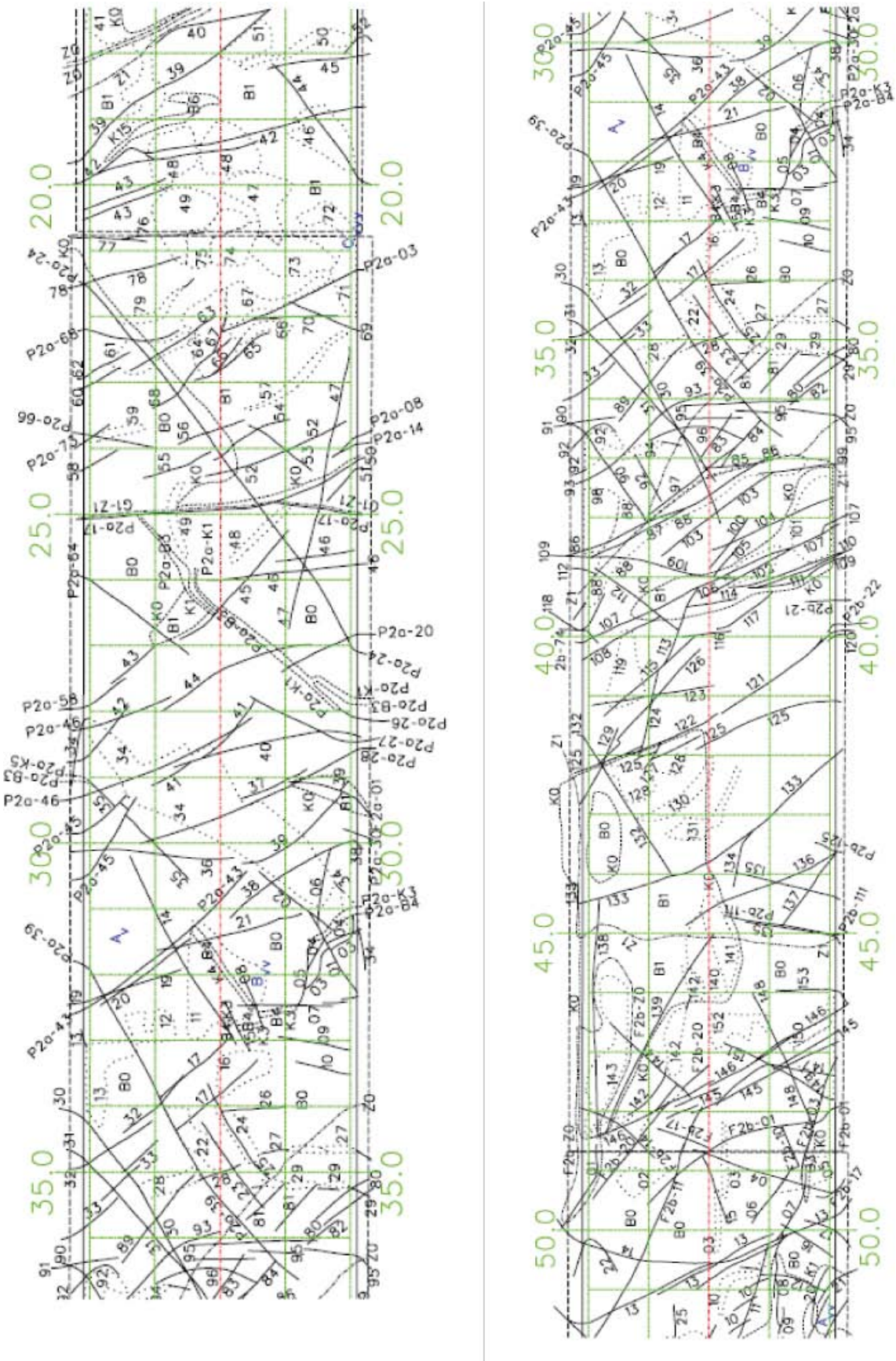

Appendix III D

3D model with the geological mapping wrapped around a theoretical tunnel model
Section: 20.74–32.94 m

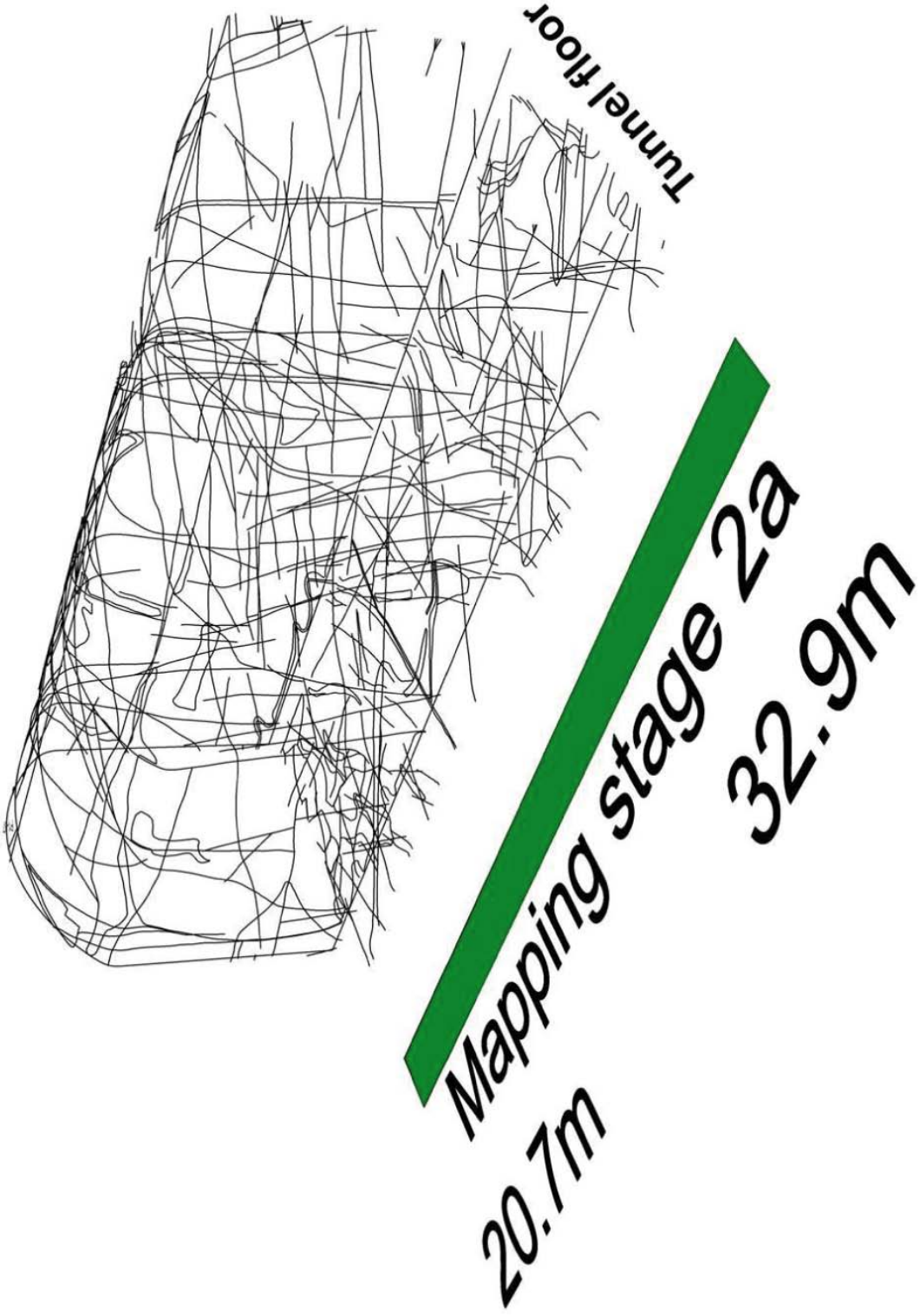

Appendix III E

3D model with the geological mapping wrapped around a theoretical tunnel model
Section: 32.94–48.67 m

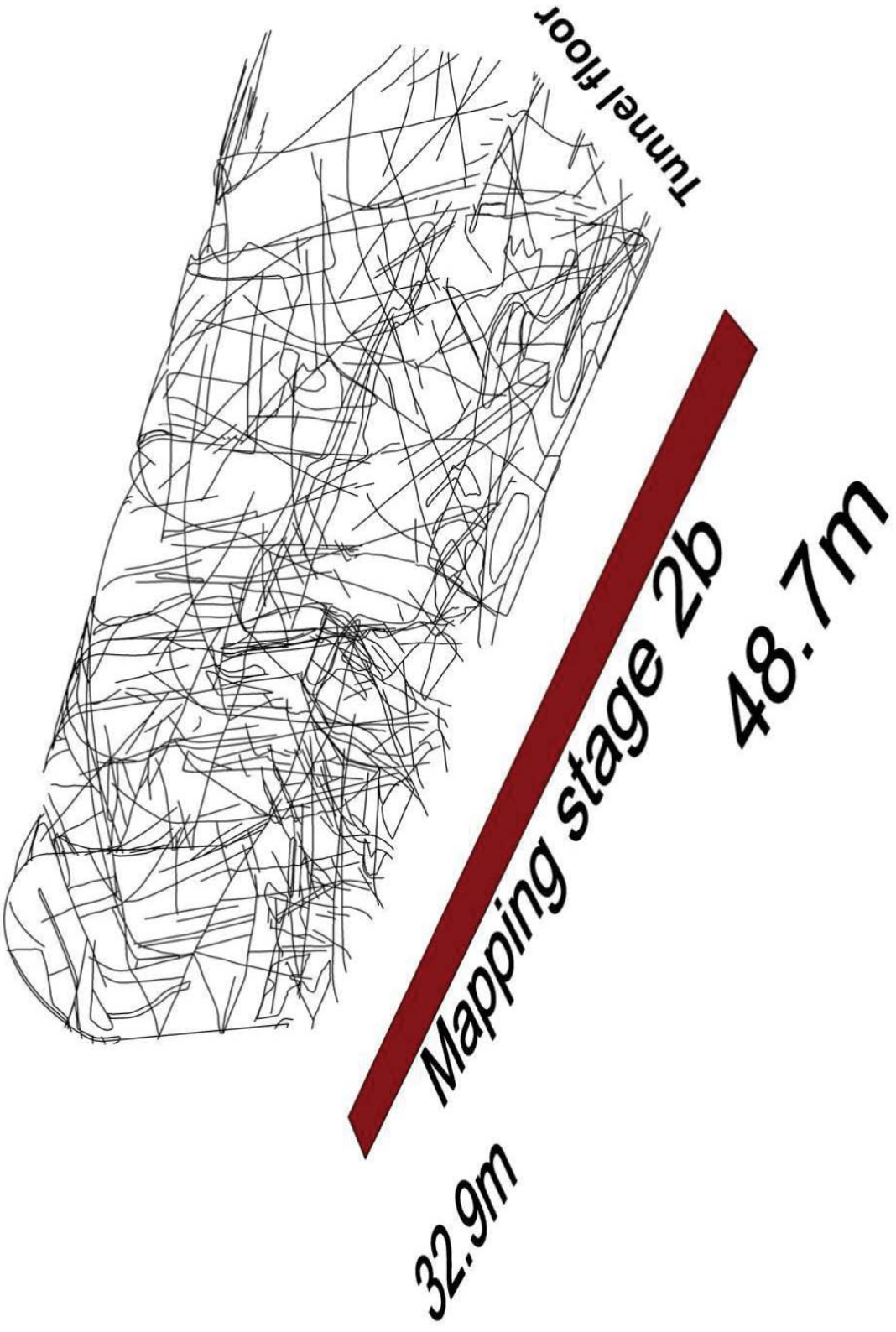

Appendix IV

Stage mapping: Stage 3, Section 48.67–64.56 m

IV A Geological map of tunnel walls and roof, with legend

IV B Geological map of tunnel floor, with legend

IV C 3D model with the geological mapping wrapped around a theoretical tunnel model

Appendix IV A

Geological map of tunnel walls and roof, with legend

Legend: P (walls and roof). Section: 48.67–64.56 m:

Rock types:

- B0 = Äspö diorite/granodiorite, grey, medium-grained (1–5 mm), porphyritic texture, showing no alteration and homogeneous structure.
- B1 = Äspö diorite/granodiorite, greyish red, fine-grained (< 1 mm), irregular texture, showing weak alteration (red staining/oxidation) and massive/irregular structure. Hybrid rock, partly oxidized Äspö diorite and partly fine-grained granite.
- B2 = Mafic rock (undifferentiated)/greenstone, black, fine-grained (< 1 mm), uniform texture, showing no alteration and homogeneous structure. With minor epidote filled fractures.
- B3 = Fine-grained granite/aplite, greyish red, fine-grained (< 1 mm), uniform texture, showing no alteration and homogeneous structure. Dyke displaced approximately 1.5 m by fracture G3-40. Dyke continuation of B6.
- B6 = Fine-grained granite/aplite, greyish red, fine-grained (< 1 mm), uniform texture, showing no alteration and shear structure. Continues from floor, but only minor amounts of Äspö diorite.
- B7 = Fine-grained granite/aplite, greyish red, medium (to fine) grained (1–5 to < 1 mm), uniform texture, showing no alteration and homogeneous structure.
- B9 = Quartz vein/dyke, white, coarse-grained (> 5 mm), uniform texture, showing no alteration and homogeneous structure.

Contacts: K0–K12 and dashed line.

Fractures: 01–144 and continuous line.

Water: A–Z and Aa–Hh and v–vv (v = occasional drops, minor seepage or patch of moisture; vv = drops, seepage or wet surface).

Scale: The squares of the grid in the drawing = 1×1 m.

Section: Numbers on the left and right-hand sides of the drawing.

Geological map: P (walls and roof). Section: 48.67–64.56 m:

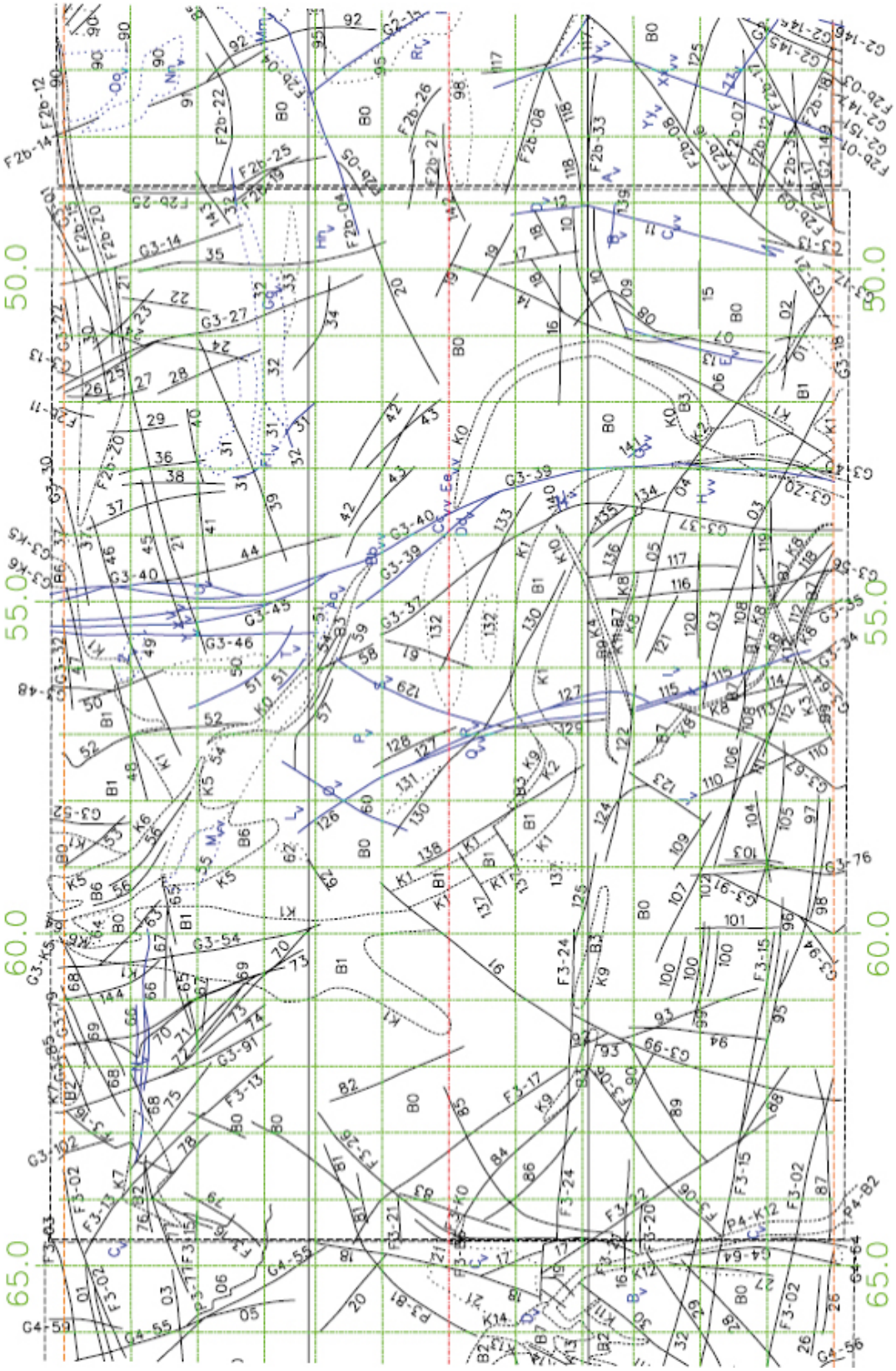

Appendix IV B

Geological map of tunnel floor, with legend

Legend: G (floor). Section: 48.67–64.56 m:

Rock types:

- B0 = Äspö diorite/granodiorite, grey, medium-grained (1–5 mm), porphyritic texture, showing no alteration and homogeneous structure.
- B1 = Äspö diorite/granodiorite, greyish red, fine-grained (< 1 mm), irregular texture, showing weak alteration (red staining/oxidation) and massive/irregular structure. Hybrid rock, partly fine-grained granite and partly oxidized Äspö diorite.
- B2 = Fine-grained granite/aplite, red, medium-grained (1–5 mm), uniform texture, showing no alteration and homogeneous structure. Granite vein/dyke, somewhat irregular orientation.
- B3 = Fine-grained granite/aplite, greyish red, fine-grained (< 1 mm), uniform texture, showing no alteration and homogeneous structure.
- B6 = Fine-grained granite/aplite, greyish red, fine-grained (< 1 mm), uniform texture, showing no alteration and shear structure. Partly coarsely laminated. Includes undefined parts of Äspö diorite/granodiorite.
- B9 = Quartz vein/dyke, white, coarse (to fine) grained (> 5 to < 1 mm), uniform texture, showing no alteration and shear structure. Coarsely laminated. Lens in lower left-hand wall homogeneous and uniform.

Contacts: K0–K6 and K12 and dashed line.

Fractures: 01–109 and continuous line.

Fracture zone: Z0 and dash-dot-dashed line. The zone category is deformation-zone proper (brittle/ductile); structure is lamellar and no alteration is seen.

Water: A–E and vv (vv = drops, seepage or wet surface).

Scale: The squares of the grid in the drawing = 1×1 m.

Section: Numbers on the left and right-hand sides of the drawing.

Geological map: G (floor). Section: 48.67–64.56 m

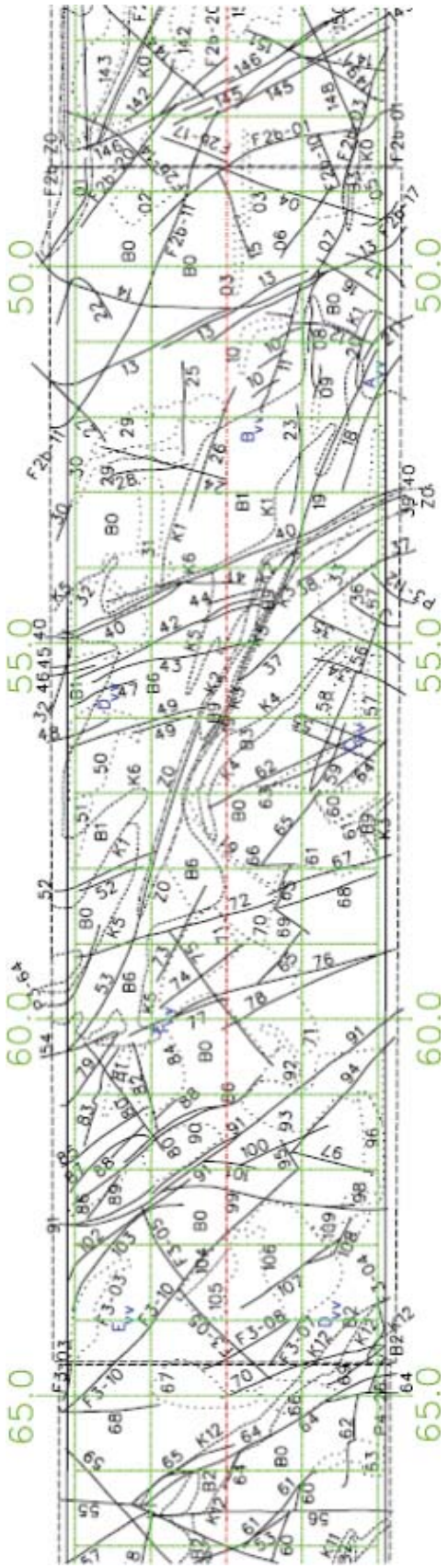

Appendix IV C

3D model with the geological mapping wrapped around a theoretical tunnel model
Section: 48.67–64.56 m

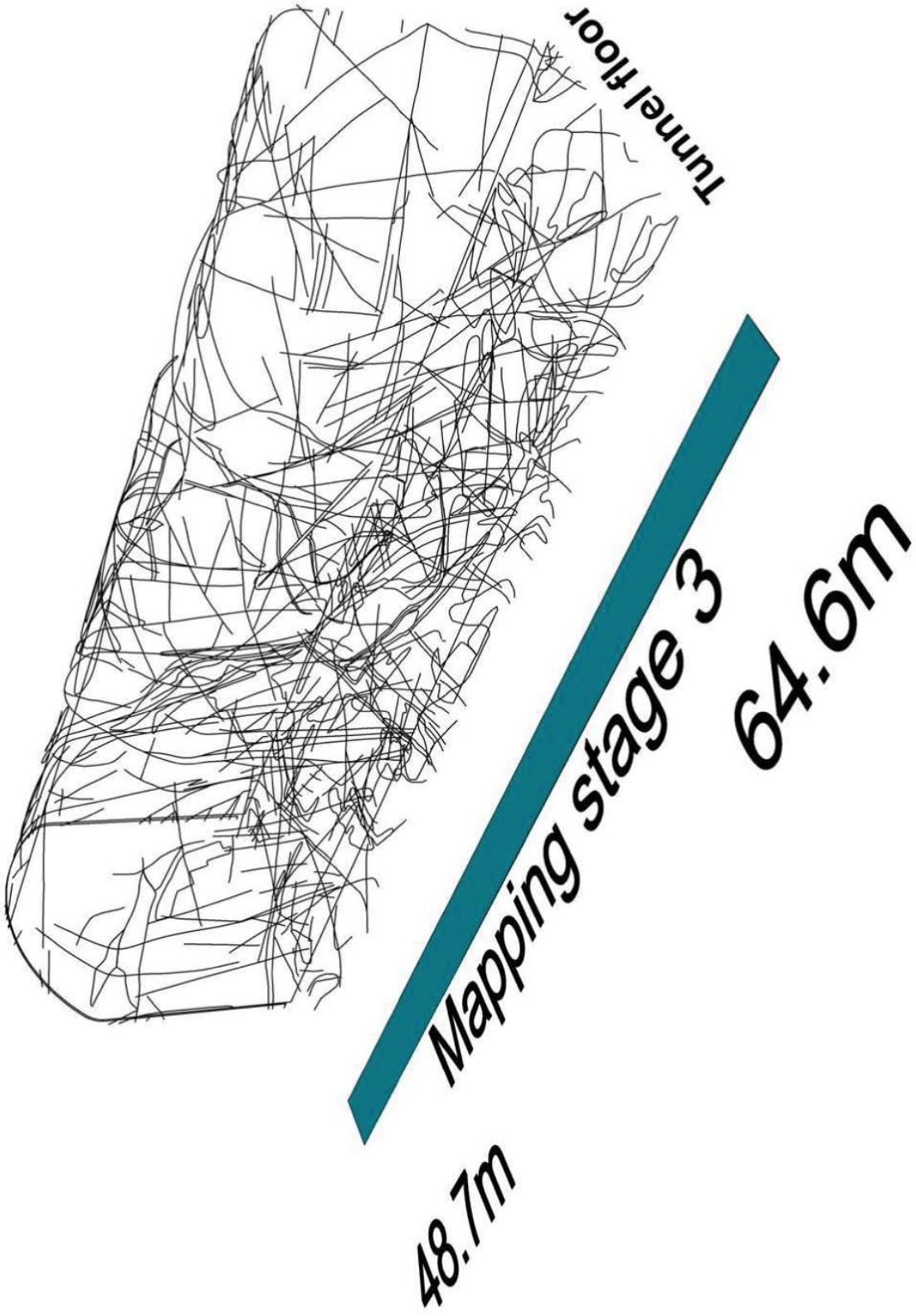

Appendix V

Stage mapping: Stage 4, Section 64.56–80.73 m

V A Geological map of tunnel walls and roof, with legend

V B Geological map of tunnel floor, with legend

V C 3D model with the geological mapping wrapped around a theoretical tunnel model

Appendix V A

Geological map of tunnel walls and roof, with legend

Legend: P (walls and roof). Section: 64.56–80.73 m:

Rock types:

- B0 = Äspö diorite/granodiorite, grey, medium-grained (1–5 mm), porphyritic texture, showing no alteration and homogeneous structure.
- B2 = Fine-grained granite/aplite, red, medium-grained (1–5 mm), uniform texture, showing no alteration and homogeneous structure.
- B3 = Fine-grained granite/aplite, greyish red, fine (to medium) grained (< 1 to 1–5 mm), uniform texture, showing no alteration and shear structure. Laminated, approximately ≤ 5 mm wide bands.
- B5 = Hybrid rock, reddish grey, medium (to fine) grained (1–5 to < 1 mm), irregular texture, showing no alteration and massive/irregular structure. Foliated to massive.
- B6 = Hybrid rock, reddish grey, medium-grained (1–5 mm), porphyritic texture, showing no alteration and massive/irregular structure. Slightly laminated, often diffuse contacts.
- B7 = Mafic rock (undifferentiated)/greenstone, black, fine-grained (< 1 mm), uniform texture, showing no alteration and massive/irregular structure. Contains small amounts of Äspö diorite.
- B8 = Fine-grained granite/aplite, red, medium-grained (1–5 mm), uniform texture, showing no alteration and gneissified structure. Foliation somewhat irregular.

Contacts: K0–K8 and K11–K14 and dashed line.

Fractures: 01–123 and continuous line.

Water: A–Z and Aa–Ii and v–vv (v = occasional drops, minor seepage or patch of moisture; vv = drops, seepage or wet surface).

Scale: The squares of the grid in the drawing = 1×1 m.

Section: Numbers on the left and right-hand sides of the drawing.

Geological map: P (walls and roof). Section: 64.56–80.73 m:

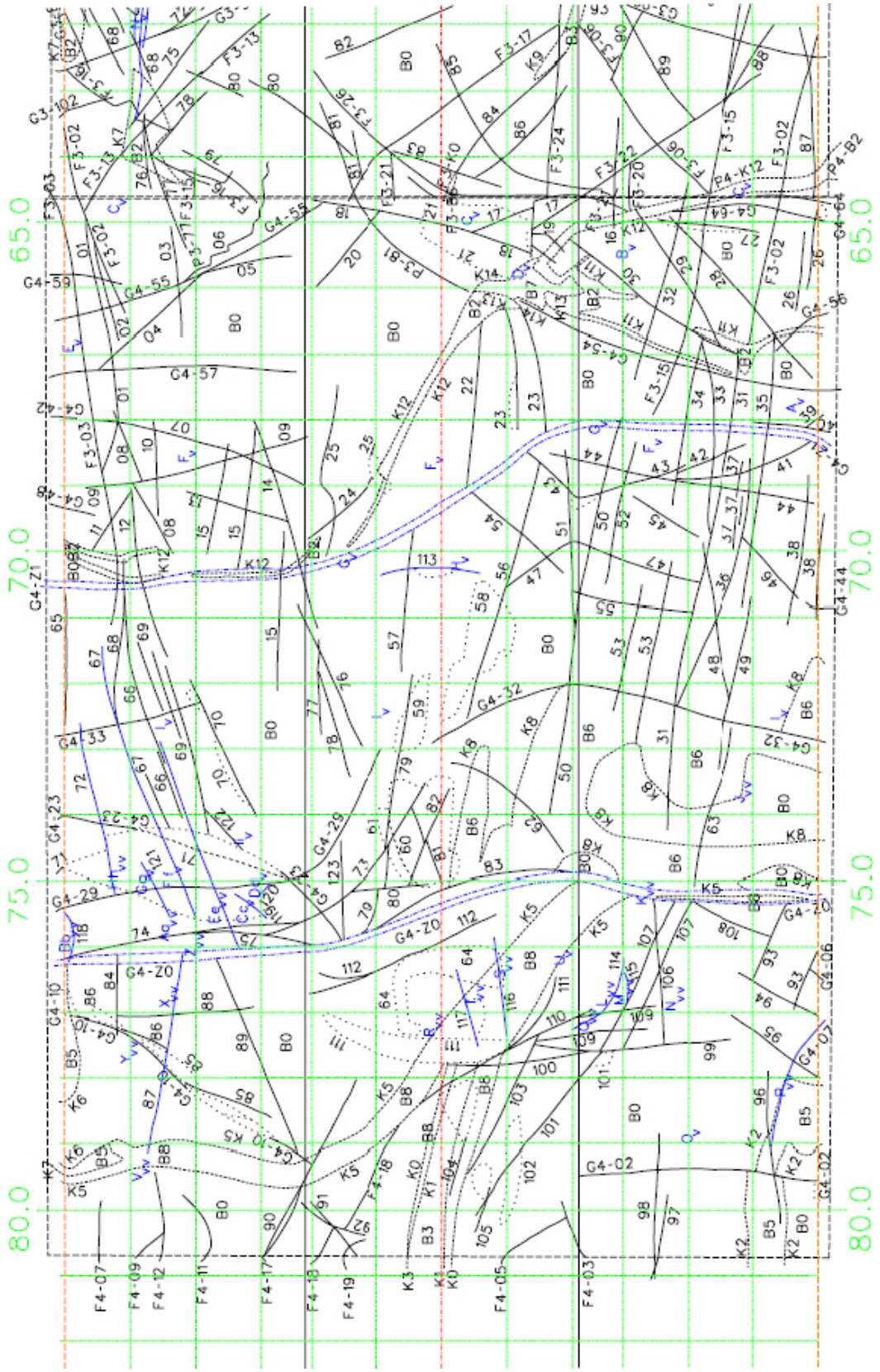

Appendix V B

Geological map of tunnel floor, with legend

Legend: G (floor). Section: 64.56–80.73 m:

Rock types:

- B0 = Äspö diorite/granodiorite, grey, medium-grained (1–5 mm), porphyritic texture, showing no alteration and homogeneous structure.
- B2 = Fine-grained granite/aplite, red, medium-grained (1–5 mm), uniform texture, showing no alteration and homogeneous structure. Granite vein/dyke, with somewhat irregular orientation.
- B3 = Fine-grained granite/aplite, greyish red, fine (to medium) grained (< 1 to 1–5 mm), uniform texture, showing no alteration and shear structure. Granite vein/dyke, somewhat irregular orientation. 1–5 mm wide bands.
- B5 = Hybrid rock, reddish grey, medium (to fine) grained (1–5 to < 1 mm), irregular texture, showing no alteration and massive/irregular structure. Irregular foliation to massive. Red fine-medium-grained granite dykes/veins and red grey medium-grained granite (Småland granite).
- B6 = Hybrid rock, reddish grey, medium-grained (1–5 mm), porphyritic texture, showing no alteration and massive/irregular structure. Slightly laminated 5–30 cm wide bands with diffuse contacts.
- B8 = Fine-grained granite/aplite, red, medium-grained (1–5 mm), uniform texture, showing no alteration and gneissified structure.

Contacts: K0–K6 and K12 and dashed line.

Fractures: 01–71 and continuous line.

Fracture zone: Z0–Z1 and dash-dot-dashed line.

Water: A–H and v–vv (v = occasional drops, minor seepage or patch of moisture; vv = drops, seepage or wet surface).

Scale: The squares of the grid in the drawing = 1×1 m.

Section: Numbers on the left and right-hand sides of the drawing.

Geological map: G (floor). Section: 64.56–80.73 m:

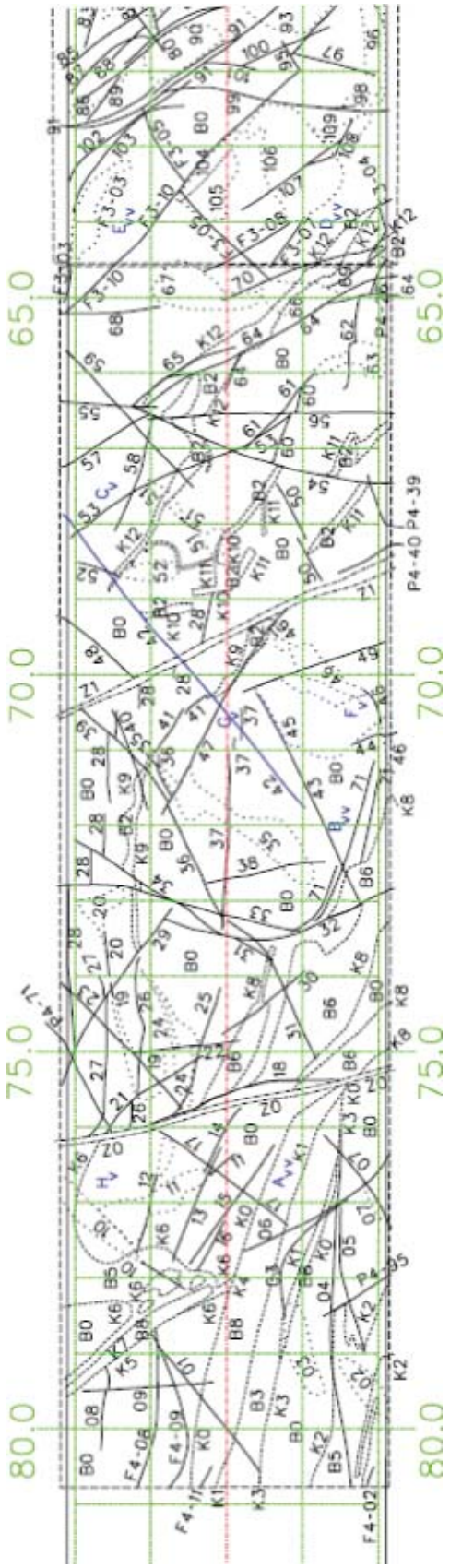

Appendix V C

3D model with the geological mapping wrapped around a theoretical tunnel model
Section: 64.56–80.73 m

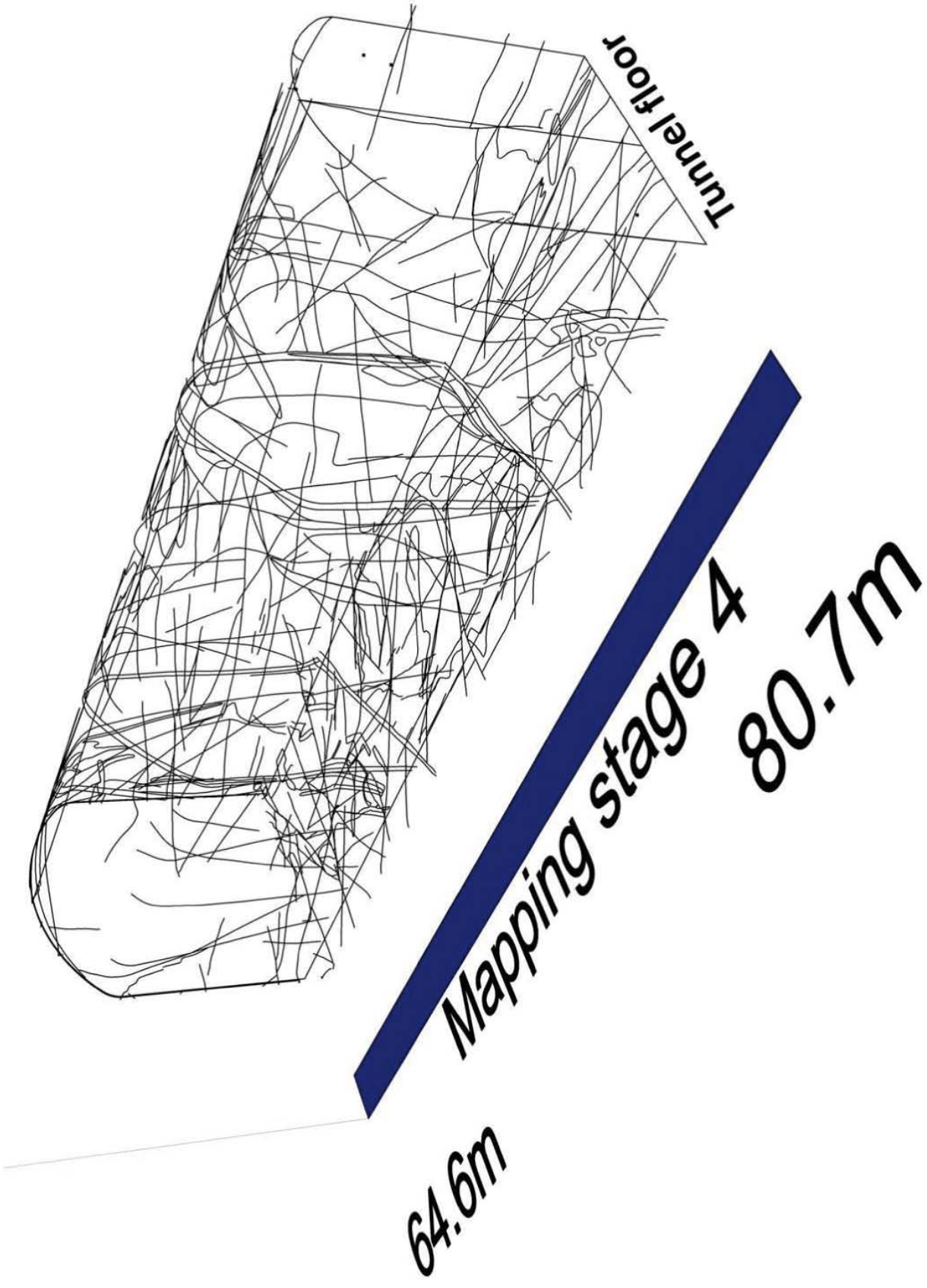

Appendix VI

Geological mapping of the EDZ-slot, with legend

Legend: P (EDZ walls, roof and floor). Section: 36.4–44.4 m:

Rock types:

- B0 = Äspö diorite/granodiorite, grey, medium-grained (1–5 mm), porphyritic texture, showing no alteration and homogeneous structure.
- B1 = Äspö diorite/granodiorite, greyish red, medium-grained (1–5 mm), porphyritic texture, showing weak alteration (red staining/oxidation) and homogeneous structure. Texture only partly porphyritic.

Contacts: K0 and dashed line.

Fractures: 01–12 and continuous line.

Fracture zone: Z1 and dash-dot-dashed line. The zone category is increased fracturing; structure is lamellar and alteration is weak.

Water: A–T and v–vvv (v = occasional drops, minor seepage or patch of moisture; vv = drops, seepage or wet surface; vvv = flow).

Scale: Section numbers (m) and height over theoretical tunnel floor (m).

Geological map of the EDZ-slot

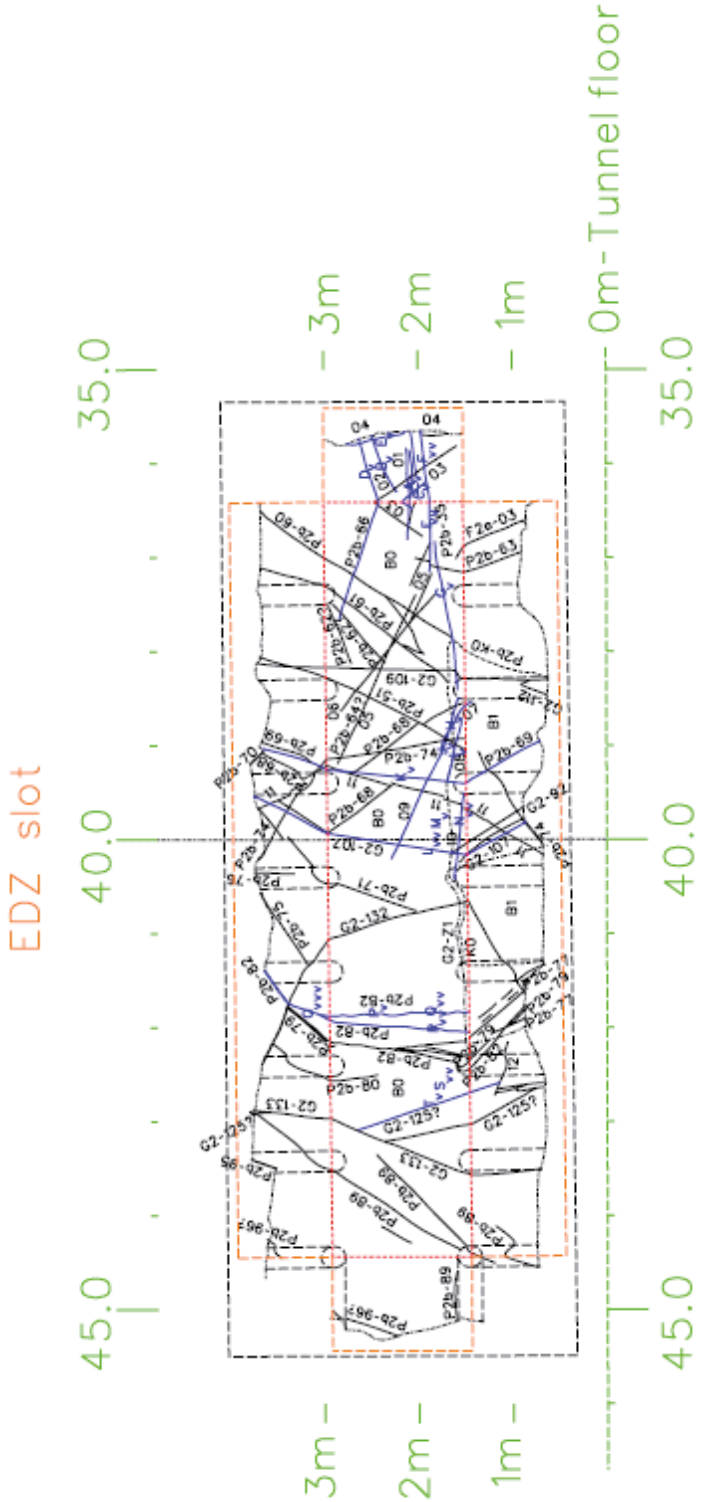

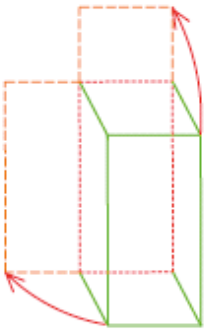

Principle drawing showing how the roof and one of the walls of the EDZ slot has been unfolded to form a plane together with the inner wall.

The projection of the geological map is made in the same manner.

Appendix VII

Rock type distribution

VII A Rock type distribution: Walls and roof of the TASS-tunnel

VII B Rock type distribution: Floor of the TASS-tunnel

VII C Rock type distribution: Faces of the TASS-tunnel

VII D Rock type distribution: The EDZ-slot (walls, roof and floor)

General abbreviations and expressions used in the Rock type distribution tables (VII A–VII C):

P = walls and roof unfolded to form one plane (see Figure 2-3). P1, P2 etc. refers to walls and roof of Stage 1 and Stage 2, etc.

F = Tunnel face (front) unfolded or down folded to vertical position. F1, F2 etc. refers to the tunnel faces of Stage 1 and Stage 2, etc.

G = Tunnel floor. G1, G2 etc. refers to the tunnel floor of Stage 1 and Stage 2, etc.

Qtz = quartz.

Fgr = fine-grained.

Mgr = medium-grained.

Cgr = coarse-grained.

Rock ID = rock type ID (B0, B1 etc) used in the geological maps.

EDZ = Excavation Damage Zone.

Appendix VII A

Rock type distribution: Walls and roof of the TASS-tunnel

Stage and Section (m)	Walls and roof (m²) (wall height approx. 4 m and tunnel width appropx. 4 m)	Rock types	Rock ID	%	m²
Stage 1 (3–20.7 m)	200	Äspö diorite	B0	75.20	150.4
P1		Äspö diorite (oxidized)	B1	13.00	26.0
		Fgr granite (fgr-mgr)	B2	4.00	8.0
		Fgr granite	B3	2.50	5.0
		Pegmatite	B4	1.50	3.0
		Hybrid (Äspö diorite)	B5	3.50	7.0
		Qtz vein/dyke (stratified)	B6	0.10	0.2
		Qtz vein/dyke	B7	0.20	0.4
				100.00	200.0
Stage 2a (20.7–32.9 m)	144	Äspö diorite	B0	94.10	135.5
P2a		Äspö diorite (oxidized)	B1	1.39	2.0
		Fgr granite	B3	0.69	1.0
		Pegmatite (w/bands)	B4	0.23	0.3
		Hybrid (Äspö diorite)	B5	3.47	5.0
		Pegmatite	B6	0.12	0.2
				100.00	144.0
Stage 2b (32.9–48.7 m)	189	Äspö diorite	B0	97.35	184.0
P2b		Äspö diorite (oxidized)	B1	2.65	5.0
				100.00	189.0
Stage 3 (48.7–64.6 m)	176	Äspö diorite	B0	91.08	160.3
P3		Hybrid (oxidized Äspö diorite and/or fgr granite)	B1	5.68	10.0
		Mafic rock	B2	0.57	1.0
		Fgr granite	B3	1.14	2.0
		Fgr granite (sheared)	B6	1.14	2.0
		Fgr granite (fgr-mgr)	B7	0.23	0.4
		Qtz vein/dyke	B9	0.17	0.3
				100.00	176.0
Stage 4 (64.6–80.7 m)	176	Äspö diorite	B0	87.50	154.0
P4		Fgr granite (fgr-mgr)	B2	2.27	4.0
		Fgr granite (sheared)	B3	1.14	2.0
		Hybrid (irregular)	B5	0.57	1.0
		Hybrid (laminated)	B6	5.11	9.0
		Mafic rock	B7	0.57	1.0
		Fgr granite (fgr-mgr, foliated)	B8	2.84	5.0
				100.00	176.0
Total area (approximately):	885				

Appendix VII B

Rock type distribution: Floor of the TASS-tunnel

Stage and Section (m)	Floor (m^2) (approx. 4 m wide)	Rock types	Rock ID	%	m^2
Stage 1 (3–20.7 m)	65	Äspö diorite	B0	27.7	18.0
G1		Äspö diorite (oxidized)	B1	55.4	36.0
		Fgr granite (fgr-mgr)	B2	5.4	3.5
		Fgr granite	B3	4.6	3.0
		Pegmatite	B4	3.1	2.0
		Hybrid (Äspö diorite)	B5	3.4	2.2
		Qtz vein/dyke	B6	0.5	0.3
				100.00	65.0
Stage 2 (20.7–48.7 m)	112	Äspö diorite	B0	81.25	91.0
G2		Äspö diorite (oxidized)	B1	17.86	20.0
		Pegmatite	B4	0.27	0.3
		Pegmatite (from P2a)	B4	0.18	0.2
		Fgr granite (from P2a)	B3	0.45	0.5
				100.00	112.0
Stage 3 (48.7–64.6 m)	64	Äspö diorite	B0	73.44	47.0
G3		Hybrid (oxidized Äspö diorite and/or fgr granite)	B1	10.16	6.5
		Fgr granite (fgr-mgr)	B2	0.31	0.2
		Fgr granite	B3	2.34	1.5
		Fgr granite (sheared)	B6	12.50	8.0
		Qtz vein/dyke (laminated)	B9	1.25	0.8
				100.00	64.0
Stage 4 (64.6–80.7 m)	64	Äspö diorite	B0	79.69	51.0
G4		Fgr granite (fgr-mgr)	B2	3.13	2.0
		Fgr granite (sheared)	B3	3.13	2.0
		Hybrid (irregular)	B5	4.69	3.0
		Hybrid (laminated)	B6	4.69	3.0
		Fgr granite (foliated)	B8	4.69	3.0
				100.00	64.0
Total area (approximately):	305				

Appendix VII C

Rock type distribution: Faces of the TASS-tunnel

Stage and Section (m)	Face (m^2) (approx. 4×4 m+2 m^2)	Rock types	Rock ID	%	m^2
Stage 1 (6.10)	18	Äspö diorite	B0	41.7	7.5
F1		Äspö diorite (oxidized)	B1	13.9	2.5
		Fgr granite (fgr-mgr)	B2	33.3	6.0
		Fgr granite	B3	11.1	2.0
				100.00	18.0
Stage 1 (8.70)	18	Äspö diorite	B0	44.5	8.0
F1		Äspö diorite (oxidized)	B1	33.3	6.0
		Fgr granite	B3	22.2	4.0
				100.00	18.00
Stage 1 (12.75)	18	Äspö diorite	B0	67.0	12.1
F1		Äspö diorite (oxidized)	B1	22.0	4.0
		Hybrid (laminated)	B2	8.0	1.4
		Fgr granite	B3	3.0	0.5
				100.00	18.00
Stage 1 (16.90)	18	Äspö diorite	B0	88.9	16.0
F1		Äspö diorite (oxidized)	B1	9.7	1.7
		Fgr granite	B3	1.4	0.3
				100.00	18.00
Stage 1 (20.74)	18	Äspö diorite	B0	71.0	12.8
F1		Äspö diorite (oxidized)	B1	11.0	2.0
		Fgr granite	B3	2.0	0.4
		Hybrid (Äspö diorite)	B5	14.0	2.5
		Pegmatite	B7	2.0	0.4
				100.0	18.0
Stage 2 (24.84)	18	Äspö diorite	B0	100.0	18.0
F2				100.0	18.0
Stage 2 (28.94)	18	Äspö diorite	B0	80.0	14.4
F2		Fgr granite	B3	6.0	1.1
		Pegmatite	B4	3.0	0.5
		Hybrid (Äspö diorite)	B5	11.0	2.0
				100.0	18.0
Stage 2 (32.94)	18	Äspö diorite	B0	100.0	18.0
F2				100.0	18.0
Stage 2 (37.50)	18	Äspö diorite	B0	100.0	18.0
F2				100.0	18.0
Stage 2 (42.14)	18	Äspö diorite	B0	100.0	18.0
F2				100.0	18.0
Stage 2 (45.72)	18	Äspö diorite	B0	98.0	17.6
F2		Mafic rock	B2	2.0	0.4
				100.0	18.0

Stage and Section (m)	Face (m^2) (approx. 4×4 m+2 m^2)	Rock types	Rock ID	%	m^2
Stage 2 (48.67)	18	Äspö diorite	B0	98.9	17.8
F2		Fgr granite (fgr-mgr)	B3	0.6	0.1
		Hybrid (irregular)	B5	0.6	0.1
				100.0	18.0
Stage 3 (52.72)	18	Äspö diorite	B0	89.0	16.0
F3		Fgr granite	B3	5.0	0.9
		Hybrid (Äspö diorite)	B5	6.0	1.1
				100.0	18.0
Stage 3 (56.77)	18	Äspö diorite	B0	83.0	14.9
F3		Fgr granite	B2	3.0	0.5
		Fgr granite (foliated)	B3	8.0	1.4
		Hybrid (Äspö diorite)	B5	3.0	0.5
		Qtz vein/dyke	B9	3.0	0.5
				100.0	18.0
Stage 3 (60.55)	18	Äspö diorite	B0	78.0	14.0
F3		Pegmatite	B4	3.0	0.5
		Hybrid (Äspö diorite)	B5	19.0	3.4
				100.0	18.0
Stage 3 (64.56)	18	Äspö diorite	B0	98.0	17.6
F3		Fgr granite	B3	1.0	0.2
		Fgr granite (fgr-mgr)	B6	1.0	0.2
				100.0	18.0
Stage 4 (68.87)	18	Äspödiorite	B0	97.0	17.5
F4		Fgr granite (fgr-cgr)	B2	3.0	0.5
				100.0	18.0
Stage 4 (73.18)	18	Äspö diorite	B0	99.0	17.8
F4		Hybrid (Äspö diorite)	B5	1.0	0.2
				100.0	18.0
Stage 4 (77.14)	18	Äspö diorite	B0	64.0	11.5
F4		Fgr granite (foliated)	B3	28.0	5.0
		Fgr granite (fgr-mgr)	B8	8.0	1.4
				100.0	18.0
Stage 4 (80.73)	18	Äspö diorite	B0	77.8	14.0
F4		Fgr granite (sheared)	B3	13.9	2.5
		Hybrid (irregular)	B5	2.8	0.5
		Fgr granite (foliated)	B8	5.6	1.0
				100.0	18.0
Total area (approximately):	360				

Appendix VII D

Rock type distribution: The EDZ-slot (walls, roof and floor)

Section (m)	EDZ-slot (m^2) Walls (approx. 1×12 m^2 +2×1.2 m^2), roof (approx. 6.4 m^2), floor (approx 6.4 m^2)	Rock types	Rock ID	%	m^2
(36.4–44.4 m)	27	Äspö diorite	B0	88.89	24.0
EDZ		Äspö diorite (oxidized)	B1	11.11	3.0
				100.00	27.0
Total area (approximately):	27				

Appendix VIII

Fractures in the TASS-tunnel; total and water-bearing

VIII A Fractures in the TASS-tunnel: walls and roof (P), floor (G), last face (F: 80.7 m) and EDZ-slot

VIII B Water-bearing fractures in the TASS-tunnel: walls and roof (P), floor (G), last face (F: 80.7 m) and EDZ-slot

Fractures in the TASS-tunnel: walls and roof (P), floor (G), last face (F: 80.7 m) and EDZ-slot

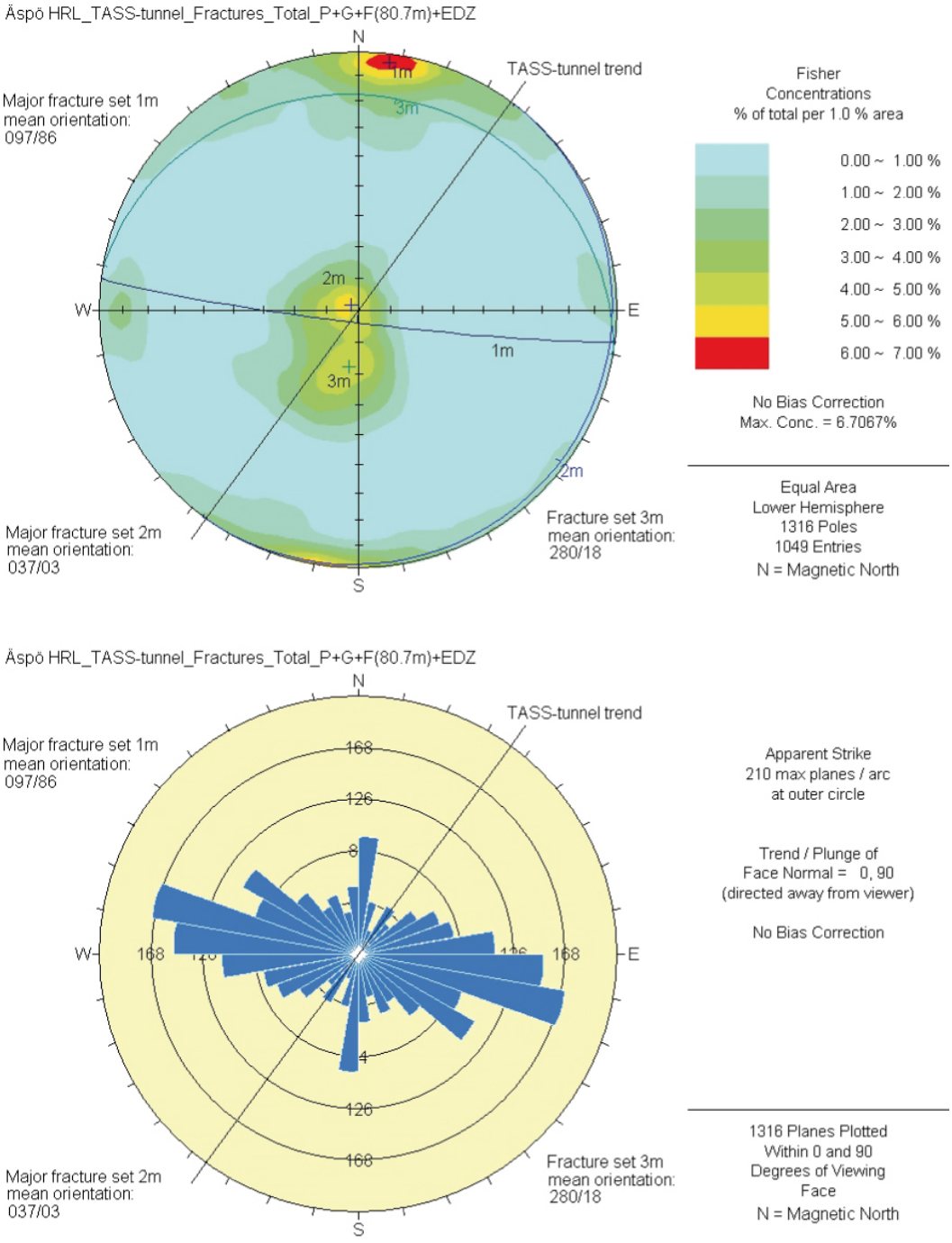

Figure VIII A. *Fracture orientations from the whole TASS-tunnel presented in Schmidt net and joint rosette diagrams. The 216° trend of the TASS-tunnel is marked as a black line. One main orientation set can be seen, 1 m: 097/86, as well as two less prominent sets, 2 m: 037/03 and 3 m: 280/18.*

Water-bearing fractures in the TASS-tunnel: walls and roof (P), floor (G), last face (F: 80.7 m) and EDZ-slot

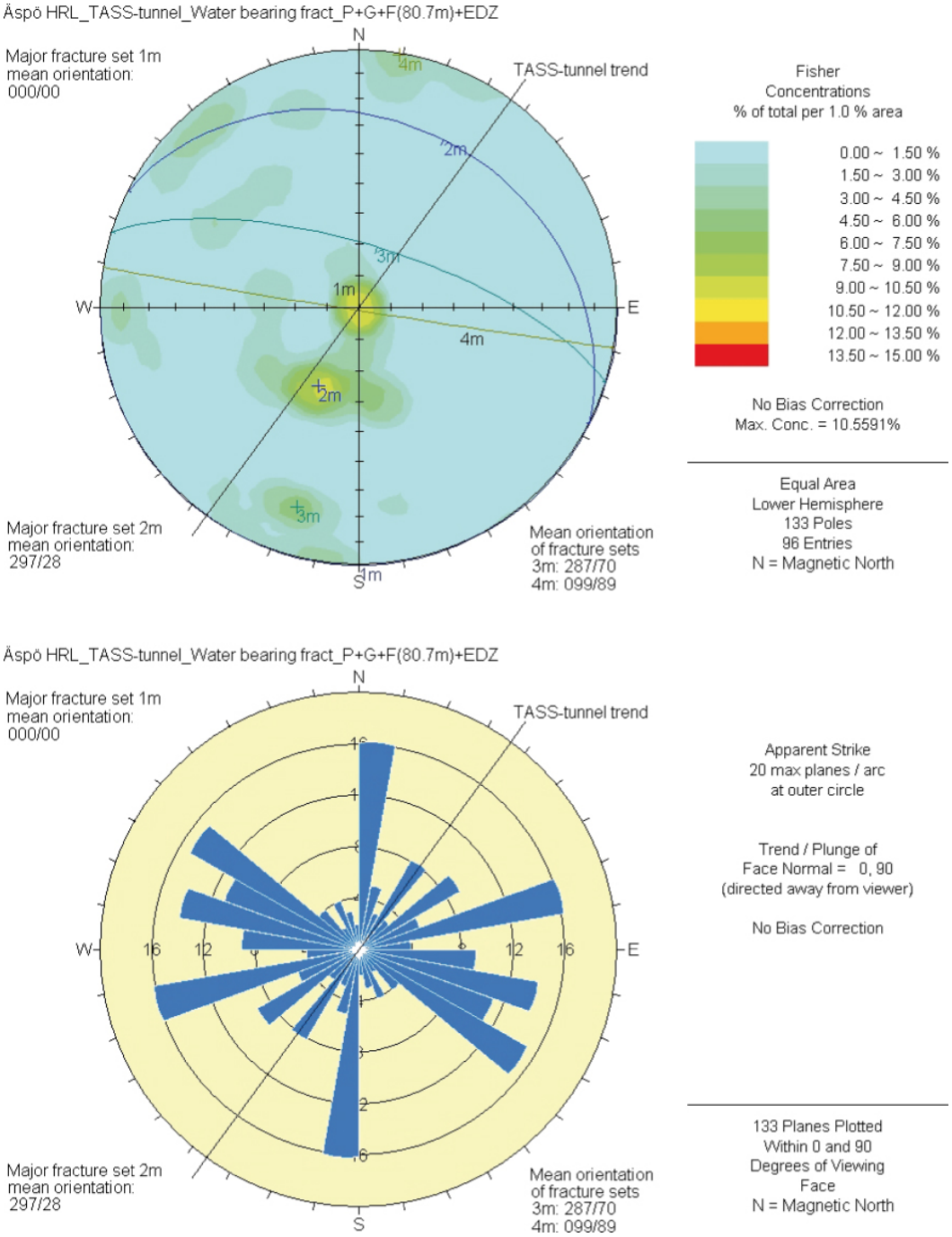

Figure VIII B. *Water bearing fracture orientations from the whole TASS-tunnel presented in Schmidt net and joint rosette diagrams. The 216° trend of the TASS-tunnel is marked as a black line. Two main orientation sets can be seen, 1 m: 000/00 and 2 m: 297/28, as well as two less prominent sets, 3 m: 287/70 and 4 m: 099/89.*

Appendix IX

TASS-tunnel, total fractures, total filling minerals

IX A Fractures containing chlorite as a fracture-filling mineral

IX B Fractures containing calcite as a fracture-filling mineral

IX C Fractures containing epidote as a fracture-filling mineral

IX D Fractures containing prehnite as a fracture-filling mineral

IX E Fractures containing epidote and prehnite as fracture-filling minerals

Appendix IX A

Fractures containing chlorite as a fracture-filling mineral

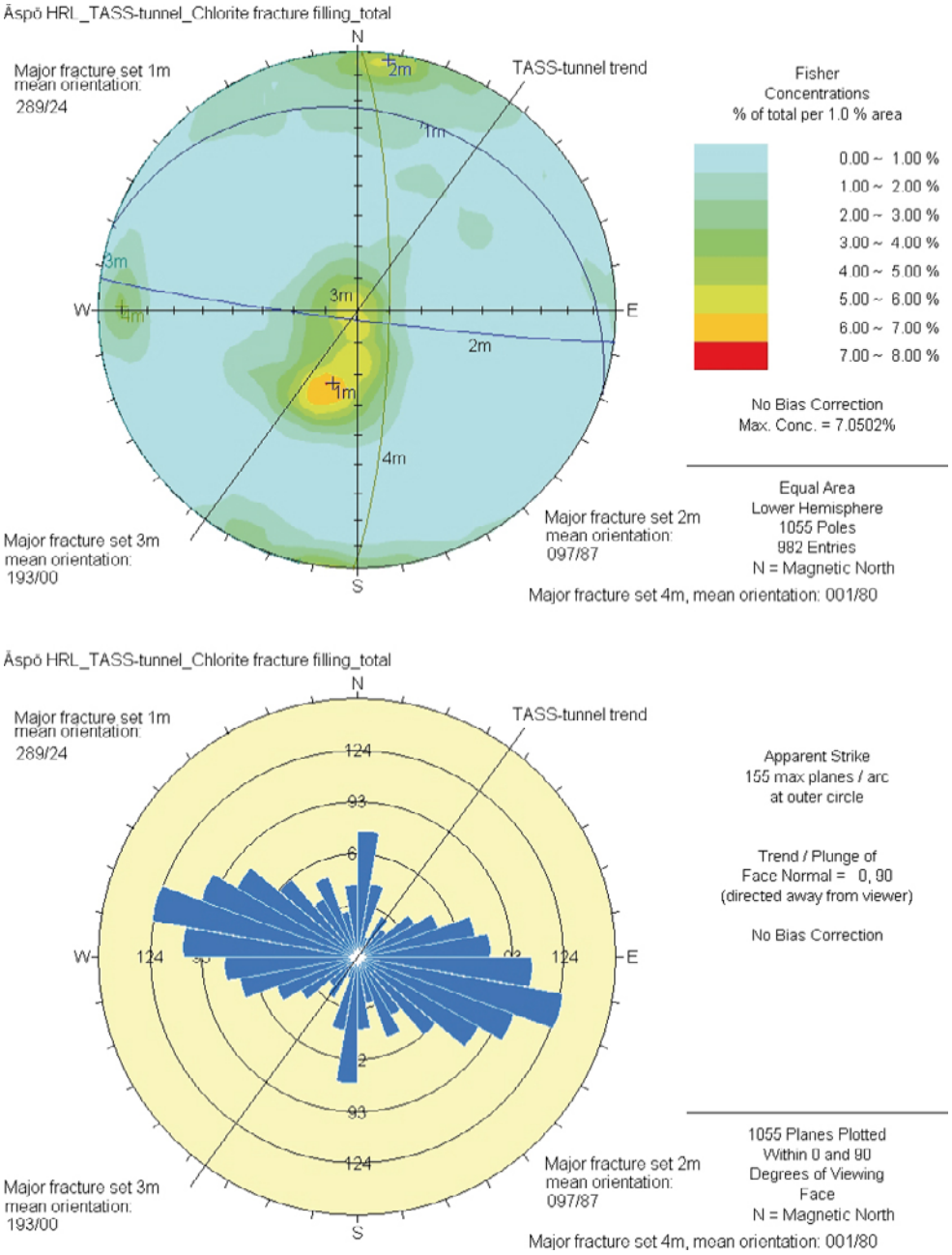

Figure IX A. *Orientation of fractures that contain chlorite as a fracture-filling mineral in the TASS-tunnel presented in Schmidt net and joint rosette diagrams. The 216° trend of the TASS-tunnel is marked as a black line. The main orientation set is 1 m: 289/24. Three less prominent sets can also be seen, set 2 m: 097/87, set 3 m: 193/00 and set 4 m: 001/80.*

Fractures containing calcite as a fracture-filling mineral

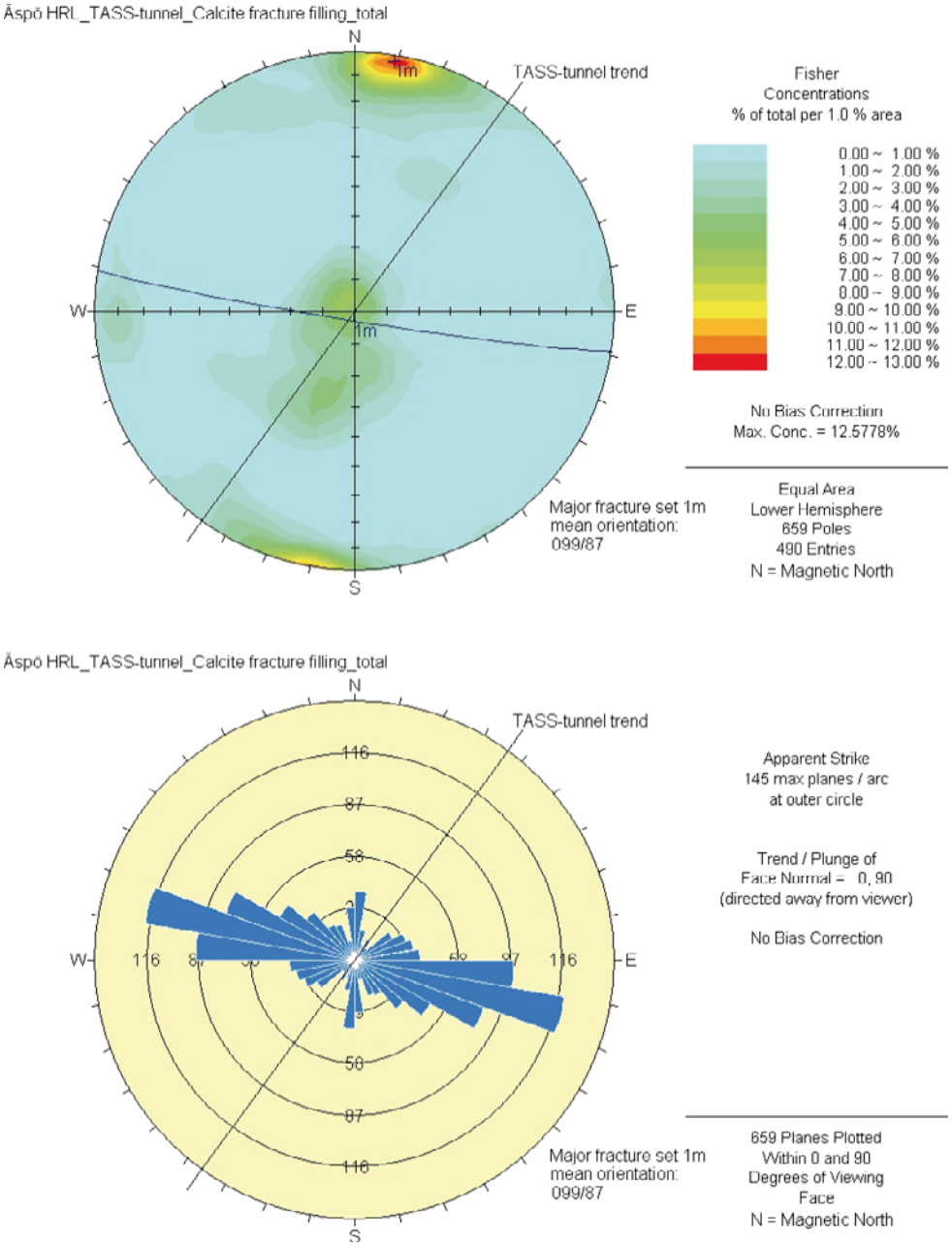

Figure IX B. *Orientation of fractures that contain calcite as a fracture-filling mineral in the TASS-tunnel presented in Schmidt net and joint rosette diagrams. The 216° trend of the TASS-tunnel is marked as a black line. The main orientation set is 1 m: 099/87.*

Appendix IX C

Fractures containing epidote as a fracture-filling mineral

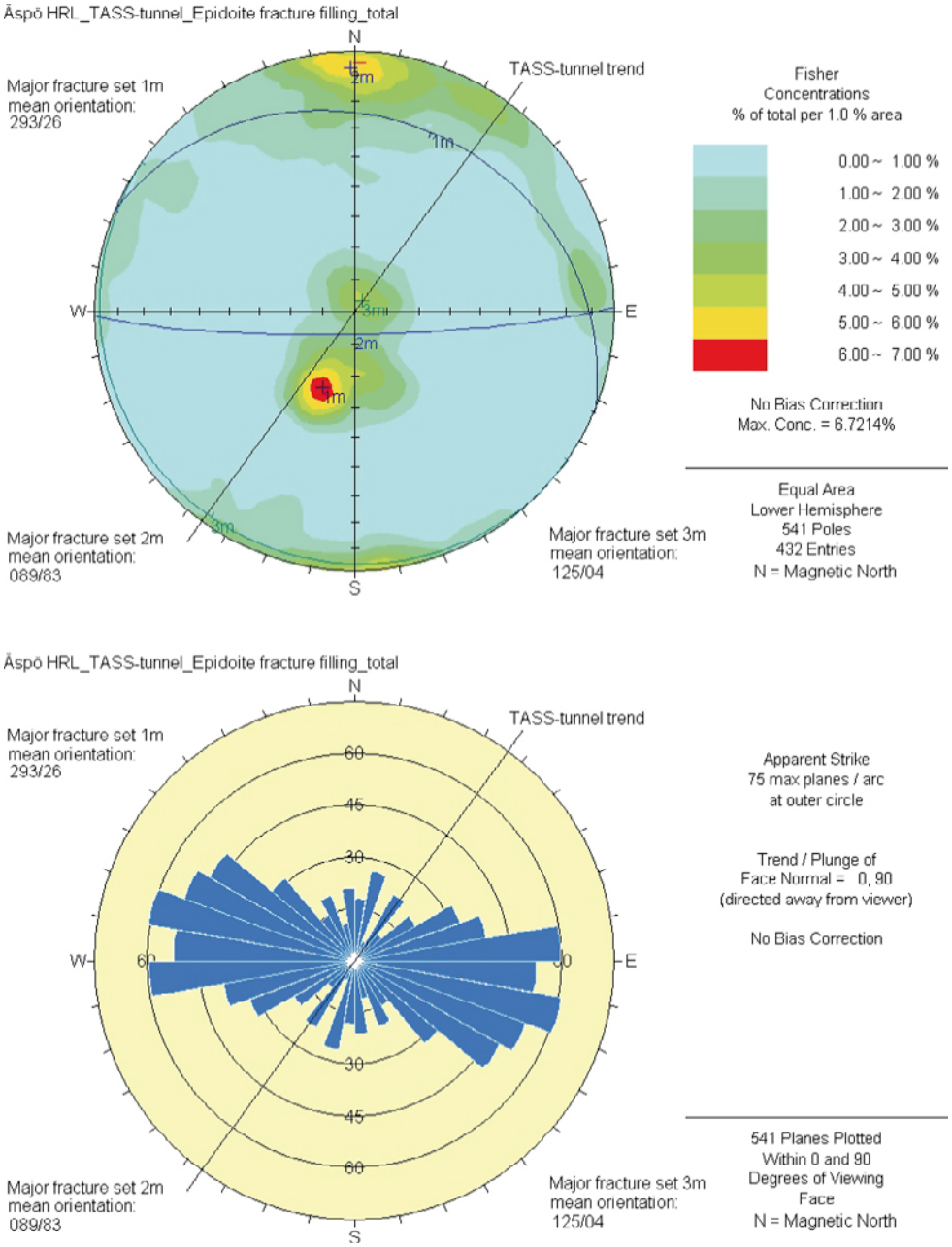

Figure IX C. *Orientation of fractures that contain epidote as a fracture-filling mineral in the TASS-tunnel presented in Schmidt net and joint rosette diagrams. The 216° trend of the TASS-tunnel is marked as a black line. The main orientation set is 1 m: 293/26. Two less prominent sets can also be seen, set 2 m: 089/83 and set 3 m: 125/04.*

Fractures containing prehnite as a fracture-filling mineral

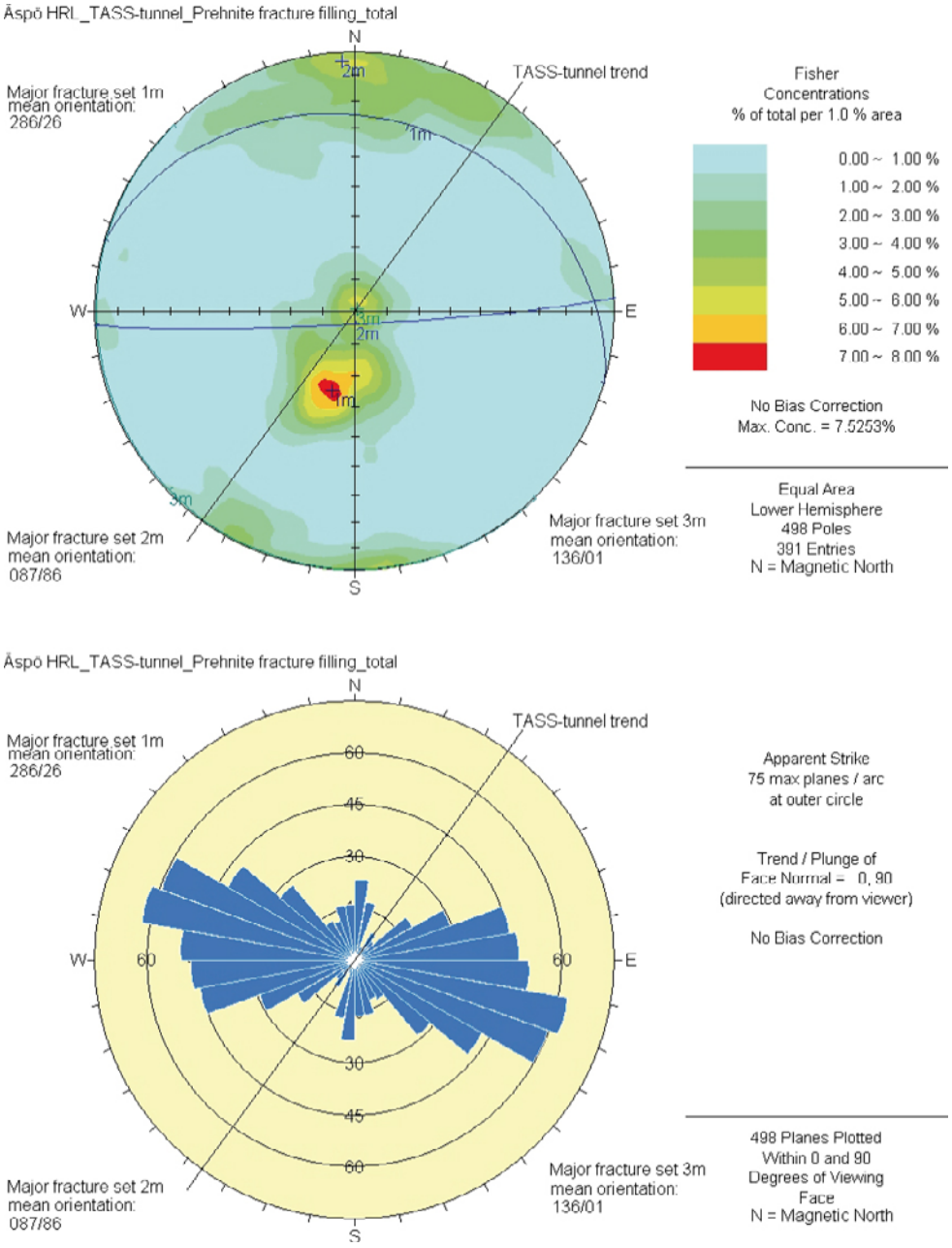

Figure IX D. *Orientation of fractures that contain prehnite as a fracture-filling mineral in the TASS-tunnel presented in Schmidt net and joint rosette diagrams. The 216° trend of the TASS-tunnel is marked as a black line. The main orientation set is 1 m: 286/26. Two less prominent sets can also be seen, set 2 m: 087/86 and set 3 m: 136/01.*

Appendix IX E

Fractures containing epidote and prehnite as fracture-filling minerals

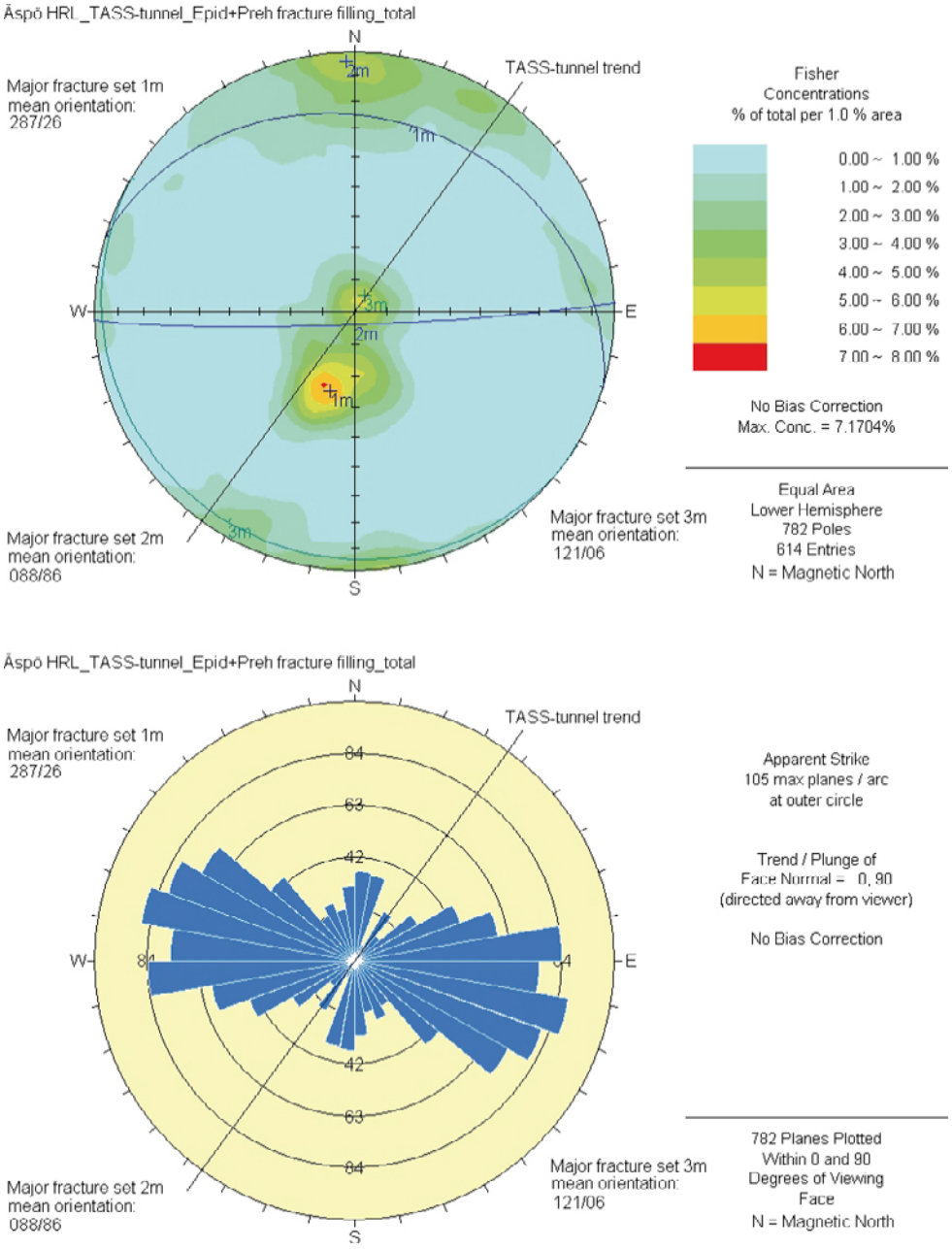

Figure IX E. *Orientation of fractures that contain epidote and prehnite as fracture-filling minerals in the TASS-tunnel presented in Schmidt net and joint rosette diagrams. The 216° trend of the TASS-tunnel is marked as a black line. The main orientation set is 1 m: 287/26. Two less prominent sets can also be seen, set 2 m: 088/86 and set 3 m: 121/06.*

Appendix X

Projection of chosen packers in borehole KI0010B01 to TASS-tunnel mapping as well as interpretations of possible intercepts of appropriate TRUE Block Scale model structures with tunnel

Stage mapping, Stages 1–4, section 3–80.7 m, walls and roof (P), floor (G).

X	Legend
XA	Stage mapping, Stage 1, section 3–20.7 m, mapping of walls and roof (P) as well as floor (G)
XB	Photographs 16–20 m
XC	Stage mapping, stage 2, section 20.7–48.7 m, mapping of walls and roof (P) as well as floor (G)
XD	Photographs 36–40 m.
XE	Photographs 40–44 m
XF	Stage mapping, Stage 3, section 48.7–64.6 m, mapping of walls and roof (P) as well as floor (G)
XG	Photographs 52–56 m.
XH	Stage mapping, Stage 4, section 64.6–80.7 m, mapping of walls and roof (P) as well as floor (G)
XI	Photographs 74–76 m.

Legend:

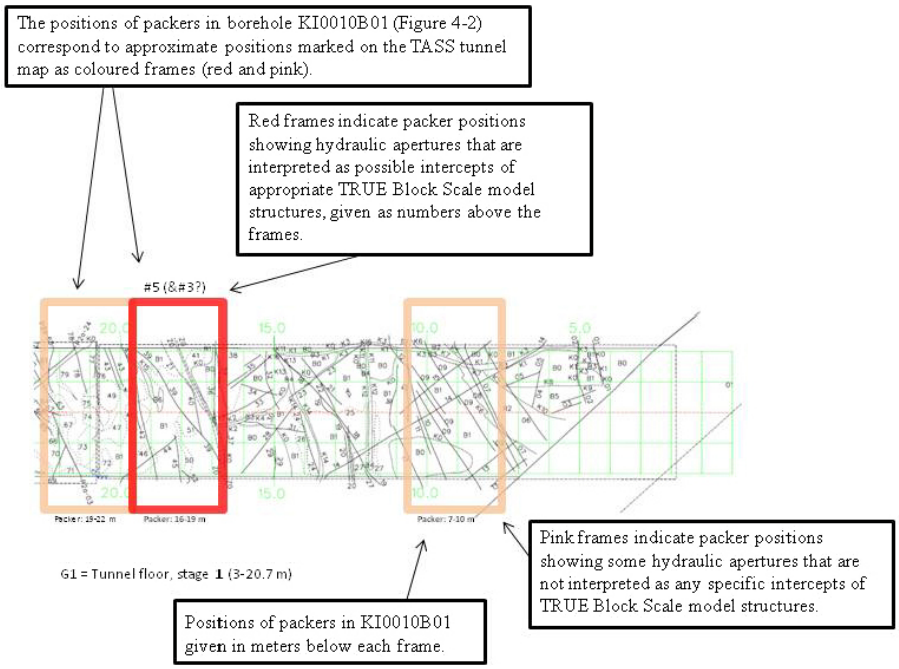

Stage mapping, Stage 1, section 3–20.7 m, mapping of walls and roof (P) as well as floor (G)

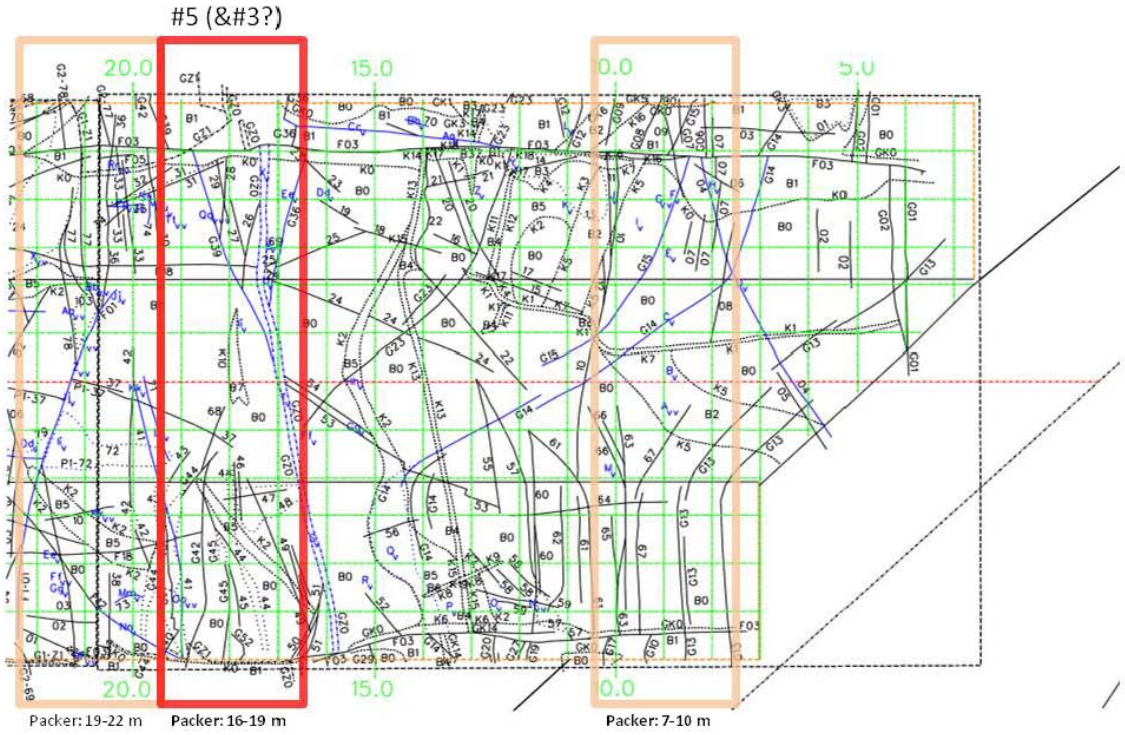

P1 = Tunnel walls & roof, stage 1 (3-20.7 m)

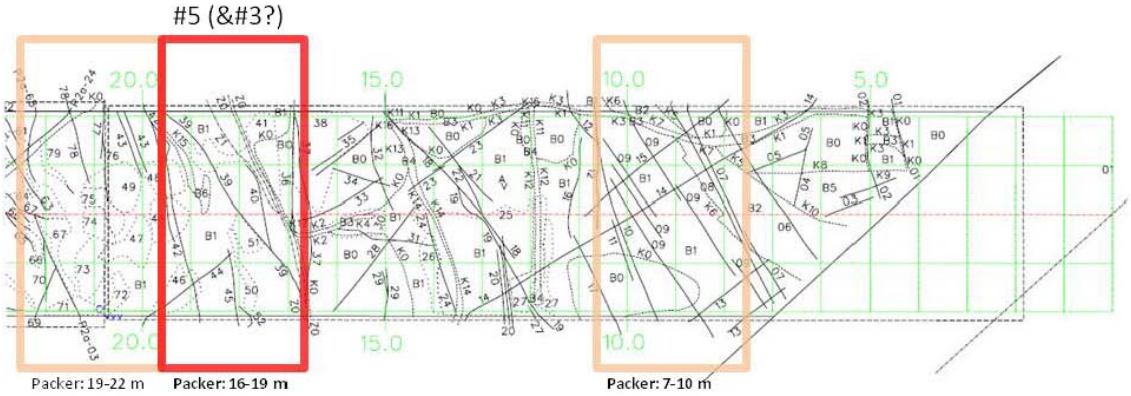

G1 = Tunnel floor, stage 1 (3-20.7 m)

Photographs 16–20 m

Arrows mark approximate positions of structures G1-Z0. Possible candidate as TRUE Block Scale model structure #5

18-20 m, right-hand side, floor and lower part of the wall

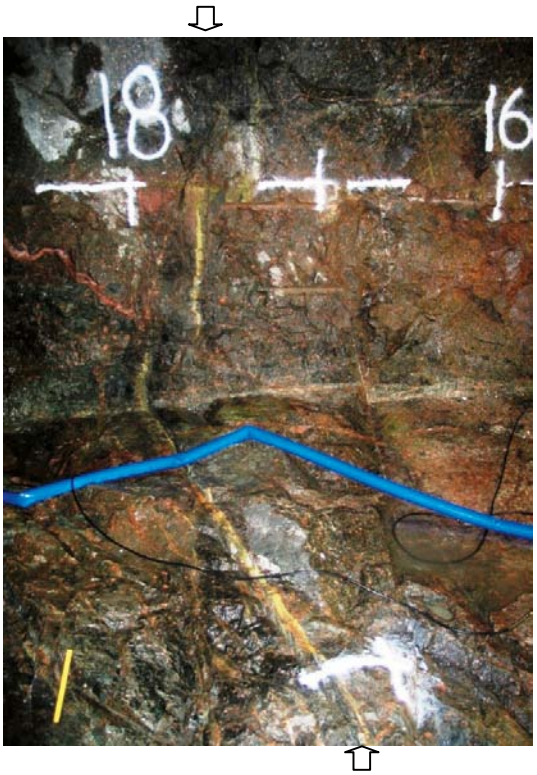

16-18 m, right-hand side, floor and lower part of the wall

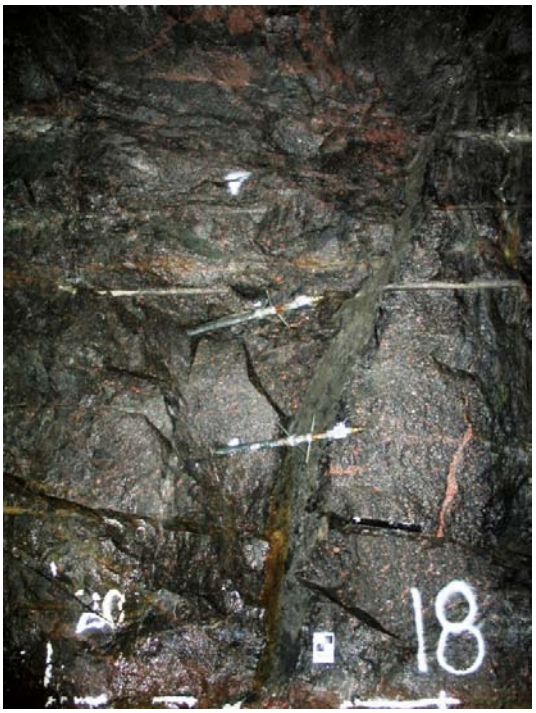

18-20 m, right-hand side, wall and shoulder

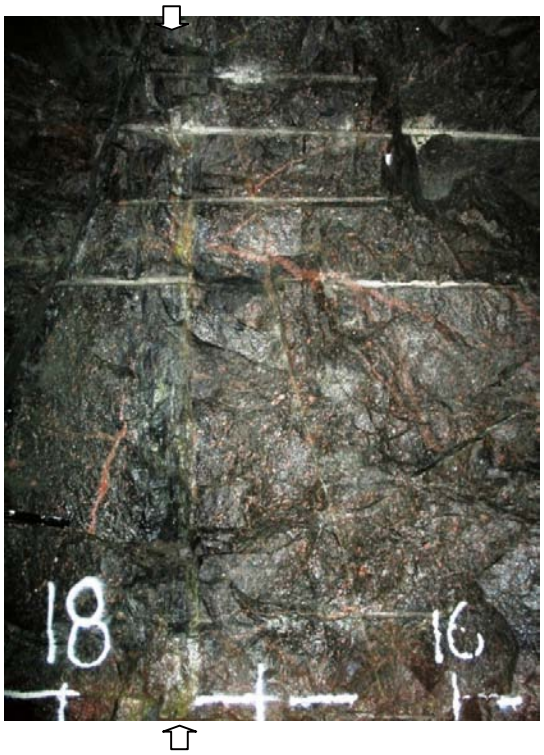

16-18 m, right-hand side, wall and shoulder

18-20 m, right-hand side, roof

16-18 m, right-hand side,roof

16-18 m, left-hand side, roof

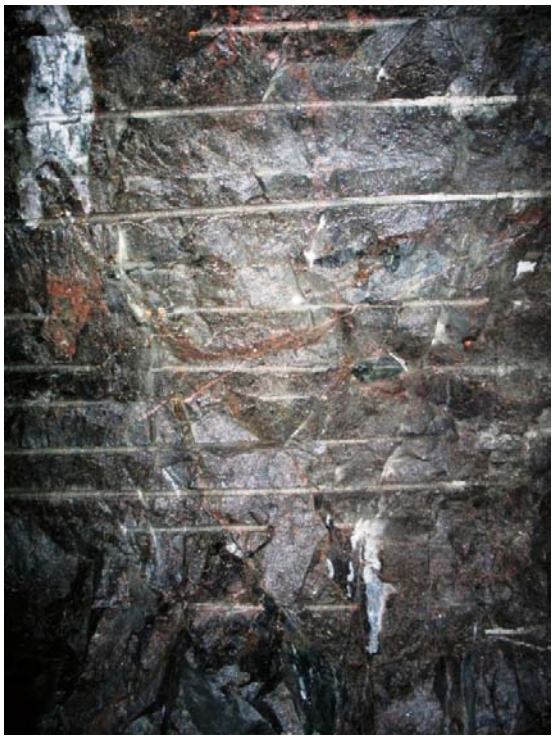

18-20 m, left-hand side, roof

16-18 m, left-hand side, wall and shoulder

18-20 m, left-hand side, wall and shoulder

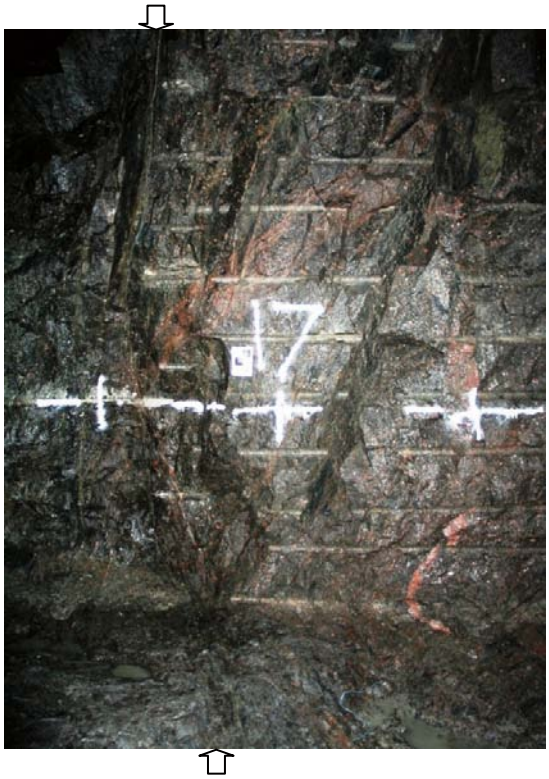

16-18 m, left-hand side, floor and wall

18-20 m, left-hand side, wall

16-18 m, left-hand side, floor and lower part of the wall

17-20 m, left-hand side, floor and lower part of the wall

Stage mapping, Stage 2, section 20.7–48.7 m, mapping of walls and roof (P) as well as floor (G)

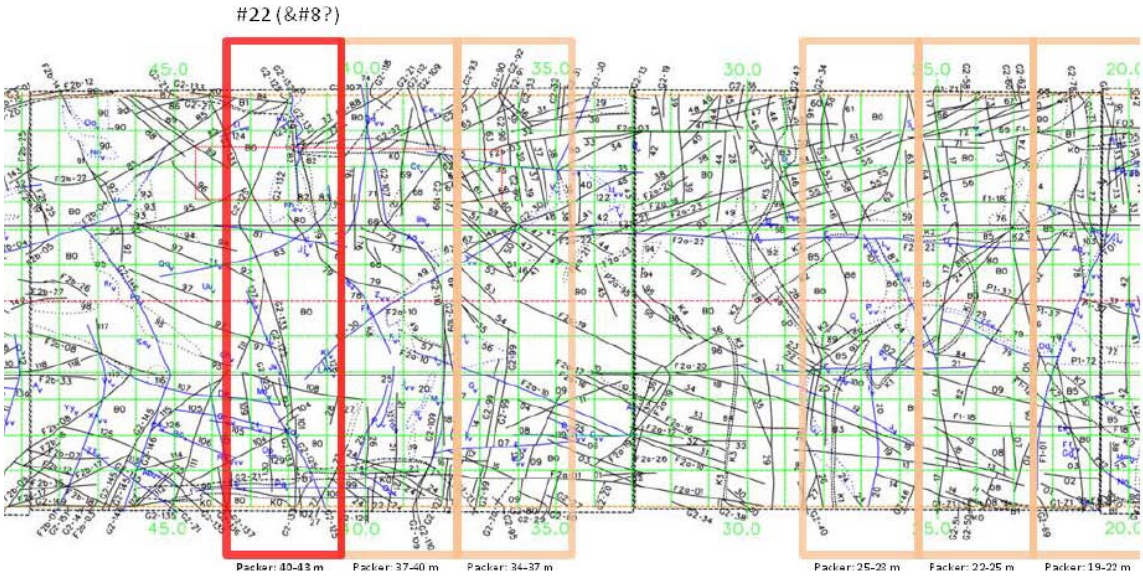

P2 = Tunnel walls & roof, stage 2 (20.7-48.7 m). Two segments P2a (20.7-32.9 m) and P2b (32.9-48.7 m)

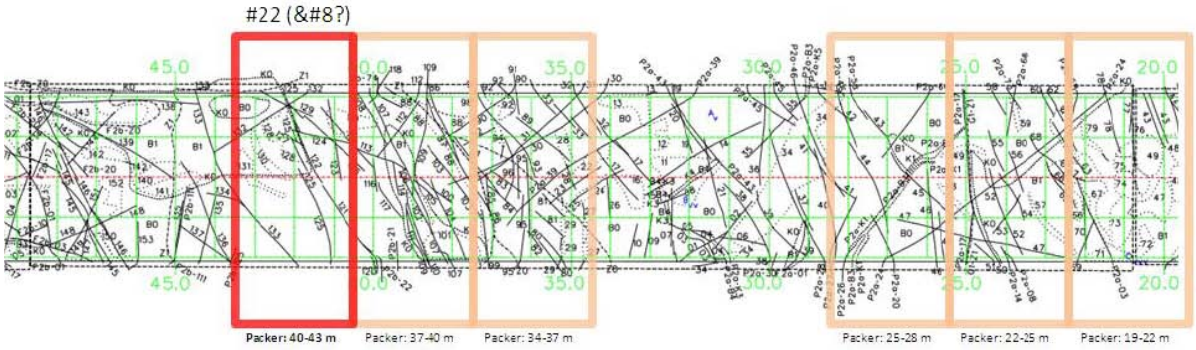

G2 = Tunnel floor, stage 2 (20.7-48.7 m)

Photographs 36–40 m

Arrows mark approximate positions of structures G2-107, 109 & 110 as well as P2b-69, 70 &71. These structures may represent #22, very uncertain.

38-40 m, right-hand side, floor and lower part of the wall

36-38 m, right-hand side, floor and lower part of the wall

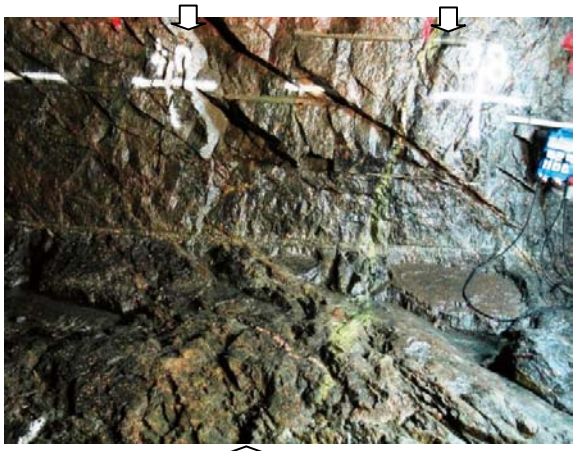

38-40 m, right-hand side, floor and lower part of the wall

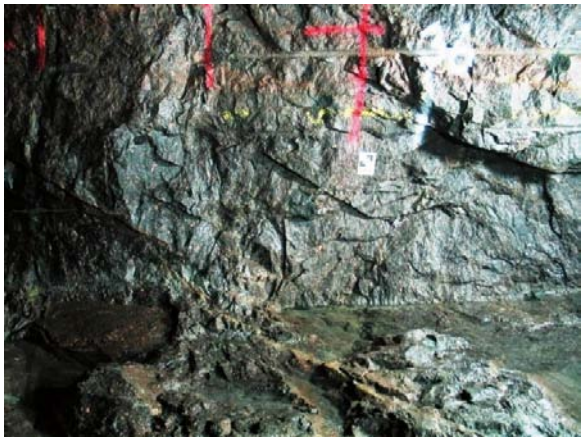

36-38 m, right-hand side, floor and lower part of the wall

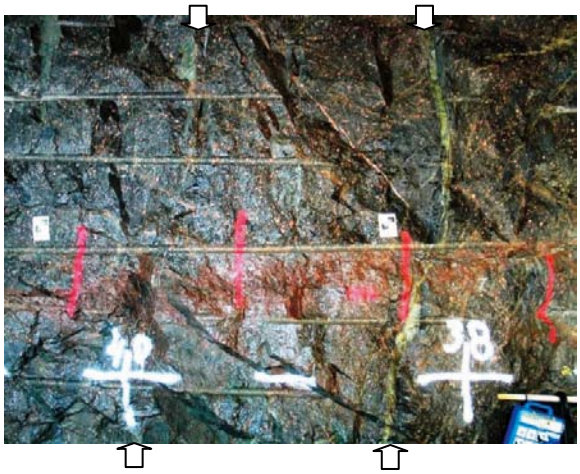

38-40 m, right-hand side, wall

36-38 m, right-hand side, wall

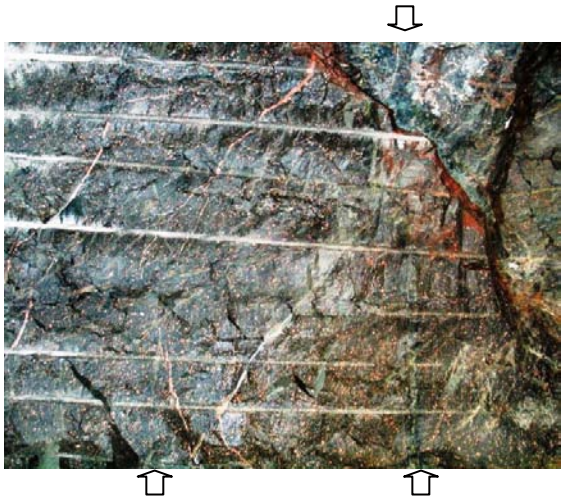

38-40 m, right-hand side, roof

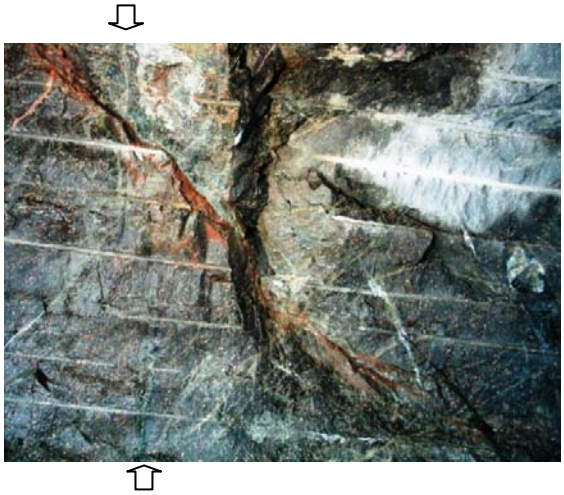

36-38 m, right-hand side, roof

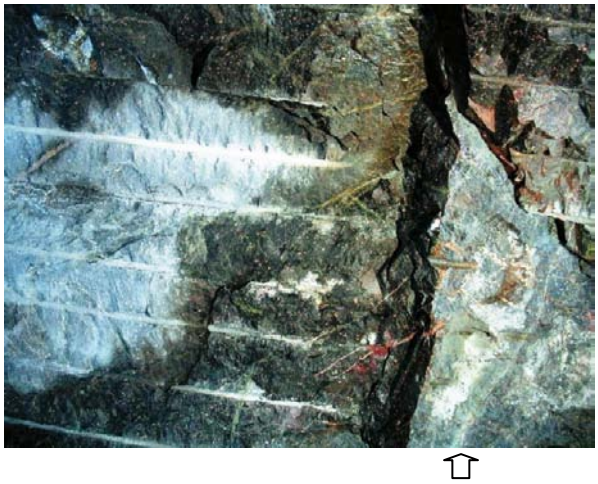

36-38 m, left-hand side, roof

38-40 m, left-hand side, roof

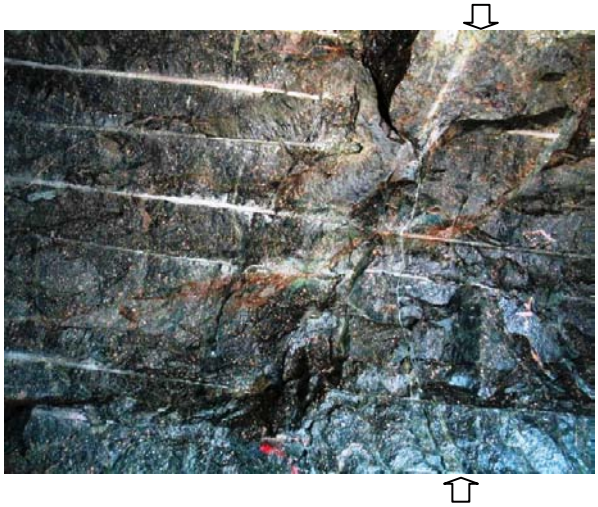

36-38 m, left-hand side, shoulder

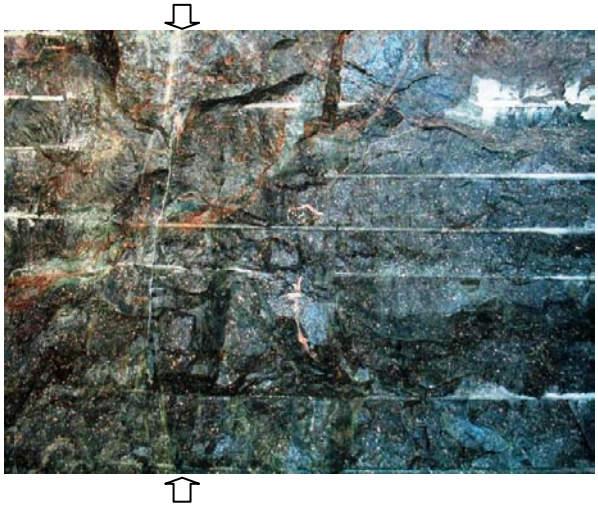

38-40 m, left-hand side, shoulder

36-38 m, left-hand side, wall

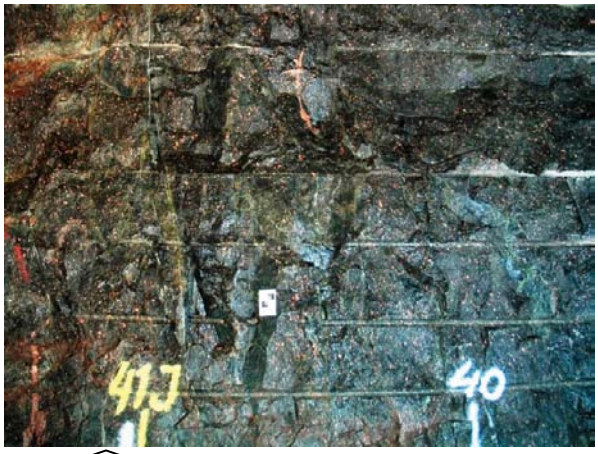

38-40 m, left-hand side, wall

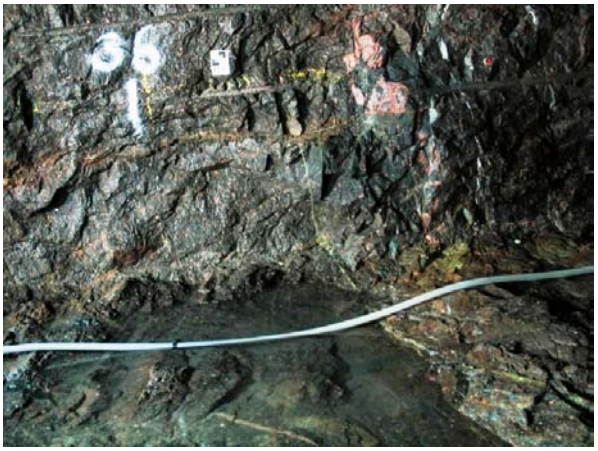

36-38 m, left-hand side, floor and lower part of the wall

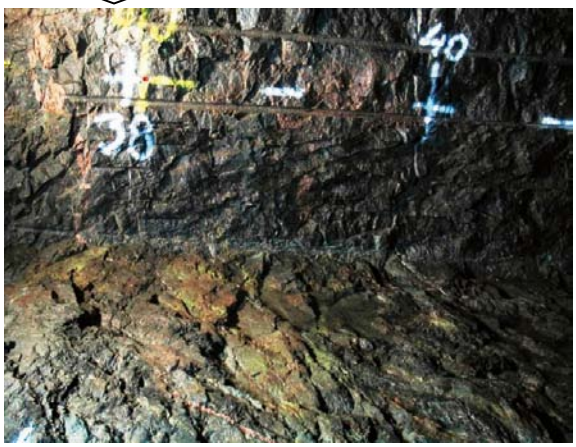

38-40 m, left-hand side, floor and lower part of the wall

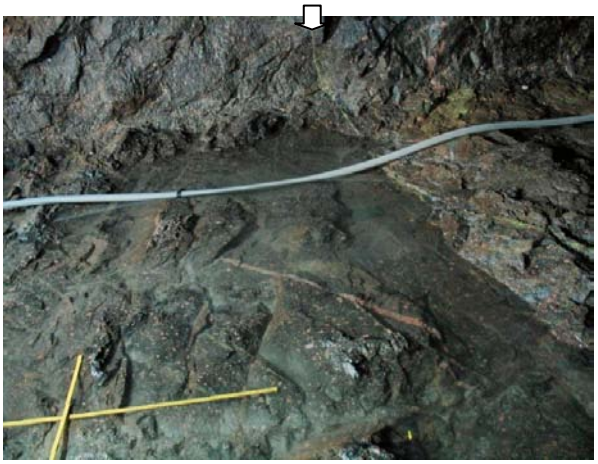

36-38 m, left-hand side, floor and lower part of the wall

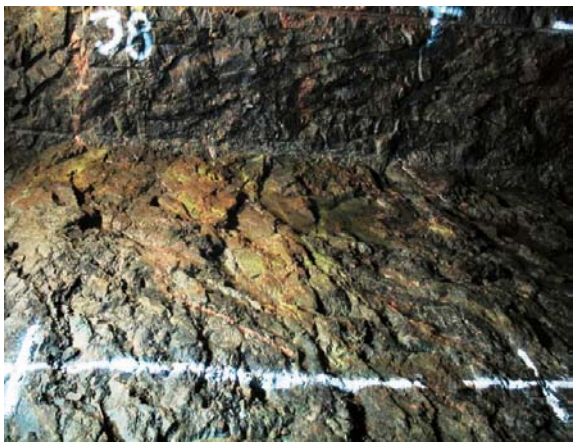

38-40 m, left-hand side, floor and lower part of the wall

Photographs 40–44 m

Arrows mark approximate positions of structures G2-122, 123, 125 & 133 as well as P2b-82. Possible candidates as TRUE Block Scale model structure #22

42-44 m, right-hand side, floor and lower part of the wall

40-42 m, right-hand side, floor and lower part of the wall

42-44 m, right-hand side, floor and lower part of the wall

40-42 m, right-hand side, floor and lower part of the wall

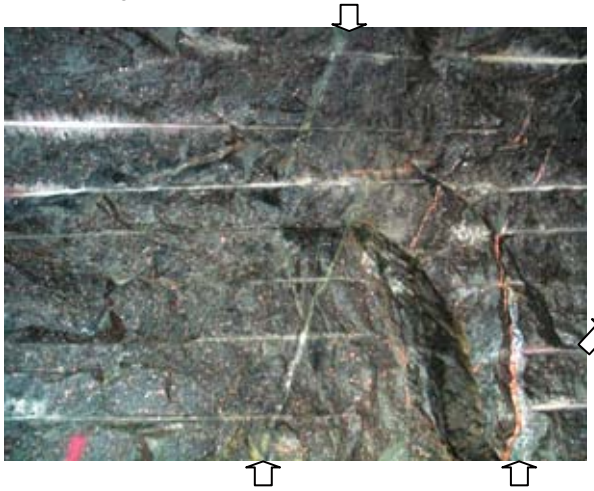

42-44 m, right-hand side, wall and shoulder

40-42 m, right-hand side, wall and shoulder

42-44 m, right-hand side, roof

40-42 m, right-hand side, roof

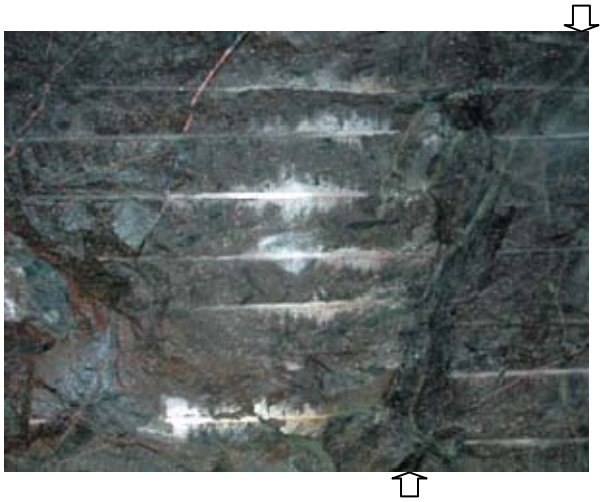

40-42 m, left-hand side, roof

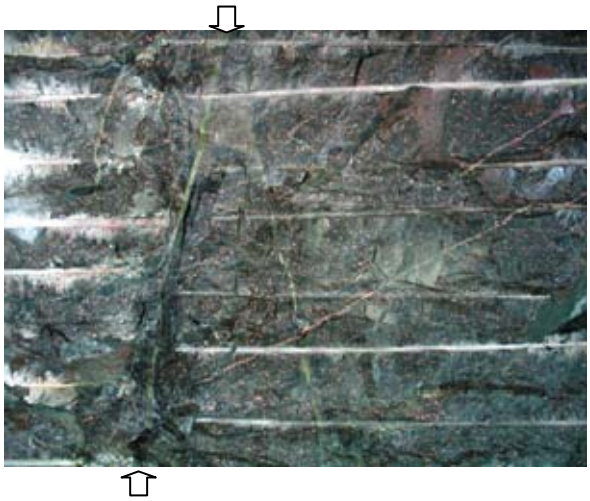

42-44 m, left-hand side, roof

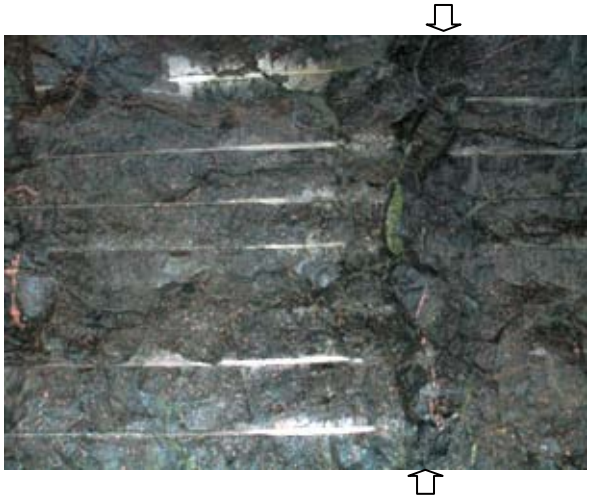

40-42 m, left-hand side, shoulder

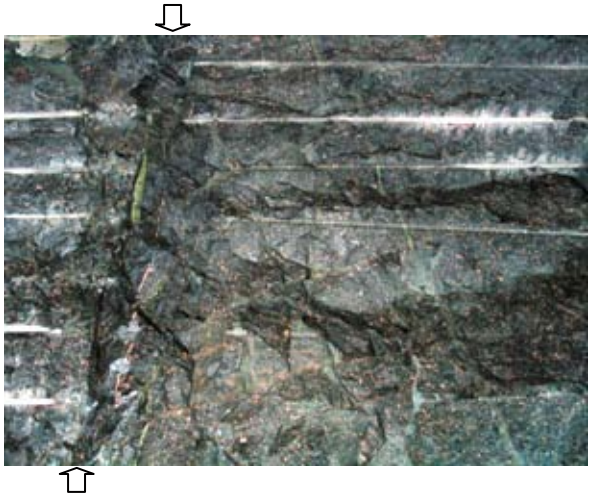

42-44 m, left-hand side, shoulder

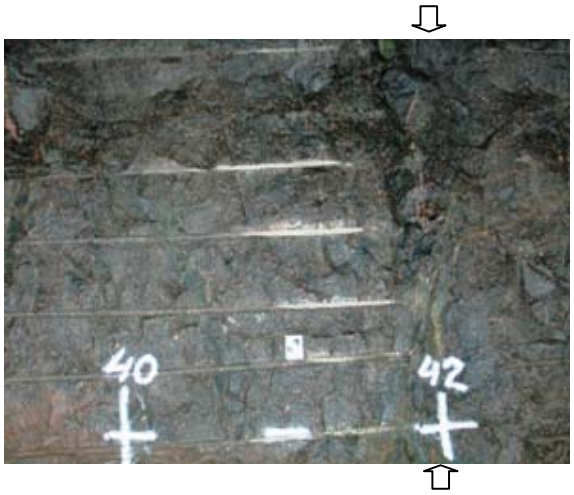

40-42 m, left-hand side, wall

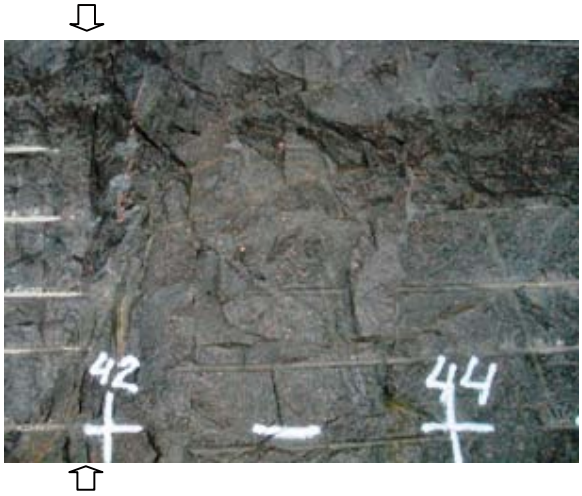

42-44 m, left-hand side, wall

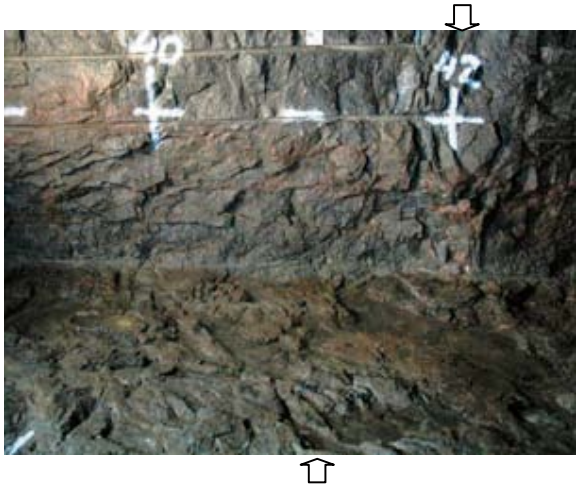

40-42 m, left-hand side, floor and lower part of the wall

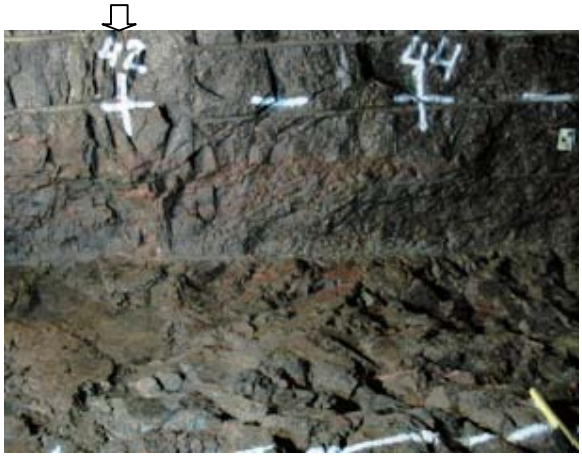

42-44 m, left-hand side, floor and lower part of the wall

40-42 m, left-hand side, floor and lower part of the wall

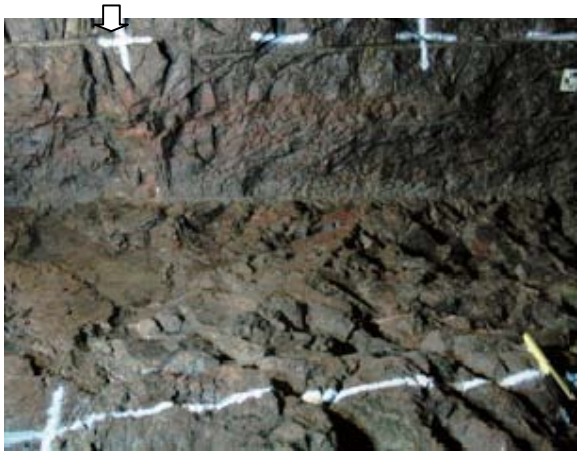

42-44 m, left-hand side, floor and lower part of the wall

Stage mapping, Stage 3, section 48.7–64.6 m, mapping of walls and roof (P) as well as floor (G)

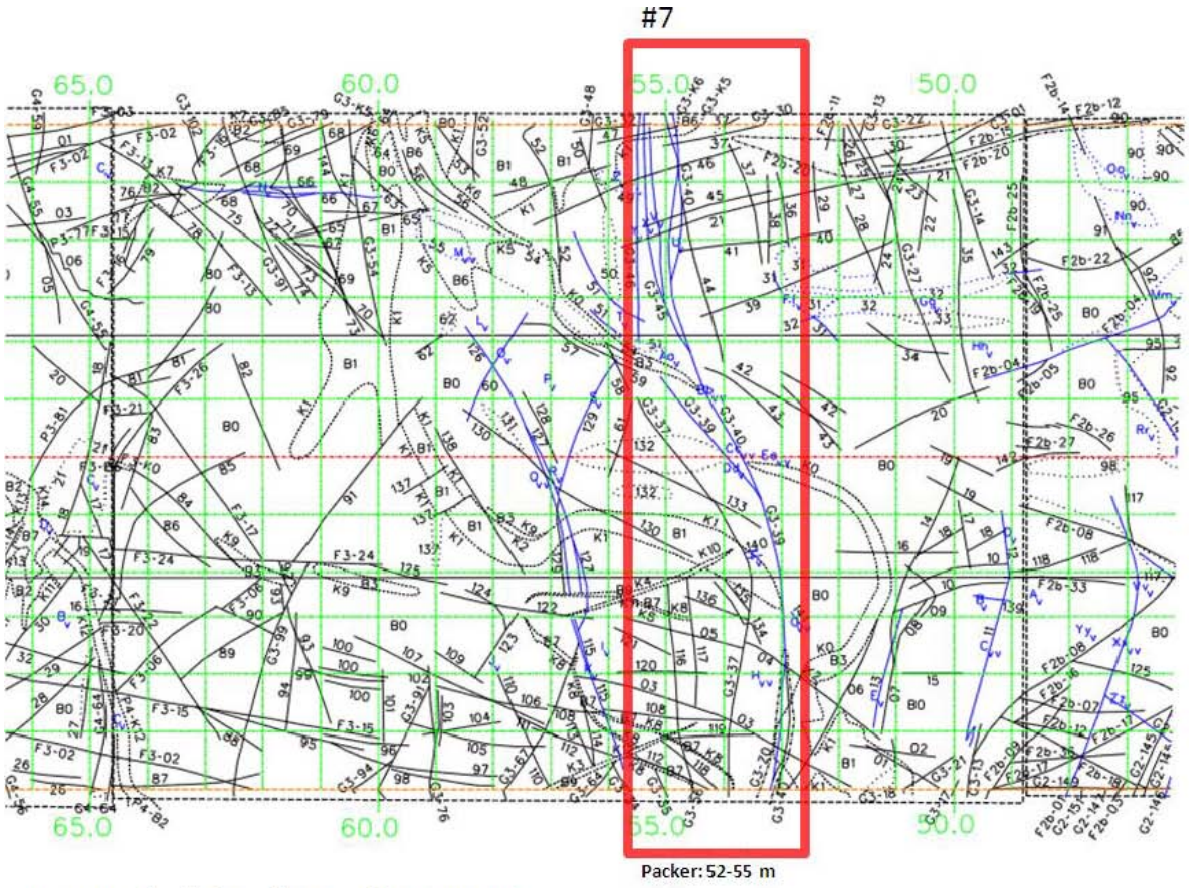

P3 = Tunnel walls & roof, stage 3 (48.7-64.6 m)

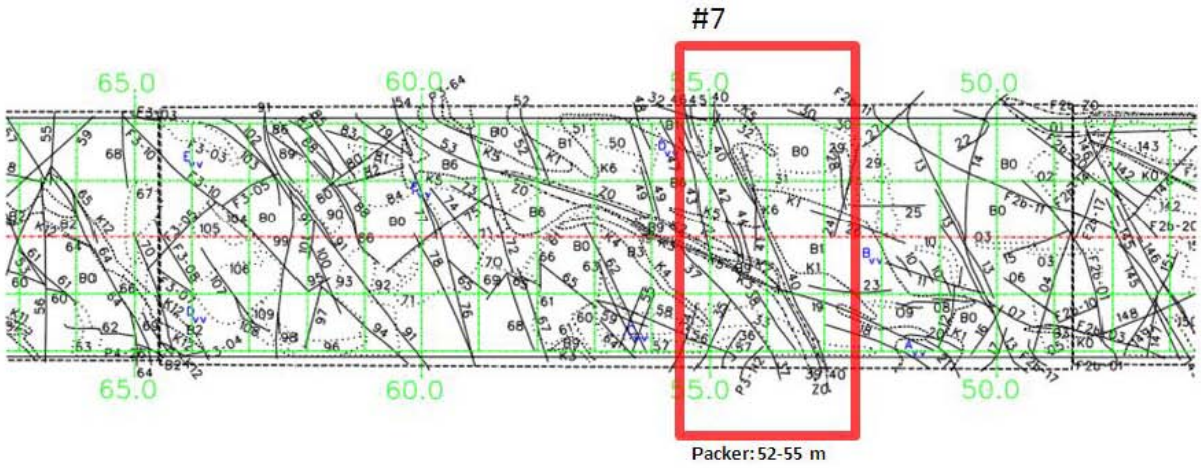

G3 = Tunnel floor, stage 3 (48.7-64.6 m)

Photographs 52–56 m

Arrows mark approximate positions of structures G3-39, 40, 42, 45 & 46 as well as G3-Z0. Possible candidates as TRUE Block Scale model structure #7

54-56 m, right-hand side, floor and lower part of the wall

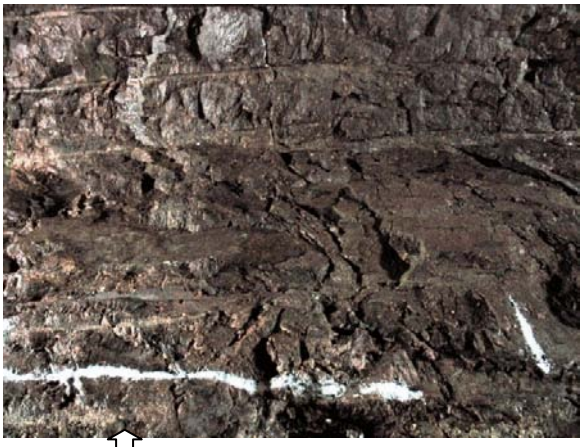

52-54 m, right-hand side, floor and lower part of the wall

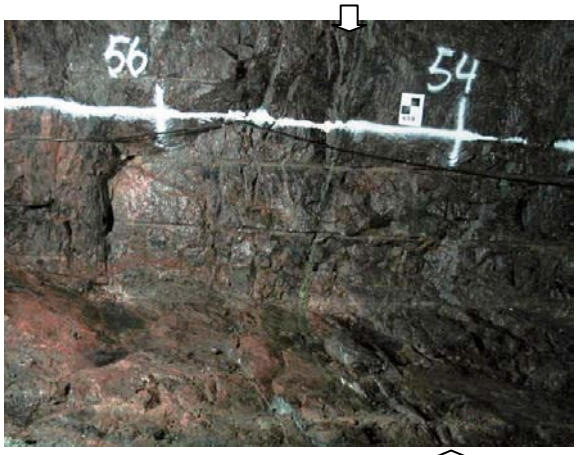

54-56 m, right-hand side, floor and lower part of the wall

52-54 m, right-hand side, floor and lower part of the wall

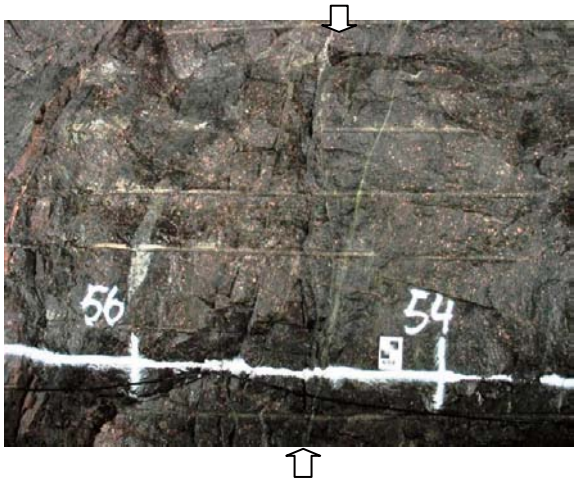

54-56 m, right-hand side, wall

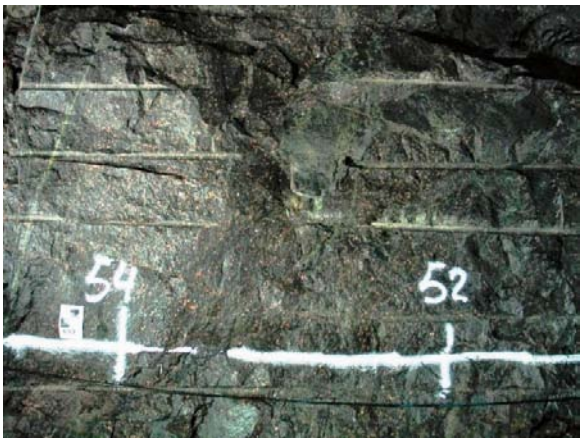

52-54 m, right-hand side, wall

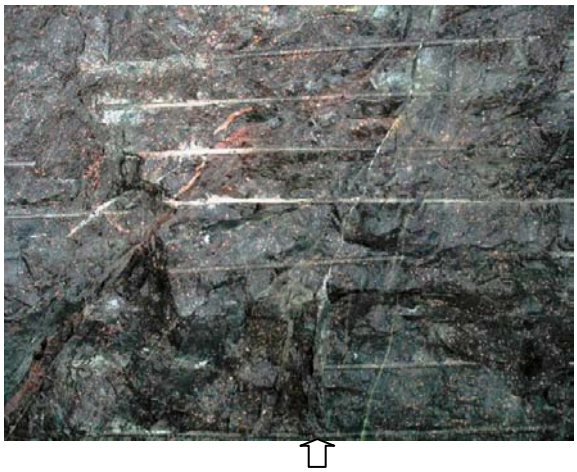

54-56 m, right-hand side, wall and shoulder

52-54 m, right-hand side, wall and shoulder

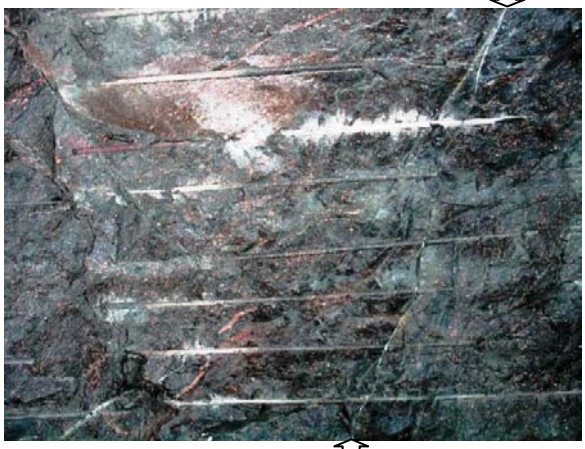

54-56 m, right-hand side, shoulder

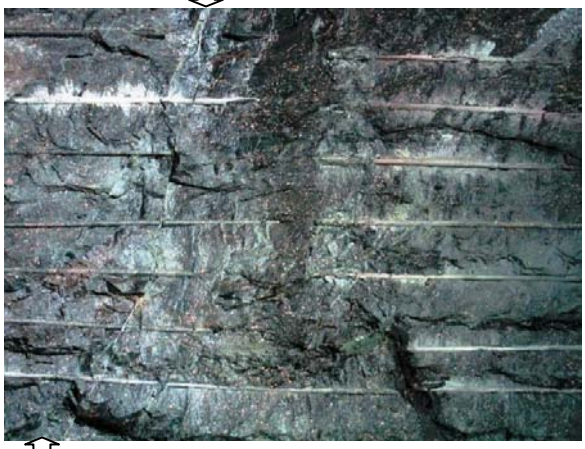

52-54 m, right-hand side, shoulder

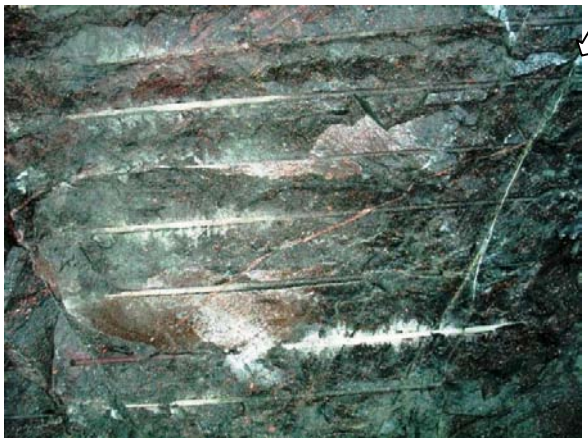

54-56 m, right-hand side, roof

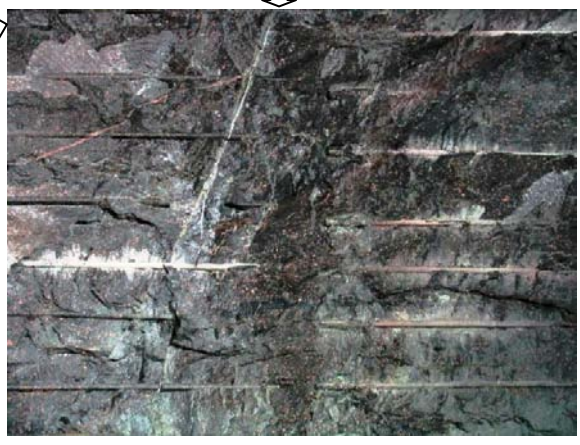

52-54 m, right-hand side, roof

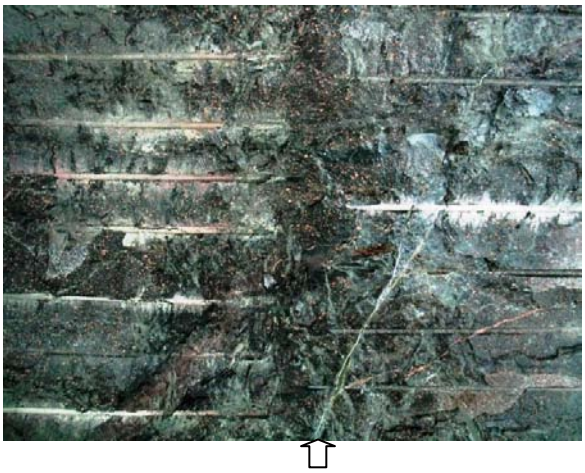

52-54 m, left-hand side, roof

54-56 m, left-hand side, roof

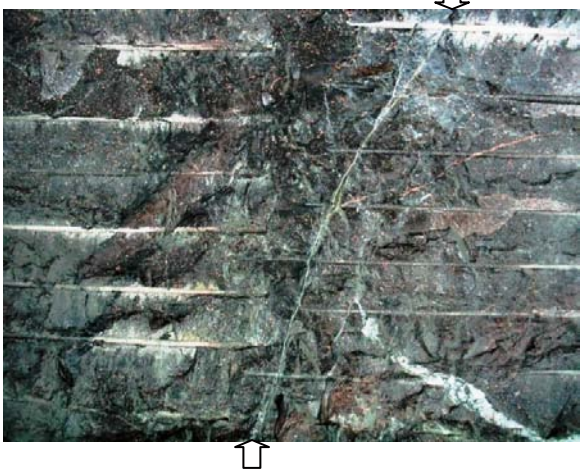

52-54 m, left-hand side, shoulder

54-56 m, left-hand side, shoulder

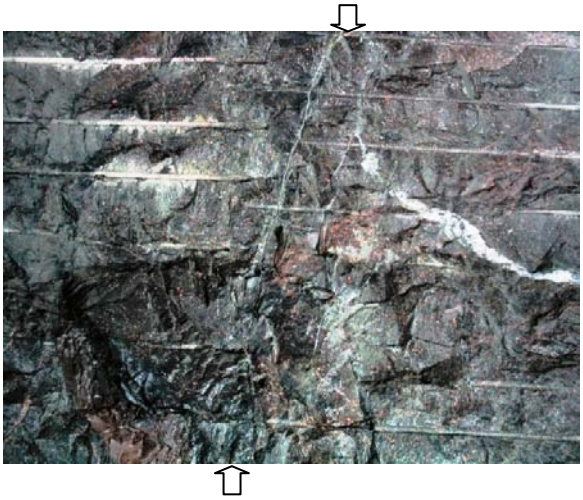

52-54 m, left-hand side, wall and shoulder

54-56 m, left-hand side, wall and shoulder

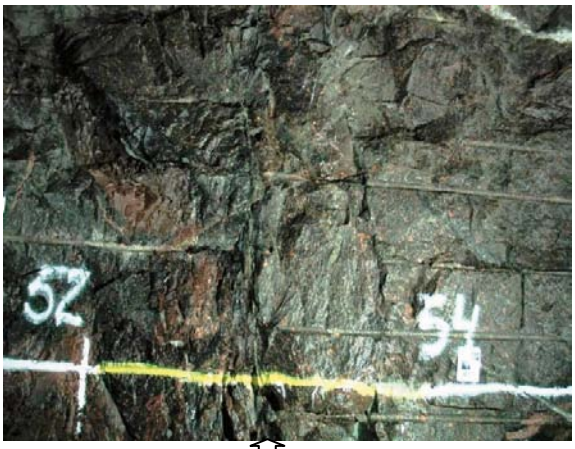

52-54 m, left-hand side, wall

54-56 m, left-hand side, wall

52-54 m, left-hand side, floor and lower part of the wall

54-56 m, left-hand side, floor and lower part of the wall

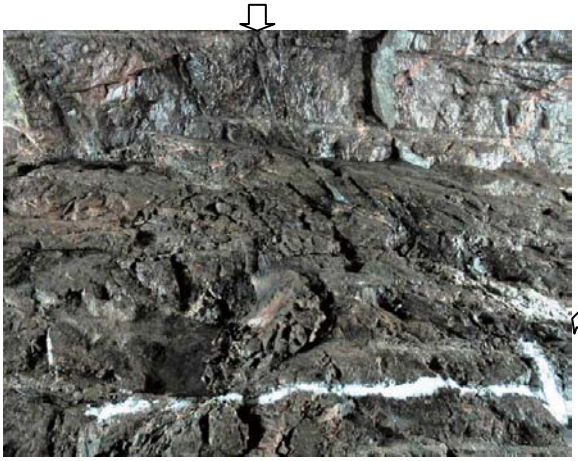

52-54 m, left-hand side, floor and lower part of the wall

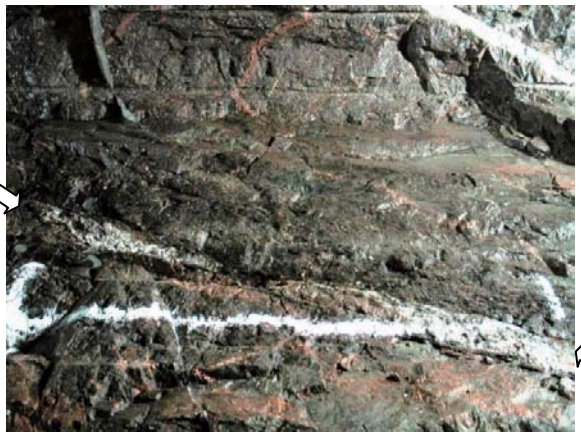

54-56 m, left-hand side, floor and lower part of the wall

Stage mapping, Stage 4, section 64.6–80.7 m, mapping of walls and roof (P) as well as floor (G)

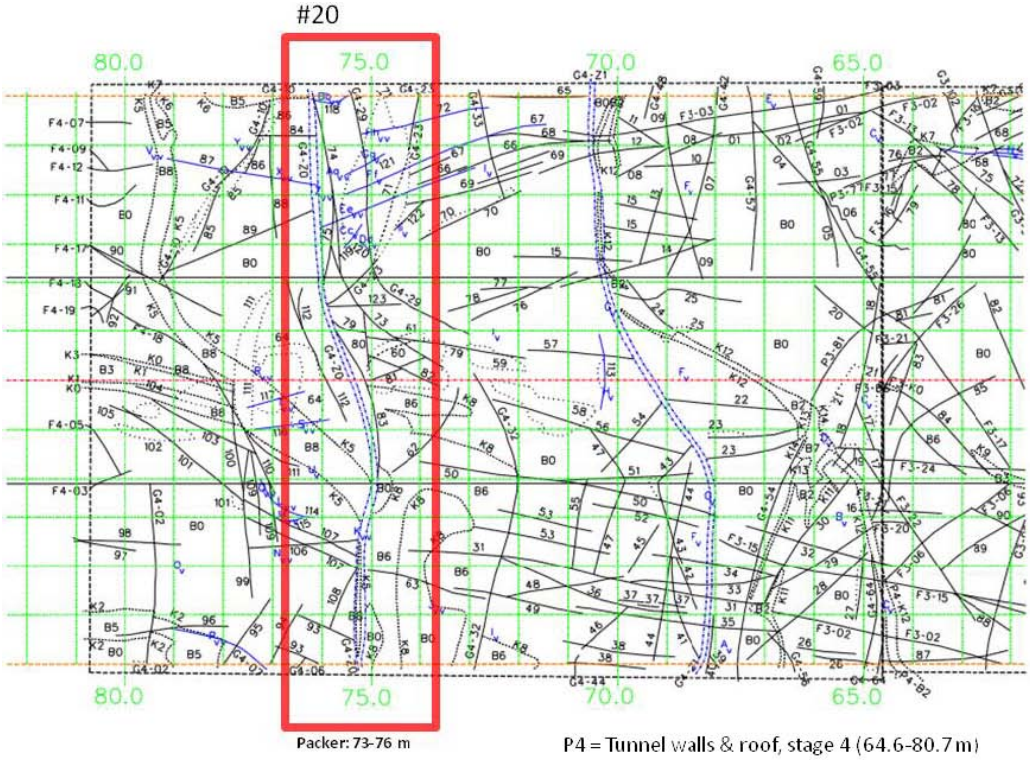

P4 = Tunnel walls & roof, stage 4 (64.6-80.7 m)

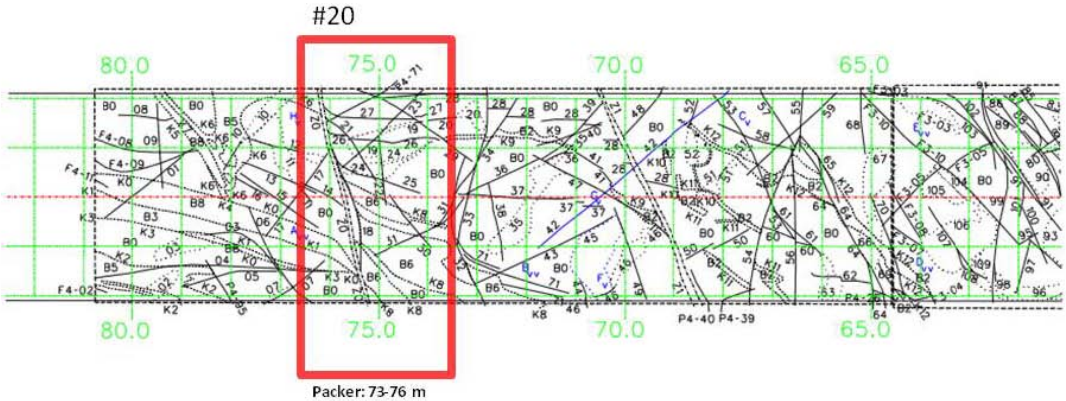

G4 = Tunnel floor, stage 4 (64.6-80.7 m)

Photographs 74–76 m

Arrows mark approximate position of structure G4-Z0. Possible candidate as TRUE Block Scale model structure #20

74-76 m, right-hand side, floor

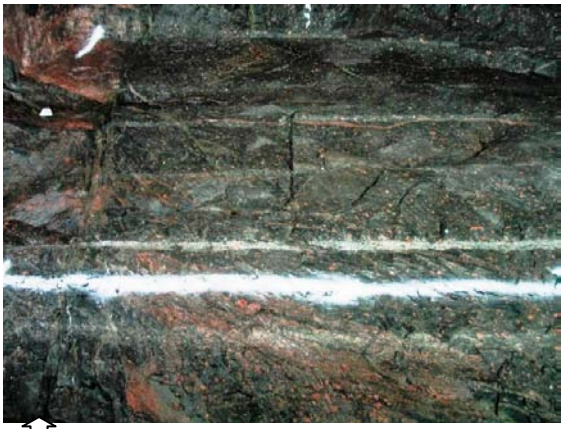

74-76 m, right-hand side, floor and lower part of the wall

74-76 m, right-hand side, floor and lower part of the wall

74-76 m, right-hand side, lower part of the wall

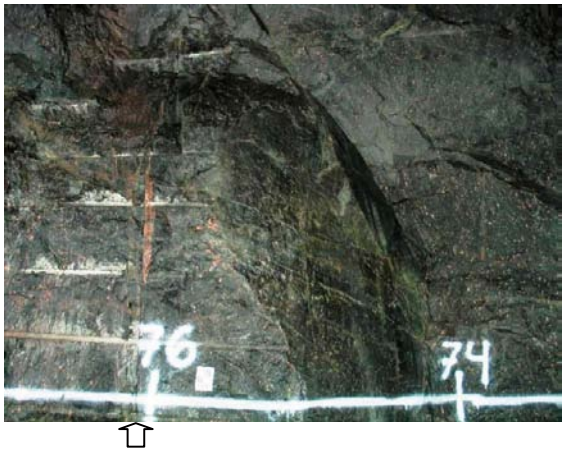

74-76 m, right-hand side, wall

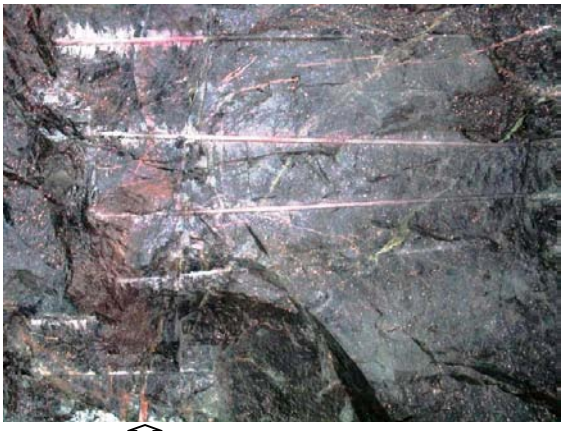

74-76 m, right-hand side, shoulder

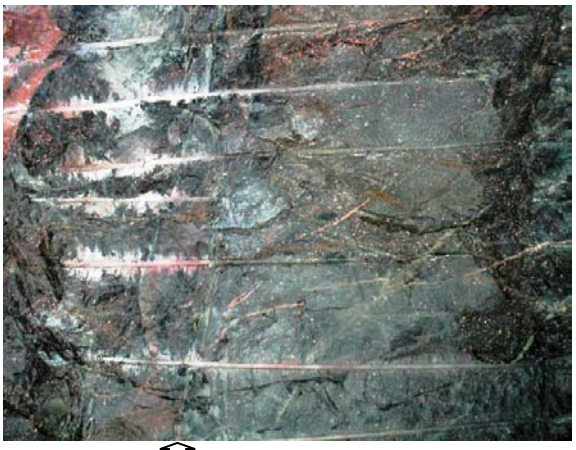

74-76 m, right-hand side, roof

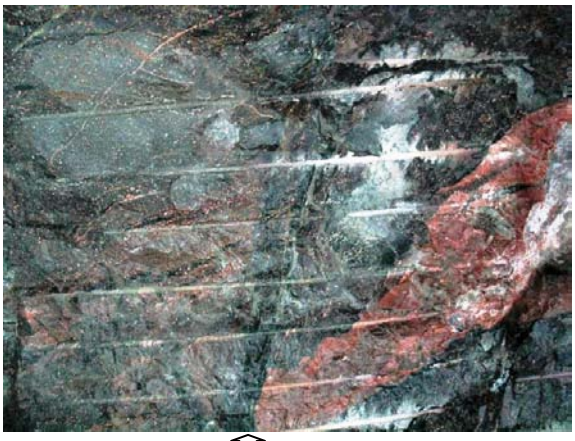

74-76 m, left-hand side, roof

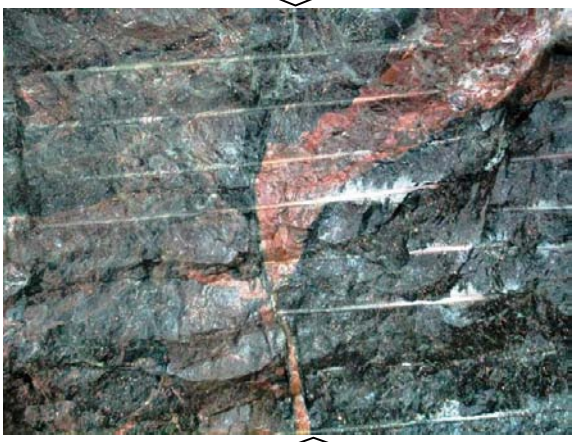

74-76 m, left-hand side, shoulder

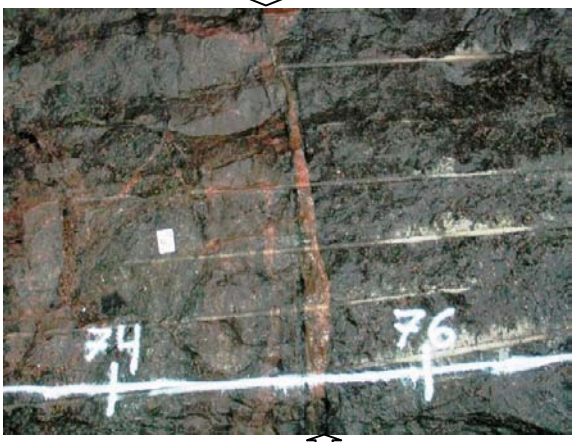

74-76 m, left-hand side, wall

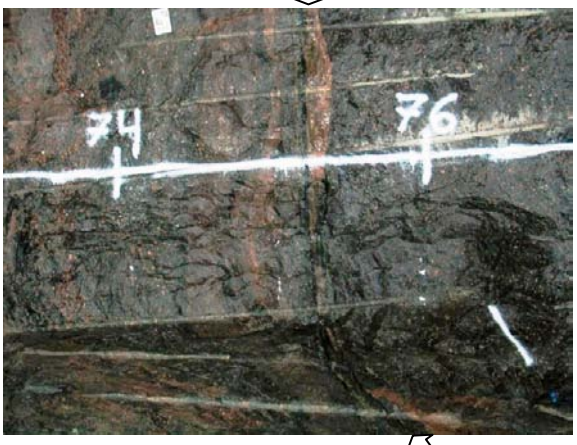

74-76 m, left-hand side, floor and lower part of the wall

74-76 m, left-hand side, floor and lower part of the wall